TESIS DE LA UNIVERSIDAD DE ZARAGOZA

2023 123

Eduardo Javier Moreo Lapieza

Use of live attenuated mycobacteria for cancer treatment in experimental mouse models

Director/es
Aguiló Anento, Juan Ignacio

ISSN 2254-7606

Prensas de la Universidad
Universidad Zaragoza

ISSN 2254-7606

Universidad Zaragoza
1542

Tesis Doctoral

USE OF LIVE ATTENUATED MYCOBACTERIA FOR CANCER TREATMENT IN EXPERIMENTAL MOUSE MODELS

Autor

Eduardo Javier Moreo Lapieza

Director/es

Aguiló Anento, Juan Ignacio

UNIVERSIDAD DE ZARAGOZA
Escuela de Doctorado

Programa de Doctorado en Bioquímica y Biología Molecular

2023

FACULTAD DE MEDICINA

Departamento de Microbiología, Pediatría, Radiología y Salud Pública

Use of live attenuated mycobacteria for cancer treatment in experimental mouse models

Memoria presentada para optar al grado de Doctor en Bioquímica y Biología Molecular por:

Eduardo Javier Moreo Lapieza

Director:

Juan Ignacio Aguiló Anento

This doctoral thesis has been elaborated in the Department of Microbiology, Pediatrics, Radiology and Public Health of the University of Zaragoza, and was ascribed to the PhD program of the Department of Biochemistry and Molecular and Cellular Biology, from the University of Zaragoza.

The PhD candidate, Eduardo Moreo, and the work showed in this thesis was funded by the Spanish Science and Innovation Ministry (RETOS COLABORACIÓN RTC-2017-6379-1 and RETOS INVESTIGACIÓN RTI2018-097625-B-I00); by the Gobierno de Aragón-Fondo Europeo de Desarrollo Regional (FEDER) 2014-2020: Construyendo Europa Desde Aragón, and by the CIBERES (Insituto de Salud Carlos III).

From the results obtained in this thesis, two articles have been produced:

- **Moreo, E., et al. Novel intravesical bacterial immunotherapy induces rejection of BCG-unresponsive established bladder tumors**. *Published in Journal for ImmunoTherapy of Cancer, 2022.*

- **Moreo, E., et al. Systemic BCG administration stimulates NK and T cell-mediated antitumor lung immunity and overcomes tumor resistance to immune checkpoint inhibition**. *In review, 2022*.

Table of contents

Summary

Since the work of William Coley at the end of the 19th century, it became clear that live microorganisms could be harnessed for cancer treatment. A plethora of preclinical and clinical studies in the 20th century led to approval of the live tuberculosis vaccine Bacillus Calmette-Guérin (BCG), for the treatment of medium and high-risk non-muscle invasive bladder cancer (NMIBC). Moreover, experimental work using mouse models clearly established that the antitumoral properties of BCG are based on stimulation of the immune system.

Although intravesical BCG therapy for NMIBC is one of the most successful immunotherapies to date, it has several shortcomings. An important fraction of patients does not respond to this type of therapy, and toxicity issues cause treatment interruption leading to modified schedules with suboptimal therapeutic efficacy. Additionally, during the past ten years BCG production has experimented a severe global shortage, forcing the use of alternative therapies or lower BCG doses. Therefore, there is an urgent need to develop treatment modalities with alternative agents for this subset of patients. Given the spectacular success of bacterial therapy in the field of bladder cancer, a more profound knowledge of its mechanism of action could lead to an improvement of this kind of treatment.

In the first part of this work, we set out to study bacterial and host factors involved in the antitumor efficacy of live-attenuated mycobacteria for bladder cancer. We took advantage of the fact that we could directly compare two different live-attenuated tuberculosis vaccines: BCG and MTBVAC. By comparing their behavior in experimental mouse models of bladder cancer, we found that the ability of the bacteria to colonize the bladder correlated with treatment efficacy. Importantly, we identified genes absent in BCG and present in MTBVAC which explained the higher therapeutic potential of the latter. Furthermore, we analyzed the antitumor immune response in the bladder, showing that intravesical bacterial treatment induced tumor-specific T cell dependent responses. Lastly, the therapeutic efficacy of intravesical MTBVAC in a mouse model of bladder cancer was greatly boosted by concurrent systemic immune checkpoint inhibition with PD-L1 blocking antibodies.

In the second part of this thesis, we devise a strategy to deliver BCG into the lungs to treat either metastatic or primary lung tumors in experimental mouse models. We observed that

intravenous administration of BCG in mice potently stimulated lung-specific antitumor immune responses (both innate and adaptive), which could be further potentiated by immune checkpoint inhibition based on PD-L1 blockade. Therefore, we propose that the success of BCG in bladder cancer and melanoma could also be applied to the field of thoracic oncology.

Resumen

Desde el trabajo de William Coley a finales del siglo XIX, quedó claro que los microorganismos vivos podían aprovecharse para el tratamiento del cáncer. Numerosos estudios preclínicos y ensayos clínicos durante el siglo XX condujeron a la aprobación de la vacuna viva para la tuberculosis, el Bacilo de Calmette-Guérin (BCG), para el tratamiento del cáncer de vejiga no músculo invasivo (CVNMI). Además, mediante el uso de modelos experimentales, quedó establecido que la actividad antitumoral de BCG se basa en la estimulación del sistema inmune.

Aunque la terapia basada en la administración intravesical de BCG para el CVNMI es una de las inmunoterapias más exitosas hasta la fecha, presenta ciertas deficiencias. Una fracción importante de los pacientes no se beneficia de este tipo de terapia, y los efectos secundarios adversos pueden provocar la interrupción del tratamiento, lo que conduce a versiones modificadas con una eficacia terapéutica subóptima. Además, durante los últimos diez años ha habido una grave escasez de BCG a nivel mundial, lo que ha obligado al uso de otras aproximaciones terapéuticas o dosis reducidas de BCG. Por lo tanto, existe una necesidad urgente de desarrollar tratamientos alternativos para esta clase de pacientes. Dado el éxito de la terapia bacteriana en el campo del cáncer de vejiga, un conocimiento más profundo de su mecanismo de acción podría conducir a una mejora de este tipo de tratamiento.

En la primera parte de este trabajo nos propusimos estudiar los factores bacterianos y asociados al huésped implicados en la eficacia antitumoral de las micobacterias vivas atenuadas para el cáncer de vejiga. Aprovechamos el hecho de que podíamos comparar directamente dos vacunas contra la tuberculosis distintas: BCG y MTBVAC. Mediante la comparación de su comportamiento en modelos experimentales de cáncer de vejiga en ratones, descubrimos que la capacidad de las bacterias para colonizar la vejiga estaba íntimamente relacionada con la eficacia del tratamiento. Es importante destacar que logramos identificar genes ausentes en BCG y presentes en MTBVAC que explicasen el mayor potencial terapéutico de esta última vacuna. Además, analizamos la respuesta inmune frente al tumor en la vejiga, mostrando que el tratamiento bacteriano intravesical era capaz de inducir respuestas dependientes de células T específicas del tumor. Por último, la eficacia terapéutica de MTBVAC intravesical en un modelo de cáncer de vejiga en ratón

se vio claramente potenciada por la administración sistémica de anticuerpos bloqueantes del punto de control inmunitario PD-1/PD-L1.

En la segunda parte de esta tesis, diseñamos una estrategia para localizar BCG en el pulmón con el objetivo de tratar tumores pulmonares primarios o metastásicos en modelos experimentales en el ratón. Se observó que la administración intravenosa de BCG en el ratón estimuló específicamente la respuesta inmunitaria antitumoral en el pulmón (tanto innata como adaptativa), que pudo potenciarse aún más mediante la inhibición del punto de control inmunitario PD-L1. Por lo tanto, con los resultados obtenidos en esta parte proponemos que el éxito de BCG en cáncer de vejiga y melanoma también podría aplicarse al campo de la oncología torácica.

"There has been a rather general feeling that the host has only a limited capacity at best to rid itself of naturally arising cancer cells. ... However, until we know how to direct the full force of specific immunity against tumor cells, the true magnitude of this potential will remain unknown. With the advances that have been made and the powerful new tools that are available, the cancer immunologist's long search for specificity may finally be rewarded"

Lloyd J. Old, 1981

General introduction

1.1 The immune system and cancer

Cancer is a disease characterized by genomic instability, in which spontaneously occurring mutations facilitate unrestricted cell growth by favouring proliferation or by avoiding intrinsic cell death mechanisms[1]. From these mutations, tumor-associated antigens can arise[2–4], which do not occur on untransformed cells or are present at lower levels. Thus, the so-called tumor-specific or tumor-associated antigens can be recognized as non-self by T lymphocytes and trigger adaptive immune responses leading to tumor elimination.

1.1.1 Cancer immunosurveillance

The notion that the immune system not only protects the host from microbial infection but can also detect and eliminate tumor cells arose 50-100 years ago, with Paul Ehrlich hypothesis that protective immunity could effectively supress cancer in long-lived organisms[5], the notion of cancer immunosurveillance introduced by Burnet and Thomas[6] and the study of experimental tumors in mice by Lloyd Old[7]. Although the idea that the immune system controls tumor growth was initially received with great scepticism and could not be experimentally proven at the time, the advent of precise gene targeting in mice and the ability to produce highly specific monoclonal antibodies directed to specific immune cell components allowed those hypotheses to be formally tested, unequivocally showing that the immune system can target and destroy tumor cells[8].

Indeed, interest in cancer immunosurveillance arose again when immune-dependent rejection of syngeneic transplanted tumors was shown to heavily depend on host IFN-γ expression[9,10]. Following this discovery, it became apparent that mice lacking key components of the IFN-γ signaling pathway, such as the IFN-γ receptor or the STAT1 transcription factor, were far more susceptible to chemically induced or even spontaneous carcinogenesis[11]. In a similar manner, mice lacking adaptive immunity by deletion of the Rag2 protein, which eliminates T and B cells in the host, presented higher rates of primary tumor development following carcinogen exposure than their wild-type counterparts (Figure 1)[11].

Following this work, a large body of literature has identified numerous immune cells and pathways which are critical for cancer immunosurveillance[8]. Among them, of particular interest are reports showing the importance of the cytolytic pore-forming protein perforin in mediating tumor elimination by immune cells, since mice lacking this molecule develop

a higher incidence of MCA-induced sarcomas and even spontaneous B cell lymphomas at higher rates than wild-type littermates[9,12,13]. Confirming these findings, genetically modified mice, such as Eμ-v-Abl or Trp53$^{+/-}$ mice, when backcrossed to a Perf$^{-/-}$ background, developed spontaneous tumors with an earlier onset than wild-type controls[12,13]. Deficiency in other components of the immune system, such as lack of the type-I IFN receptor[14], IL-12[15] or depletion of NK cells by antiNK1.1 or antiAsialo-GM1 administration[12,16] also entails higher incidence of carcinogen-induced tumors and/or spontaneous carcinogenesis. These highlighted results, among many others, have validated a critical role for the immune system in suppressing tumor growth.

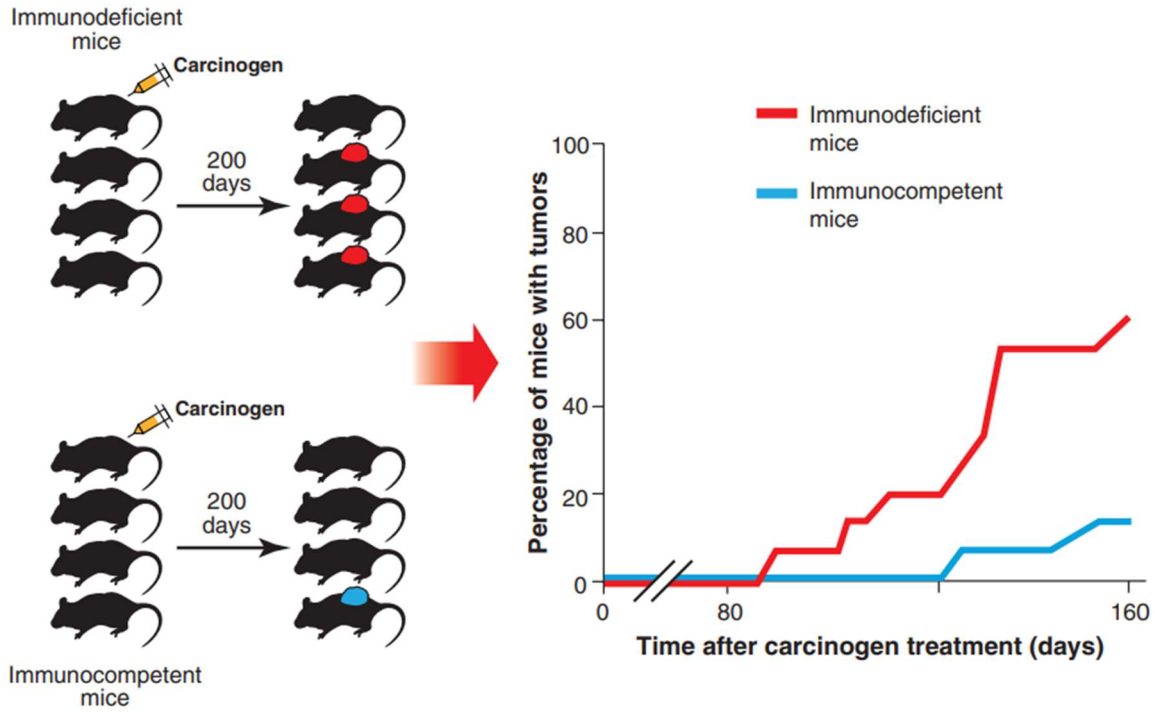

Figure 1. Higher incidence of MCA-induced sarcomas in Rag2$^{-/-}$ immunodeficient mice compared with wild-type immunocompetent mice. *Taken from Schreiber et al. (2011)*[17].

Although the importance of the IFN-γ signaling axis in the host had been clearly stablished, subsequent work demonstrated that the tumor cell itself is a physiologically important target for IFN-γ mediated tumor rejection. Particularly, Meth A tumor cells engineered to be insensitive to IFN-γ showed more aggressive growth than parental IFN-γ sensitive tumor cells when transplanted into syngeneic mice[18]. Using a different approach consisting in generation of carcinogen-induced tumor cell lines in an IFN-γ receptor knock-out (IFNγR$^{-/-}$) background, it was shown that tumor cell lines derived from this background were highly

tumorigenic when transplanted into wild-type hosts, compared to tumor cell lines coming from a wild-type background[19]. Importantly, genetic recomplementation of these tumor cell lines with wild-type IFNγR reverted this effect and elicited tumor rejection, except when IFN-γ neutralizing antibodies were administered or mice were depleted of $CD4^+$ or $CD8^+$ T lymphocytes[20]. Altogether, these works, among others, suggested that T cell-derived IFN-γ is a critical mediator of antitumor immunity.

Later work has demonstrated that IFN-γ enhances tumor cell immunogenicity by upregulating multiple components of the antigen presentation machinery, being of particular importance the MHC-I pathway function, which enables targeting by antigen-specific cytotoxic $CD8^+$ T cells. However, accessory antitumor functions such as direct antiproliferative/proapoptotic activity on tumor cells[21,22], the induction of lymphocyte chemoattractant molecules such as CXCL9 and CXCL10[23], and inhibition of angiogenesis have also been described for IFN-γ[24]. Notwithstanding the potent antitumor effects of IFN-γ on tumor cell themselves, this immune cell-produced cytokine also regulates immune cell activity, for example by maintaining a $CD4^+$ Th1-polarized immune cell response, by generating "M1-like" macrophages which can carry out diverse antitumor functions or by triggering NK cell activation[25].

Lastly, although the immune system directly targets tumor cells to restrict their growth, its ability to eliminate pathogens can also contribute to cancer immune surveillance. The most direct evidence is the control of viruses such as Merkel Cell polyomavirus, human papillomavirus, Epstein-Barr virus, Kaposi's sarcoma virus or hepatitis B and C virus, which are known to be tumorigenic drivers in humans[8]. Indeed, AIDS patients present elevated frequencies of malignancies[26]. Moreover, triple knock-out mice lacking GM-CSF, IL-3 and IFN-γ, which were highly susceptible to bacterial infection, displayed chronic inflammation in multiple organs and developed spontaneous tumors at increased rates[27]. Chronic inflammation and tumor development in these mice was abrogated upon treatment with broad-spectrum antibiotics from birth[27], evidencing that immune control of infections which can drive chronic inflammation can restrict cancer development. Not only does immune-mediated control of virus and bacteria influence the development of cancer, but a strong influence of the intestinal microbiota on antitumor immunity has become apparent in the recent years[28], as well as the existence of a tumor microbiome[29] and mycobiome[30],

which could conceivably modulate intratumoral immune cells or affect the immunogenicity of tumor cell themselves.

1.1.2 Cancer immunoediting

The role of the immune system in cancer progression is two-fold: as we have discussed, it is now clear that diverse immune cell subsets and pathways can target tumor cells and restrict their growth. However, it has become apparent that the evolutionary pressure exerted by the immune system over cancer cells favours the emergence of clones that evade recognition by the immune system, a process known as cancer immunoediting[31]. Cancer immunoediting comprises three phases: elimination, equilibrium and escape (Figure 2)[32].

○ Elimination

Although the elimination phase will be described in more detail in the next section (see Section 1.3.3 The cancer-immunity cycle) here I will briefly describe its main components. The first stage in the elimination phase requires detection of the developing tumor. This has been proposed to be mediated by tumor cell secretion of type I IFNs or damage-associated molecular patterns (PAMPs) such as HMGB1 or RAGE, secreted by dying cells or as a consequence of tissue damage generated by a growing tumor mass[33,34]. All these agents possess the ability to activate dendritic cells, which are the cellular subset responsible for driving adaptive immune responses[35,36]. Tumor cell expression of activating ligands (RAE-1, MICA/B) for components of the innate immune system such as NK lymphocytes can trigger the release of proinflammatory cytokines, which would aid in the development of adaptive immune responses[37,38]. Although the innate immune system can effectively target tumor cells, it is believed that adaptive immune responses are generally needed for complete tumor rejection[32]. Most importantly, the generation of adaptive immune responses targeting tumor-specific antigens warrants the development of immunological memory against those antigens[39]. This memory responses are best exemplified by the protection conferred by the rejection of a primary tumor cell transplant against a secondary challenge with the same tumor cell line, which is often observed in mice. In summary, the elimination phase comprises the detection of transformed cells by the innate immune system, which in turn guides the development of adaptive immune responses targeting specific tumor antigens.

The ability of the immune system to shape tumor immunogenicity is now well stablished. This was elegantly demonstrated by Robert Schreiber's group, showing that tumor generated in $Rag2^{-/-}$ mice are more immunogenic that those coming from immune competent mice, suggesting that the immune system sculpts developing tumors selecting for less immunogenic variants[11]. An independent study confirmed these results: when genetically engineered mouse models of sarcoma driven by KRAS and P53 mutations and expressing the SIINKEFL model antigen were used, immune competent mice selected tumor cell variants in which the locus containing the exogenously introduced SIINKEFL antigen had been epigenetically silenced. Importantly, this was not observed in immunocompromised $Rag2^{-/-}$ mice, so it was driven by the adaptive immune system[40,41]. Other work showed that the innate immune system can also edit the immunogenicity of developing tumors, since cell lines generated in $Rag2^{-/-}$ x $\gamma c^{-/-}$ mice, which lack NK lymphocytes in addition to T and B cells, were more immunogenic than those generated in $Rag2^{-/-}$ mice[42]. Interestingly, in this work NK cell-derived IFN-γ was shown to polarize M1 like-macrophages to drive tumor rejection in $Rag2^{-/-}$ mice[42].

It is worth noting that techniques such as whole exome sequencing and bioinformatic tools have allowed us to identify tumor neoantigens in human (and mouse) tumors and prove T cell reactivity against those antigens[43,44]. Importantly, tumor mutational burden and lymphocyte infiltration into tumors correlate with good prognosis and response to immunotherapy in some instances, evidencing that cancer immunosurveillance also exists in humans[45]. This year, evidence of pancreatic cancer immunoediting in humans was finally provided: recurrent tumors from long term survivors progressively lost immunogenic neoantigens when compared to primary resected tumors in the same patient[46].

○ Equilibrium

The equilibrium phase refers to a stage in which the immune system keeps tumors in a dormant state. Although this phase is not easily modelled in mice, several observations suggest that tumors can remain in an occult dormant state and emerge under certain conditions. For example, injection of low dose MCA in mice did not induce the development of overtly growing tumors in most individuals. However, depletion of T cells or neutralization of IL-12 or IFN-γ 200 days after the primary challenge allowed tumor outgrowth in 50 % of mice, whereas NK cell depletion did not[47]. These results evidenced a

specialized role of the adaptive immune system in maintaining the equilibrium phase in cancer.

Interestingly, tumors which escaped the equilibrium phase after depletion of immune system components were highly immunogenic when reimplanted in immunocompetent hosts, whereas sarcomas spontaneously escaping immune control in immunocompetent mice, which rarely happened, presented very low immunogenicity upon transplantation, evidencing editing by the immune system[47].

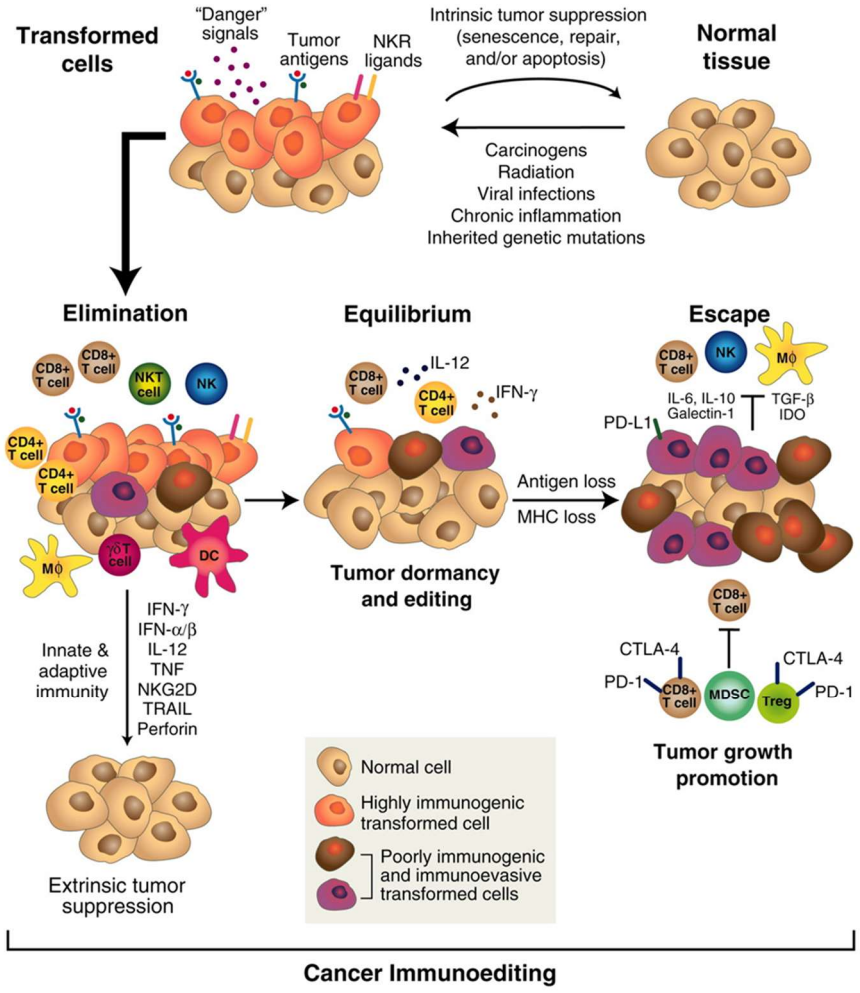

Figure 2. The three E's of cancer immunoediting: elimination, equilibrium and escape. Transformed cells can be targeted at a very early stage by cytotoxic lymphocytes ($CD8^+$, γδ T cells, NKT, NK), which can drive tumor elimination. However, some tumor cells may undergo editing due to selective pressure exerted by the immune system, and enter a phase of tumor dormancy, where edited tumor cells are kept at bay by immune cells. Further immunoediting of some tumor cell clones allow them to avoid the immune system and progressively grow. This is the escape phase, which is characterized by immune suppressive mechanisms and promotion of tumor growth. *Taken from Schreiber et al. (2011)*[17].

Histological analysis of dormant tumors revealed that a high proportion of cells were labelled by TUNEL and had lower expression of the proliferation marker Ki67$^+$ compared to progressively growing tumors, evidencing that a higher proportion of cells were undergoing cell death and were overall less proliferative in tumors which are actively controlled by the immune system[47]. Other studies revealed that tumor cells progressively acquire immune-evading properties during the equilibrium phase: longer periods of dormancy were accompanied by higher PD-L1 expression in tumor cells in a mouse model of leukaemia, allowing escape from CD8$^+$ T cell-mediated cytotoxicity[48]. Re-emergence of tumors following CD8$^+$ T cell depletion has also been observed in mouse models of ultraviolet B radiation-induced skin cancers[49] or in *Ret*-driven models of melanoma, confirming findings in MCA-induced sarcoma models[50]. In an interesting study, the coordinated action of immune cell derived IFN-γ and TNF prevented proliferation and induced tumor cell senescence[51].

In humans, the equilibrium phase is best exemplified in patients which relapse years after primary tumor surgical removal[52], or instances in which tumor outgrowth was observed when organs from patients lacking signs of malignancy were transplanted into immunosuppressed patients[53].

○ Escape

In the escape phase, tumor cells that have acquired the capacity to evade the immune system progressively grow. Broadly, progression from equilibrium to escape can be attributed to: (1) changes in the tumor cell allowing escape from immune cell recognition or (2) immunosuppression or immune exhaustion elicited by the growing tumor mass, via mechanisms which induce immune cell dysfunction[54,55]. Focusing first on tumor cells, resistance to immune cell targeting can arise by losing the ability to present neoantigens to T cells, which can occur by several different mechanisms: emergence of clones lacking strong immunogenic antigens, loss of MHC-I proteins or mutations in components of the antigen presentation machinery (TAP1, TAP2 or the immunoproteasome) or in IFN-γ receptor signalling components (IFNγR, JAK1, JAK2)[56]. Additionally, tumor cells become resistant to immune cell mediated cytotoxicity by upregulating anti-apoptotic mechanisms for enhanced survival, as STAT3, BCL-XL or FLIP.

Alternatively, tumors can also actively escape by driving immune cell dysfunction or exclusion[57]. For instance, establishment of a so called immune suppressive microenvironment can negatively impact the function of T and NK lymphocytes. For example, expression of immunoregulatory molecules such as PD-L1, galectin-9, IDO, HLA-E or HLA-G by the tumor dampen the cytotoxic activity of lymphocytes. Additionally, chronic exposure to tumor antigens can drive exhaustion of $CD8^+$ T lymphocytes, an epigenetically imprinted state which hinders the ability of these cells to respond to subsequent stimuli in a manner which is reminiscent to chronic viral infections[58].

Another critical way in which the tumor evades the immune system is the recruitment of regulatory immune cells. These can come in many flavours: $Foxp3^+$ regulatory T cells can inhibit effector T cells by producing IL-10 and TFGβ, by expressing CTLA-4 or PD-L1 and by depleting IL-2 from the environment, due to the expression of a higher affinity receptor for this T cell prosurvival cytokine[59]. Importantly, regulatory T cells function physiologically to maintain peripheral tolerance but are hijacked by being actively recruited to the tumor microenvironment (TME), where they exert potent immunosuppressive activities[59]. The importance of these cells in driving immune escape is evidenced by a plethora of studies showing that their depletion, normally by using Foxp3-DTR mice, unleashes immune responses to drive tumor rejection.

Tumors can favour the expansion of myeloid-derived suppressor cells (MDSCs) by deregulating bone marrow (BM) hematopoiesis. Production of certain cytokines and growth factors such as GM-CSF, G-CSF or PGE_2 by tumors elicits the generation of this heterogeneous group of cells comprising immature neutrophils and monocytes, which are then recruited to the TME in a chemokine-dependent manner[60]. Induction of MDSCs by the growing tumor mass also supresses immune function at a systemic level, facilitating the seeding of tumor cells in other organs besides the primary tumor, a process known as metastasis[61]. Blocking the recruitment of MDSCs into the tumor or their generation in the BM can boost antitumor immune responses, evidencing their important role in driving tumor escape from the immune system[60]. Tumorigenesis also alters other branches of haematopoiesis, for example by precluding the development of type 1 conventional dendritic cells (cDC1s), which are critical drivers of tumor-specific T cell responses, as described later[62,63].

Although the role of regulatory T cells and MDSCs in the immune response to cancer is somewhat clear, tumor-associated macrophages (TAMs) can both inhibit or favour effective antitumor immunity by multiple mechanisms. For instance, IL-10, TGFβ, ROS or L-arginine production, promotion of stromal development and hypoxia, generation of a dysfunctional vasculature or recruitment of other regulatory populations are some of the mechanisms that TAMs use to supress antitumor responses[64]. Normally, the phenotype of these immune suppressive TAMs reflects that of tissue-remodelling or tissue-repair macrophages. However, when properly activated, TAMs can also exert antitumor functions, such as T cell recruitment and priming, secretion of immunostimulatory cytokines or even direct tumor cell killing, reminiscent of their role in defence against bacterial or viral pathogens. The importance of this cellular subset in tumor immunology is evidenced by the undergoing preclinical and clinical development of numerous TAM-directed therapeutic strategies, either by depleting them or by modulating their activity[65,66].

In summary, the balance between immune inhibitory and stimulatory mechanisms determines whether the growing tumor mass escapes or not the vigilance of the immune system and its growth rate. Conceivably, progressively growing tumors reach a point of no return in which the immune system is overwhelmed by inhibitory signals, and immune-mediated rejection is no longer possible. This is best exemplified by the fact that therapies that target the immune system are far more effective at earlier stages of tumor growth, when immune-stimulatory signals overcome inhibitory mechanisms. At later stages, the balance is shifted into immune-inhibition and therapeutic interventions are less effective at controlling tumor growth and completely incapable of driving tumor rejection.

1.1.3 The cancer-immunity cycle

For an effective antitumor immune response leading to tumor growth control to happen, a series of sequential steps are required (visually summarized in Figure 3). Critically, these steps can function in an iterative self-propagating manner in order to amplify the ongoing immune response. This is what has become to be known as the cancer-immunity cycle[67].

The first step (1) requires the release of tumor neoantigens to be captured by DCs for processing. Different triggers exist for inducing initial cell death and release of tumor antigens: tumor cells can initially be targeted by innate immune cells such as NK or NKT cells, or cell death can be induced by treatment such as radiotherapy, chemotherapy or

adoptive T cell therapy. In the recent years it has become apparent that the way in which tumor cells die is critical for the subsequent priming of antigen-specific responses[68]. For instance, optimal priming requires cell death to be immunogenic as opposed to tolerogenic, being characterized by the release of proinflammatory cytokines (type I IFN) and alarmins such as ATP, HMGB1 or STING ligands, which trigger the activation and maturation of DCs[69]. Recent reports suggest that necroptotic, pyroptotic or ferroptotic cell death could be more immunogenic than apoptosis, and efforts are undergoing to induce specific modes of death in tumor cells to enhance priming of adaptive immune responses[70]. Remarkably, cell death induced by cytotoxic lymphocytes is particularly immunogenic[71].

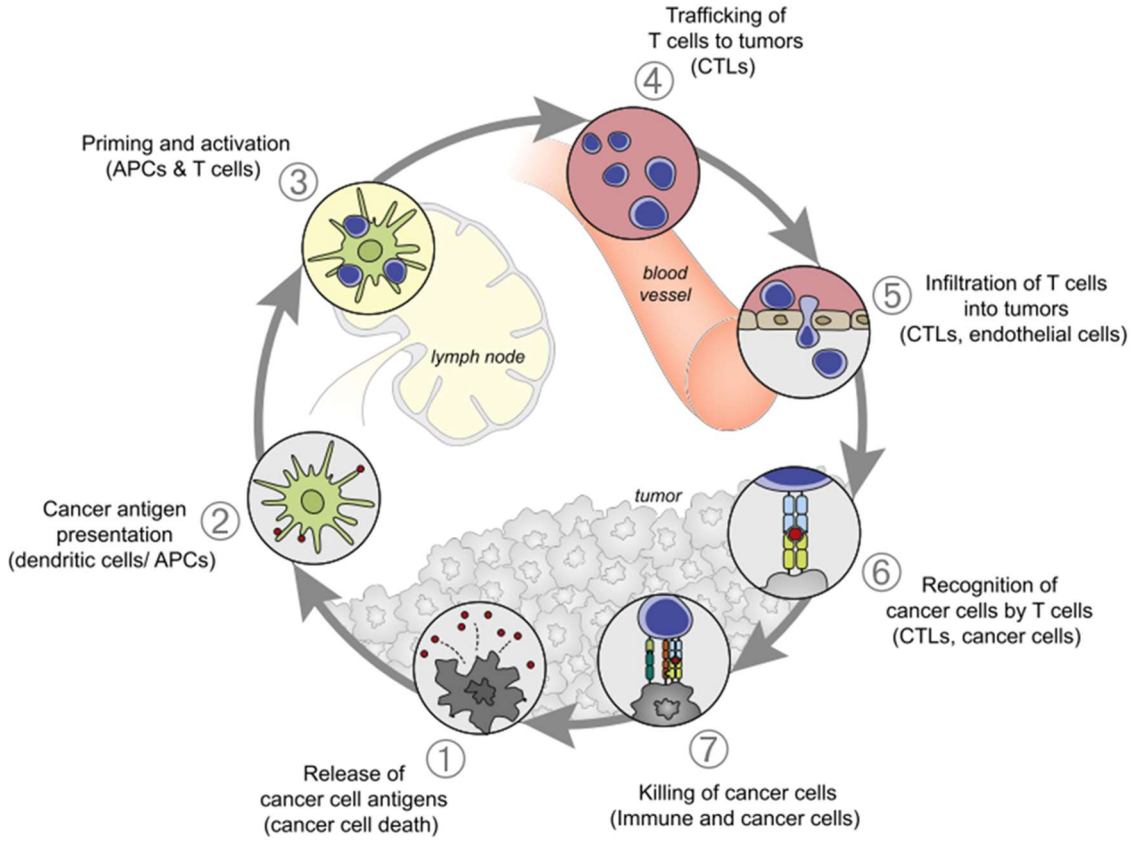

Figure 3. The seven steps of an effective antitumor immune response. *Taken from Mellman et al. (2013)*[67].

Following capture of tumor antigens, DCs are the cellular subset responsible for tumor antigen presentation to T cells (2). This event primarily happens in the tumor-draining lymph nodes (tdLNs) and requires the maturation of DCs which have acquired tumor antigens for their optimal processing into peptides, for migration to the tdLNs by a

mechanism dependent on CCR7 expression, and for providing T cells optimal costimulatory cues to guide their development into effector cells (3)[72].

It is important to note that presentation of exogenously acquired tumor antigens to $CD8^+$T cells via MHC-I, a pathway which classically was thought to drive presentation of peptides derived from endogenous proteins, requires a process known as antigen cross-presentation. Importantly, it is type 1 conventional dendritic cells that are specialized in cross-presentation of tumor-antigens to $CD8^+$ T cells, and their depletion completely abrogates antitumor adaptive immune responses[73]. The concept of cross-presentation took years to be established[74], and although we are starting to understand it more[75,76], it is still not fully discerned at the molecular level, and specially why is it restricted to cDC1s *in vivo*.

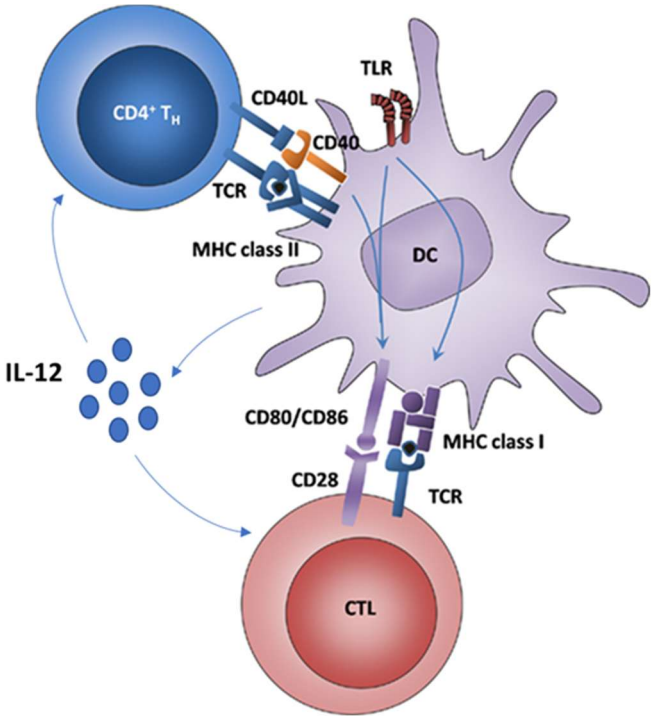

Figure 4. cDC1s prime tumor-specific T cells in the tumor draining lymph node. First, damage sensing by TLRs allows maturation and migration of DCs to the lymph node, where they prime and become licensed by tumor specific $CD4^+$T helper cells. Licensed cDC1s by CD40-CD40L interactions then go on to prime tumor-specific $CD8^+$ T cells, aided by costimulation signals (CD28-CD80/CD86) and cytokine secretion (IL-12). *Adapted from Kurts et al. (2011)*[77].

Effective priming of T cells in the tdLN (Figure 4) requires costimulatory signals provided by the DC (CD80/86 mediated engagement of CD28 in the T cell) as well as an appropriate cytokine milieu (IL-2, IL-12). It has become increasingly clear that cDC1s must be first licensed by CD40/CD40L interactions to allow effective priming of tumor-specific $CD8^+$

T cells, as deletion of CD40 in cDC1s abrogates antitumor T cell responses[78,79]. CD40-dependent licensing is thought to be provided by CD40L expressing-$CD4^+$ T cells, conforming the historical concept of T cell help[74]. In some instances, cDC1s are indispensable for priming tumor-specific $CD4^+$ T cell responses by MHC-II dependent antigen presentation[79]. Of note, MHC-II restricted neoantigens and tumor-specific $CD4^+$ T cell responses are required for the development of efficient antitumor immunity and response to immunotherapy[80].

Following priming in the tdLN, effector T cells must then traffic to the tumor (4) guided by gradients of chemokines such as CCL5, CXCL9 or CXCL10[81] and extravasate from the circulation to the tumor bed, a process that can be hindered by a tumor-induced abnormal vasculature (5)[82]. Finally, infiltrated T cells need to recognize their cognate antigen through interactions between their TCR and tumor MHC-I molecules (6) to kill their target cell. Killing of target tumor cells causes release of additional tumor antigens, kickstarting the cancer immunity cycle once again (7).

Although here we have described a successful antitumor immune response, it is clear that in patients with overt tumor growth the cancer-immunity cycle has failed at some point. Briefly, tumor antigens may not be immunogenic enough or treated as self, T regulatory cells can overcome effector responses, or T cell homing into tumors might be precluded[83]. Most importantly, the TME can suppress the activity of correctly primed and recruited $CD8^+$ T cells[83].

As discussed before, tumor cells can escape $CD8^+$ T cell targeting by losing MHC-I expression or other components of the antigen presentation machinery. Interestingly, loss of tumor MHC-I expression, which is an inhibitory ligand for NK cells, can facilitate targeting and killing by this innate cellular subset. It is now clear that NK cells play an important role in the cancer-immunity cycle both for MHC-I sufficient and deficient tumors, as well as for the prevention of metastatic spread[84].

1.1.4 Natural Killer cells in the cancer-immunity cycle

In stark contrast to T cells, NK cell-mediated killing of tumor cells relies on an intricate balance between inhibitory and activating signals provided by target cells (Figure 5). Inhibitory receptors expressed by NK cells mostly recognize target MHC-I (HLA in

humans) molecules. Therefore, this innate cellular subset preferentially kills targets that have lost MHC-I expression, a phenomenon that has become to be known as "missing-self" recognition[85]. In humans, inhibitory receptors are encoded by the killer-cell immunoglobulin-like receptor (KIR) family of genes[86], whereas in mice seven lectin-like Ly49 receptors play a similar role[87]. Importantly, in mice and humans different inhibitory receptors recognize distinct class I molecules. An interesting aspect of NK cell biology is that inhibitory receptors are randomly distributed amongst individual NK cells in an overlapping manner[88]. Indeed, as much as 30.000 distinct NK cell phenotypes, regarding inhibitory receptor expression, have been found in individual humans[89]. Therefore, if a tumor cell loses even one class I molecule, it could be recognized by the subset of NK cells which only express the corresponding inhibitory receptor. Inhibitory signals are transduced to NK cells via immunoreceptor tyrosine-based inhibitory motifs (ITIMs) present in their cytoplasmic regions. Apart from KIRs, the NK cell CD94-NKG2A inhibitory receptor recognizes the non-classical HLA-E molecule in humans and the corresponding Qa-1 molecule in mice[90].

Regarding activating receptors, NK cells express high-affinity Fc receptors (CD16/32), which allows them to bind antibody-coated cells to trigger antibody-dependent cellular cytotoxicity and cytokine release[91]. Other examples of activating receptors include natural cytotoxicity receptors (NKp30, NKp46), some of the KIRs and Ly49 receptors and C-type lectins such as NK1.1 and NKG2D[92]. These receptors mostly recognize ligands which are preferentially expressed in stressed cells, such as virally infected or transformed cells. The most studied NK cell receptor, NKG2D, binds numerous ligands, such as MICA/B, the ULBP family, the RAE1 family members in mice, MULT1, H60 and others[93]. Adhesion molecules also play an important role in NK cell activation. For instance, NK cell expressed LFA-1 binds to ICAM-1, enhancing their cytotoxic potential by organizing the cytoskeleton to facilitate granule exocytosis. DNAM-1 (CD226) also activates NK cell migration and activation upon binding CD155, which interestingly also interacts with the inhibitory receptors TIGIT and CD96.

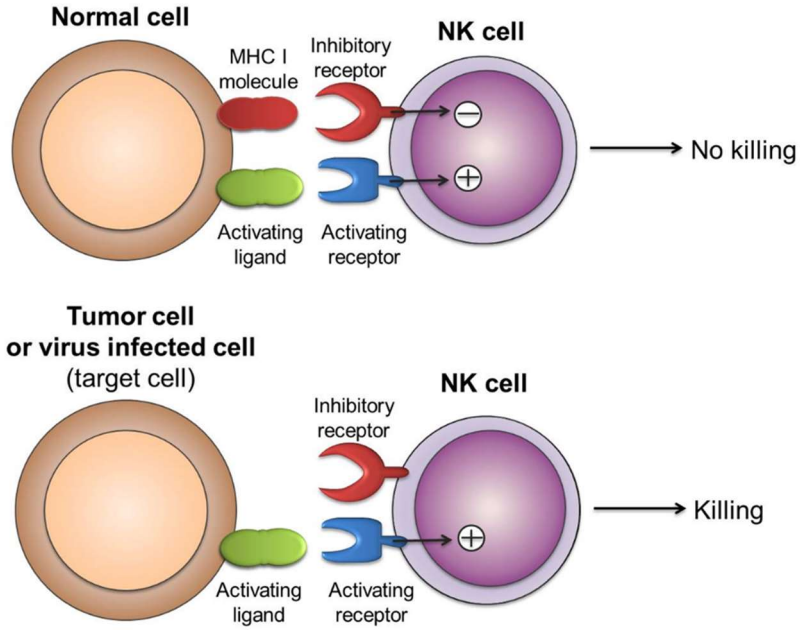

Figure 5. The cytotoxicity of NK lymphocytes towards target cells is balanced by a series of activating (e.g., MICA/B, ULBP, RAE1) and inhibitory (e.g., HLA) ligands. *Taken from*[94].

○ Natural Killer cells in the control of metastatic disease

The prominent role of NK cells in controlling metastasis has been clearly established in numerous preclinical studies, which usually rely on tail vein injection of melanoma cells or spontaneous metastasis of primary mammary carcinomas[95]. It is believed that epithelial to mesenchymal transition (EMT) in tumor cells, required for efficient metastasis to secondary organs, favours their recognition by NK cells as it entails a higher expression of activating receptors for these cells[96–98], which could explain their crucial role in preventing metastatic spread.

Evidencing their critical contribution to metastatic control, depletion of NK cells by antiNK1.1 or anti-asialoGM1 administration greatly increases tumor burden in lungs, liver and bone marrow after intravenous inoculation of tumor cells in mice[99,100]. Seminal studies showed that expression of both perforin and IFN-γ (and TRAIL in some instances) was critical for the antimetastatic activity of NK cells[101–103]. Subsequent work showed that abrogation of key steps in NK cell development and maturation, survival, activation or trafficking to tumors greatly impaired control of experimental metastasis[104–108]. In a complementary manner, boosting NK cell function confers robust protection against metastasis in multiple preclinical mouse models[105,109,110].

Whereas the role of NK cell in the control of metastatic spread and hematological malignancies is clearly stablished, their role in controlling primary solid tumors is more controversial[95]. Although some studies showed a role for NK cells in the control of MCA-induced sarcomas[111], other studies evidence that NK cell deficiency does not affect the growth of established subcutaneously transplanted tumors[112]. Importantly, NK cell infiltration into solid tumors is often very low compared to other lymphocytes[113,114], and the immunosuppressive TME exerts potent inhibitory effects on these cells[115]. Tumor cells actively employ multiple mechanisms to subvert NK cell-mediated control. A prominent example encompasses downregulation of activating ligands or inhibitory ligand upregulation, including the PD-1/PD-L1 axis, TIGIT/CD155 interactions, or ligation of shed MICA/MICB decoys by NKG2D, all of which can be therapeutically targeted for enhancing NK cell antitumor activity[116]. In a similar manner to adaptive immunity, immunosuppressive cytokines or signaling molecules such as IL-10, PGE_2 and TGF-β, regulatory immune cells like T regulatory cells, MDSCs and TAMs and an hypoxic TME have also been shown to inhibit the antitumoral activity of NK cells[116].

○ Activation and effector functions of NK cells in the TME

As discussed before, following recruitment of NK cells to the TME, relying on a complex interplay between multiple chemokines and chemokine receptors, NK cell activation is determined based on a balance between inhibitory and activating signals provided by the tumor cell. Additionally, it has become clear that type I IFN is required for optimal induction of NK cell antitumor activity, and its production requires the activation of the cGAS/STING DNA sensing pathway in tumor cells[117,118]. Chromosomic instability is a characteristic of cancer cells, and the accumulation of cytosolic DNA activates the cGAS/STING pathway which serves as an innate sensor of tumorigenesis[119]. The production of cyclic GMP-AMP (cGAMP) leads activation of STING, which can happen either in the tumor or in surrounding myeloid cells[119]. In any case, the result is the production of type I IFN, which is an activating stimulus for NK cells[117]. Evidencing the critical importance of this pathway, host STING deficiency abrogates spontaneous NK cell and T cell-mediated antitumor responses in mice[117,120]. Importantly, this pathway can be therapeutically harnessed, as administration of STING agonists potently stimulates NK cell activity via enhanced type I IFN and IL-15 expression by $CD11c^+$ myeloid cells in the

TME[121]. Proper NK cell activation also requires cytokines provided by other immune cells, with the common γ chain cytokines IL-2 and IL-15, IL-12 and IL-18 being the most prominent examples. These cytokines critically regulate NK cell proliferation, survival, maturation, and acquisition of effector function[116].

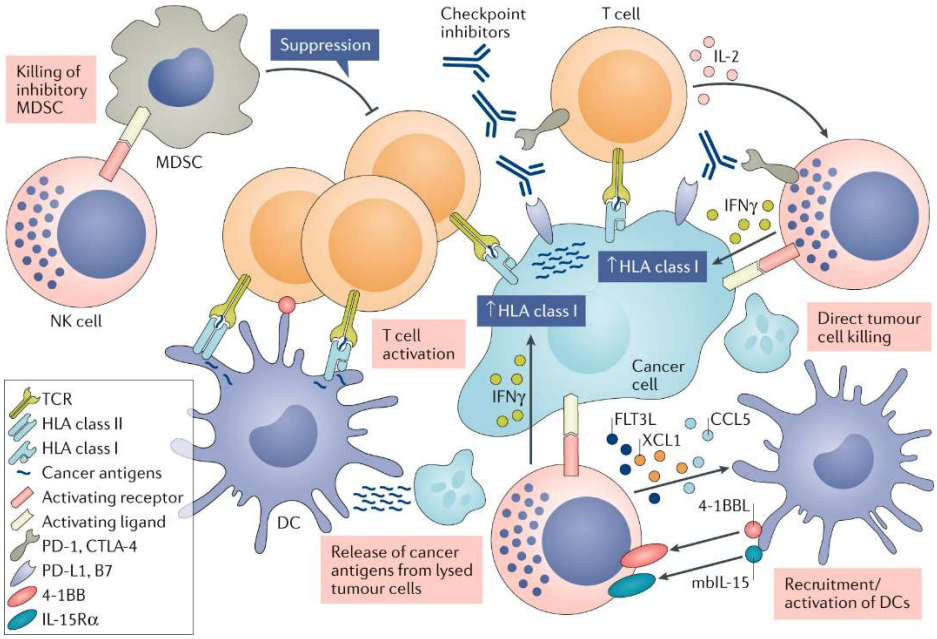

Figure 6. The complex role of NK cells in orchestrating antitumor immunity. NK cells can directly kill tumor cells, facilitating antigen uptake by dendritic cells. Dendritic Cell influence NK cell function via 4-1BBL/4-1BB or IL-15/IL-15R interactions, while NK cells recruit Dendritic Cells to the tumor bed and facilitate their survival via chemokine and growth factor secretion. Secretion of IFN-γ by NK cells can directly activate T cells and upregulate MHC-I in tumor cells, facilitating their recognition by T cells. NK cells can also be cytotoxic towards MDSCs, alleviating immune suppression in the TME. *Taken from Campana et al. (2020)*[122].

Properly activated NK cells can detect tumor cells and kill them, a process which is generally dependent on perforin and granzyme expression, but that can also rely on FASL, TRAIL or IFN-γ/TNF[123]. However, NK cell infiltration in solid tumors is generally low, raising the question whether direct cytotoxic activity is the only role that NK cells play in the cancer-immunity cycle[124]. In the recent years it has become increasingly clear that NK cells have a critical role in driving the initiation and maintenance of adaptive T cell-dependent responses. For instance, initial killing of tumor cells by NK cells provides antigens for cross-presentation and priming of T cells, and production of certain cytokines such as IFN-γ, GM-CSF, TNF or FLT3LG and chemokines (CCL5, XCL1) influences the maturation status and recruitment of cDC1s to the tumor bed[125–128]. Interestingly, NK cells

can also edit the DC compartment by killing immature DCs[129]. In summary, NK cells can exert direct cytotoxic activity towards tumor cells, modulate adaptive T cell responses and influence DC function in the TME.

1.1.5 Targeting the immune system for cancer treatment

Whereas chemotherapy, radiotherapy and oncogene-directed therapies target tumor cells to kill them or slow their growth, immunotherapeutic approaches seek to enable immune-mediated control of tumor growth. Following a series of fits and starts during the 20th century, the first immunotherapies approved by the FDA for use in cancer were the live-attenuated bacteria Bacillus Calmette-Guérin (BCG) and the immune-stimulatory cytokines IFN-α and IL-2. These first approaches evidenced that cancers could be effectively controlled by the immune system in humans, when properly activated, even achieving some durable complete responses in small subsets of patients.

Here, we will briefly review the development and mechanism of action of several types of immunotherapies for cancer treatment. Due to space constraints, immunotherapies which are most related to this thesis will be prioritized, leaving behind others such as adoptive T cell therapies, cancer vaccines or cytokines. Of note, therapeutic approaches which *a priori* were not thought to engage the immune system, such as chemotherapy, radiotherapy, or targeted therapy, have also been described to influence antitumor immunity, and in most instances require a functional immune system to be effective.

○ Innate immune stimulants

The first instances of immunotherapy can be traced back into 1900, when Robert Coley found that erysipelas infection was associated in some cases with spontaneous tumor regressions in patients. Then, he applied this observation to treat patients with mixtures of *S. pyogenes* and *S. marcescens* ("Coley's toxins") to boost antitumor immunity[130]. Although some responses were observed, the advent of radiotherapy and chemotherapy left these ideas behind[131]. During the 20th century, the antitumor properties of the tuberculosis vaccine BCG were thoroughly studied in animal models, with the idea that unspecific stimulation of the immune system could slow tumor growth. Importantly, these studies helped in shaping the concept of tumor immunology. The history of BCG and its use in human cancer will be covered in section 1.2. Today, BCG therapy is a first-line therapy for a subset of non-muscle invasive bladder cancer (NMIBC) patients. Overall, these findings

brought forward the idea that utilizing the privileged ability of microorganisms (or parts of them) to activate the innate immune system could in turn favor the development of tumor-specific responses.

Perhaps the best-known example of cancer treatment with a living microorganism is virotherapy[132]. Inside this category, the most prominent agent is T-VEC, based on a herpes simplex virus (HSV) approved by the FDA for use in a subset of melanoma patients[133]. Viral therapies can be based on replicating on non-replicating viruses. Non-replicating viruses are normally engineered to deliver toxins, immune stimulants (GM-CSF, 4-1BB, FLT3LG, IL-12…) or tumor-associated antigens into the TME[134]. On the contrary, replicating oncolytic viruses function by a combination of (1) immunogenic tumor cell death caused by selective tumor tropism of the virus and subsequent release of tumor antigens and (2) stimulation of innate immune responses via recognition of viral particles by host pattern recognition receptors (PRRs), driving T/NK cell recruitment into the TME and DC maturation[135]. Oncolytic viruses can be further engineered to express immunostimulatory cytokines such as type I IFNs or GM-CSF. This type of immunotherapy is thought to work best to ignite adaptive immune responses in cold tumors with low immunogenicity. Importantly, preclinical and human studies have shown that immune checkpoint blockade can greatly improve the efficacy of oncolytic virotherapy[136,137].

We can also include in this section the administration of innate immune receptor agonists, such as TLR or STING ligands, since their mechanism of action is somewhat related to the administration of live microorganisms[138]. A clear difference between them is that innate immune stimulants can be synthesized to target specific pathways, and the safety concerns of administrating a living organism are eliminated. However, these therapies are not completely devoid of side-effects, and administration of live organisms can conceivably achieve the activation of multiple innate immune pathways at once in a more physiological manner which is reminiscent of their natural role in detecting microbial infection.

The main idea behind the use of innate immune stimulants agonists is the activation of innate immune pathways that are critical for the optimal development adaptive immune responses, and which are normally supressed at the tumor site[139].

Generally, following their recognition by pattern recognition receptors (PRRs), innate immune receptor agonists trigger the release of type I IFN, induce the maturation of DCs and elicit proinflammatory cytokine release by TAMs. In some instances, TLR3 agonists such as PolyI:C or its derivative BO-112 can directly trigger tumor cell death, providing tumor antigens to DCs[140,141], whereas administration of STING agonists, such as cyclic dinucleotides, rely on type I IFN production by tumor cells, DCs and macrophages, triggering NK cell-mediated cytotoxicity[119,121,142,143]. Contrary to simulation of the STING pathway, agonists of the RNA sensing protein RIG-I, such as 5'-triphosphorilated RNA, rely on triggering cell death in tumor cells, which augments the availability of tumor antigen with the subsequent boost in $CD8^+$ T cell responses[144,145]. Therefore, PRRs and pathways which physiologically serve to detect invading pathogens and/or cell intrinsic damage, can be hijacked to stimulate antitumor immunity.

Another important example in this category is the topical administration of imiquimod, a TLR7 agonist, for cutaneous malignancies. In mice, the efficacy of imiquimod therapy was shown to rely on NK cell and $CD4^+$ T cell recruitment and activation at the tumor site[146]. An improved version of LPS, a TLR4 agonist, was shown to activate TAMs and drive improved T cell-mediated antitumor responses in mouse models of breast cancer[147]. Finally, and among many others, CpG oligodeoxynucleotides, which are TLR9 agonists, are currently in clinical trials for several types of cancer[148].

In summary, results from preclinical studies involving the use of innate immune receptor agonists have evidenced their unique potential to engage innate immunity to drive tumor antigen-specific responses and tumor growth control. The hurdles that these types of therapies face for translation into the clinical are mostly related to safety and side effects, particularly in the case of live virus or bacteria-based treatments. It has become evident that efficacy of TLR/STING/RIG-I agonists is usually highest when delivered intratumorally[149,150], which can be done for some tumor types (melanoma, bladder, brain) but could be hard to implement for others (lung, pancreas, ovarian). Additionally, the persistence of these agents in the body is generally low, so multiple administrations are usually needed for achieving an antitumoral effect.

Immune checkpoint blockade

Work by Jim Allison's group in the 1990s revealed that a protein known as cytotoxic T lymphocyte antigen-4 (CTLA-4) negatively regulated T cells, functioning as a physiological "brake" to avoid the generation of autoimmune responses[151,152]. Mechanistically, following T cells activation CTLA-4 is expressed in the cell surface, where it outcompetes CD28 in binding to the costimulatory molecules CD80 and CD86 and delivers an inhibitory signal to the T cell, precluding its proliferation and activation. Allison devised that blocking the CTLA-4 axis could bypass this control mechanism and allow supraphysiological activation of T cells. Indeed, blocking CTLA-4 with a monoclonal antibody led to rejection of transplanted tumors in several mouse models[152]. In subsequent years, this therapeutic strategy moved to the clinic and is nowadays approved for the treatment of advanced melanoma.

The other example of successful immunotherapy targeting an immune checkpoint is the administration of antibodies targeting either side of the PD-1/PD-L1 axis. Expression of the cell surface receptor Programmed Cell Death 1 (PD-1) is induced in T cells following their activation, and upon binding its cognate ligand PD-L1, generates intracellular signalling events which drive reduced production of effector cytokines (IL-2, IFN-γ, TNF), reduced ability to proliferate and increased proclivity to undergo cell death. In contrast to CTLA-4, PD-1 ligation regulates signalling downstream of the TCR to attenuate the activity of T cells[153].

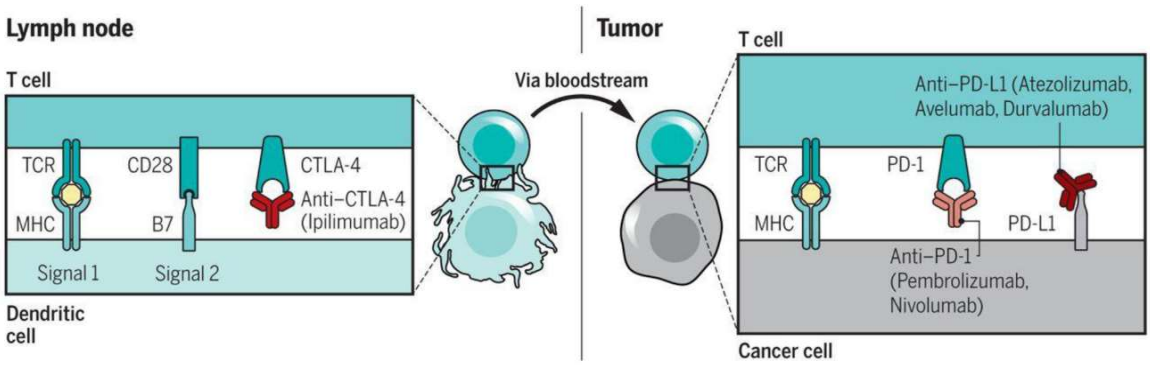

Figure 7. Mode of action of CTLA-4 and PD-1/PD-L1 blocking antibodies. Whereas CTLA-4 blocking antibodies avoid the CTLA-4/B7 interaction allowing CD28-B7 costimulation, PD-1 or PD-L1 blocking antibodies avoid PD-1/PD-L1 interactions. *Taken from Ribas et al. (2018).*[154]

As with CTLA-4, PD-1 receptor signalling functions physiologically to maintain peripheral tolerance and avoid immunopathology. Indeed, mice lacking PD-1 are prone to develop autoimmune disorders and suffer from exacerbated inflammation during infection. The PD-1 ligand, PD-L1, is expressed by many cells and is mainly upregulated in response to pro-inflammatory cytokines.

Upon recognition of their cognate antigen presented in MHC molecule by tumor cells, T cells release proinflammatory cytokines, such as IFN-γ. As explained before, IFN-γ drives upregulation of the antigen presentation machinery in tumor cells, facilitating recognition by $CD8^+$ T cells. However, IFN-γ is the strongest stimulator of reactive PD-L1 expression by tumor cells and by surrounding myeloid cells[155]. Therefore, chronic antigen stimulation of T cells results in upregulated PD-L1 in the TME, and chronic PD-1 signalling in T cells drives an epigenetically regulated program of exhaustion[156]. Several studies have suggested that PD-L1 expressed by host myeloid cells in the TME is primarily responsible for driving $CD8^+$ T cell exhaustion, and not PD-L1 expressed by the tumor cells themselves, as was previously hypothesized[157–160]. Indeed, the antitumoral effect of PD-1/PD-L1 axis blockade in transplanted tumors in mice was phenocopied by genetic deletion of PD-L1 specifically on DCs, and not on macrophages or tumor cells, underscoring the importance of this cellular subset in driving T cell exhaustion[160].

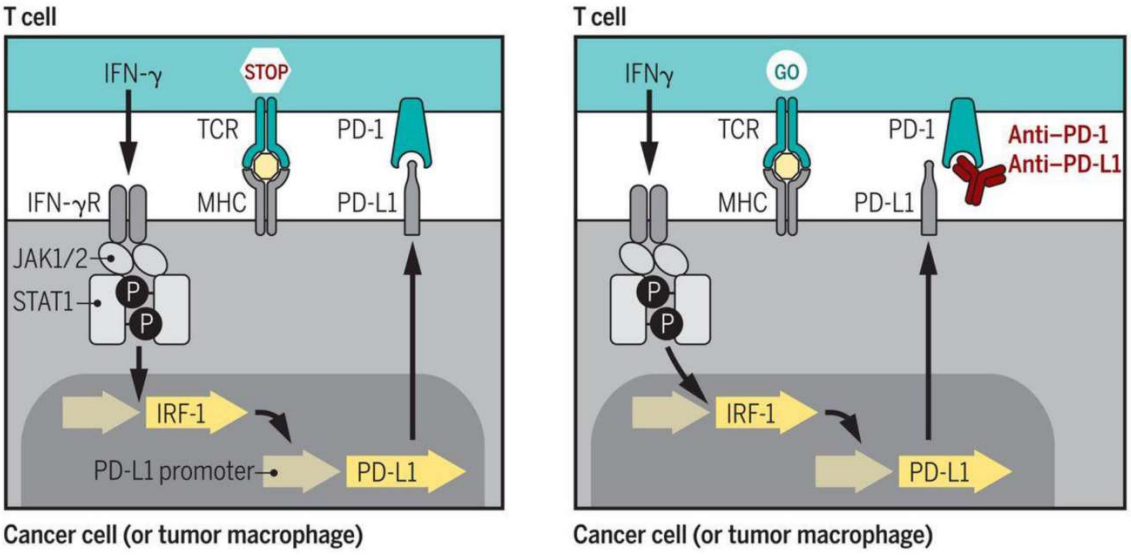

Figure 8. Mode of action of PD-1/PD-L1 checkpoint blockade. An ongoing antitumor response is characterized by IFN-γ production by tumor infiltrating lymphocytes. IFN-γ signals through its receptor un JAK1/2-STAT1 pathway, driving the expression of PD-L1 on the membrane of tumor cells or macrophages. Membrane-bound PD-L1 interacts with PD-1 on lymphocytes, interfering in

their activation. Blocking this interaction allows correct activation and antitumor function of T lymphocytes. *Taken from Ribas et al. (2018).*[154]

Mechanistically, PD-1/PD-L1 axis blockade with monoclonal antibodies is thought to drive tumor rejection by reinvigorating and restoring the activity of exhausted $CD8^+$ T cells[161]. However, the population of exhausted T cells is highly heterogeneous[162], and it has been proposed that a small population termed as "precursor-exhausted" $CD8^+$ T cells, which express TCF1, are the ones responsible for the proliferative burst following PD-1/PD-L1 blockade which generates effector T cells and drives tumor rejection[163]. Interestingly, a recent article posed that PD-1/PD-L1 blockade does not reinvigorate $CD8^+$ T cells in the TME, but instead favors the differentiation of tumor-specific T cell populations in the tumor draining LNs characterized by canonical memory characteristics and that undergoes proliferation and infiltration into the tumor upon therapeutic blockade of this axis[164]. Indeed, this study builds on several works which have demosntrated that the draining LNs are a critical reservoir of $CD8^+$ T cells which mediate responses to therapeutic PD-1/PD-L1 blockade[165–167].

Intriguingly, other targets of PD-1/PD-L1 blockade besides T cells have been described. For instance, PD-1 expression in macrophages restrains their ability to ingest tumor cells by phagocytosis. In turn, therapeutic blockade of PD-1 facilitated tumor cell phagocytosis by macrophages and slowed tumor growth in mouse models[168]. Another study revealed that tumor-driven PD-1 expression by myeloid progenitors and mature myeloid cells triggers an immunosuppressive state on these cells, dampening antitumor immunity. Upon genetic deletion of PD-1 specifically on the myeloid lineage, accumulation of MDSCs was prevented[169]. Lastly, the effect of blocking the PD-1/PD-L1 axis on NK cell function is controversial, since some groups have observed almost negligible PD-1 expression in intratumoral NK cells[114,170], while others have shown that PD-1 is expressed on the NK cell surface upon release of cytotoxic granules[171], or that blocking PD-1 induces antitumor immunity dependent on NK cells[172,173]. Nonetheless, PD-1/PD-L1 blockade could conceivably influence NK cell function indirectly through T cell or macrophage derived cytokines.

Although its precise mechanism of action is still being figured, blockade of the PD-1/PD-L1 axis with monoclonal antibodies such as Nivolumab, Pembrolizumab or Atezolizumab

is used nowadays in the clinic in a wide array of tumors as diverse as refractory melanoma, advanced non-small cell lung carcinoma (NSCLC), Merkel cell carcinoma, urothelial carcinomas, renal cell carcinoma, hepatocarcinoma and microsatellite-unstable cancers of any origin[154]. In the recent years, a great interest is arising in the rational combination of checkpoint blockade immunotherapies with other modalities such as TLR/STING agonists, radiotherapy, chemotherapy, and oncogene-targeted therapies in an attempt to boost therapeutic responses[154].

○ Targeting immunosuppressive tumor-associated macrophages

In the recent years it has become apparent that NK and T cell function is greatly hampered in the TME. First, physical barriers preclude the infiltration of lymphocytes into the tumor. Indeed, structures such as dense layers of fibroblasts and/or abnormal extracellular matrix formation can trap immune cells and prevent them to reach their targets. Furthermore, a hypoxic environment or metabolic restrictions imposed by the growing tumor mass negatively also negatively influence antitumor immunity. Although these factors undoubtedly have a critical effect on antitumor immune responses and can be therapeutically targeted, in this section we will focus on therapies that target immunosuppressive mechanisms driven by immune cells themselves, particularly tumor-associated macrophages (TAMs).

Macrophages are often the most abundant immune cell type in the TME, and historically there has been a great enthusiasm in therapeutically modulating their activity to enable effective antitumor immune responses[174]. Tumor-associated macrophages can exert both antitumor and protumor roles in the TME (Figure 9)[175]. Until now, antitumor macrophages have generally been classified as “M1” or immunostimulatory macrophages, while protumor macrophages have been coined “M2”, alternatively activated, anti-inflammatory or tissue-remodeling macrophages. In the recent years it has become clear that this classification oversimplifies the heterogeneity of the TAM population, which most likely exists in a spectrum between the archetypic M1 and M2 extremes[176]. Further complicating TAM biology, they can arise both from recruited BM derived monocytes or from tissue resident populations of embryonic origin and play different roles during tumor progression[177]. Importantly, both BM-derived macrophages and tissue-resident populations have the capacity to exert antitumor roles. Briefly, TAMs can directly kill tumor cells via

TNF or nitric oxide (NO), ingest tumor cells by phagocytosis, present antigens to T cells and secrete NK and T cell stimulatory cytokines such as IL-12[178]. However, their protumor roles include production of tissue invasive and angiogenic mediators, the secretion of tumor growth factors, or inhibition of innate and adaptive immunity via production of immunosuppressive molecules such as IL-10, TGF-β or PGE_2[178].

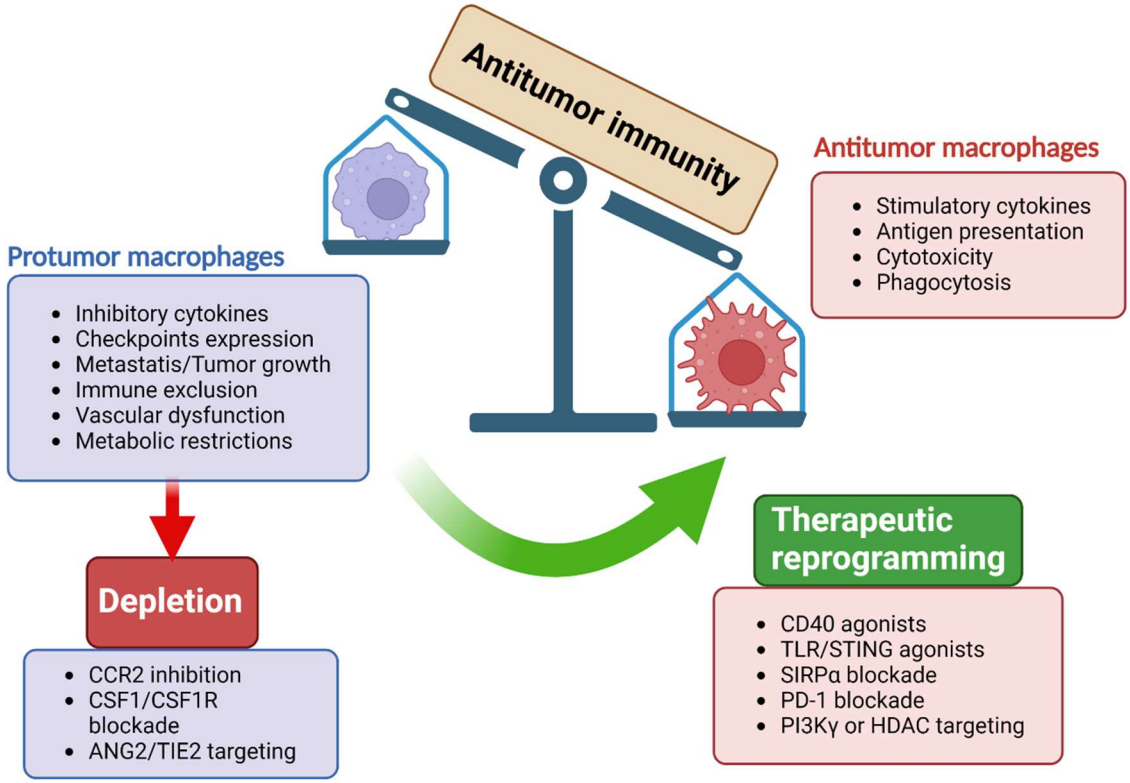

Figure 9. Dual role of TAMs in antitumor immunity and therapeutic targets. *Created with BioRender.com.*

TAM-directed therapeutic strategies can be divided into those aimed at reducing their numbers in the tumor and those that reprogram them into an antitumor phenotype (Figure 9)[179].

Normally, TAMs are polarized into an immunosuppressive phenotype in the TME by tumor and immune cell derived factors[180,181]. Therefore, depletion of TAMs can be harnessed to unleash efficient antitumor immunity which was otherwise blocked by this population. For instance, since an important fraction of TAMs arises from circulating inflammatory monocytes, blocking CCL2/CCR2 signalling responsible for monocyte recruitment readily reduces TAM numbers in tumors[182–184]. This strategy has been shown to enhance the therapeutic effect of radiotherapy, chemotherapy, and immunotherapy in preclinical models

by multiple studies, and clinical trials are ongoing[185]. Importantly, a biomarker study of a clinical trial involving this approach reported that CCL2/CCR2 inhibition facilitated T cell infiltration into the tissue. An important limitation of this strategy is that it cannot target TAMs already residing in the tumor, or those arising from tissue-resident populations. Another option is targeting macrophage survival factors, such as the CSF-1/CSF1R axis to eliminate this population. Inhibition of CSF-1/CSF1R signalling drives TAM depletion in most preclinical models[186–188], although in the case of glioma its therapeutic activity was associated with repolarization of the TAM population[189–191]. Regardless of the mechanism of action, CSF1R inhibition has been shown to facilitate antitumor T cell responses in many preclinical models, mostly when combined with radiotherapy, chemotherapy, immune checkpoint blockade or antiCD40 agonistic antibodies, and clinical trials are ongoing testing these approximations[192,193].

An important caveat of blocking macrophage recruitment or survival is that their potential immunostimulatory roles as a professional phagocyte and antigen presenting cell are lost. Therefore, efforts are being made to find ways to repolarize this population into an antitumoral "defender" phenotype to sustain immune surveillance against cancer[64]. In preclinical models, TAMs can be polarized into an "M1" antitumor phenotype by various TLR or STING agonists, especially when combined with IFN-γ[194–196]. Another relevant example the use of CD40 agonistic antibodies, which strongly stimulate the antitumor function of macrophages[197,198], although this surface molecule is not macrophage specific since DCs and B cells also express it and respond to this therapeutic approach[199,200]. Nonetheless, CD40 agonism synergizes with chemotherapy and immune checkpoint blockade by unleashing potent T cell-dependent antitumor responses in preclinical models and is expected to be tested in the clinic[201–203]. Interestingly, intravesical administration of CD40 agonistic antibodies demonstrated therapeutic effect as a monotherapy in several mouse models of bladder cancer. In this case, efficacy of CD40 agonism was attributed to stimulation of cDC1s and not macrophages[204].

Other promising therapeutic approaches that target TAM biology and are currently being investigated include the blockade of CD47, which interacts with SIRPα expressed on macrophages inhibiting efficient phagocytosis of tumor cells[205,206], the epigenetic reprogramming of TAMs by inhibiting histone deacetylases (HDAC)[207], or targeting the

PI3Kγ pathway, which is activated in TAMs and is a master regulator of their immunosuppressive activities[208].

1.2 BCG as an immunostimulatory agent

The discovery of the antitumor properties of mycobacteria can be traced back to the 20th century. In 1929, Robert Pearl reported a lower incidence of cancer in patients dying of tuberculosis, while cancer survivors presented a higher incidence of active or latent tuberculosis than those dying of cancer[209,210]. Although he did not manage to explain these findings at the time, a link between mycobacterial infection and cancer was established for the first time. In this chapter I will first describe the development of BCG as a tuberculosis vaccine, followed by the application of BCG immunostimulatory properties to cancer treatment and the recently described ability of BCG to train innate immune responses and confer non-specific protection against diseases other than tuberculosis.

1.2.1 BCG as a tuberculosis vaccine

The BCG vaccine was obtained in 1921 by Albert Calmette and Camille Guérin at the Pasteur Institute in Lille, following the isolation of a virulent *Mycobacterium bovis* strain from a cow with tubercular mastitis. This virulent strain was passaged 231 times along 13 years in a medium containing cow bile, glycerin and potatoes. During the subcultivation process, Calmette and Guérin observed a gradual loss of virulence in guinea pigs and in calves. Finally, experiments using guinea pigs revealed that following 231 passages, the bacterium had lost it virulence and was protective against tuberculosis infection in a guinea pig model. This live-attenuated strain became to be known as bacillus Calmette-Guérin, or BCG[211].

Given its initial success, BCG was subsequently distributed all over the world. Importantly, cryopreservation of glycerol stocks was not stablished until 1960. Before then, BCG was kept by serial subcultivation, which entailed the appearance of multiple substrains (Figure 10)[212,213]. Of note, BCG strains used in this thesis are comprised in the Group IV, namely BCG Tice, BCG Connaught, and the BCG Pasteur reference strain 1173 P2.

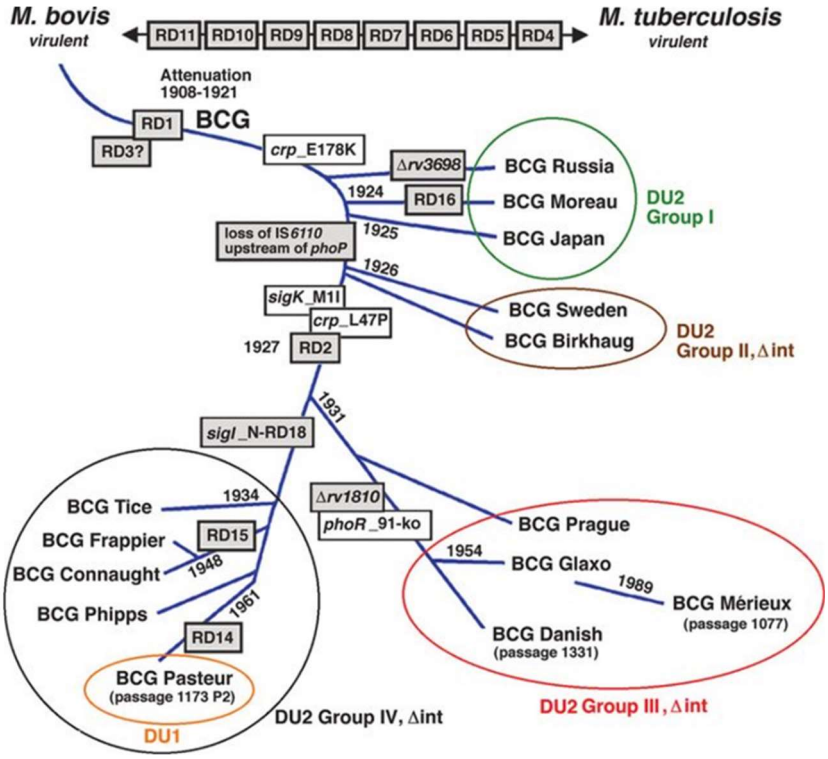

Figure 10. Genealogy of BCG vaccines, showing genetic regions of difference (RD) with reference to *M. tuberculosis*. *Taken from Brosch et al. 2007*[212].

It is now well established that BCG confers an 80 % degree of protection against disseminated forms (miliary and meningeal) of tuberculosis in young children[214]. On the contrary, protection against pulmonary disease in adults is still debated and efficacy ranges from as low to 0 % to 70 %, depending on the study[215]. These differences had been ascribed to race of vaccinees, geographical location and previous exposure to other mycobacteria or the strain, dose and route of administration used in the studies, although causes are not currently completely clear[216].

In this line, although WHO recommends the intradermal route for vaccination, recent studies have shown that alternative routes, such as mucosal (intranasal or aerosolized) or systemic (intravenous), are far superior at preventing *M. tuberculosis* infection than the intradermal in mouse and macaque models due to superior simulation of lung-specific immune protective mechanisms[217,218]. Additionally, BCG vaccination given at birth confers non-specific protection against other causes of mortality not related to tuberculosis, raising the question whether the protection that BCG vaccination confers against *M. tuberculosis*

infection relies on the induction of antigen-specific T cell responses or on stimulation of innate immune cells such as monocytes, neutrophils, macrophages, or NK cells[219,220].

1.2.2 Antitumoral properties of BCG

The spread of Coley's work, the worldwide distribution of BCG and the increasing interest in the study of transplant and tumor immunology using inbred mice strains allowed the investigation of BCG as a potential cancer therapy as early as in 1950. Here I will outline the two bodies of work which lead to the evaluation of BCG as an anti-cancer agent in multiple clinical trials, with the resulting approval of intravesical BCG for the prevention of recurrence and progression of non-muscle invasive bladder cancer (NMIBC) in 1990.

- Systemic infection with BCG leads to resistance to transplanted tumors in mice

In a seminal study from 1959[221], Lloyd Old *et al.* applied previous observations reporting that endotoxins, zymosan or BCG infection enhanced the activity of the reticulo-endothelial system, which today we know as macrophages, in the host. They hypothesized that since the reticulo-endothelial system was present and altered in transplanted tumors, stimulating its phagocytic function could prevent tumor growth. To test this idea, he inoculated mice with 1 mg of BCG by the intravenous route, and subsequently transplanted mice with different tumor cell lines.

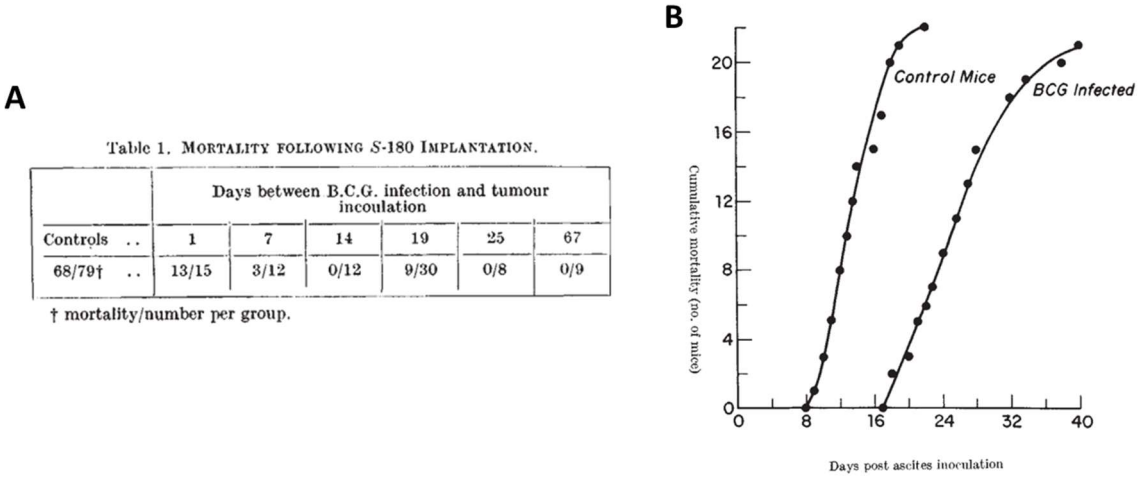

Figure 11. (A) Intradermal S-180 tumor growth inhibition in Swiss mice previously infected with BCG. Data shows the proportion of mice succumbing due to tumor burden. (B) Cumulative mortality following intraperitoneal Ehrlich ascites tumor inoculation in Swiss mice infected or not with BCG 17 days prior to tumor challenge. Adapted from *Old et al. 1959*[221].

As seen in Figure 11A, transplanted S-180 tumors progressed normally in 68 out of 79 control non-infected Swiss mice, and when tumors were inoculated one day after BCG infection, no differences were observed. However, when tumors were grafted 7, 14, 19, 25 or 67 days after BCG inoculation, mice were almost completely resistant to tumor growth. Importantly, Old observed that, in protected mice, tumors grew for the first 7-14 days and then quickly regressed, meaning that protection was not due to an inability of the tumor cells to initially form a growing tumor mass, suggesting a delayed action of (immune) cells stimulated by BCG infection. Old tested this approximation in a different tumor model, consisting in the intraperitoneal inoculation of Ehrlich ascites tumor in Swiss mice. As seen in Figure 11B, BCG-infected mice were also significantly protected from tumor growth compared to controls[222].

In the following years, Old hypothesized that BCG antitumor activity was indirect and mediated by the host immunological system, and not due to direct cytotoxic activity on tumor cells. Indeed, BCG and LPS were found to exert potent effects on macrophages, stimulating their phagocytic and bactericidal abilities, and at that time it was known that macrophages could directly kill cancer cells by production of oxygen intermediates[223]. Subsequent work by Old *et al.* revealed that inoculation of microbial agents such as BCG, zymosan, LPS or *C. parvum* triggered the appearance of a tumor cytotoxic agent in the serum of mice, which became known as tumor necrosis factor, or TNF[224,225]. Altogether, Old's work provided first-time solid evidence that BCG could be harnessed for cancer treatment.

- Local administration of BCG

Lloyd Old's work relied on systemic inoculation of BCG, while intravesical BCG treatment for bladder cancer relies nowadays on local administration of the vaccine. Alvaro Morales established BCG therapy for bladder cancer in 1976[226], and his idea was inspired by Burton Zbar's works conducted in the previous decade.

Zbar and colleagues worked with transplanted tumors in guinea pigs and studied whether the co-injection of BCG and tumor cells at the same time, or the inoculation of BCG into established tumors could restrain tumor growth. Importantly, tumor growth inhibition was only observed when BCG was injected directly into the tumor and in an adequate dose (Figure 12A). In Figure 12B, tumor growth follow-up in guinea pigs is depicted after

intratumoral injection of BCG at day 7. Interestingly, BCG injected tumors grew quicker than controls for the first week and then progressively regressed. Of note, excision of the primary tumor, a transplanted carcinogen-induced hepatocarcinoma, did not prevent the appearance of palpable lymph node metastases, while intratumoral BCG treatment prevented it in 2 out of 8 animals tested (Figure 12A)[227]. Although not considered at the time, this could very well be due to the fact that local BCG treatment was capable of inducing systemic tumor-specific T cell memory responses, precluding metastatic spread of tumor cells. This important study showed for the first time that established palpable tumors could be controlled by inducing an immune response against antigens unrelated to the tumor. Of important note, the antitumor effect of BCG was attributed by Zbar and colleagues to a host immune response (termed by them a delayed hypersensitivity type immunological response), since *in vitro* experiments discarded cytotoxic effects of BCG towards tumor cell lines[228,229].

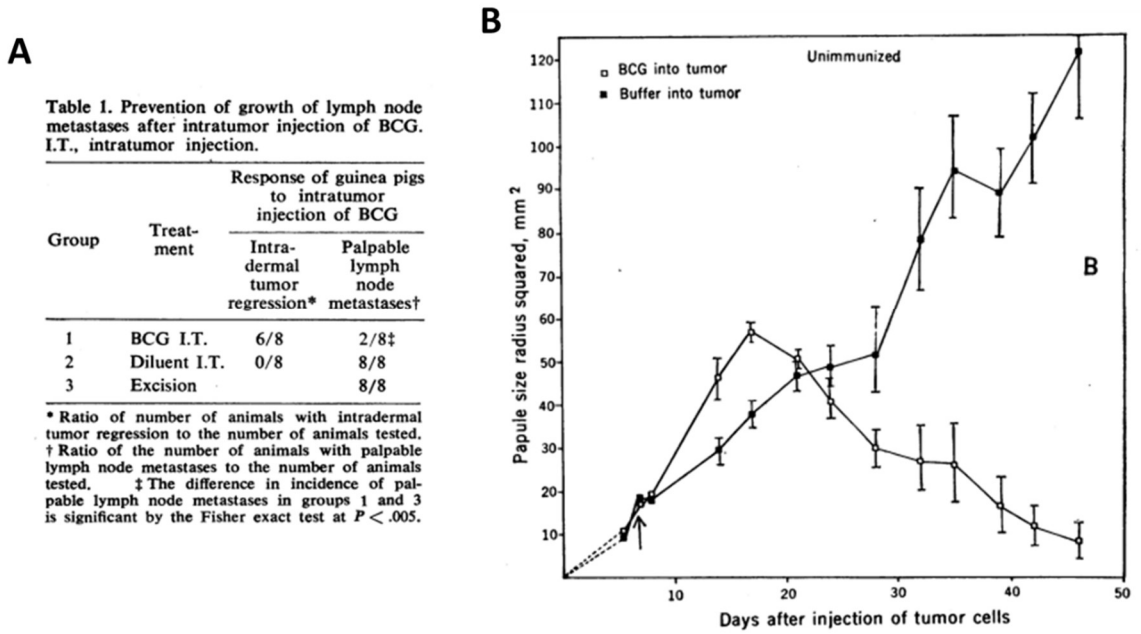
A

Table 1. Prevention of growth of lymph node metastases after intratumor injection of BCG. I.T., intratumor injection.

Group	Treatment	Response of guinea pigs to intratumor injection of BCG	
		Intradermal tumor regression*	Palpable lymph node metastases†
1	BCG I.T.	6/8	2/8‡
2	Diluent I.T.	0/8	8/8
3	Excision		8/8

* Ratio of number of animals with intradermal tumor regression to the number of animals tested. † Ratio of the number of animals with palpable lymph node metastases to the number of animals tested. ‡ The difference in incidence of palpable lymph node metastases in groups 1 and 3 is significant by the Fisher exact test at $P < .005$.

Figure 12. Tumor growth inhibition in guinea pigs following intratumoral BCG injection (10^7 CFUs). (A) Guinea pigs inoculated intradermally with 10^6 cells of ascites tumor cell line 10 were treated with BCG or diluent intratumorally, or the primary tumor was excised. Results show the proportion of guinea pigs undergoing primary tumor regression and the proportion of mice developing palpable lymph node metastases. In (B), follow-up of tumor growth of guinea pigs treated intratumorally with BCG or diluent is shown. *Adapted from Zbar et al. (1971)*[227].

Following this experimental work with transplanted tumors in guinea pigs, Zbar and colleagues established four criteria required for successful BCG therapy[230,231]:

1. An immunocompetent host
2. Low tumor burden
3. Close contact between tumor cells and BCG
4. An adequate dose of live BCG

Importantly, these criteria were referred by Morales for the establishment of BCG therapy for bladder cancer and laid the foundations of this type of treatment[226,232]. However, although BCG has only found success for the treatment of bladder cancer in humans, its use against other types of cancer was tested in numerous clinical trials in the 1970-80 decades[233].

- First clinical trials using BCG in humans

Clinical use of BCG as a cancer immunotherapy started in 1969, when Mathé *et al.* found that chemotherapy-induced remissions in acute lymphoblastic leukaemia were prolonged by percutaneous BCG adjuvant treatment[234]. At the same time, in the United States, Morton *et al.* observed regression of metastatic melanoma in 5 out of 8 patients treated with intratumoral BCG[235], and in 1975 he reported successful treatment of a bladder cancer patient following transurethral intralesional injection of BCG[236]. These successful reports in humans, coupled with the work that Zbar and colleagues were conducting in animal models at the time, ignited interest in the use of BCG as an anticancer therapy. In the subsequent years, BCG therapy was used in clinical trials against melanoma, lung, prostate, colon, kidney and bladder cancers.

In the case of lung cancer, intrapleural and intradermal injection of BCG were used, mostly as an adjuvant in small cell lung cancer patients (SCLC) following curative chemotherapy and/or radiation. Generally, results obtained were poor[237–239], which could be ascribed to the fact that intrapleural or intradermal administration cannot reliably achieve close contact between BCG and the tumor, which is needed for effective treatment, at least considering Zbar's preclinical studies and its success in bladder cancer and melanoma. Surprisingly, a recent 60-year follow-up study revealed lower incidence of lung cancer in American Indian and Alaska Native populations receiving intradermal BCG vaccination at birth[240], although mechanisms behind this finding are unknown and probably are not related to the use of BCG in a therapeutic setting. This is not the only report of BCG's ability to prevent cancer development in humans, since in 1970 work by Rosenthal[241] and Davignon[242] separately

evidenced that the incidence of acute leukaemia was reduced in individuals which had received BCG vaccination at birth.

BCG therapy was also studied for prostate cancer in several clinical trials around 1980, administered either intraprostatic or intradermally. Overall, results were modest[243,244], although a study reported that adjuvant intradermal BCG prolonged the survival of advanced prostate cancer patients undergoing conventional chemotherapy or estrogen therapy[245]. Despite these results, use of BCG in prostate cancer was discontinued in the following years.

Besides bladder cancer, the only other tumor in which BCG has been successfully applied leading to recommendation by health authorities is melanoma, concretely for stage III inoperable subtypes, although currently it is not a first-line treatment[246]. The success found with BCG in melanoma could be explained by the ease of performing intratumoral BCG injections, considering Zbar's guidelines for successful BCG therapy. Intralesional BCG therapy started in the early 1970s, with a series of clinical trials that demonstrated regressions in 15%–20% of treated patents[247,248]. In 1993, pooled analysis of 15 different clinical trials found that intralesional BCG resulted in complete responses in 19% and extended survival in 13% of stage III melanoma patients[249]. Recent studies have examined intralesional BCG combinated with the topical TLR7 agonist imiquimod, achieving a high proportion of tumor regressions across two studies[250,251], or with the immune-checkpoint inhibitor ipilimumab[252].

Lastly, as already mentioned, adjuvant intravesical BCG treatment of superficial bladder tumors, following endoscopic eradication of the tumor was developed by Morales *et al*. in 1976. BCG adjuvant therapy in this first study prevented the recurrence of superficial bladder tumors, which frequently appeared following initial resection of the tumor, in the seven patients tested[226]. Indeed, intravesical inoculation of a solution containing BCG into the bladder represented a unique opportunity, since no other cancer allowed the possibility to locally administer BCG into the tumor, to maintain BCG for a fixed time period at the tumor site and then to be released by urinating. Keeping in mind Zbar criteria for successful BCG therapy, it is not surprising that it is in bladder tumors where BCG has found the highest success across all cancer types studied. Today, almost 50 years later, adjuvant BCG immunotherapy is still the front-line treatment in NMIBC patients to delay recurrence and

disease progression. The use of BCG in bladder cancer will be further developed in section 1.3.

1.2.3 BCG-induced trained immunity

In the last two centuries, vaccines have represented one of the most significant public health interventions, reducing child mortality and morbidity due to protection against the specific pathogen targeted by the vaccine. The most notable examples include the smallpox, BCG, the polio, and measles vaccines. It is now clear that protection conferred by vaccines can be primarily attributed to the generation of immunological memory against antigens present in the pathogen. However, in the recent years it has become increasingly studied that vaccines, and especially live vaccines given at birth, confer protection against all-cause mortality that goes beyond protection against their respective target pathogen[253]. For instance, epidemiological studies have shown that vaccination with BCG, measles or oral polio vaccines reduce all-cause mortality independently of their efficacy against measles polio or tuberculosis disease. The heterologous effects that vaccines confer against unrelated pathogens, against tumor growth or against all-cause child mortality have been termed "off-target" or non-specific effects[254].

Non-specific or heterologous effects have been primarily described with live vaccines, and one of the most studied examples has been BCG, due to its widespread use worldwide as a vaccine against tuberculosis. In a pioneer study in Guinea-Bissau, BCG administration at birth reduced mortality rate by 40 % in the first month following vaccination[255,256]. In Spain, an epidemiological study reported a 70 % decrease in hospitalization due to respiratory infections not related to tuberculosis in 10–14-year-old children who had received BCG at birth, compared to those who did not[257,258]. Importantly, these observations have been replicated across several studies and locations and are not restricted to resource poor settings or to children. Indeed, in a recent clinical trial in which elderly patients were vaccinated with BCG, the incidence of respiratory tract viral infections was significantly lower in the vaccinated group.

Mechanistically, the fact that a vaccine designed to target a specific pathogen influences the host immune response against subsequent unrelated challenges has been explained either by the induction of heterologous lymphocyte responses or by the generation of innate immune memory through metabolic changes and epigenetic modifications[254].

In the last decade, it has been thoroughly demonstrated that the ability to respond to a secondary challenge quicker and stronger (i.e., immunological memory) is not circumscribed to the adaptive branch of the immune system but can also be observed in innate immune cells[253]. Innate immune memory, or trained immunity, refers to a mechanism of long-term adaptation of innate immune cells leading to altered (either stronger or weaker) responses to a secondary stimulus (Figure 13). Importantly, different innate immune system stimuli (e.g., BCG, β-glucan, LPS) can lead to distinct trained immunity programmes (Figure 13)[259]. It is generally believed that training of the innate immune system is mediated by metabolically driven epigenetic reprogramming of transcriptional pathways in innate immune cells, which can lead to easier access and more efficient transcription of genes involved in innate immune responses such as proinflammatory cytokines[259].

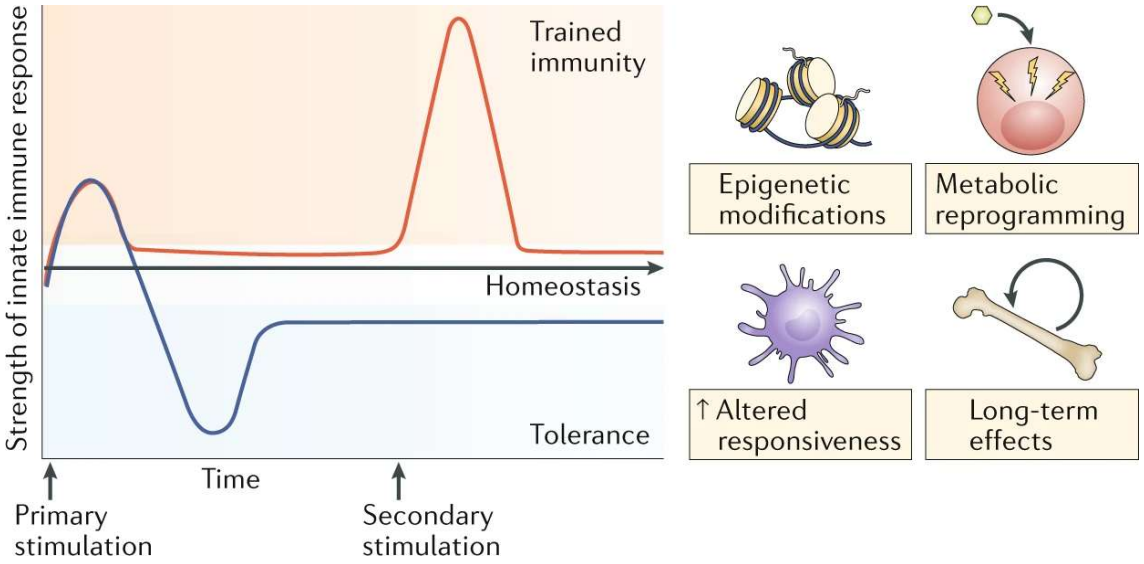

Figure 13. Innate immune memory refers to the ability of the innate immune system to, following a primary challenge and subsequent return to baseline, mount a weaker (tolerance) or stronger (trained immunity) "modified" response to a secondary stimulus. Trained immunity involves metabolic reprogramming of innate immune effectors as well as epigenetic modifications leading to altered transcription of genes involved in the inflammatory response. *Taken from Netea et al., (2020)*[254].

Although initially trained immunity was thought to happen in circulating myeloid cells, this hypothesis met with the problem that mature myeloid cells, such as monocytes or neutrophils, are very short-lived in humans and mice (about 1 week for monocytes and less for neutrophils). Therefore, to explain that trained immunity could be maintained in humans

and mice for longer periods of times, ranging from months to years, it became apparent that immune cell progenitors in the bone marrow should be involved, and this has been experimentally demonstrated in the recent years[254]. Indeed, β-glucan or BCG can train bone marrow myeloid progenitors[260–262], leading to the generation of mature myeloid cells with enhanced responses to subsequent challenges. Additionally, tissue-resident immune cells, such as alveolar macrophages, can also present traits of trained immunity after bacterial or viral challenges[263,264], as well as NK cells[265] or non-immune cells such as stromal or epithelial cells[259,266].

The ability of BCG vaccination to confer resistance to infection by unrelated pathogens has been thoroughly studied in animal models and observed in human studies[267–270]. Moreover, the resistance that intravenous inoculation of BCG confers against tuberculosis infection was ascribed to training of hematopoietic myeloid progenitors in the bone marrow, which lead to the generation of macrophages which more effectively restricted *M. tuberculosis* growth. Importantly, this was not observed when BCG was administered subcutaneously, and functioned by a mechanism dependent on IFN-γ[260]. More recently, intravenous BCG was found to be far superior to other administration routes such as intradermal or aerosolized at preventing tuberculosis infection in a rhesus macaque model, although this was not solely ascribed to the induction of trained immunity[218].

As described in previous sections, myeloid cells are driven into a dysfunctional state in the TME and acquire potent immunosuppressive traits. At least hypothetically, therapeutic training of innate immune cells and/or progenitors could change the ways in which myeloid cells respond to tumor-derived factors, perhaps precluding their acquisition of a protumor phenotype[271]. Additionally, tumorigenesis also engages hematopoiesis in the bone marrow, favoring the generation of immature suppressive populations of neutrophils and monocytes. Rebalancing this aberrant hematopoiesis via trained myelopoiesis with agents such as β-glucan or BCG might overcome the generation of an immunosuppressive microenvironment[272].

Indeed, recent evidence suggests that intravesical BCG efficacy for bladder cancer treatment involves local trained immunity mechanisms in the bladder[273–275], perhaps even conferring protection against respiratory infections. In animal models, prophylactic β-glucan administration favors antitumor responses driven either by trained neutrophils in

subcutaneously transplanted tumors[276] or monocyte-derived macrophages in orthotopic pancreatic tumors[277]. Additionally, a trained immunity-inducer nanotherapeutic facilitated the control of transplanted B16-F10 tumors in mice and sensitized this tumor to immune checkpoint blockade[278]. In two of those studies, training of bone marrow myeloid progenitors was observed, and protection could be conferred by transferring bone-marrow cells to naïve mice. Interestingly, β-glucan was already being explored as a cancer therapy well before the emergence of the trained immunity concept. However, epigenetic reprogramming of innate immune cells can also facilitate tumor growth in some instances, as observed following myocardial infarction in humans and mouse models of breast cancer[279].

Summarizing, although pioneer studies have shown that trained immunity mechanisms can be therapeutically harnessed for cancer treatment, more studies are needed in order to understand the underlying mechanism of action, especially to avoid the reprogramming of innate effectors into a protumoral state. Ideally, trained immunity-based approaches could be used to potentiate other therapies such as immune checkpoint blockade or chemotherapy, since myeloid cells have been shown to preclude their efficacy. However, besides their potential prophylactic use, it remains to be studied whether trained-immunity stimuli can overcome the (negative) effects of cancer on myeloid cells and hematopoiesis once the tumor is already present, which will be the scenario found in the clinic. Additionally, whether the training of other innate immune effectors besides monocytes and neutrophils, such as NK cells or DCs, can influence antitumor responses remains to be studied.

1.3 Bladder Cancer

In this chapter, generalities regarding the anatomy of the bladder and the epidemiology and pathogenesis of bladder cancer are briefly described. Then, existing and emerging treatment options for urothelial carcinomas will be discussed, with a special focus on intravesical BCG therapy for NMIBC.

1.3.1 Disease pathogenesis

The healthy bladder tissue is composed by 3 anatomic structures (Figure 14):

- A thin mucosal layer, comprising a transitional epithelium (urothelium) and the supportive lamina propria.

- A submucosal layer composed of connective tissue.
- A muscle layer that allows voiding upon contraction.

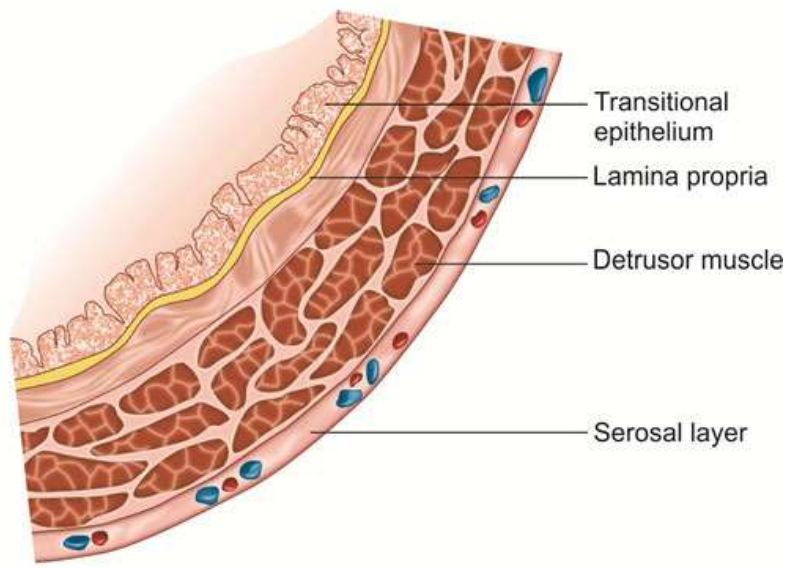

Figure 14. Anatomical structure of the bladder. *Taken from Singh et al. (2016)*[280].

In the innermost section of the urothelium, a layer of cells known as umbrella cells are linked together through very tight junctions, and this, together with the secretion of the so-called uroplakin proteins establishes a highly impermeable layer which is needed to prevent urine leakage through the epithelium and to isolate toxic substances carried by urine from the rest of the organism. Interestingly, the high degree of impermeability makes the bladder an organ relatively unexposed to pathogens, except for urinary tract infections caused by *E. coli,* which can effectively invade underlaying bladder tissue. This is in stark contrast with other mucosal layers of the organism, such as the lung or the intestine, which are continuously exposed to microorganisms, making the bladder mucosa a unique anatomical site[280].

Bladder cancer is the 9th most common cancer and the 13th most common cause of cancer-related death worldwide. Interestingly, it is the 4th most common cancer in the male population in developed countries, with a significantly lower incidence in the female population, with almost a 3:1 ratio[281]. The most common symptom leading to diagnosis is the (painless) appearance of blood in the urine, i.e., hematuria.

Risk factors for developing bladder cancer include cigarette smoking, which has been estimated to underly almost half of the cases, and other factors such as urban living, exposure to food or water polluted with arsenic, alcohol intake, or occupational exposure to carcinogens such as those found in aluminium and iron processing, gas manufacturing or industrial painting. Overall, bladder cancer has been described to be most common in industrial areas, its incidence is almost three times higher in more developed regions and is tightly linked to carcinogen exposure[282].

Tumors arising in the innermost layer of the urothelium, composed of transitional epithelial cells, comprise almost 90 % of all bladder cancers. A smaller fraction of patients develops squamous cell carcinomas, which are tightly linked to environmental exposure to *Schistosoma haematobium*, the causal agent of schistosomiasis also known as bilharzia[282,283].

Classification of transitional cell carcinoma or urothelial carcinoma is based on staging, which measures the extent of cancer spread into bladder tissue (Figure 15), and grading, which measures the degree of differentiation of tumor cells. A clear distinction is made between non-muscle invasive bladder cancer (NMIBC) and muscle-invasive bladder cancer (MIBC), which critically differ in prognosis, management, and choice of treatment[283,284].

Regarding grading and following the WHO-recommended classification, G1 tumors are the most differentiated, resembling normal urothelial cells. In contrast, "high-grade" G3 tumors present numerous cytologic abnormalities and are comprised by highly undifferentiated tumor cells. Importantly, high-grade urothelial tumors have a much higher propensity for invading underlying submucosal and muscle layers[283].

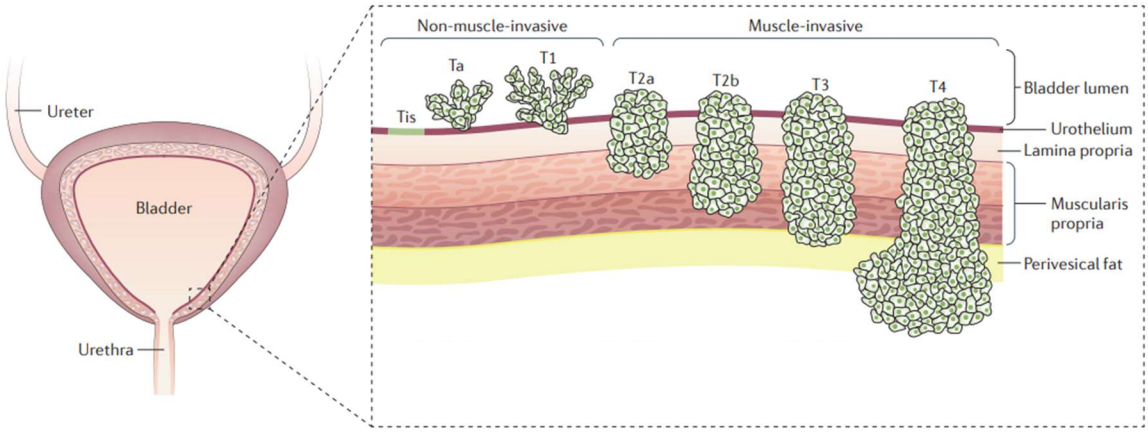

Figure 15. Bladder cancer staging following the Tumor, Node, Metastasis (TNM) system. Bladder

cancer usually originates in the epithelium (urothelium) of the bladder. Ta or T1 tumors are papillary tumors growing towards the lumen of the bladder that are confined to the mucosa (Ta) or invade the lamina propria (T1). Carcinoma *in situ* (CIS; Tis) are flat, high-grade tumors confined to the mucosa. Ta, T1 and Tis tumors are termed non-muscle invasive. T2 tumors have invaded superficially (T2a) or deeply (T2b) the muscle layer. T3 tumors have invaded the perivesical fat and T4 tumors have bypassed bladder tissue, invading either the prostate, uterus, vagina, bowel, or abdominal walls. *Taken from Sanli et al. (2017)*[283].

Patient survival depends mostly on bladder tumor stage at the time of diagnosis: for patients with localized disease such as papillary tumors, the five year-survival is as high as 92 %, falling to 40 % in muscle-invasive tumors and 6 % in metastatic bladder cancer. Urothelial carcinomas can progress to a higher stage or grade or recur to the same stage/grade following the recommended therapy. The risk of progression and recurrence is estimated based on several clinical and pathological parameters, heavily influencing the choice of therapy, which will be discussed in the following section[283].

Regarding urothelial tumorigenesis, generally there are two accepted pathways which generate two different phenotypic tumor variants greatly differing in prognosis, risk of recurrence and progression and treatment choice (Figure 16)[285].

A first group of low-grade differentiated papillary tumors originate via hyperplasia, and their most prominent characteristic are the presence of activating point mutations in the fibroblast growth factor receptor 3 (FGFR3) and the telomerase reverse transcriptase (TERT), and the deletion of chromosome 9[286]. Low-grade papillary tumors are often multifocal and recurrent, and rarely progress into muscle-invasive tumors. Low-grade papillary tumors account for almost 80 % of all urothelial carcinomas[283].

The remaining 20 % of urothelial carcinomas are comprised by muscle-invasive variants that are thought to arise from high-grade undifferentiated flat dysplasia and CIS driven by diverse defects in the TP53 and RB1 tumor suppressor pathways. It is thought that progression from flat dysplasia confined to the mucosa to muscle-invasive subtypes could be caused by loss of cyclin-dependent kinase inhibitor 2A (CDKN2A)[286]. Interestingly, high-grade undifferentiated papillary tumors (Ta stage) can also develop from flat dysplasia, and they have a higher risk of generating muscle-invasive tumors than papillary tumors which are low grade or highly differentiated. Overall, these types of urothelial carcinomas have a high risk of progressing into metastatic disease[286].

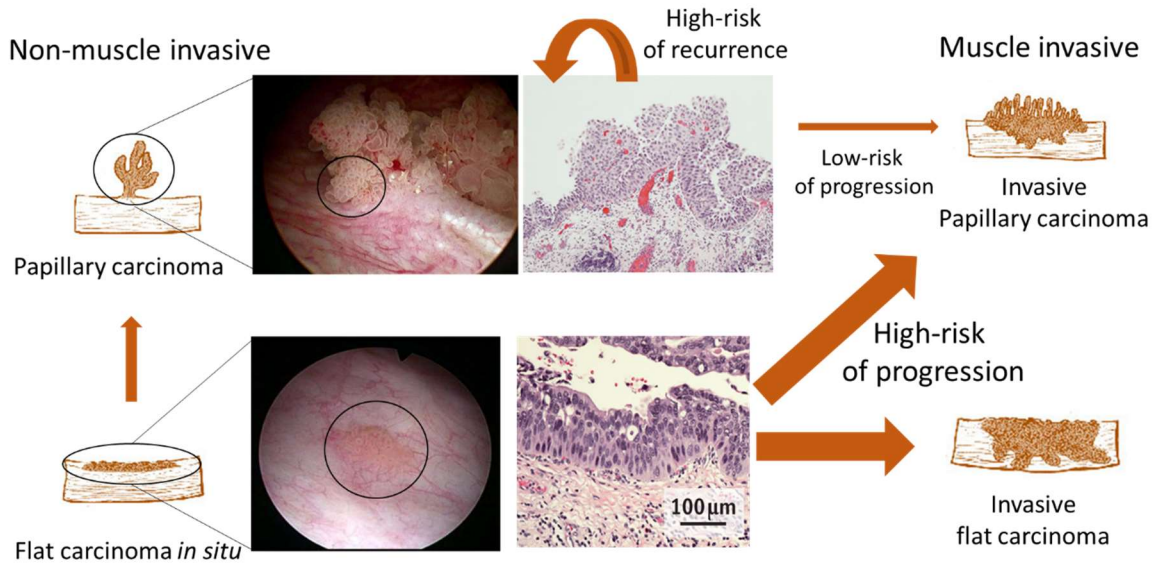

Figure 16. Progression pathways of urothelial carcinomas. Shown are schematic depictions, cystoscopy images and haematoxylin and eosin (H&E) staining of bladder tumors. *Adapted from several sources: cystoscopy images*[287]*, (H&E) staining images*[283]*, schematic depictions*[288].

1.3.2 Treatment options

Treatment choice in non-muscle invasive bladder cancer (NMIBC) is heavily influenced by parameters such as histology, grade, and depth of invasion into the muscle layer, which in turn estimate the risk of progression or recurrence[289]. Generally, newly diagnosed bladder tumors, detected either by appearance of hematuria or dysuria, undergo surgery and subsequent adjuvant therapy that depends on the stage and grade of the tumor[290].

Following diagnosis, bladder tumors undergo endoscopic resection, a procedure known as transurethral resection of bladder tumors (TURBT). This procedure has both a diagnostic intent to determine stage and grade of the tumor, as well as a therapeutic curative role. Most superficial non-muscle invasive bladder tumors, which are often multifocal, can be easily resected, although depending on stage and grade some patients present high risk of tumor recurrence and progression[289]. To avoid this, different adjuvant therapies are administered by the intravesical route. Of note, CIS cannot be fully resected by TURBT[283].

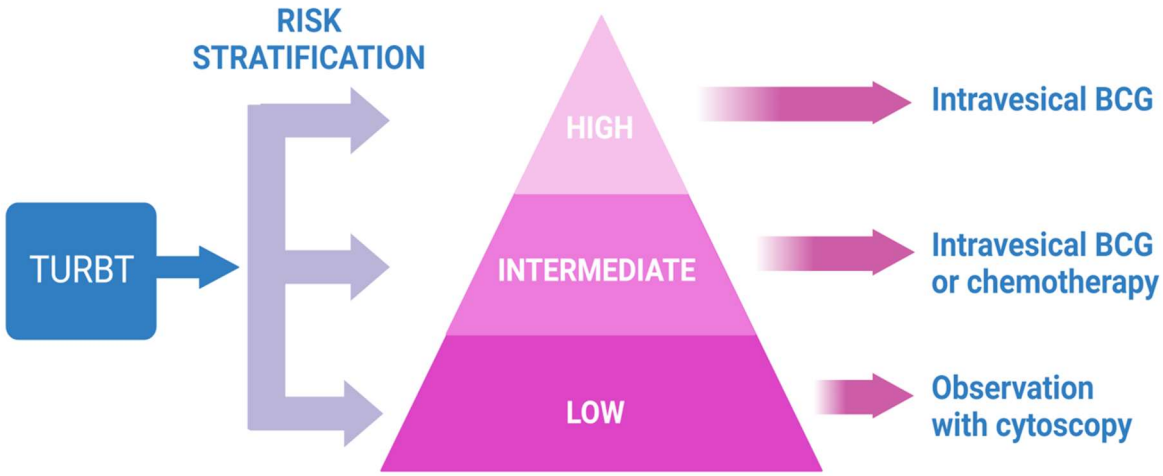

Figure 17. Treatment guidelines for NMIBC, as recommended by the European Association of Urology (2022)[291]. TURBT: transurethral resection of bladder tumor. *Created with BioRender.com.*

In NMIBC, adjuvant therapy is chosen depending on the stage and grade of the tumor determined after TURBT, which are used to estimate the risk of progression and recurrence[290,291]:

- The low-risk group comprises solitary low-grade small papillary Ta tumors. Following TURBT, these patients are followed up and observed with cystoscopy.
- Intermediate-risk tumors are multifocal, large, or recurrent Ta and T1 bladder tumors. For these cases, repeated adjuvant intravesical therapy with 1 year of maintenance is recommended. In this group, both intravesical chemotherapy and BCG are used.
- High-risk tumors are superficial high-grade Ta or T1 lesions or CIS, with a high risk of recurrence and progression are preferentially treated with intravesical BCG therapy, which is particularly effective for CIS with complete responses ranging 70-90 % in some studies.

For MIBC patients, radical cystectomy with pelvic node dissection is the most common approach, often accompanied with systemic chemotherapy (platinum-based) or immunotherapy (avelumab, pembrolizumab, atezolizumab) in cases of metastatic disease[283].

1.3.3 Intravesical BCG therapy

Adjuvant intravesical BCG therapy is currently the gold-standard therapy for intermediate and high-risk NMIBC and consists in 6 weekly instillations initiated two weeks after TURBT (Figure 17). Treatment design was proposed empirically by Morales et al. in 1976, as explained in previous sections[226].

Interestingly, BCG dosage is usually measured in mg, and depending on the commercial preparation (Connaught, Tice, RIVM…), the proportion of live bacteria among the total lyophilized weight varies. Generally, an estimated dose between 10^8 and 10^9 CFUs is administered in 50 ml of saline[226,292]. The solution containing BCG is maintained in the bladder for two hours, after which the patient is allowed to void. Importantly, some clinical studies have reported differences in antitumoral efficacy between BCG strains[293], although others have not found any significant differences[294].

The initial period of 6 weekly intravesical instillations is referred to as the induction phase and is usually followed by a maintenance phase (Figure 18). The recommended maintenance regimen consists in 3 weekly instillations at month 3, month 6 and then every 6 months up to 3 years, although the benefit of maintenance regimens is currently being questioned[283].

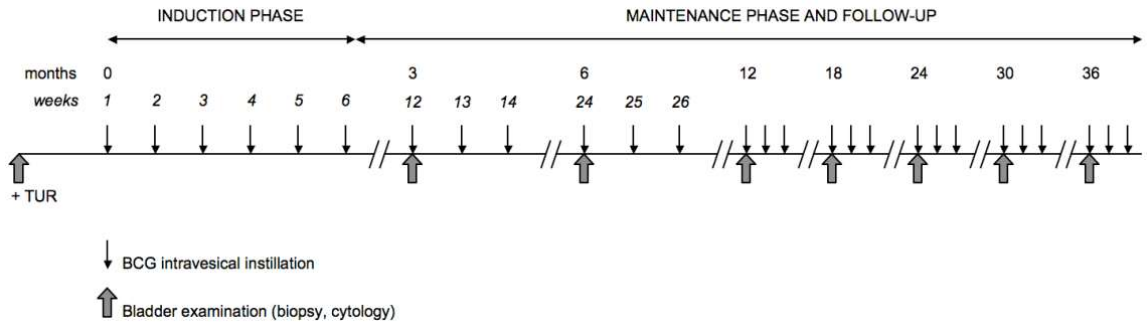

Figure 18. Schematic of recommended intravesical BCG therapy regimen. *Taken from Biot, (2012)*[295].

Following the pioneer study of Morales in 1976, in which BCG therapy precluded recurrence of non-muscle invasive urothelial carcinomas in 7 out of 10 patients, subsequent studies showed that BCG eradicated CIS, delayed progression to muscle-invasive stages, and avoided recurrence, overall improving the survival of high-risk patients with superficial

bladder cancer, proving much superior efficacy to intravesical chemotherapy in numerous clinical trials such as those showed in Figure 19. This makes BCG one of the most successful immunotherapies to date, with complete responses as high as 55-65 % for high-risk papillary tumors and 70-75 % for CIS. It is important to note that non-muscle invasive bladder tumors recur in 60 % and progress in 50 % of patients after TURBT without adjunctive post-resection therapy[290].

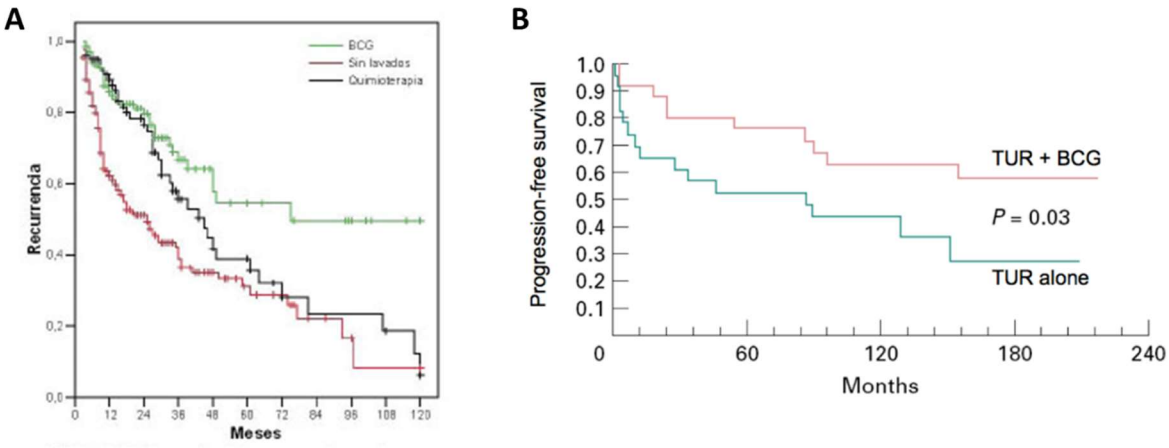

Figure 19. (A). Time to recurrence in 419 T1 high-grade superficial bladder tumor patients following TURBT and adjuvant intravesical BCG (green), chemotherapy (black) or no adjuvant treatment (red). *Taken from García Rodríguez et al, (2007)*[296]. (B) T1 high-grade bladder tumor patients received either TUR alone or TUR + adjuvant BCG and followed for 15 years. *Taken from Herr et al, (1997)*[297].

Despite its success, several problems can arise during BCG therapy. First, as many as 30-45 % patients do not benefit from therapy and as much as 40 % relapse. Moreover, BCG therapy entails many adverse effects, with 20 % of patients being intolerant and leading to suboptimal treatment schedules[284].

Patients who do not respond to BCG (BCG-unresponsive) can be classified into three categories: BCG refractory, BCG intolerant and BCG relapsing[298].

- BCG intolerant: BCG intolerant patients are those who cannot tolerate one induction course of intravesical BCG. BCG-associated toxicities can be local or systemic. Local toxicities include irritative urinary symptoms, hematuria and bladder contracture, and are generally transient and more manageable than systemic side effects. Systemic side-effects include fever, which may indicate systemic BCG infection (BCG-itis) if it is persistent. Although very rare (1 % of cases), systemic

BCG infection must be treated with antibiotics and causes treatment interruption, since it could progress to sepsis and multiorgan failure.

- BCG relapsing: BCG relapse referrers to the reappearance of a tumor after an apparent disease-free state. In these cases, in spite of an initial response, one or more recurrent tumors can appear, even with a higher stage or grade, or new CIS lesions.
- BCG refractory: BCG refractory tumors do not respond to BCG therapy and persist as a high-grade non-muscle invasive tumor both at 3 and 6 months after treatment initiation. Alternatively, refractory tumors can progress and become muscle-invasive.

The gold-standard treatment for BCG-unresponsive disease is radical cystectomy. Although bladder-preserving strategies are being developed, most of them are still in the experimental phase and are considered clinically inferior to radical cystectomy. Removal of the bladder is a life-changing intervention and an invasive procedure associated with significant morbidities, so there is an urgent need to investigate novel bladder-sparing therapies for these patients[283].

Here I will briefly review the most promising immunotherapy-based alternatives for adjuvant BCG therapy in NMIBC, either as replacement or in combination with BCG, as well as bladder-sparing strategies for BCG-unresponsive NMIBC.

- Immune checkpoint blockade: Antibodies blocking either PD-1 or PD-L1 have already shown durable objective responses in muscle-invasive and metastatic bladder cancer scenarios and are being progressively applied in the management of NMIBC. Interestingly, high PD-L1 expression in the TME has been associated with BCG-unresponsive disease[299], and numerous clinical trials are evaluating the combination of PD-1/PD-L1 blockade (durvalumab, atezolizumab, sasanlimab, avelumab) with intravesical BCG or as a monotherapy in NMIBC BCG-naïve patients[300]. Additionally, pembrolizumab (antiPD-1) was recently granted approval for BCG-unresponsive NMIBC, and it is currently the only approved bladder-preserving approach[301]. Moreover, pembrolizumab is also being tested in combination with intravesical BCG for BCG-unresponsive disease[300]. Interestingly, intravesical administration of pembrolizumab was recently shown to be safe in a small cohort of NMIBC patients and represents a promising strategy to deliver

antibodies directly into bladder tumors while reducing potential systemic toxicities[302].

- IL-15 receptor superagonist (ALT-803): This agent promotes both adaptive and innate immune responses driven by NK and $CD8^+$ T cells and demonstrated robust antitumor activity in a carcinogen-induced bladder cancer rat model[303]. This approach is currently being tested in a phase II clinical trial, combined with intravesical BCG in BCG-unresponsive patients, since the combination of both agents displayed synergy in preclinical studies. In a preliminary phase I/II trial, 9 BCG-naïve patients with intermediate-/high-risk NMIBC were found completely disease-free at 24 months[304].
- Targeted molecular approaches: Since FGFR mutations are often found in urothelial carcinoma, an interesting approach for BCG-unresponsive NMIBC patients harboring FGFR mutations is targeted therapy with erdafitinib, a FGFR1/4 inhibitor, which is currently being tested in phase II clinical trials. The FGFR1/3 inhibitor pemigatinib is also under investigation in phase II clinical trials for BCG-naïve NMIBC patients, as well as the oral FGFR inhibitor BGJ398[300].
- CD40 agonism: Recent preclinical work evidenced strong efficacy of Fc-optimized antiCD40 antibodies given by the intravesical route in three different orthotopic mouse models of bladder cancer[204]. Mechanistically, stimulation of CD40 in cDC1s in the bladder TME induced $CD8^+$ T cell-dependent antitumor responses in BCG-unresponsive bladder tumors. This approach is currently being tested in BCG-unresponsive NMIBC patients in a phase I clinical trial[305].
- Nadofaragene firadenovec: This approach consists in the intravesical administration of a replication-deficient recombinant adenovirus which delivers human IFNα cDNA into the bladder epithelium as an immune stimulant. Recently, this strategy has been tested in BCG-unresponsive NMIBC patients in a phase III clinical trial. Interestingly, as much as 53,4 % of patients underwent complete responses, which is a notable feat in an already difficult to treat BCG-unresponsive scenario[306]. This agent has been granted approval by the FDA for BCG-unresponsive NMIBC in December 2022.
- Oncolytic virotherapy: Intravesical administration of CG0070 showed efficacy in preclinical mouse models of bladder cancer[307] and has shown strong responses in

phase I and II clinical trials in the BCG-unresponsive NMIBC scenario[308]. CG0070 is an oncolytic serotype 5 adenovirus encoding GM-CSF and replication selective for retinoblastoma pathway-deficient tumors, which is often the case in urothelial carcinomas[307]. Therefore, both direct tumor cell lysis and stimulation of immune cells by GM-CSF are thought to drive the efficacy of this agent. A recent study reported surprising efficacy (88,9 % were complete responses) of CG0070 in combination with pembrolizumab in BCG-unresponsive NMIBC patients[309].

- NKG2A blockade: Recent work by the group of Amir Horowitz suggests that human bladder tumors with high levels of T cell infiltration could still be resistant to PD-L1 blockade therapy due to high expression of another checkpoint molecule expressed by $CD8^+$ T cells and NK cells: NKG2A, an inhibitory receptor which binds tumor HLA-E molecules[310]. Indeed, also working with patient-derived tumor specimens, this group showed that intravesical BCG therapy was associated with an increase of PD-L1 and HLA-E expression in tumor cells, which could explain BCG failure. Therefore, PD-1/PD-L1 blockade might not be enough to stimulate NK and $CD8^+$ T cells in BCG-unresponsive NMIBC patients, so targeting other immune checkpoints such as NKG2A could represent an interesting strategy to induce curative antitumor immune responses[311,312].

Thus, although interesting alternatives to BCG are starting to appear, especially to avoid radical cystectomy when BCG fails, none has yet been able to substitute in the clinic the gold-standard therapy for intermediate and high risk NMIBC for almost 30 years. Taking into consideration the success of bacterial-based immunotherapy in the context of urothelial carcinoma, another feasible strategy is to develop bacterial-based treatments which improve BCG activity in NMIBC, for example by employing a different bacterial agent (genetically modified BCG strains, *Salmonella* strains, other mycobacteria…). Although efforts are undergoing, no agent has been able so surpass BCG.

1.3.4 Immunological mechanism of action of intravesical BCG therapy

Although the precise mechanism of action of intravesical therapy for bladder cancer is still incompletely understood, it is well established that it involves an immune response mediated by the host against the tumor.

To discuss the antitumoral activity of BCG in the context of bladder cancer, here I have divided current knowledge based on human data and experimental studies in three different topics: 1) Interaction between BCG and the urothelium, 2) stimulation of innate immune responses, and 3) role of T cells and tumor-specific immunity.

1) Interaction between BCG and the urothelium

Following intravesical inoculation, the first interaction between BCG and the host is contact with the bladder epithelium, either healthy or tumoral. Analysis of urine in patients undergoing BCG instillations suggests local persistence of BCG in the bladder of patients only in the short term, since BCG was absent in the urine from most patients by 4 days following instillation. In a similar manner, BCG was detected by PCR in less than 10 % of biopsies taken 3 months after the first course of 6 weekly BCG instillations[313].

In mice, it has been described that BCG can attach to urothelial cells in a process involving interaction between bacterial fibronectin attachment proteins (FAPs, such as Ag85B) and host fibronectin[314]. Confirming the importance of this step, blocking of BCG attachment to the bladder via fibronectin abrogated the antitumor efficacy of BCG in animal models of bladder cancer[315].

Although BCG clearly can attach to the bladder wall, it is still unknown whether it is internalized by urothelial or immune cells in the bladder *in vivo*. In an attempt to answer this question, several studies have reported that bladder cancer cell lines readily internalize BCG *in vitro,* although very high ratios of BCG to bladder cancer cells were used[316,317]. Indeed, at such high ratios even a certain degree of cytotoxicity exerted by BCG can be observed. Whether this mechanism is relevant in an *in vivo* scenario is unclear. Interestingly, BCG interaction with tumor cells could influence their phenotype and behavior: a recent study reported that BCG internalization by bladder cancer cell lines *in vitro* induced downregulation of surface HLA-I expression, which could preclude targeting by $CD8^+$ T cells and difficult immune-mediated rejection, driving BCG therapy failure[318]. Interestingly, HLA-I downregulation caused by BCG in tumor cells was accompanied by the secretion of cytokines associated with an immune-suppressive TME. These results can help us in understanding BCG failure in a fraction of patients, although this phenomenon remains to be confirmed *in vivo* in murine tumor models.

Therefore, the fate of BCG in the bladder following intravesical instillation is an understudied topic. Analysis of human urine following BCG instillations suggests that the vast majority of BCG is voided after instillation. However, two critical questions remain unanswered: 1) are persisting bacteria internalized by urothelial cells or immune cells in the bladder? and 2) is bacterial persistence in the bladder needed to trigger an inflammatory response and subsequent antitumor immune responses? Indeed, if persistence of BCG in the bladder tissue is needed to trigger an innate immune response, improving the ability of the bacteria to colonize the bladder could be harnessed to enhance the efficacy of this type of treatment.

2) Stimulation of innate immune responses

BCG has been described to activate numerous PRRs: TLR2, TLR4, TLR9, NOD2, dectin-1, DC-SIGN, etc. TLR signaling depends on MyD88, and a recent study showed that the beneficial effect of intratumoral BCG treatment was abrogated in MyD88 deficient mice[319], suggesting that recognition of BCG derived PAMPs is needed for antitumoral effect, at least in this model. However, this observation could have another explanation: sensing of immunogenic cell death also depends on TLR4 and MyD88 signaling. Indeed, shRNA mediated silencing in MB49 cells of HMGB1, a TLR4 ligand secreted by tumor cells undergoing cell death, abrogated the efficacy of BCG in mouse models of bladder cancer[320].

The role of macrophages in intravesical BCG therapy is still not very clear. A recent study showed that high numbers of $CD163^+$ $CD68^+$ "M2" macrophages in bladder cancer patients predicted recurrence following BCG therapy[321,322]. Whether intravesical BCG can change the phenotype and functionality of macrophage in bladder tumors remains to be tested in experimental mouse models and in human samples.

Following BCG therapy, neutrophils are the most abundant immune cell subtype in the urine[323]. Moreover, *in vitro* BCG-stimulated neutrophils can secrete the cell death ligand TRAIL and exert cytotoxicity against human bladder cancer cell lines[324]. Interestingly, in orthotopic models of bladder cancer, neutrophil depletion abrogated the therapeutic effect of BCG[325,326]. These results support a role for PMNs in the mechanism of action of intravesical BCG, although their precise role is still unclear. Whether BCG-stimulated neutrophils exert significant cytotoxicity against tumor cells remains to be verified *in vivo*.

Alternatively, neutrophil recruitment to the bladder following BCG instillation could represent a first step in the local inflammatory reaction driving effective antitumor responses by other immune cells, such as NK or T cells. Indeed, in naïve mice, neutrophil depletion abrogated recruitment of $CD4^+$ T cells to the bladder following intravesical BCG instillation, suggesting that BCG-activated neutrophils could be responsible for the recruiting T cells[326].

Indeed, NK lymphocytes can become activated by exposure to BCG, which enhances their cytotoxic activity towards human bladder cancer cells *in vitro*[327]. Additionally, BCG-infected bladder cancer cells are more susceptible to NK lymphocytes cytolytic activity[328]. Importantly, the cytotoxic activity of BCG-stimulated NK cells was completely dependent on perforin[329–331]. In the MB49 orthotopic mouse model of bladder cancer, NK cell depletion abrogated the therapeutic benefit of intravesical BCG[332], indicating that this subset is required for the efficacy of this kind of therapy. However, conclusive evidence about the precise role of NK cells following intravesical BCG therapy is still lacking, especially in experimental mouse models *in vivo*.

Lastly, in stark contrast to other types of immunotherapies, the role of DCs, and especially Batf3-dependent cDC1s, in BCG therapy for bladder cancer has been somewhat overlooked, given their specialized ability to prime tumor-specific T cell responses. Importantly, DCs have been found in the urine of patients undergoing BCG instillations[333]. However, whether DCs and Batf3-dependent cDC1s are needed for BCG efficacy in the context of bladder cancer remains unknown. Besides their role in priming adaptive immune responses, DCs can also influence the activation status of NK, NKT and γδ T cells in the tumor. Indeed, in humans, BCG-activated DCs improved the cytolytic activity of NKT and γδ T cells against bladder cancer cell lines *in vitro*[334]. Another interesting hypothesis that remains to be tested in experimental mouse models is whether exposure to BCG could impact the functionality of bladder DCs, either by enhancing their maturation status or their expression of costimulatory molecules, or even by facilitating their migration to the draining LNs, where they could better prime T cells.

Therefore, although innate immune populations are clearly activated by intravesical BCG *in vivo* or by BCG *in vitro*, data concerning their specific roles in the orchestration of effective antitumor responses in the bladder is still lacking.

3) Role of T cells and tumor-specific immunity

The importance of T cells in BCG immunotherapy was established in seminal studies using experimental mouse models of orthotopic bladder cancer: intravesical BCG was totally ineffective in mice lacking T cells[335], and depletion of either $CD8^+$ and $CD4^+$ T cells abrogated treatment efficacy[336]. In humans, following BCG therapy, T cells can be detected in the urine[323] and infiltrating the bladder mucosa, even months after instillation[337]. Interestingly, these T cells found in the urine and bladder mucosa are predominately of the $CD4^+$ lineage. Regarding the function of this recruited $CD4^+$ T cells, BCG induces a Th1-skewed response in the bladder, detected by increased IL-2, IL-12, IFN-γ, IL-18, IL-8, TRAIL, and TNF cytokine levels in the urine of patients[338]. Indeed, mice bearing bladder tumors and genetically lacking IL-12 or IFN-γ are insensitive to BCG therapy, whereas knock-out of IL-10 potentiates therapeutic effect[339], so it is likely that the ability of BCG to induce a Th1-skewed response plays a significant role in the antitumoral mechanism of action.

It is still debated whether intravesical BCG therapy requires the development of tumor-specific T cell-dependent immunity. What has become clear is that BCG-specific T cells might participate in the antitumoral effect of BCG. First, a critical body work by Biot *et al.* showed that subcutaneous vaccination with BCG before intravesical treatment in an orthotopic mouse mode of bladder cancer greatly accelerated T cell recruitment to the bladder and improved tumor rejection. In the same work, NMIBC patients with a positive PPD skin test, which indicates previous exposure to mycobacteria, responded better to intravesical BCG therapy than those with a negative test[340]. These results suggest that the immune response to mycobacteria determines the therapeutic efficacy of BCG. Second, Ji *et al.* found that both BCG-specific and tumor-specific αβ T cells, as well as γδ T cells, were needed for the therapeutic effect of intratumoral BCG in subcutaneous MB49 tumors[341]. Third, Antonelli *et al.* recently found that mice cured of MB49 bladder tumors following intravesical BCG therapy developed tumor-specific immune memory dependent on $CD4^+$ T cells[342]. Therefore, the existing literature suggests that both BCG-specific and tumor-specific T cells are needed for the antitumoral effect of intravesical BCG. However, a better understanding of the link between the BCG-specific and the tumor-specific T cell response is still lacking.

1.4 MTBVAC

The closest relative to the tuberculosis vaccine BCG is MTBVAC[343]. Although both are live-attenuated vaccines obtained from a virulent *Mycobacterium* strain, MTBVAC was generated by rational attenuation of a clinical isolate of the human pathogen *M. tuberculosis*, by stable deletion of the *phoP* and *fadD26* genes, in contrast to BCG which was attenuated by serial in vitro subcultivation from a *M. bovis* strain[344–346]. Deletion of *phoP* and *fadD26* markedly alters the phenotype of the mycobacteria, including both the composition of the cell envelope and the expression of secretion systems (Figure 20), explaining the attenuation of MTBVAC with respect to its parental *M. tuberculosis* virulent strain. MTBVAC has become the first live-attenuated vaccine based on *M. tuberculosis* to be tested in clinical trials (phase I and II)[347]. Critically, MTBVAC confers protection against pulmonary tuberculosis infection in several preclinical models[348–350], and has been shown to be safe and immunogenic in humans[351].

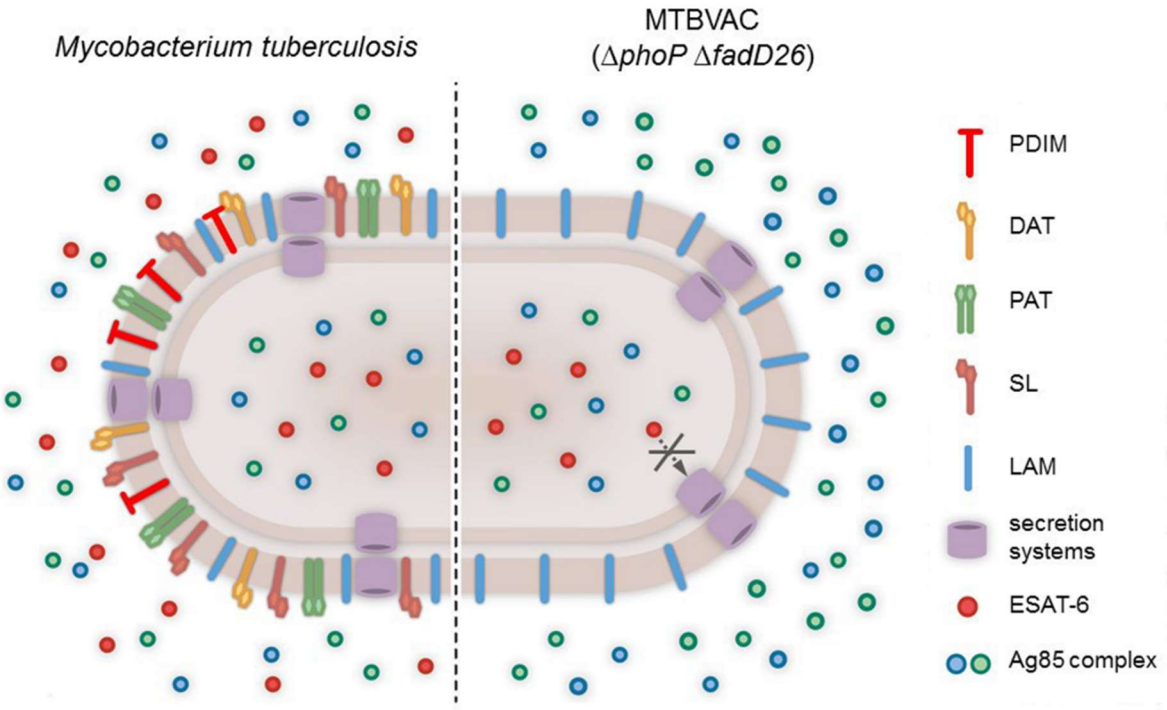

Figure 20. Main phenotypic differences between *M. tuberculosis* and MTBVAC, a *phoP* and *fadD26* mutant. ESAT-6: Early secreted antigen target 6, Ag85: Antigen 85, PDIM: phthiocerol/phthiodiolone dimycocerosate, DAT: diacyltrehaloses, PAT: penta-acylated trehaloses, SL: sulfolipids, LAM: lipoarabinomannan. *Adapted from Gonzalo-Asensio et al. (2017)*[344].

In a recent study, the superior efficacy of intradermal MTBVAC vaccination compared to BCG at preventing *M. tuberculosis* infection in mouse models was explained by the fact that MTBVAC conserves strong immunogenic proteins such as ESAT-6 and CFP10, which are expressed by *M. tuberculosis* during pulmonary infection but that were lost during the attenuation process of *M. bovis* leading into the BCG vaccine[352]. Importantly, intradermal vaccination with MTBVAC triggered ESAT6 and CFP10-specific immune responses in humans, while BCG did not[352].

As we have explained, the protection conferred by BCG against *M. tuberculosis* and other infections cannot be solely ascribed to the induction of antigen-specific immune responses[353]. For this reason, candidates to replace BCG as a tuberculosis vaccine must demonstrate a comparable ability to non-specific effects. With MTBVAC, this has been recently demonstrated in mice[354], and will be an important aspect to be evaluated in phase III clinical trials, which recently started in tuberculosis endemic countries (NCT04975178).

It is noteworthy that MTBVAC resulted more effective than BCG (Pasteur) as an anticancer agent in a mouse model of bladder cancer, owing to an increased ability to infect several mouse and human bladder cancer cell lines when compared to BCG[355]. Further studies will be needed to explain how genetic differences between distinct mycobacteria shape their antitumor properties, especially in the context of bladder cancer.

Materials and methods

2.1 Mice

C57BL/6JR mice were purchased to Janvier Biolabs or bred in the facilities of the Centro de Investigaciones Biomédicas de Aragón (CIBA). Mouse strains deficient for IFN-γ, Perforin, Batf3, Granzyme B, Rag1 or TLR4 were bred in the facilities of the Centro de Investigaciones Biomédicas de Aragón (CIBA).

The use and care of animals for experimental work were performed in agreement with the Spanish Policy for Animal Protection RD53/2013 and the European Union Directive 2010/63 for the protection of animals used for experimental and other scientific purposes. Experimental procedures were approved by Ethic Committee for Animal Experiments of University of Zaragoza. Mice were housed and maintained in specific pathogen-free conditions and observed for any sign of disease.

Mice were acclimatized during one week before experiments started. Food and water were provided *ad libitum* and room temperature was 20-24 ºC, humidity 50-70% and light intensity 60 lux with the light-dark cycle of 12 hours.

Female mice aged 8 to 12 weeks were used for implantation of bladder tumors and intravesical treatments, due to (our) inability to perform intravesical instillation in male mice. For experiments involving intravenous inoculation of B16-F10 cells, female mice were used due to lower tumor take observed in male mice, which is described in the literature[356]. For the remaining experiments, female and male mice were used indistinctly.

2.2 Cell lines

The MB49 cell line is a urothelial carcinoma line originally obtained by exposing bladder epithelial cells obtained from a C57BL/Icrf-a' mouse to the carcinogen 7,12-dimethylbenz[a]anthracene (DMBA) for 24 h. This transformed cell line was shown to generate carcinomas when transplanted into syngeneic mice[357]. MB49 cells used in our laboratory were purchased from the ATCC. MB49 expressing the fluorescent protein GFP (MB49-GFP) were given by Dr. Denise Nardelli-Haefliger[358]. MB49 expressing the fluorescent protein ZsGreen and the reporter luciferase (MB49-ZsGreenLuc) were made in the laboratory as described below. MB49 cells lacking MHC class I (MHC-I) expression were made in the laboratory as described below. Res50 cells were derived from a MB49 bladder tumor arising at day 50 post tumor cell inoculation in a mouse receiving MTBVAC intravesical treatment.

The B16-F10 line is a melanoma cell line originally obtained from a pulmonary melanoma nodule after 10 passages of the B16 parental cell line by intravenous inoculation in C57BL/6 mice[359]. B16-F10 cells used in laboratory were purchased from the ATCC. B16-F10 expressing the lymphocytic choriomeningitis virus (LCMV) antigen gp_{33-41} were given by Dr. Hans Pircher (Freiburg, Germany)[360]. B16-F10 cells lacking MHC-I expression were made in our laboratory as described below. B16-F10 cells expressing the fluorescent protein ZsGreen and the reporter luciferase were made in our laboratory.

The LLC (from Lewis Lung Carcinoma) cell line was originally established from the lung of a C57BL/6 mouse bearing a tumor resulting from the implantation of a primary Lewis Lung Carcinoma, which originally arose as a spontaneous carcinoma in the lung of a C57BL/6 mice[361]. LLC cells used in our laboratory were given by Dr. David Sancho and were originally purchased from the ATCC. LLC cells expressing ZsGreen and luciferase were made in the laboratory. LLC cells lacking MHC-I were made as described below.

The KC8.1 lung adenocarcinoma cell line was established in our laboratory from a lung carcinoma arising in a GEM mouse bearing the Cre recombinase-inducible allele $Kras^{LSLG12Vgeo}$. The generation of this cell line is described in detail in chapter 2 section 2.

The HEK-293T-GP2 (293T) cell line used for lentivirus production was given by Dr. Julián Pardo and was originally purchased from the ATCC. The X63Ag8653 cell line is a murine myeloma transfected with a plasmid encoding granulocyte-monocyte colony stimulating factor (GM-CSF)[362] and was given by Dr. Julián Pardo. The L929 cell line was used as a source of monocyte colony stimulating factor (M-CSF) and was given by Dr. Julián Pardo.

All cell lines were cultured in DMEM (Gibco) or RPMI (Gibco, for X63Ag8653) supplemented with 10 % heat inactivated fetal bovine serum (FBS; Gibco), Glutamax (Sigma) and penicillin-streptomycin (Sigma). Adherent cells were routinely passaged by addition of trypsin/EDTA (Sigma) and were always used with less than 10 passages from thawing. Cell lines were stored frozen in liquid nitrogen at a concentration of $3\text{-}5x10^6$ cells ml^{-1} in complete DMEM supplemented with 10 % dimethyl sulfoxide (Sigma-Aldrich). *Mycoplasma* contamination was routinely checked in cell culture supernatants. Cell line authenticity was not checked.

2.3 Generation of cell lines expressing ZsGreen and luciferase

The *E.coli* strain containing the pHIV-Luc2-ZsGreen plasmid encoding the proteins ZsGreen and Firefly Luciferase (Luc2) and the strains containing the plasmids necessary for lentivirus packaging and production (psPAX containing GAG and POL genes, and pM2D-G containing VSV-G) were given by Dr. Julián Pardo. Bacterial strains were grown in LB with Ampicillin and plasmid DNA was purified with a Plasmid Maxi Kit (Qiagen). 293T cells were seeded in 10 cm Petri dishes and transfected with 5 µg psPAX, 2,5 µg pM2D-G and 7 µg of pHIV-Luc2-ZsGreen in the presence of polyethyleneimine (Sigma-Aldrich). 72 h later, supernatants containing lentivirus were harvested following centrifugation for 5 min at 1250 rpm, to eliminate cell debris. For lentiviral transduction, tumor cells were seeded in 6-well plates and 2 ml of lentivirus-containing supernatant was added in the presence of 8 µg ml^{-1} of polybrene (Sigma-Aldrich). Upon reaching confluence, transfected tumor cells were detached and sorted by fluorescence-activated cell sorting (FACS) in a SH800S Cell Sorter (Sony) to generate tumor cell lines stably expressing ZsGreen. Before each *in vivo* experiment performed with these cell lines, ZsGreen expression was validated by flow cytometry.

2.4 Generation of cell lines lacking MHC-I expression

Tumor cell lines were transfected with CRISPR plasmids (SantaCruz Biotechnology) containing three different sgRNAs targeting the β_2-microglobulin gene, a puromycin resistance gene and RFP for selection of transfected populations. For efficient transfection, UltraCruz transfection reagent was used following the manufacturer instructions. Briefly, CRISPR plasmids diluted in transfection reagent and 1 ml of complete DMEM were added to tumor cells seeded in 6-well plates. Following overnight incubation, media was changed, and cells allowed to grow for 1-2 days more. Then, cells were selected with puromycin at the optimal concentration previously titrated for each cell line. After one week of selection in the presence of puromycin, growing cells were FACS-sorted based on lack of MHC-I expression after staining with an APC-conjugated $H2K^b/D^b$ antibody, and sorted again if necessary. When a pure tumor cell population completely lacking MHC-I was obtained, cells were incubated for 24 h in the presence of 50 ng ml^{-1} of mouse recombinant IFN-γ (Miltenyi) and analyzed by flow cytometry to confirm lack of $H2K^b/D^b$ expression.

2.5 Generation and culture of bone marrow derived macrophages (BMDMs) and dendritic cells (BMDCs)

Conditioned media containing M-CSF for BMDM generation was obtained from the supernatant of L929 cell cultures. Conditioned media containing GM-CSF for the generation of BMDCs was obtained from the supernatant of X63Ag8563 cell cultures.

BM cells were flushed out from the tibias and femurs of mice with RPMI medium, the obtained cell suspension was filtered through a 70 µm mesh and red blood cells were lysed in 1 ml Red Blood Cell Lysing Buffer (Sigma-Aldrich) for 1 min.

Then, for BMDM generation, cells were counted, resuspended in DMEM with 10 % FBS, Glutamax, penicillin/streptomycin and 10 % of L929 supernatant and $10x10^6$ cells seeded in a 10 cm Petri dish. Cells were cultured for 7 days and then detached with Trypsin/EDTA and a cell scraper for use in subsequent experiments.

For BMDC generation, cells were counted and resuspended in RPMI with 10 % FBS, Glutamax, penicillin/streptomycin and 10 % of X63Ag8563 supernatant. $10x10^6$ cells were seeded in a 10 cm Petri dish. Fresh medium was added at day 3, and at day 6 the cells in suspension were collected, spun and seeded in fresh medium in another 10 cm Petri dish. At day 9, cells in suspension were collected and used in subsequent experiments. Expression of the dendritic cell markers CD11c and MHC-II was checked in the resulting cell population by flow cytometry.

2.6 Bacterial strains

Mycobacterial strains used in this study were grown at 37°C in Middlebrook 7H9 broth (BD Difco) supplemented with 0.05% Tween 80 (Sigma) and 10% Middlebrook albumin dextrose catalase enrichment (ADC; BD Biosciences), or on solid Middlebrook 7H10 agar (BD Difco) supplemented with 10 % ADC (BD Biosciences). Mycobacteria were grown to mid-log phase in liquid 7H9 supplemented broth, and cultures were centrifuged and resuspended in PBS with 0.05 % Tween 80. Bacterial suspensions were kept for 10 minutes at room temperature to allow clump sedimentation, and the resulting supernatants were centrifuged to remove additional clumps at 1400 rpm for 10 minutes. Supernatants were kept and stored frozen at -80ºC after the addition of glycerol to achieve a final concentration of 5 %. One week after freezing the cultures, a vial of the batch was thawed, plated on solid

Middlebrook 7H10 agar and 3 weeks later colonies were counted to determine the CFU concentration of each batch. All experiments were performed with bacteria from quantified stocks kept at -80ºC.

BCG Tice was originally obtained and cultured from a commercial vial of OncoTICE (used for NMIBC treatment) and BCG Connaught from a commercial vial of ImmuCyst (used for NMIBC treatment). The BCG Pasteur reference strain 1173P2 and BCG Pasteur recomplemented with the genomic region RD1 (BCG::RD1) were a gift from Roland Brosch (Institut Pasteur, France). BCG Moreau was obtained and cultured from a commercial vial of ImunoBCG (Biofabri). GFP-expressing MTBVAC and BCG Tice strains were generated in the laboratory by transformation with the pJKD6 plasmid (a kind gift from Luciana Leite, Butantan Institute, Brazil). The MTBVAC strain lacking ESAT6 and CFP10 (MTBVAC ΔE6C10) was constructed and characterized in our laboratory[352]. The MTBVAC parental strain was constructed and characterized in our laboratory[343].

Heat-killed (HK) BCG Pasteur was prepared by incubating the desired inoculum for 30 min at 90ºC and allowed to cool for 2 hours before inoculation. The resulting inoculum was plated in solid medium to confirm lack of viability.

2.7 Experimental murine tumor models

For tumor cell inoculation, cells were cultured as described, detached with trypsin/EDTA, counted and resuspended at the desired concentrations in serum-free RPMI.

For the induction of subcutaneous tumors, tumor cells at the desired concentration were inoculated subcutaneously in the shaved flanks of mice in a volume of 100 µl. The size of subcutaneous tumors was measured every 2 days with a digital caliper and determined by using the following formula: $[(\text{tumor width})^2 \times (\text{tumor length})]/2$. Mice were sacrificed when tumor volume exceeded 1 cm^3 or became ulcerated.

For the induction of lung tumors, tumor cells at the desired concentration were inoculated into the tail vein of mice in a volume of 200 µl in serum-free RPMI.

For the induction of orthotopic bladder tumors, female mice were anesthetized with isoflurane and intravesically instilled with 50 µl of a 0.01% poly-L-lysine (Sigma) solution using a 24-gauge catheter (BD Insyte) attached to a syringe. The poly-L-lysine solution was maintained in the bladder for 20 minutes, and then the catheter was removed and the

bladder emptied by manually applying gentle pressure. Then, 50 µl of a solution containing $4x10^5$ tumor cells was intravesically instilled and retained in the bladder for 1 h, after which the bladder was emptied, and the mice allowed to recover from anaesthesia.

2.8 Intravesical treatments

Bacteria from frozen quantified stocks were resuspended in PBS at a concentration of $1x10^8$ CFUs ml^{-1}. Part of the inoculum used in every experiment was plated in solid 7H10 medium and counted 3 weeks later for CFU determination and quality control. Mice were anesthetized with Isoflurane using a vaporizer (5 % for induction and 1,5 % for maintenance) and intravesically instilled using a 24-gauge catheter with 50 µl of the bacterial suspension and maintained in the bladder for 2 hours. Then, the bladder was manually emptied and the mice were allowed to recover from anesthesia. Treatment schedules followed in the experiments are detailed in the Figures along the results section.

2.9 Intranasal inoculation

Bacteria from frozen quantified stocks were resuspended in PBS at the desired concentrations. Part of the inoculum was plated in solid medium for CFU determination and quality control. Mice were anesthetized and intranasal administration was performed with two sequential instillations of 20 µl of the bacterial suspension by adding it drop by drop into the mice nostrils.

2.10 Intravenous inoculation

Bacteria from frozen quantified stocks were resuspended in PBS at the desired concentrations. Part of the inoculum used for treatment was plated in solid medium for CFU determination and quality control. Bacterial suspensions at the desired concentrations were inoculated into the tail vein of mice in a volume of 200 µl.

2.11 Subcutaneous inoculation

Bacteria from frozen quantified stocks were diluted in PBS at the desired concentrations and 200 µl were injected subcutaneously.

2.12 Antibody based cell depletion and treatments

For $CD4^+$ and $CD8^+$ T cell depletion, mice were injected intraperitoneally with 200 µg of anti-CD4 (clone GK1.5, BioXCell) or 200 µg of anti-CD8α (clone 2.43, BioXCell) two

days before tumor challenge or the day before bacterial treatment, depending on the experimental setting. For NK cell depletion, mice were injected with an initial dose of 200 µg of anti-NK1.1 (clone PK136, BioXCell) following a schedule that depended on the experimental setting and is detailed in the corresponding Figures. Repeated doses of 100 µg were administered twice a week to achieve continuous depletion if needed. Depletion of cell populations was confirmed at endpoint in all experiments by flow cytometry analysis and representative examples are shown below.

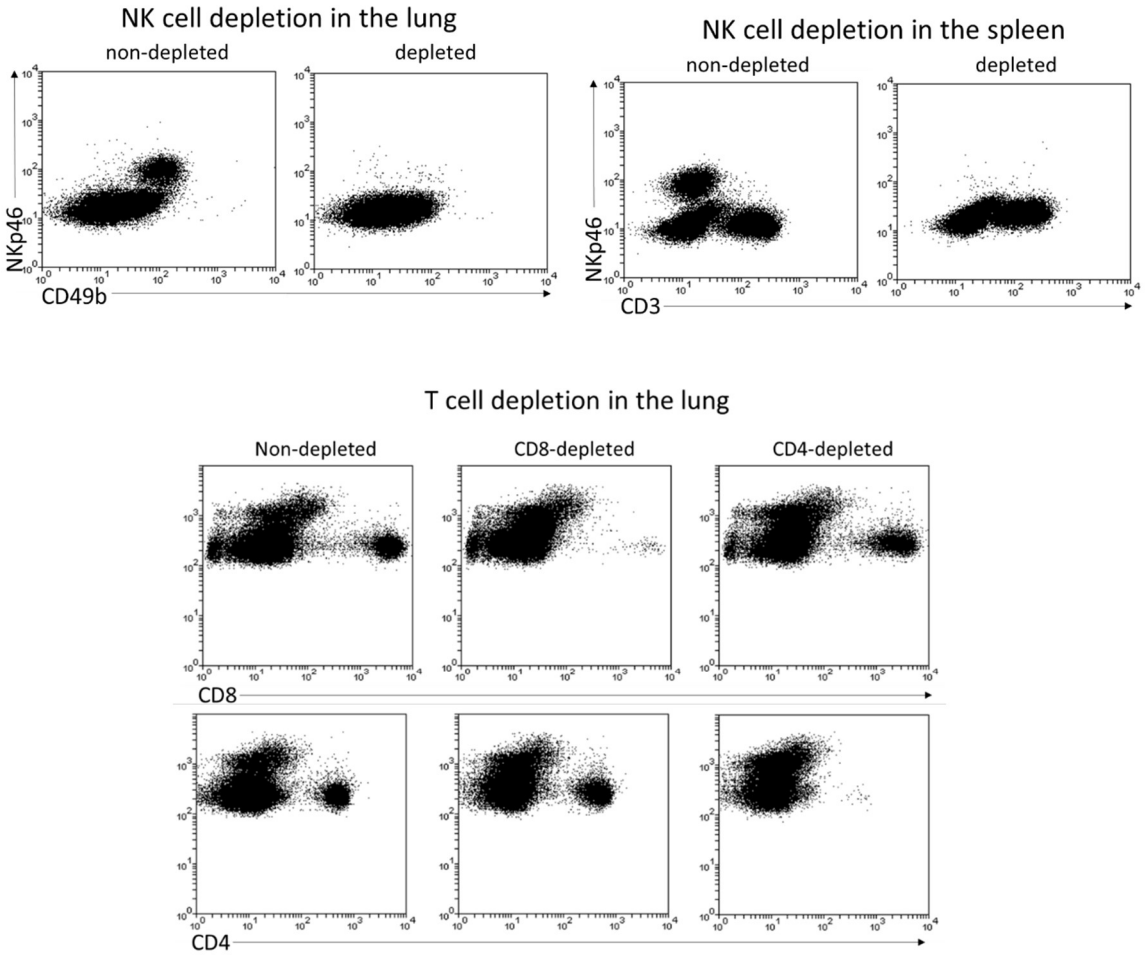

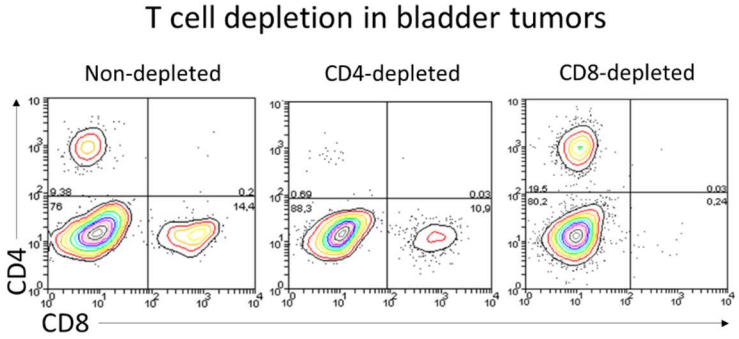

For antibody-based treatments, 200 µg of anti-PD-L1 (clone 10F.9G2, BioXCell) was administered intraperitoneally twice a week for a total of 4 doses.

2.13 *In vivo* CD45 labeling

For intravenous CD45 labeling, mice were intravenously inoculated with 2 µg of CD45-PerCP-Vio700 (Clone REA737, Miltenyi) diluted in 200µl of PBS 5 min before euthanasia. After euthanasia, lungs were immediately placed in 20 ml of RPMI medium to allow dilution of unbound antibodies and processed as described below.

2.14 Bacterial load determination in mouse tissues

Bladders, bladder draining lymph nodes and kidneys were aseptically harvested from mice were homogenized using a GentleMacs dissociator (Miltenyi) in 1 ml of H_2O and kept at -80ºC. After unfreezing, serial dilutions were prepared in PBS, plated in solid 7H10 medium supplemented with 10% ADC and 3 weeks later bacterial colonies were counted.

2.15 Preparation of single cell suspensions from the bladder

Bladders or bladder tumors were harvested from mice and processed first by manual dissection using scissors and a scalpel, followed by vigorous pipetting and digestion in RPMI containing 0.17 U ml^{-1} Liberase TM (Roche), 2 mg ml^{-1} Collagenase D (Roche) and 40 U ml^{-1} DNAse I (ApplyChem) for 45 min at 37ºC, followed by filtration through a 70 µm cell strainer (Miltenyi). Red blood cells (RBC) were lysed in 1 ml Red Blood Cell Lysing Buffer (Sigma-Aldrich) for 1 min. Cells were resuspended in PBS with 2 % FBS and stained for surface and intracellular markers.

2.16 Preparation of single cells suspensions from lymph nodes

Lymph nodes were mashed with the back of a syringe in 24-well plates in 1 ml of RPMI with 2 mg ml^{-1} Collagenase D and 40 U ml^{-1} DNAse I, incubated for 30 min at 37ºC after vigorous pipetting and strained through a 70 µm cell strainer. Cells were resuspended in PBS with 2% FBS and stained for surface and intracellular markers.

2.17 Preparation of single cell suspensions from the spleen

Spleens were mashed with the back of a syringe in 6-well plates in 5 ml of RPMI with 2 mg ml^{-1} Collagenase D and 40 U ml^{-1} DNAse I, incubated for 30 min at 37ºC after vigorous pipetting and strained through a 70 µm cell strainer before lysing erythrocytes with RBC Lysing Buffer for 1 min. Single cells were resuspended in PBS with 2% FBS and stained for surface and intracellular markers or in complete RPMI, depending on the experiment.

2.18 Preparation of single cell suspensions from the lung

Lungs were harvested from mice and homogenized in 5 ml of RPMI containing 40 U ml^{-1} DNAse I and 2 mg ml^{-1} collagenase D using a GentleMacs dissociator (Miltenyi) according to manufacturer's instructions for lung tissue. After vigorous pipetting, lungs were incubated at 37°C for 30 min and further homogenized with the GentleMacs dissociator. The homogenates were filtered through a 70 µm cell strainer and erythrocytes were lysed with RBC Lysing Buffer for 1 min. Single cells were resuspended in PBS with 2% FBS and stained for surface and intracellular marker or in complete RPMI, depending on the experiment.

2.19 Restimulation and intracellular cytokine staining

For the detection of cytokine secreting cells, single cell suspensions were stimulated *in vitro* in complete RPMI medium (supplemented with with non-essential aminoacids, 10 mM HEPES and 50 µM 2-mercaptoethanol) with 50 ng ml^{-1} phorbol-12-myristate 13-acetate (PMA, Sigma-Aldrich) and 1 µg ml^{-1} ionomycin (Sigma-Aldrich) in the presence of Brefeldin A (eBioscience) for 4 h at 37ºC. Alternatively, for T cell stimulation single cell suspensions were stimulated with 2 µg ml^{-1} of plate bound αCD3 and 5 µg ml^{-1} of soluble αCD28 in complete supplemented RPMI containing for 4 h at 37ºC in the presence of Brefeldin A. For NK cell stimulation, single cell suspensions were stimulated with 40 µg ml^{-1} of plate bound αNK1.1 in complete supplemented RPMI in the presence of

Brefeldin A and αCD107 antibody, for the detection of degranulating cells, for 4 h at 37ºC. For DC restimulation and IL-12 detection, single cell suspensions were stimulated with 10 ng ml^{-1} of LPS (from *E. coli* O111:B4, Sigma Aldrich) and 10 ng ml^{-1} of mouse recombinant IFN-γ (Miltenyi). After restimulation, cells were stained for extracellular and intracellular markers as described. In all experiments cells were stimulated for 1 hour and then Brefeldin A was added for the remaining 3 hours of the assay.

2.20 IFN-γ ELISpot

Single cell suspensions prepared from the spleen as described were counted, and 5 x 10^5 cells were seeded in 96-well ELISpot plates (MSIP PVDF-plates, Millipore) which were pre-coated overnight with primary anti-mouse IFN-γ antibody (clone AN18, Mabtech), and incubated overnight with either only media as a control or 10 µg ml^{-1} of different peptides (Table 1).The next day, IFN-γ producing colonies were detected using a biotinylated anti-mouse IFN-γ detection antibody (clone R4-6A2, Mabtech) following manufacturer instructions. Spot forming units (IFN-γ spots) were automatically counted using AID ELISpot Reader (GmbH). Results were expressed as the difference between the number of IFN-γ spots obtained in response to a given peptide and the number of IFN-γ spots obtained when incubated with media alone.

Peptide	*Sequence*	*MHC Allele*	*Source*
OVA$_{257-265}$	SIINKEFL	H2-K^b	Genscript
HY Uty$_{246-254}$	WMHHNMDLI	H2-D^b	Genscript
HY Dby$_{608-622}$	NAGFNSNRANSSRSS	H2-A^b	Genscript
LCMV gp$_{33-41}$	KAVYNFATM	H2-D^b	Genscript
MuLV p15E	KSPWFTTL	H2-K^b	Genscript

Table 1. Peptides used for splenocyte stimulation

2.21 Splenocyte cytotoxicity assay

1x10^4 MB49-ZsGreenLuc, B16-F10-ZsGreenLuc or LLC-ZsGreenLuc tumor cells were seeded in dark flat 96-well plates (ThermoFisher) as target cells. Splenocytes from tumor bearing mice were obtained as described, counted, and seeded at a 100:1 ratio over the target cells in complete RPMI supplemented with non-essential aminoacids, 10 mM HEPES and 50 µM 2-mercaptoethanol. After 20 h, live tumor cells were detected by adding

150 µg ml^{-1} of Xenolight D-luciferin Potassium Salt (Perkin Elmer) to the wells and incubating for 15 min at 37ºC. The resulting luminescence was measured in an Epoch Microplate reader (BioTek). Percentage cytotoxicity was calculated in reference to wells incubated without splenocytes.

2.22 NK cell cytotoxicity assay

$1x10^4$ tumor cells labelled with CellTrace Violet (CTV; Invitrogen) were seeded in flat 96-well plates as target cells. NK cells were isolated from the spleens of mice by magnetic separation with anti-CD49b (DX5) microbeads (Miltenyi). Purity of NK cells isolated by this method was around 70 %, analysed by flow cytometry in every experiment. Isolated NK cells were seeded over target tumor cells at different effector to target ratios in triplicates in complete RPMI supplemented with non-essential aminoacids, 10 mM HEPES and 50 µM 2-mercaptoethanol. After 20 h, cells were detached with trypsin-EDTA, stained with FITC-conjugated Annexin V (Miltenyi) and 7-AAD (Miltenyi) and analysed by flow cytometry. Cell death was analysed in the CTV^+ tumor cell population.

2.23 Proliferation assay

BMDCs prepared as described were loaded with 1 µg ml^{-1} of LCMV gp_{33-41} peptide (Table 1) for 2 h at 37 ºC. Lung single cell suspensions from tumor-bearing mice prepared as described were stained with CTV following manufacturer instructions. Then $2,5x10^5$ lung cells were mixed with $4x10^4$ loaded BMDCs in round 96-well plates and incubated for 72 h. Then, cells were stained with CD45, CD3 and CD8-directed antibodies and CTV dilution was analysed in $CD3^+$ $CD8^+$ T cells. Results were expressed as the percentage of cells that have undergone proliferation.

2.24 Staining of single cell suspensions with fluorochrome-conjugated antibodies

Single cell suspensions were first incubated with mouse Fc receptor blocking reagent (Miltenyi) for 20 min at 4ºC in FACS buffer (PBS, 2 % FBS, EDTA 2 mM), washed, stained with different combinations of fluorochrome-conjugated antibodies (Table 2) for 20 min at 4ºC in FACS buffer, washed again and fixed in 4 % paraformaldehyde (PFA) for 20 min at room temperature. For staining of intracellular proteins, cells were further fixed

and permeabilized with the FoxP3 staining set (Miltenyi) and stained with fluorochrome-conjugated antibodies (Table 3) for 30 min at room temperature.

ANTIBODY	CLONE	SOURCE	FLUOROCHROME
CD45	REA737	Miltenyi	Vioblue,FITC, PerCP-Vio700
CD11b	REA592	Miltenyi	PerCP-Vio700, PE
CD11c	REA754	Miltenyi	PE, FITC
F4/80	REA126	Miltenyi	PE
CD4	REA604	Miltenyi	FITC, APC-Vio770
CD8	REA601	Miltenyi	PE, FITC, APC
CD3	REA641	Miltenyi	PerCP-Vio700, PE
MHC-II	REA813	Miltenyi	Vioblue, APC
XCR1	REA707	Miltenyi	APC
SIRPα	REA1201	Miltenyi	APC-Vio770
CCR7	4B12	Biolegend	PE
H2K^b/D^b	REA932	Miltenyi	APC, PE
CD86	REA1190	Miltenyi	VioBright, PE
CD40	REA965	Miltenyi	VioBright
NKp46	REA815	Miltenyi	FITC, PE
CD49b	DX5	Miltenyi	APC-Vio770
CD64	REA286	Miltenyi	APC-Vio770, PE
SIGLECF	REA798	Miltenyi	APC, PE
LY6C	REA796	Miltenyi	APC
LY6G	REA526	Miltenyi	Vioblue
PD-L1	MIH5	BD	PE
CD206	C068C2	Biolegend	PerCP-Cy5.5
PD-1	J43	BD	APC
PD-1	REA802	Miltenyi	PerCP-Vio700
TIM-3	5D12/TIM-3	BD	BV421
KLRG1	2F1	Miltenyi	APC-Vio770
QA-1^b	6A8.6F10.1A6	BD	PE
GALECTIN9	RG9-35.7	Miltenyi	PE-Vio770

LAG-3	C9B7W	Miltenyi	FITC
CD69	REA937	Miltenyi	FITC
ICOS	7E.17G9	Miltenyi	PE
CD107a	1D4B	BD	FITC
CD49a	Ha31/8	Biolegend	AF647
CD44	IM7.9.1	Miltenyi	Vioblue
CD48	REA1238	Miltenyi	PerCP-Vio700
CD34	REA383	Miltenyi	FITC
CD150	Q38-480	BD	BV421
FLT3	A2F100.1	BD	PE-CF594
c-KIT	REA791	Miltenyi	APC
SCA-1	D7	BD	APC-Cy7
TER119	Ter-119	Miltenyi	PE
B220	RA3-6B2	Miltenyi	PE

Table 2. Fluorochrome-conjugated antibodies for extracellular staining

ANTIBODY	CLONE	SOURCE	FLUOROCHROME
IFN-γ	REA638	Miltenyi	FITC, PE, APC
TNF	MP6-XT22	BD	PE
IL-2	JES6-5H4	BD	FITC
IL-12 (p40/p70)	REA136	Miltenyi	PE
iNOS	REA982	Miltenyi	PE, FITC
T-BET	REA102	Miltenyio	PE
GATA3	REA174	Miltenyi	APC
GRANZYME B	REA226	Miltenyi	FITC, PE
TCF1/7	S33-966	BD	AF488
CCL5	2E9/CCL5	Biolegend	PE
STAT1	1/STAT1	BD	AF647
STAT3	M59-50	BD	PerCP-Cy5.5
pSTAT1 (PY701)	4a	BD	BV421
CLEAVED CASPASE 3	C92-605	BD	AF647

Table 3. Fluorochrome-conjugated antibodies for intracellular staining

2.25 Dextramer staining

For staining with gp33-specific (KAVYNFATC) H2-D^b Dextramers (Immudex), lung or spleen single cell suspensions were blocked with Fc receptor blocking reagent, washed, and stained with fluorochrome-conjugated dextramer for 10 min at room temperature in FACS buffer. Without washing, antibodies for extracellular proteins were added and incubated for 20 min at 4ºC. Then, cells were washed 5 times in FACS buffer, fixed in 4 % PFA and further stained for intracellular markers if needed.

2.26 Flow cytometry

Cells were acquired using a Gallios flow cytometer (Beckman Coulter). Fluorescence minus one (FMO) stained controls were used for the discrimination of negative and positive populations and for the correction of fluorescence spill-over of the different fluorochromes. Data concerning optimization and compensation of the different flow cytometry antibody panels used in this study is not shown although it was performed for each panel described. Flow cytometry results were analysed using Weasel software (version 3.0.2), following the gating strategies described below. Results have been expressed either as the percentage of cells staining positive for a marker inside a given population of cells, or as the Mean Fluorescence Intensity (MFI) of a marker inside a population of cells.

Generic gating strategies and FMOs for bladder and lung tumors are shown below, although more detailed descriptions and specific gating strategies are given throughout the results section.

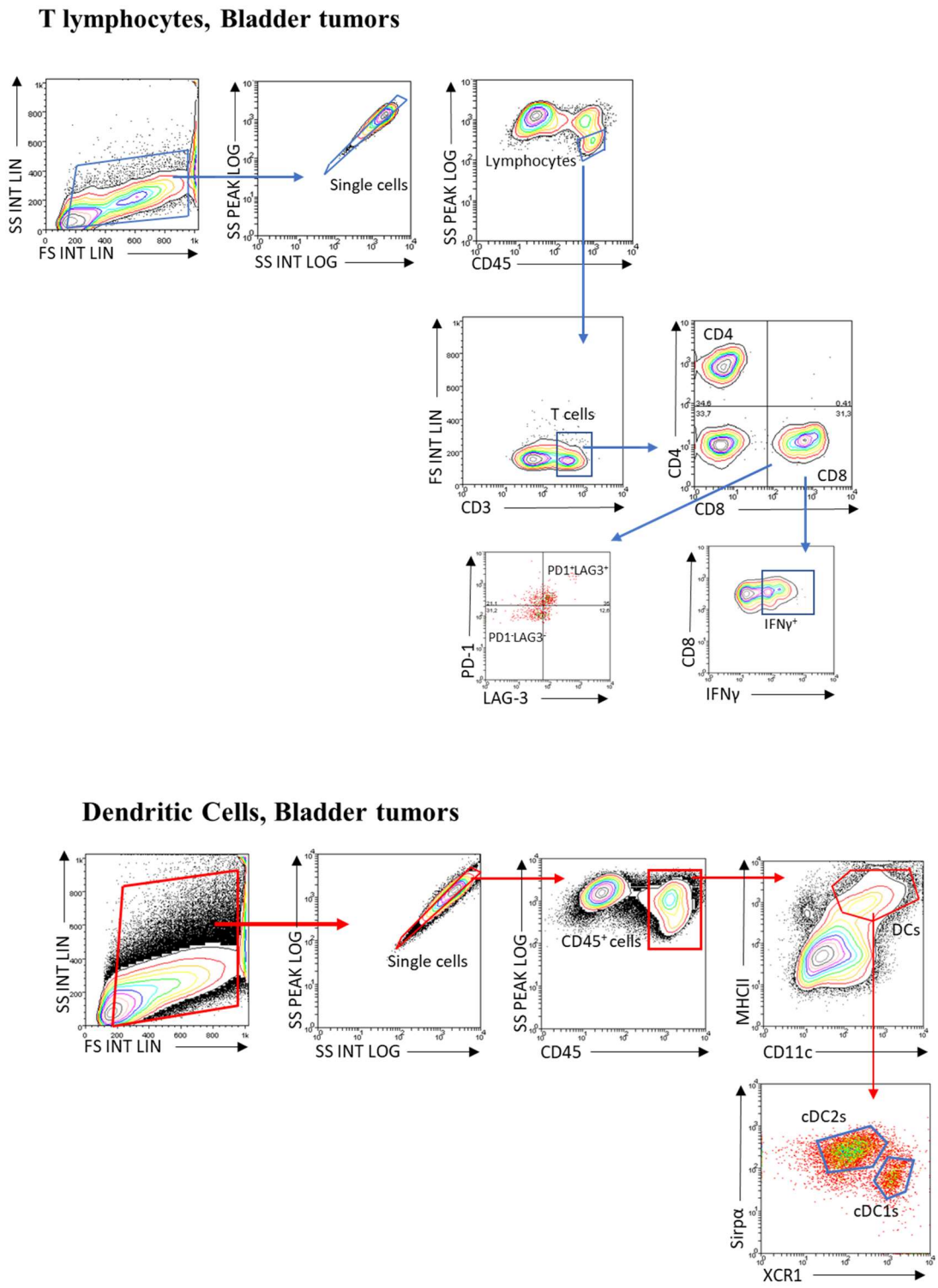

Flow cytometry gating strategy for T cell and DC identification in bladder tumors.

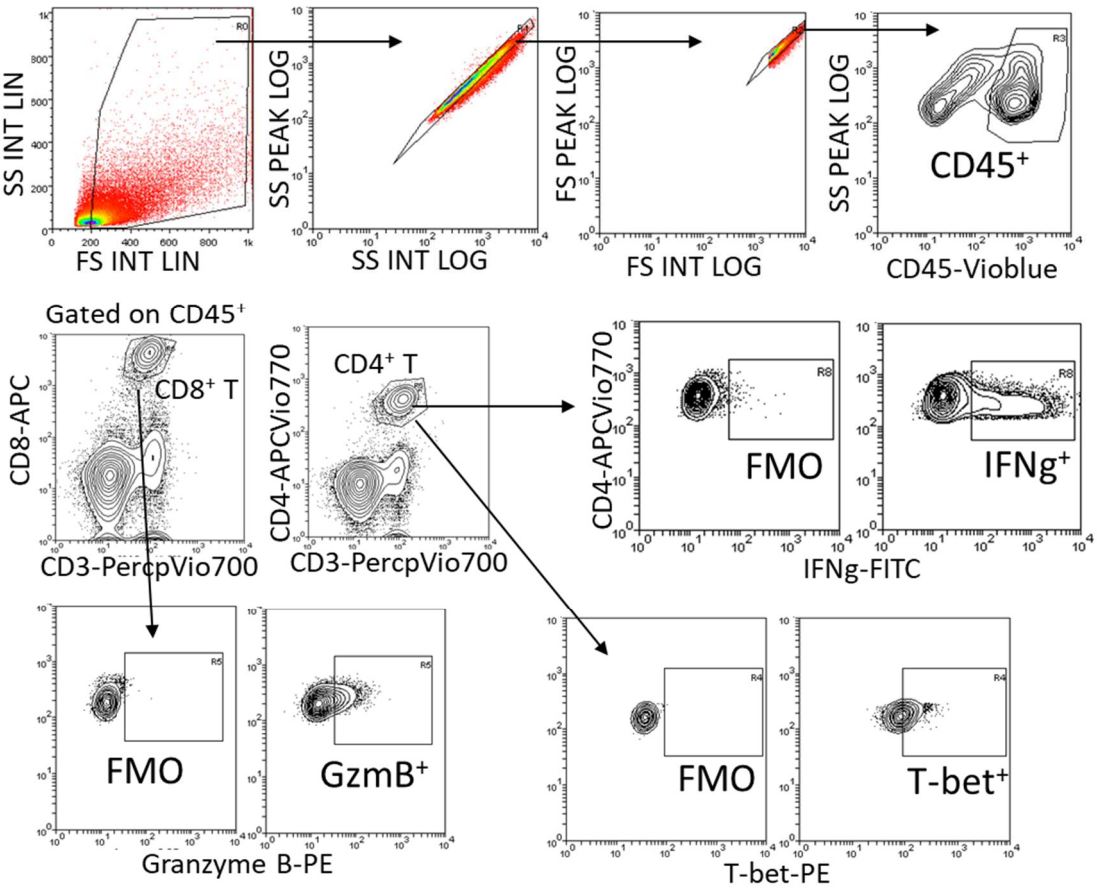

Flow cytometry gating strategy for T cell identification in the tumor-bearing lung and FMOs for specific markers.

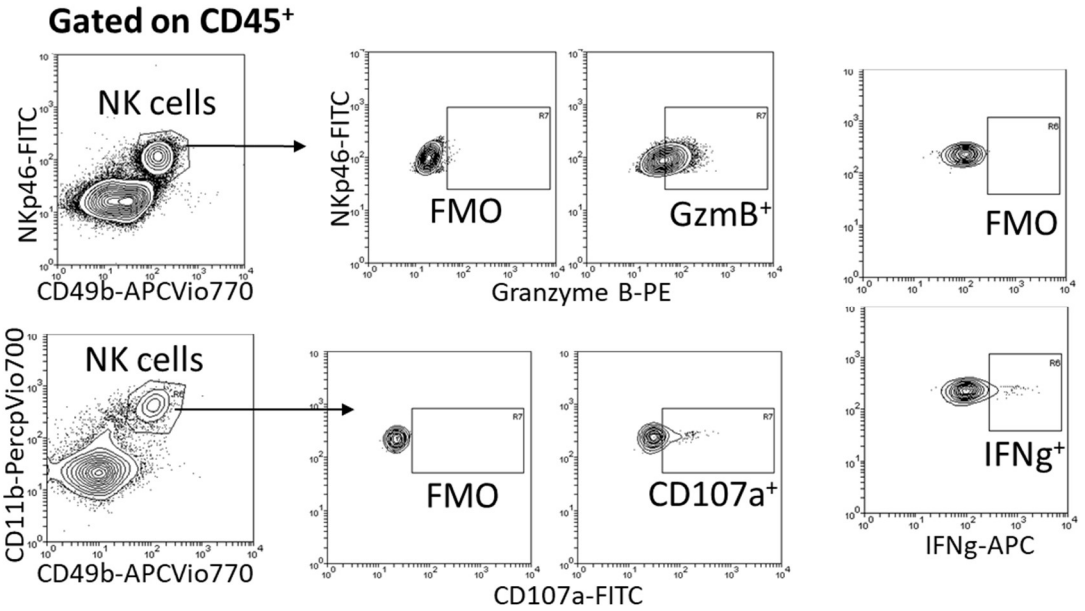

Flow cytometry gating strategy for NK cell identification in the tumor-bearing lung and FMOs for specific markers.

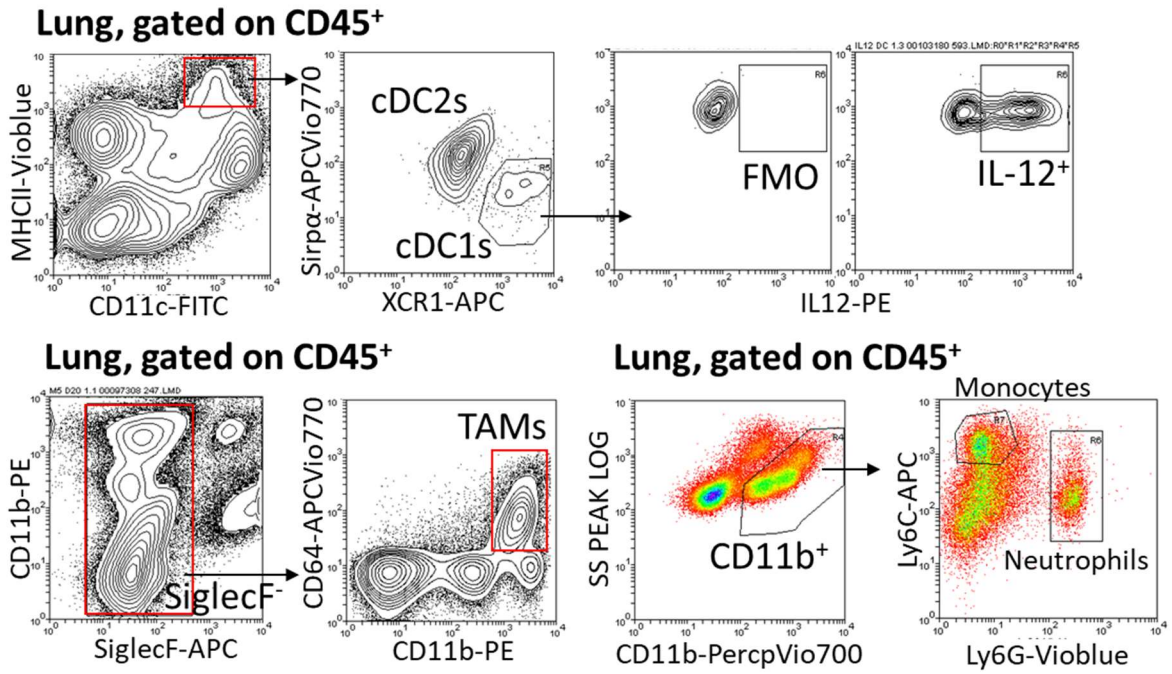

Flow cytometry gating strategy for myeloid cell identification in the tumor-bearing lung.

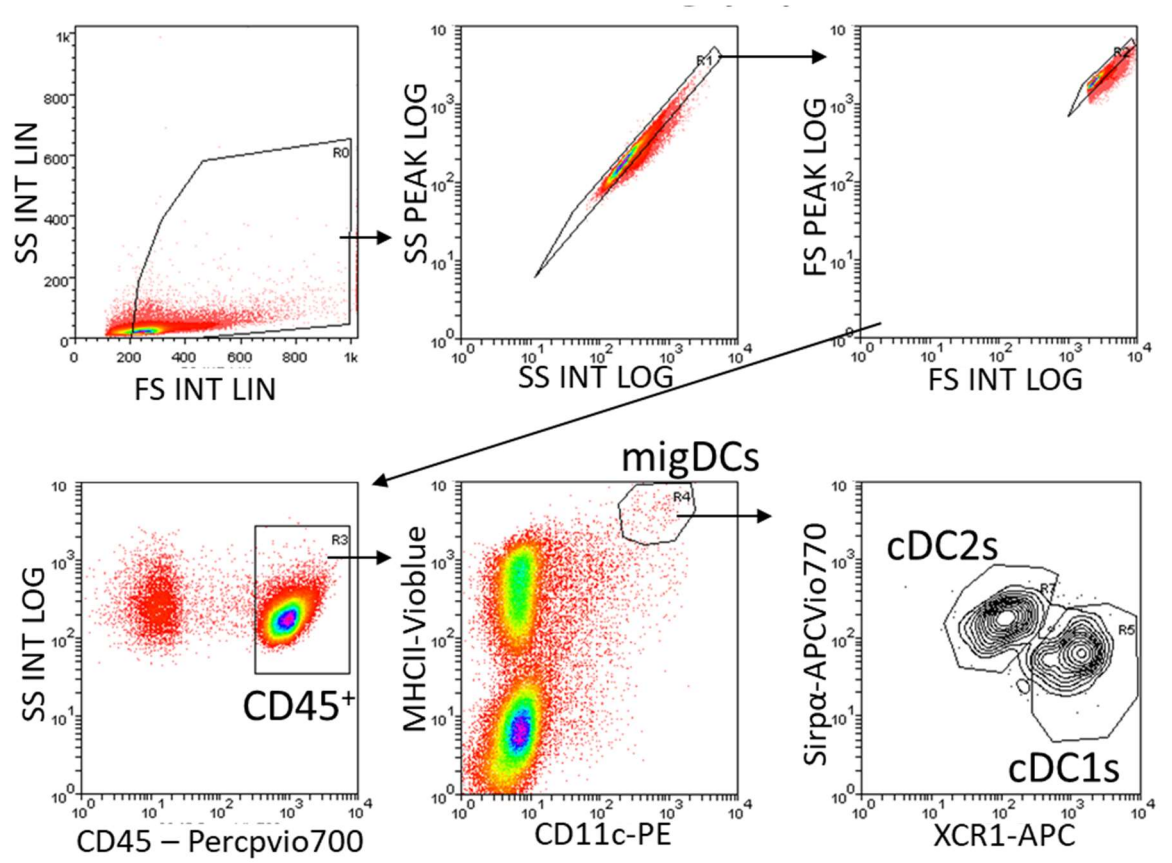

Flow cytometry gating strategy for DC identification in the mediastinal and bladder draining lymph nodes.

2.27 Histological analysis

For lung histopathology analysis, lungs were aseptically removed and fixed in 4 % formaldehyde for 24 h prior to hematoxylin-eosin (H&E) staining. Histological staining was performed in the Pathological Anatomy Service from CIBA (Zaragoza, Spain) and images were obtained with a Leica DM5000B optical microscope.

2.28 Protein extraction from tissue

Lung tissue was weighted and homogenized in a GentleMacs Dissociator in serum-free RPMI medium using a protocol for protein extraction. The homogenates were spun at 1500 rpm for 5 min and the supernatant was collected. Then, cOmplete Protease Inhibitor Cocktail (Roche) was added to the supernatants following manufacturer instructions and samples were kept frozen at -80ºC until protein determination.

2.29 Cytokine measurements

Cytokine concentration in lungs lysates or coculture supernatants was measured by ELISA (CCL5: Mouse CCL5/RANTES DuoSet, R&D Systems; IFN-γ: ELISA Flex Mouse IFN-γ, Mabtech; IL-12: ELISA Flex Mouse IL-12, Mabtech), and expressed as amount of cytokine per mg of tissue homogenized.

2.30 Study design and statistical analysis

Mice were randomized into different treatment groups after tumor inoculation. To avoid cage-associated variability, each cage contained mice from every experimental group, when possible. The number of biological replicates and repetitions for each experiment are indicated in figure legends. Animal monitoring and data analysis were not blinded.

Data from all biological replicates were included for analysis unless there were technical issues with experimental setup or data collection (flow cytometry). Outliers were not excluded. GraphPad Prism software (version 8) was used for graphical representation and statistical analysis. Kolmogorov-Smirnov test was used to check normal distribution of the data. To compare two group means, two-tailed unpaired Student's t-test (for normal distribution of data) or Mann-Whitney test (not normal) were used. To compare means between more than two groups, unpaired one-way ANOVA (for normal distribution of data) with Bonferroni's multiple comparisons post test or Kruskal-Wallis (not normal) with

Dunn's multiple comparisons test were used. For survival analysis, log-rank Mantel-Cox test was used. *P* values < 0,05 were considered significant: * $p < 0,05$, ** $p < 0,01$, *** $p < 0,001$, **** $p < 0,0001$. Data shown in graphs depicts mean +/- standard error of the mean (SEM).

Following initial optimization, studies designed for analysis of immune populations in tumor-bearing mice were generally planned to end on day 12 for bladder tumors or day 20 for lung tumors after tumor inoculation. If changes in body condition or other health issues required euthanasia before said timepoints, those mice were sacrificed and excluded from the study. In studies involving bladder tumors, absence of hematuria was considered as a sign of failed tumor implantation and those mice were excluded.

3 Objectives

In the first part of this PhD project, we optimized an orthotopically transplanted model of bladder cancer in mice in order to test different intravesical treatments with live-attenuated mycobacteria, such as BCG or MTBVAC. We studied the genetic differences between both vaccines in order to explain their differential efficacy against bladder tumors, unveiling bacterial factors that can influence antitumor potency in this context. Next, we hypothesized that intravesical MTBVAC could function by inducing tumor-specific responses against bladder tumors relying on the cross-presenting activity of cDC1s, and experimentally tested this idea. Furthermore, we devised a therapeutic strategy combining intravesical administration of bacteria with systemic antiPD-L1 mAbs which drove tumor rejection in most mice bearing bladder tumors.

In the second project of this thesis, we hypothesized that contact of BCG with the tumor may be a key factor behind its antitumor efficacy, and therefore conceived a strategy for the treatment of lung tumors consisting in intravenous inoculation of BCG, a route of administration which had previously been shown to be highly efficient at preventing tuberculosis infection. We hypothesized that BCG given by this route could strongly stimulate tumor-specific immunity in the lung, as well as modulate the TME to favour adaptive immune responses.

The main objectives of this thesis will be:

- To identify the genetic determinants which explain the differential efficacy of the live-attenuated mycobacterial vaccines BCG and MTBVAC when used as intravesical therapy for bladder cancer.
- To study the mechanism of action of bacterial immunotherapy for bladder cancer, focusing on the induction of tumor-specific adaptive immune responses and the requirement for Batf3-dependent cDC1s.
- To establish a combined immunotherapeutic approach to potentiate antitumor immune responses in mice bearing orthotopic bladder tumors.
- To devise a strategy to deliver BCG into the lung TME for inducing efficient antitumor immunity.
- To decipher which immune cell compartments and pathways participate in successful intravenous BCG immunotherapy against tumors growing in the lung.

"If some resistance based on an immunological response exists to the development and progression of spontaneous neoplasms, the BCG infected host with its greatly enhanced capacity to respond to antigenic stimulation deserves special attention in studies concerning tumor immunity."

Lloyd J. Old, 1959 "Effect of BCG Infection on Transplanted Tumours in the Mouse"

Chapter 1

Bacterial and host factors involved in intravesical therapy for bladder cancer with live-attenuated mycobacteria

---

4.1 Chapter introduction

BCG therapy of NMIBC is one example of successful immunotherapy in the clinic and offers us a unique opportunity to study immunological mechanisms that drive tumor rejection. Following decades of work in the antitumor properties of BCG[230], Morales and colleagues devised the use of 6 weekly instillations of BCG following resection of the tumor[231,363], which is still today the standard of care for high-risk NMIBC, namely carcinoma *in situ* and high-grade Ta/T1 bladder tumors[364].

In NMIBC patients receiving BCG, relapses or resistances appear in approximately 50 % of cases. Currently, there are limited options for BCG-unresponsive disease besides radical cystectomy, a life-changing intervention. Recently, pembrolizumab was granted approval for BCG-unresponsive NMIBC (KEYNOTE-057, NCT02625961), although less than 18 % complete responses without recurrence at 1 year were observed[301].

Given the historical success of BCG in the treatment of NMIBC, there have been numerous efforts to genetically modify this vaccine to make it more effective for bladder cancer treatment[365–367]. Recent examples include the recombinant BCG strain VM1002BC[368,369], currently in clinical trials, a cyclic-di-AMP overexpressing BCG strain[370,371] or engineered strains expressing immunostimulatory cytokines such as IFN-α[372]. Another strategy is finding other bacteria different from BCG that could improve it. Recent examples studied in preclinical models include Ty21a/Vivotif, a commercial vaccine against typhoid fever that showed improved efficacy in an orthotopic model of bladder cancer compared to BCG[358], or *Mycobacterium brumae*[373,374]. It is interesting to note that even *a priori* very similar BCG strains differ in their antitumoral efficacy in human bladder cancer patients, as has been reported in several independent studies[293,375]. Therefore, an effort should be made to improve this already successful immunotherapy, especially given the fact that since its approval in 1990, no agent has come close in replacing BCG for the management of this subset of NMIBC patients. Understanding its mechanism of action, considering both bacterial factors and host immune system components which drive efficient curative antitumor responses, is the first step in order to rationally improve this treatment.

The ability of bacteria to restrict tumor growth in the context of bladder cancer is thought to be a consequence of stimulation of the innate immune system, which in turn aids in the development of tumor-specific adaptive immunity, although this has yet to be formally proven.

In this chapter, first we will optimize a mouse model of bladder cancer based on orthotopic implantation of MB49 cells. Then, we will focus on studying the genetic differences between BCG and MTBVAC that explain their differential antitumor potency when delivered intravesically into tumor-bearing mice. Lastly, we will dissect the immune pathways that are triggered by intravesical administration of MTBVAC to drive effective antitumor immunity, shedding light on the mechanism of action of bacterial immunotherapy for bladder cancer.

4.2 Optimization of an orthotopic mouse model of bladder cancer

In order to study the therapeutic effect of live-attenuated mycobacteria for bladder cancer, first we needed to develop a mouse model which allowed us to recapitulate the biology of the disease. We chose to use orthotopic transplanted tumors, meaning that the tumor grows in its organ of origin. Importantly, orthotopically transplanted tumors resemble the TME and immune contexture found in human tumors more faithfully than the traditional subcutaneously grown models, which was important for us since we wanted to mechanistically dissect the immune response against bladder tumors[376,377]. Also, the clinical practice of intravesical BCG treatments cannot be faithfully modeled in subcutaneous models as in orthotopic bladder tumors.

For bladder cancer, orthotopically transplanted tumors have already been described[378,379] and are based on intravesical inoculation of tumor cells into the bladders of mice. Different tumor cell lines can be used to this end, although the MB49 bladder cancer cell line is the most used in the field. MB49 derived epithelial tumors grow towards the bladder lumen in an aggressive manner without invading the muscle, mimicking the Ta and T1 stage of human NMIBC. Tumor establishment is usually confirmed by appearance of hematuria, which generally occurs between 6 and 8 days after tumor cell inoculation. Indeed, mice which do not show hematuria do not develop tumors and are excluded from survival experiments.

In our pilot experiments with the MB49 model, tumor take and kinetics of survival were highly variable, which prompted us to optimize different parameters before carrying out therapeutic efficacy experiments. Our goal was to reflect as closely as possible human disease and the clinical procedure of BCG instillation.

We identified appearance of tumors in the upper urinary tract and kidneys in a considerable number of mice as the first problem in our model, since it would not allow us to properly evaluate survival to bladder tumors. We thought that this could be due to using an inadequate volume for instillations (100 µl), which would cause vesico-ureteral reflux of tumor cells[380]. Indeed, volumes of 50 µl are used in the literature[340,381]. Lowering the volume from 100 µl to 50 µl and performing the instillation at a low rate (approximately 10 µl every 10 seconds)[382], allowed us to solve the issue of tumor implantation in the kidneys because of vesico-ureteral reflux.

Next, we titrated the number of cells to be inoculated (Figure 22), finding that the dose of tumor cells inversely correlated with median survival of mice. We chose a medium dose of $4x10^5$ cells, since we wanted enough therapeutic window to administer at least 2 or 3 weekly intravesical bacterial treatments (indicated by arrows in Figure 22), mirroring the clinical practice, and at the same time aiming for a 100 % tumor take to minimize the number of mice to be used in each experiment.

Importantly, we also observed that the passage number of MB49 cells is a critical parameter determining tumor take and survival kinetics. In our hands, a higher number of *in vitro* passages decreased the tumorigenic potential of MB49 cells. Therefore, in all the experiments shown, MB49 cells were used with less than 5 passages from thawing.

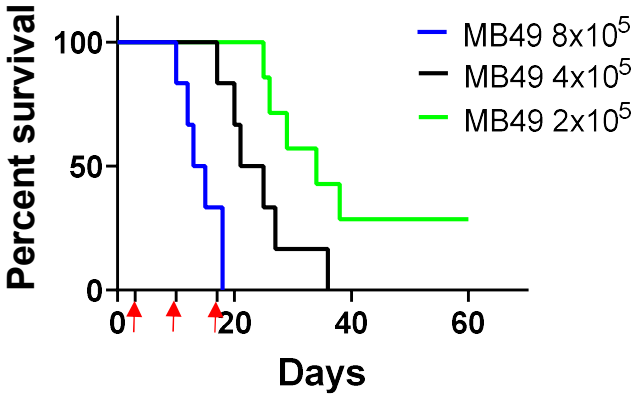

Figure 22. Survival of mice implanted with MB49 cells orthotopically in the bladder with the indicated doses of MB49 cells. Red arrows indicate the timepoints in which we would want to perform the intravesical bacterial treatments (days 3, 10 and 17).

In the MB49 model of NMIBC, mice usually succumb either because of inability to urinate, which causes rapid weight loss, or due to prolonged high tumor burden in the bladder. The fact that tumor cells inoculated intravesically can be established in any area of the bladder makes this model highly variable in terms of mice survival[383]. Concretely, we have observed that tumors established near the urethra can obstruct it, which causes rapid weight loss due to inability to urinate. Other tumors that are established further away from the urethra can grow without affecting the ability of to urinate, and therefore these mice survive longer. This phenomenon can be observed my manual palpation of the bladder. By applying gentle pressure to the bladder, mice urinate only if the urethra is not obstructed by the tumor. Therefore, we can find mice that succumb as early as 15 days post-tumor cell inoculation, or as late as 50 days. We have also consistently found cases of tumor recurrence in the bladder. In some cases, mice apparently cured from bladder tumors in which hematuria disappeared and there were no palpable signs of tumor for 20 or more days, can suddenly go on to develop again hematuria and signs of a visible growing tumor, succumbing as late as 60 days post tumor cell inoculation.

Lastly, cases of MB49 metastasis to the lung were rarely detected, and only in mice which survived for long periods of time. In these cases, when mice were sacrificed due to tumor burden in the bladder and rapid weight loss, small but visible tumor foci were detected in the lung. These tumor foci were generally small (< 1 mm), most likely not affecting mouse survival as the primary bladder tumor.

In summary, we developed a mouse model of NMIBC which recapitulates some aspects observed in human bladder cancer, such as presence of hematuria, tumors growing towards the lumen of the bladder without invading the muscle layer and episodes of recurrence in apparently cured individuals.

4.3 Intravesical treatment of bladder tumors with live-attenuated mycobacteria

Once we had an optimized model of bladder cancer, we went on to test intravesical treatments with different live-attenuated mycobacteria. First, we wanted to study the efficacy of BCG in our model. We used the Tice strain of BCG, which we cultured from a commercial vial of OncoTice®, used in clinical practice for bladder cancer treatment. We initially tested BCG Tice starting the three weekly treatments one day after MB49 tumor cell inoculation in the bladder (Figure 23) because in the literature, BCG administered following this schedule generally drives an antitumoral effect[332,342,355,379]. In these experimental conditions, we found a therapeutic effect of BCG Tice (Figure 23), with slightly more than 50 % of mice surviving in the BCG group compared to 2 % in the PBS controls. Therefore, our model of NMIBC responds to intravesical BCG when the treatment is initiated very early, which agrees with the existing literature.

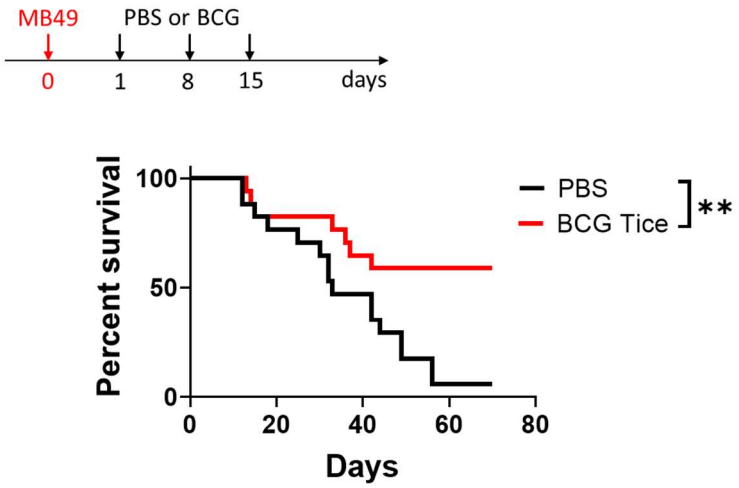

Figure 23. Survival of mice implanted with MB49 cells in the bladder and treated with intravesical PBS or BCG Tice following the indicated schedule. *n* = 20 PBS, *n* = 18 BCG, pooled from 2 independent experiments. ***P*<0.01, log-rank (Mantel-Cox) test.

Next, we chose to delay the weekly intravesical treatments until day 3 after tumor cell inoculation (Figure 24). Under these experimental conditions, generally BCG is not capable

of improving mice survival[204,340]. Therefore, delaying intravesical treatments until day 3 could be considered as a strategy to model BCG-unresponsive NMIBC in order to test new therapeutic approaches for this condition[204].

Previously, we demonstrated that MTBVAC was superior to BCG Pasteur in this experimental setting[355], although we wanted to confirm this finding with our refined protocols and with a BCG strain used in clinical practice (BCG Tice "OncoTice"). We observed that weekly intravesical treatment with MTBVAC improved mice survival compared to BCG Tice (65 % tumor-free survival in MTBVAC vs 2 % in BCG), which was completely ineffective in slowing tumor growth compared to PBS controls in this experimental setting (Figure 24).

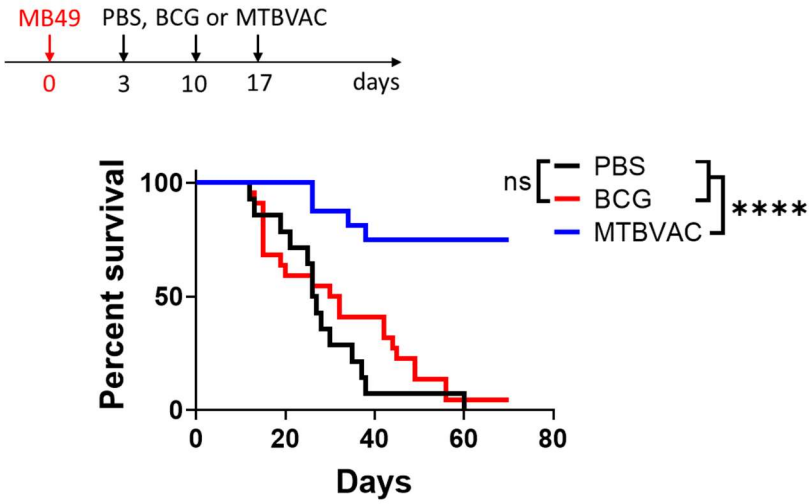

Figure 24. Survival of mice implanted with MB49 cells in the bladder and treated with intravesical PBS, BCG or MTBVAC following the indicated schedule. *n* = 22 PBS, *n* = 18 BCG, *n* = 16 MTBVAC, pooled from 2 independent experiments. ns: not significant, ****$P<0.0001$, log-rank (Mantel-Cox) test.

Therefore, we confirm our previously published results and describe that the live-attenuated mycobacterial vaccines BCG and MTBVAC differ in their efficacy against orthotopically-transplanted MB49 bladder tumors. Importantly, MTBVAC showed antitumoral efficacy in a BCG-unresponsive scenario.

4.4 Bacterial colonization of the bladder following intravesical instillation

Next, we set out to explain the improved antitumoral efficacy of MTBVAC compared to BCG, given that they are similar mycobacteria with a high degree of genetic homology

(>99 %)[352]. However, genetic differences between both bacteria are mostly defined, facilitating the identification of potential factors behind this phenomenon.

Colonization of the bladder by the bacteria has been described as a key factor behind its antitumoral activity in the context of intravesical therapy for bladder cancer in mice and humans[384]. Indeed, BCG attachment to the bladder epithelium through fibronectin-attachment proteins is a prerequisite for antitumoral efficacy[314,315,385], and low attachment may cause treatment failure[386,387]. Therefore, we initially hypothesized that MTBVAC could be more efficient than BCG either in adhering to the bladder epithelium or in infecting tumor cells.

To test this, we induced MB49 bladder tumors and performed 3 weekly intravesical treatments with either BCG or MTBVAC. At day 18, we analyzed the bacterial load in bladder tumors and bladder-draining lymph nodes (bdLNs), also known as the periaortic or iliac lymph nodes[204], by plating tissue homogenates in solid mycobacterial growth medium. Our results revealed a higher amount of MTBVAC bacilli both in the bladder and bdLNs compared with BCG Tice, which was barely detected in both compartments (Figure 25).

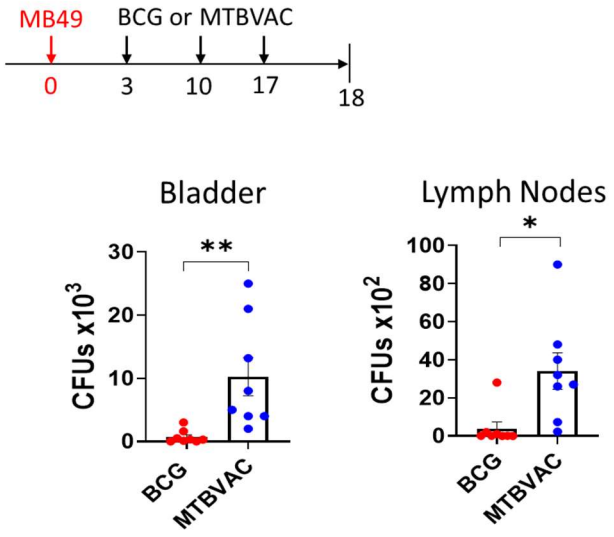

Figure 25. Enumeration of BCG and MTBVAC CFUs in the bladder and bdLNs of tumor-bearing mice treated as shown in the figure. *n* = 8 mice per group, pooled from 2 independent experiments. **P*<0.05, ***P*<0.01, unpaired t-test.

This result could mean either that MTBVAC is superior to BCG in adhering to the bladder epithelium, at infecting bladder tumor or epithelial cells or better fitted to survive in the bladder. The higher bacterial load observed in bdLNs most likely is a result of the higher

load in the bladder in the case of MTBVAC-treated mice. Since mycobacteria are intracellular pathogens, they travel to the lymph nodes inside DCs, at least in the case of *M. tuberculosis* infection[388]. Therefore, myeloid cells may be infected in bladder tumors by mycobacteria and allow transport to the bdLNs.

Therefore, we hypothesized that intravesically administered mycobacteria do not infect tumoral or epithelial cells, but that they initially attach to the bladder epithelium and, in cases of tissue damage such as presence of tumor or following resection, exposed myeloid cells may be internalizing them. Clasically, BCG has been described to infect diverse bladder tumor cell lines[317,389,390], but these experiments are peformed *in vitro* in 2D cultures in which simply by gravity bacteria are forced to enter in contact with seeded tumor cells. This does not accurately model intravesical instillation of mycobacteria into the bladder.

To determine which bladder cellular subsets internalize mycobacteria *in vivo*, we inoculated tumor-bearing mice with BCG Tice or MTBVAC strains engineered to express GFP, which originally allowed us to detect infected cells in the lungs after intranasal inoculation[264], and here were used for detecting infected cells in bladder tumors following intravesical instillation. Since we expected a low number of infected cells, we performed the analysis 2 hours after the last intravesical instillation to maximize detection (Figure 26A).

Flow cytometry analysis of digested bladder tumors revealed that fluorescent bacteria-containing cells could be detected when compared to control PBS-treated mice, specially in MTBVAC-GFP treated mice (Figure 26B). Confirming our results obtained by plating bladder homogenates, MTBVAC was more efficient than BCG in colonizing bladder tumors, evidenced by a higher percentage of GFP^+ infected cells among total isolated cells (Figure 26C).

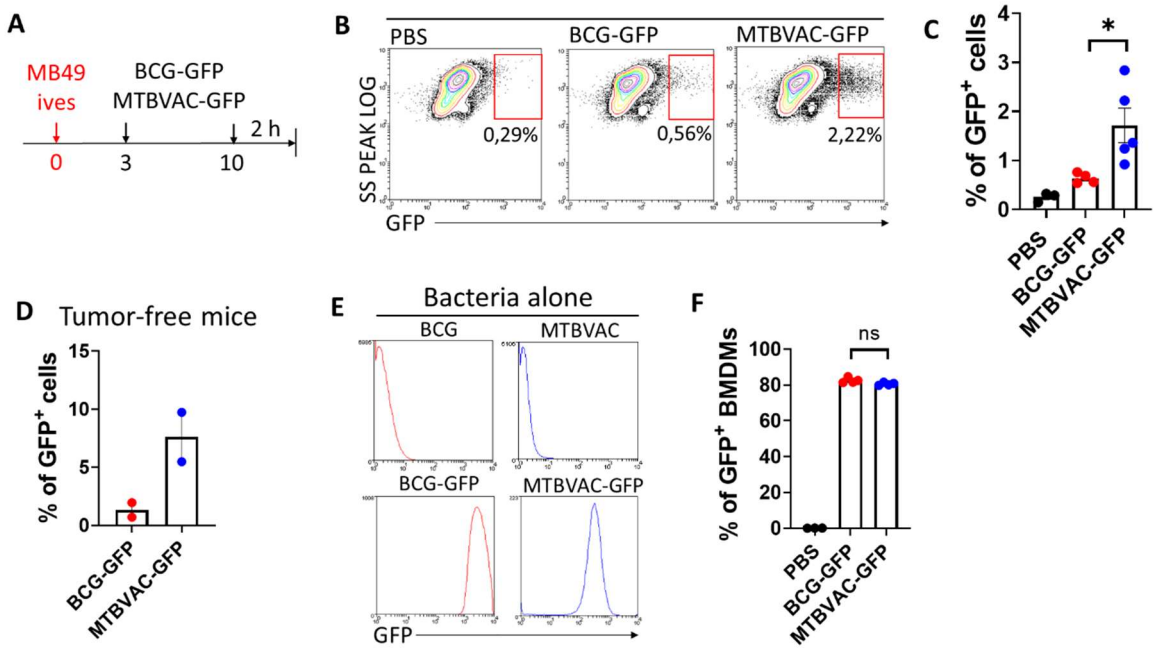

Figure 26. Mice were treated as in (A) and bladders processed into single cell suspensions. (B,C) Representative flow cytometry contour plots for identification of infected GFP$^+$ cells in bladder tumors and quantification of the % of infected cells among total cells, *n* = 3 (PBS), *n* = 4 (BCG Tice-GFP) and *n* = 5 (MTBVAC-GFP), from one experiment. (D) Mice were treated as in (A) but without bladder tumor induction. Shown is the % of infected cells among total cells in the bladder, *n* = 2 mice/group, from one experiment. (E) Flow cytometry representative contour plots of GFP expression by BCG Tice and MTBVAC wild-type strains and their GFP-expressing counterparts. (F) DIifferentiated BMDMs were infected with GFP-tagged mycobacteria at a 10:1 MOI. 4 h later, BMDMs were detached and % of infected F4/80+ cells analyzed by flow cytometry. n = 3-4 experimental replicates per group, from one independent experiment.

This finding was replicated in tumor-free mice, meaning that live-attenuated mycobaceria were also capable of colonizing healthy bladder tissue (Figure 26D). As a control, GFP fluorescence intensity of the two bacterial strains was compared, finding that BCG-GFP was not less fluorescent than MTBVAC-GFP, therefore the observed differences were not due to higher GFP expression by MTBVAC-GFP bacilli (Figure 26E). We also evaluated whether MTBVAC-GFP was more efficiently internalized by BMDMs in vitro compared with BCG-GFP, but found no differences in the percentage of infected BMDMs after 4 h of incubation at a MOI of 10:1 (Figure 26F). Therefore, enhanced phagocytosis by myeloid cells does not explain the increased ability of MTBVAC to colonize the bladder .

We further analyzed which cellular subsets contained fluorescent bacteria in bladder tumors following intravesical inoculation. Strikingly, in all mice analyzed for both BCG and MTBVAC, around 95 % of all GFP$^+$ infected cells were CD45$^+$ immune cells (Figure 27).

Less than 5 % of infected cells were $CD45^-$, a population comprising tumor cells, untransformed epithelial cells and fibroblasts (Figure 27). Therefore, although mycobacteria can infect bladder tumor cells *in vitro*, this does not seem to happen *in vivo*, at least in our specific model.

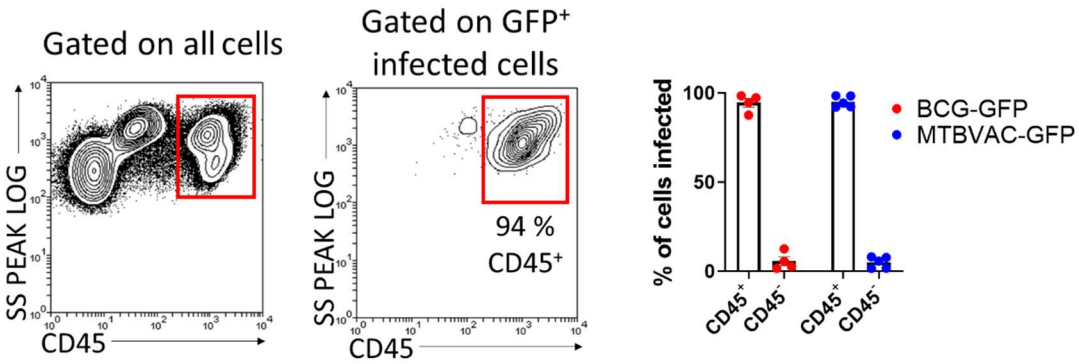

Figure 27. Mice were treated as in Figure 26. Shown are representative contour plots for defining the phenotype of infected GFP^+ cells in bladder tumors, and quantification of infected cell distribution among $CD45^-$ and $CD45^+$ subsets. *n* = 4-5 mice/group, from one experiment.

To analyze specifically which immune cells were harbouring mycobacteria in bladder tumors, here we will focus on MTBVAC-GFP treated mice since they had more infected cells, making the analysis easier, although similar results were obtained with BCG-GFP (Figure 28).

Our results revealed that most infected cells (around 90 %) in bladder tumors stained positive for CD11b (Figure 28), suggesting myeloid origin. Further analysis of the $CD11b^+$ subset revealed that bacteria were contained in monocytes ($CD11b^+$ $Ly6C^+$), neutrophils ($CD11b^+$ $Ly6G^+$) and other cells which stained negative for Ly6G and Ly6C (Figure 28). Further analysis of this population revealed that a fraction of macrophages ($CD11b^+$ $F4/80^+$ $CD64^+$) also harboured GFP-tagged mycobacteria. A $CD11b^+$ population lacking F4/80 and CD64 also contained MTBVAC-GFP, which could represent $CD11b^+$ DCs or even NK cells.

Using a separate panel, we found that $CD11b^+$ $CD11c^+$ $MHCII^+$ $Sirp\alpha^+$ cDC2s and $CD11b^-$ $CD11c^+$ $MHCII^+$ $XCR1^+$ cDC1s (probably representing the $CD11b^-$ infected population observed before) also harboured GFP-tagged MTBVAC. Therefore, inside the immune cell fraction, neutrophils appeared to be the prominent cellular subset containing mycobacteria, although they were proportionally the most abundant subset in MB49 bladder tumors

(Figure 28). Overall, we could detect GFP-tagged MTBVAC in all cell types which are known to be phagocytic: macrophages, neutrophils, monocytes and DCs.

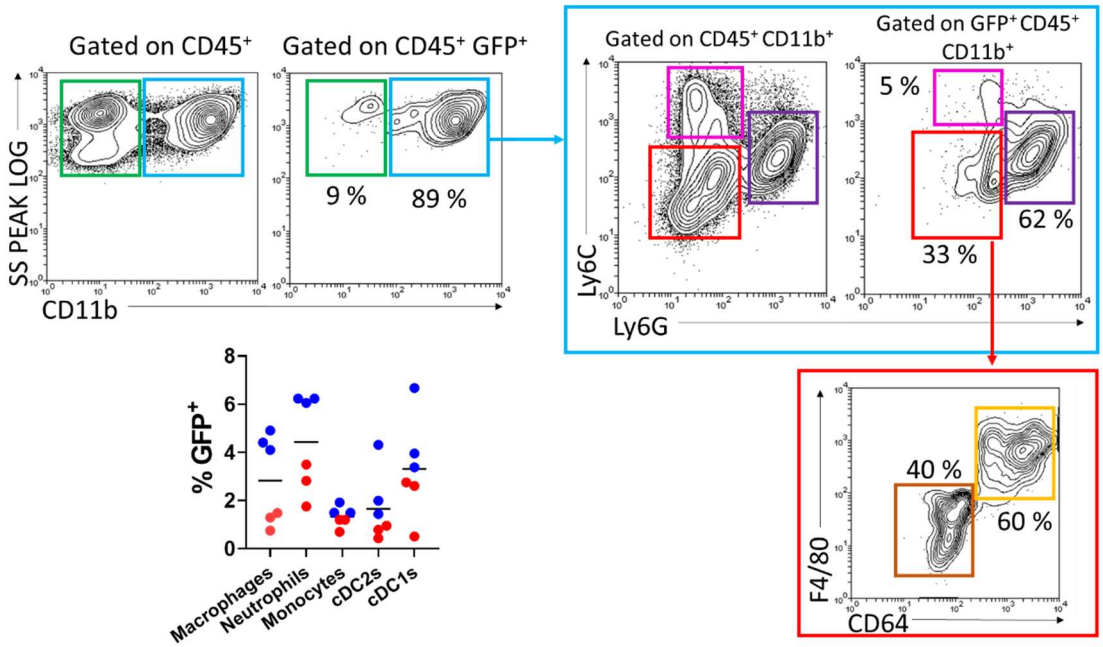

Figure 28. Mice were treated as in Figure 26. Shown are representative contour plots to phenotype infected GFP+ cells in bladder tumors, and quantification of infected cells among distinct myeloid cellular subsets. Blue dots represent MTBVAC-GFP-treated mice and red dots represent BCG-Tice-GFP treated mice. *n* = 5 mice/group, from one experiment.

Although MTBVAC-GFP could be detected in immune cells in bladder tumors, the proportion of cells containing bacteria were generally low (Figure 28). Further research is needed to determine whether internalization of mycobacteria modifyes the phenotype of infected immune cells, whether infected populations change over time, and overall whether infection of immune cells is relevant for antitumoral effect.

Next, we thought that the observed differences in bladder colonization between BCG and MTBVAC could be due to differential attachment to bladder tumor cells. To test this, we infected MB49 cells *in vitro* with a low MOI (1:1) of BCG and MTBVAC for a short period of time (2 h), to model as much as possible *in vivo* conditions when bacteria are instilled into the bladder. After 2 h of infection, a timepoint at which few MB49 cells are infected, we detached MB49 cells and stained them with an anti-TB polyclonal antibody, which binds to mycobacteria. This allowed us to detect cells with mycobacteria attached to their surface, whereas ingested bacteria are protected from staining. Results showed that after 2 h of infection, MTBVAC was more efficient at adhering to the cell surface of MB49

cells than BCG, evidenced by a higher percentage of tumor cells with bacteria attached to their surface (Figure 29),

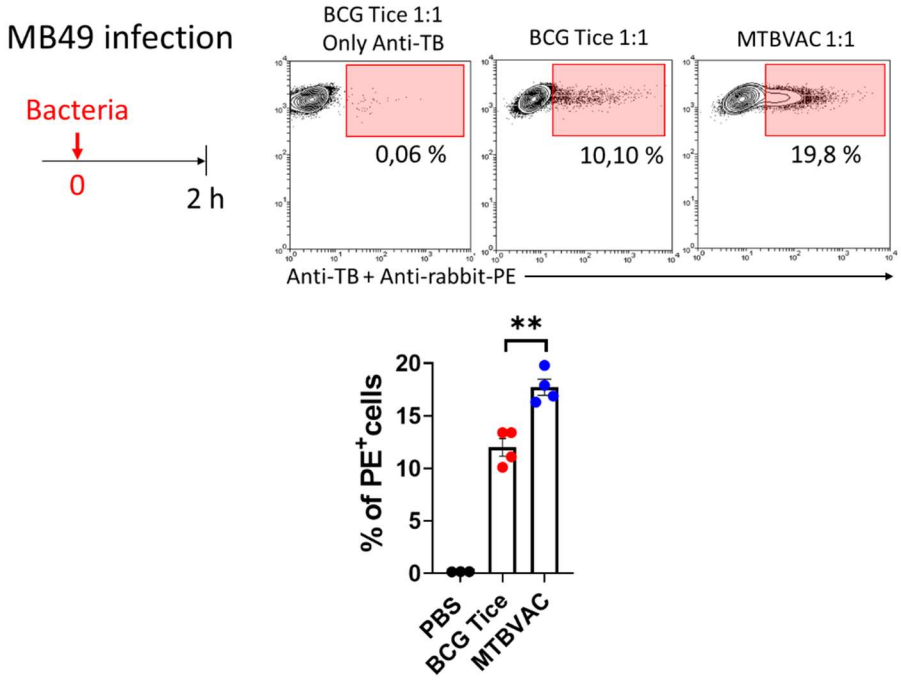

Figure 29. MB49 tumor cells were infected with mycobacteria as indicated in the Figure. In the upper side, representative contour plots after staining of MB49 cells with anti-TB polyclonal rabbit antibody + anti-rabbit-PE secondary antibody are shown, as well as quantification of the percentage of PE^+ cells for *n* = 4 experimental replicates per group, from one independent experiment.

Considering these results, we propose a mechanism by which intravesically administered mycobacteria adhere to the bladder epithelium and then are ingested by phagocytic cells. The improved ability of MTBVAC to adhere to bladder epithelium, either healthy or tumoral, would explain its higher capacity to colonize the bladder, which we have shown using two different approaches: (1) by culture of viable bacteria from bladder homogenates and (2) by identification of GFP-tagged bacteria in bladder immune cell populations by flow cytometry.

4.5 The expression of ESAT6 and CFP10 proteins by mycobacteria is critical for colonization of the bladder

Next, we wanted to study whether the observed differences in colonizing the bladder also extended to other BCG strains, since previous experiments were performed with BCG Tice. We also included in our experiments two MTBVAC strains lacking either the Antigen 85B,

which has been described as a fibronectin-attachment protein[391], or the ESAT6/CFP10 proteins, which are involved in adherence to the lung epithelium during *M. tuberculosis* infection[352,392]. The purpose of using these strains was to explain the improved capacity of MTBVAC over BCG to adhere to the bladder epithelium and colonize the bladder. Importantly, BCG does not express ESAT6 or CFP10, since they are contained in the RD1 genomic region which BCG lost during its attenuation process[393], but are expressed by MTBVAC[344]. Additionally, BCG does not secrete the Ag85B[352], as it has been predicted that a polymorphism in the Ag85B encoding gene (*fbpB*) causes an unstable protein[394], whereas Ag85B is detected in the extracellular fraction of MTBVAC cultures[352]. Therefore, we hypothesized that the expression of these proteins previously involved in adherence to the epithelium could confer MTBVAC a higher capacity to colonize the bladder.

To test this, we treated bladder tumor-bearing mice with the same dose ($5x10^6$ CFUs) of different mycobacterial strains and at day 18 bladder homogenates were plated to determine bacterial load (Figure 30).

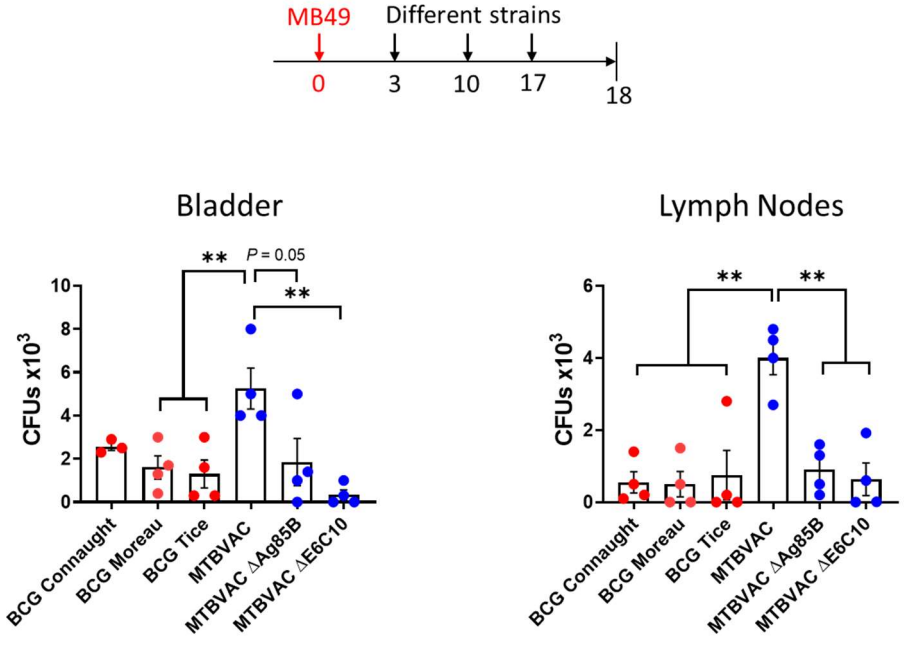

Figure 30. Enumeration of bacterial CFUs in the bladders and bdLNs of tumor-bearing mice treated as shown in the figure. *n* = 4 mice per group, from one experiment. ***P*<0.01, One-way ANOVA with Bonferroni post test.

Our results revealed that the BCG strains Connaught and Moreau behaved similarly to BCG Tice, since less CFUs were obtained from bladder tumors compared with MTBVAC.

Interestingly, the MTBVAC strain lacking Ag85B was less efficient than the parental strain (p = 0.05), whereas loss of ESAT6 and CFP10 completely abrogated the ability of the bacteria to colonize the bladder (Figure 30). Bacterial load in the bdLNs was also evaluated, finding that it correlated well with what was found in the bladder. Concretely, all three BCG strains were present at smaller numbers compared to parental MTBVAC in the bdLNs, while loss of Ag85B or ESAT6/CFP10 reverted this phenomenon (Figure 30). These results suggest that the improved ability of MTBVAC over different BCG strains to colonize bladder tumors and migrate to the bdLNs could be driven by the expression of proteins such as Ag85B and specially the ESAT6/CFP10 dimer, which are absent in BCG.

4.6 Loss of ESAT6 and CFP10 compromises antitumor efficacy

Next, we tested whether the bacterial load found in bladder and bdLNs following intravesical instillation correlated with immune cell recruitment into the bladder. We focused on three strains: BCG Tice, MTBVAC and the MBTVAC strain lacking ESAT6 and CFP10 (MTBVAC ΔE6C10), since this strain displayed the highest differences in attachment to the bladder compared to parental MTBVAC. We decided to analyze immune cell recruitment in the absence of bladder tumors, to avoid variability inherent to tumor implantation.

First, we confirmed that in non-tumor bearing mice, MTBVAC still showed a higher capacity to colonize bladder tissue compared with BCG Tice, and was also dependent on ESAT6/CFP10 expression (Figure 31A,B). Of note, to further validate our findings, we used a BCG Pasteur strain genetically complemented with the RD1 genomic region, which contains ESAT6 and CFP10 (among other proteins). As a control, a BCG Pasteur strain was used. CFU enumeration in the bladder showed that RD1 reconstitution in BCG enhanced colonization (Figure 31C), meaning that proteins contained in this region, most likely ESAT6 and CFP10, are critical for the observed differences between BCG and MTBVAC.

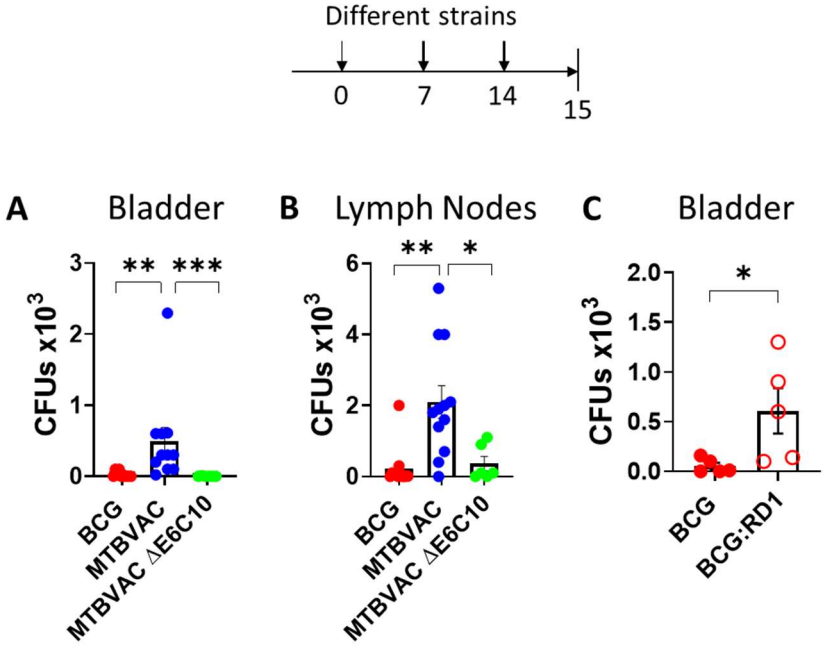

Figure 31. Enumeration of bacterial CFUs in the bladder or bdLNs of naïve mice treated as shown in the figure. *n* = 5-10 mice per group, from two independent experiments (A,B), *n* = 5 mice per group, from one experiment (C).***P*<0.01, One-way ANOVA with Bonferroni multiple comparisons test (B), Kruskal Wallis with Dunn's multiple comparisons test (A) or unpaired t-test (C). **P*<0.05, ***P*<0.01, ****P*<0.001.

Next, we evaluated immune cell recruitment to the bladder in non-tumor bearing mice (Figure 32A), focusing on $CD4^+$ T, $CD8^+$ T and NK cells since they are critical for antitumor immunity. Flow cytometry analysis of bladder digests at day 15 revealed that intravesical MTBVAC recruited significantly more $CD45^+$ immune cells, as well as $CD4^+$, $CD8^+$ and NK cells to the bladder than BCG Tice or MTBVAC ΔE6C10 (Figure 32B,C,D,E). Interestingly, T cell infiltration into the bladder following intravesical instillation correlated with bacterial load in the bdLNs of the same mice (Figure 32E,F), meaning that bacterial access to the lymph node is critical for mediating T cell recruitment to the bladder. At the same time, when the ability of the bacteria to colonize the bladder is reduced, as in BCG and MTBVAC ΔE6C10, its potential to migrate to the bdLNs is hindered, as is its capacity to induce T cell recruitment to the bladder.

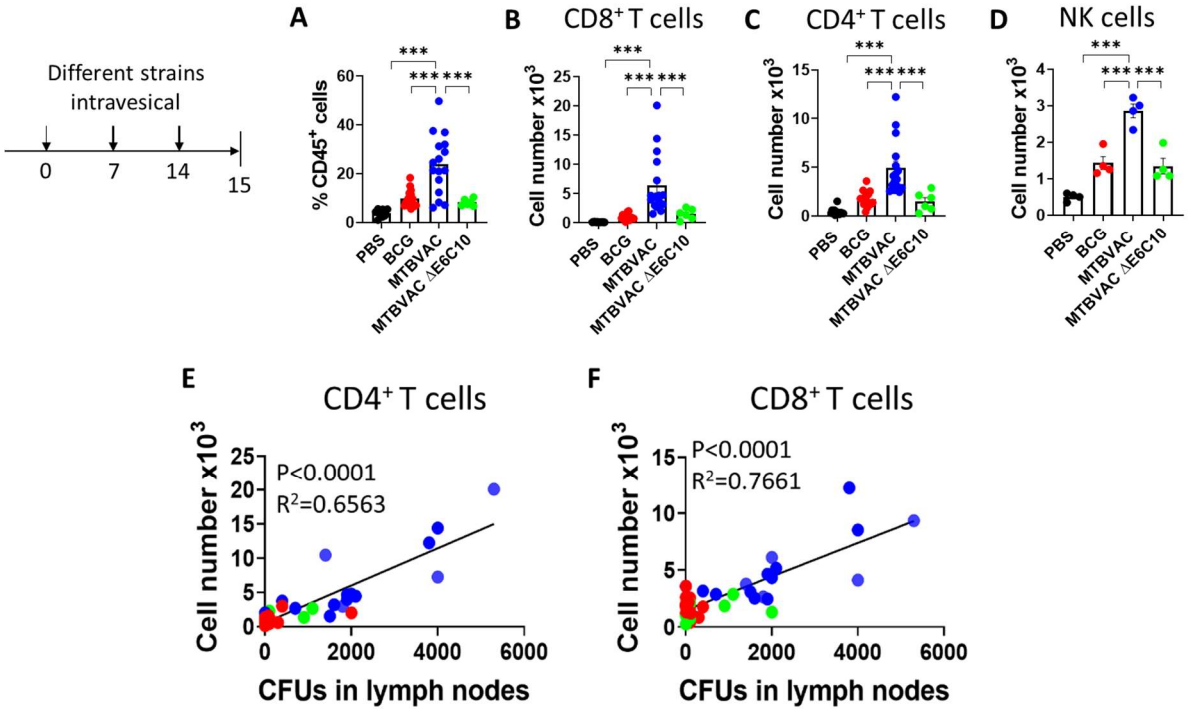

Figure 32. Mice were treated intravesically weekly with $5x10^6$ CFUs of different live-attenuated mycobacteria. At day 15, bladders were processed into single cell suspensions and distinct immune cell subsets were quantified by flow cytometry (A-D). In E and F, correlation between absolute numbers of $CD4^+$ and $CD8^+$ T cells and bacterial CFUs cultured from bladder draining LNs are shown. *n* = 6-16 mice/group, from two independent experiments.

Lastly, to determine whether the observed differences between strains influenced the antitumor efficacy of the bacteria following intravesical treatment, we conducted survival experiments in mice bearing MB49 bladder tumors. The therapeutic efficacy of the MTBVAC ΔE6C10 strain was substantially reduced to that observed with BCG Tice, with only 8% of the mice surviving at the end of the follow-up, in contrast to 60 % of mice becoming tunor-free in the MTBVAC-treated group (Figure 33). Thus, our results suggest that the expression of ESAT6 and CFP10 proteins by MTBVAC enhances its ability to colonize the bladder as well as its efficacy against MB49 bladder tumors, whereas their absence compromises the efficacy of BCG.

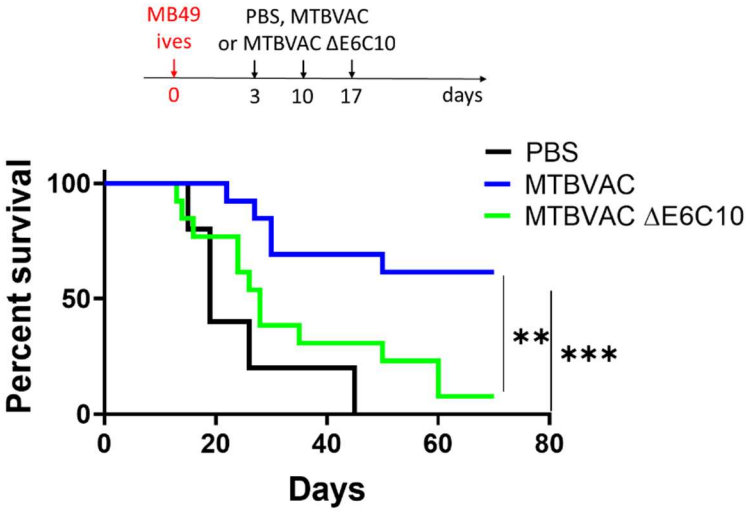

Figure 33. Survival of mice implanted with MB49 cells in the bladder and treated with intravesical PBS, MTBVAC or E6C10 MTBVAC mutant following the indicated schedule. *n* = 12 mice per group, from two independent experiments.

4.7 Immunological mechanism of action of MTBVAC intravesical therapy for bladder cancer

In the next section we turn away our focus from the bacteria to the host immune system and study the antitumor immune responses induced against MB49 bladder tumors to reveal the mechanism of action of bacterial immunotherapy for bladder cancer.

4.7.1 $CD4^+$ and $CD8^+$ T cells but not NK cells control the growth of MB49 bladder tumors

First, to better understand immunological aspects of our model, we induced bladder tumors and treated mice with depleting antibodies to study the contribution of different immune cell subtypes to tumor control. We found that both $CD4^+$ and $CD8^+$ T cells were required for controlling tumor growth of MB49 tumors, since mice separately depleted of these cells quickly succumbed due to tumor burden in the bladder (median survival of 14 and 16 days vs 35 days in control non-depleted mice, Figure 34).

In contrast, tumors were not more aggresive in mice undergoing NK cell depletion (median survival: 37 days) compared to control mice, showing that these cells are not involved in bladder tumor control at least in the absence of treatment (Figure 34). Thus, MB49 bladder tumors are preferentially controlled by $CD4^+$ and $CD8^+$ T cells.

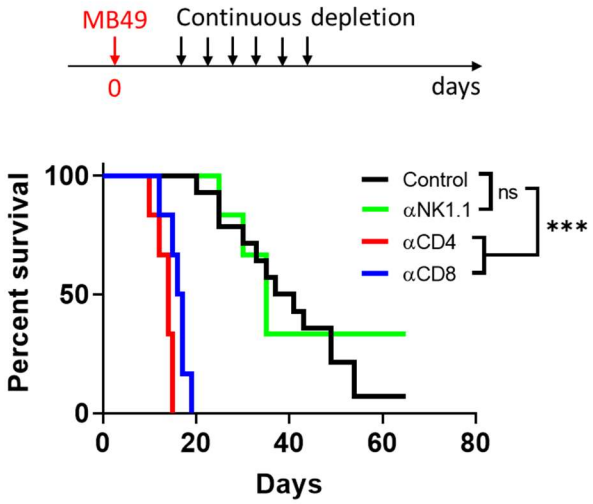

Figure 34. Survival of mice implanted with MB49 cells in the bladder and treated with immune cell depleting antibodies from day 2 until endpoint. *n* = 6-12 mice per group, from two independent experiments.

4.7.2 Immunological pathways required for effective bacterial immunotherapy

BCG immunotherapy for bladder cancer has been demonstrated to rely on the adaptive immune system in preclinical animal models[335,336], and a key role for $CD4^+$ and $CD8^+$ T cells has been suggested in humans[395]. To determine which immune pathways are involved in the antitumoral mechanism of action of intravesical immunotherapy for bladder cancer with MTBVAC, we used different mouse strains lacking key molecules involved in antitumor immunity.

First, intravesical MTBVAC treatment was completely ineffective in MB49-bladder tumor bearing mice lacking either IFN-γ or perforin (Figure 35). Loss of efficacy in the absence of IFN-γ was already described for intravesical BCG[396], and together with our findings evidence that bacterial immunotherapy does not rely on direct tumor cell cytotoxicity by bacterial infection, but on a coordinated antitumor immune response in which IFN-γ plays a key role. Loss of efficacy of bacterial therapy in the absence on perforin suggests that the cytotoxic activity of either $CD8^+$ T cells, NK cells or other subsets of innate-like lymphocytes mediated by the perforin/granzyme pathway is required for treatment success.

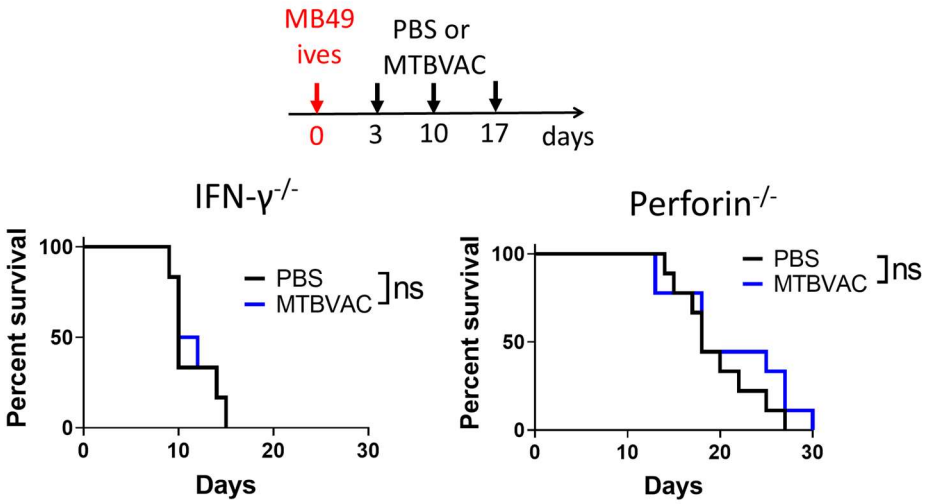

Figure 35. Survival of mice implanted with MB49 cells in the bladder and treated with intravesical PBS or MTBVAC following the indicated schedule. *n* = 6 mice per group for IFN-γ$^{-/-}$ from one experiment and *n* = 12 mice per group for Perf$^{-/-}$ mice, from two independent experiments.

Next, we induced bladder tumors in Rag1$^{-/-}$ mice, which lack T and B cells, and thus do not have a functional adaptive immune system. Intravesical MTBVAC minimally extended the survival of Rag1$^{-/-}$ mice bearing MB49 bladder tumors. Although statistical significance was reached between control and treated groups, intravesical MTBVAC only improved median survival by 2 days and no complete remissions were observed, in contrast to WT mice in previous experiments (Figure 36). This result, coupled with the lack of antitumor activity in mice lacking perforin, suggests that perforin-mediated killing of tumor cells by T cells is critical for the success of this type of therapy.

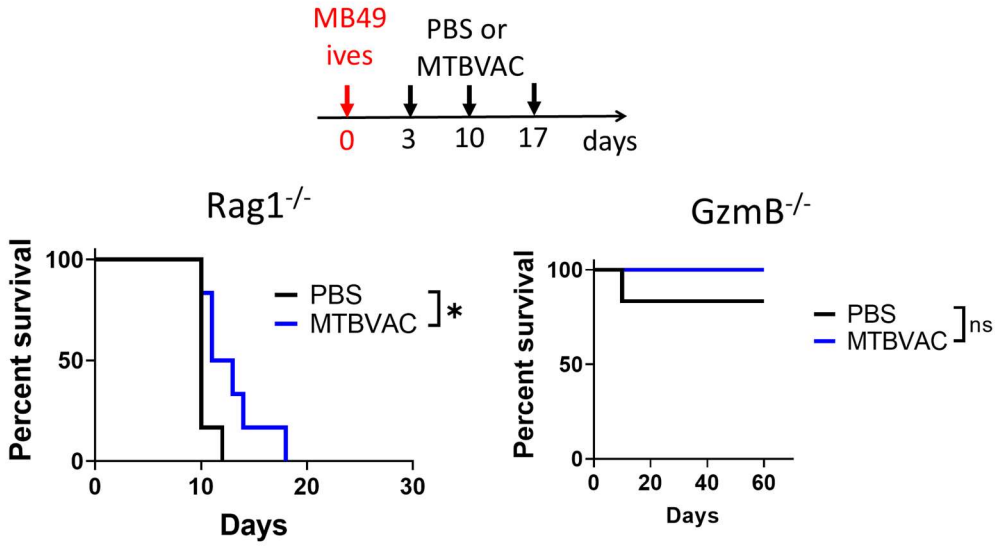

Figure 36. Survival of mice implanted with MB49 cells in the bladder and treated with intravesical PBS or MTBVAC following the indicated schedule. *n* = 6 mice per group, from one experiment.

Surprisingly, mice lacking Granzyme B ($GzmB^{-/-}$) were completely protected from tumor growth in the bladder (Figure 36). Although we did not further follow this line of research, this result is consistent with previous work describing that $GzmB^{-/-}$ mice are protected from tumor growth since T regulatory cells (Tregs) are able to kill effector $CD8^+$ T cells by a GzmB-dependent mechanism[397]. Unpublished results from Julián Pardo laboratory (personal communication) also show that EL-4 tumors are rejected in $GzmB^{-/-}$ mice, and we also have observed that $GzmB^{-/-}$ mice inoculated with B16-F10 melanoma cells by the intravenous route fail to develop lung metastases, in contrast to their WT counterparts (data not shown).

Additionally, if we compare the growth rate of bladder tumors in WT mice to three of the KO strains described in the untreated setting (Figure 37), we observe that IFN-γ, perforin and the adaptive immune system contribute to spontaneous immunity against bladder tumors even in the absence of treatment.

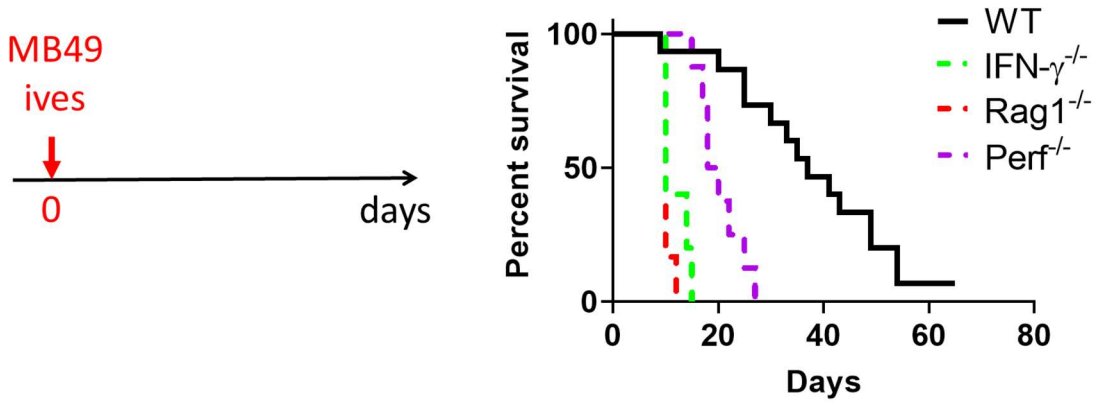

Figure 37. Survival of mice implanted with MB49 cells in the bladder. *n* = 6 mice per group and *n* = 12 for WT, pooled from various experiments.

Next, we inoculated mice deficient for Toll-like receptor 4 ($Tlr4^{-/-}$) with MB49 cells in the bladder and followed-up tumor growth. Results showed that $Tlr4^{-/-}$ mice treated with intravesical MTBVAC did not survive more than the control group, meaning that host TLR4 expression is needed for successful bacterial immunotherapy for bladder tumors (Figure 38).

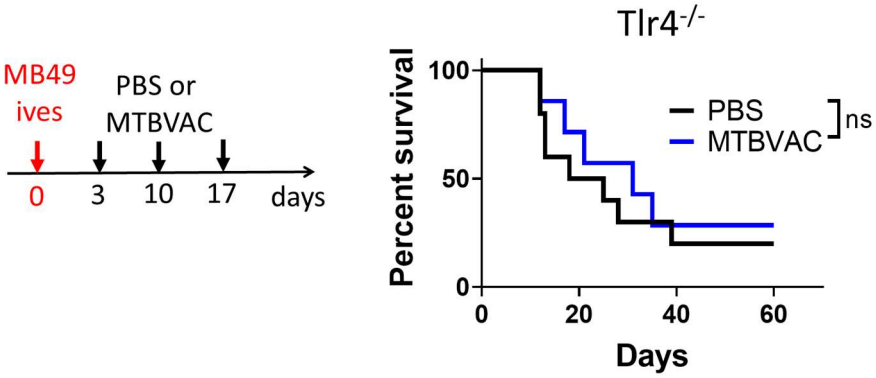

Figure 38. Survival of mice implanted with MB49 cells in the bladder and treated with intravesical PBS or MTBVAC following the indicated schedule. *n* = 7 mice per group, from one experiment.

Although further research is needed, this finding could mean that TLR4-mediated sensing of MTBVAC triggers an initial inflammatory response which would be needed for inducing efficient antitumor immune responses in the bladder. Alternatively, TLR4 could be required for sensing immunogenic bladder tumor cell death by DCs, driving their maturation and subsequent priming of tumor-specific T cells in the LNs.

4.7.3 Recognition of MHC-I in bladder tumor cells by $CD8^+$ T cells is required for bacterial immunotherapy

Given that intravesical bacterial immunotherapy critically depended on IFN-γ and perforin and that $CD8^+$ T cells were needed for the control of MB49 tumors in the untreated setting, we wondered whether disrupting the MHC-I/TCR interaction between tumor cells and the $CD8^+$ lymphocytes would affect tumor growth, both in the untreated and treated scenarios. To test this, we disrupted the β2-microglobulin gene in MB49 cells (MB49-$B2m^{-/-}$) using CRISPR/Cas9, abolishing surface MHC-I expression even when cells were exposed to IFN-γ for 24 hours (Figure 39).

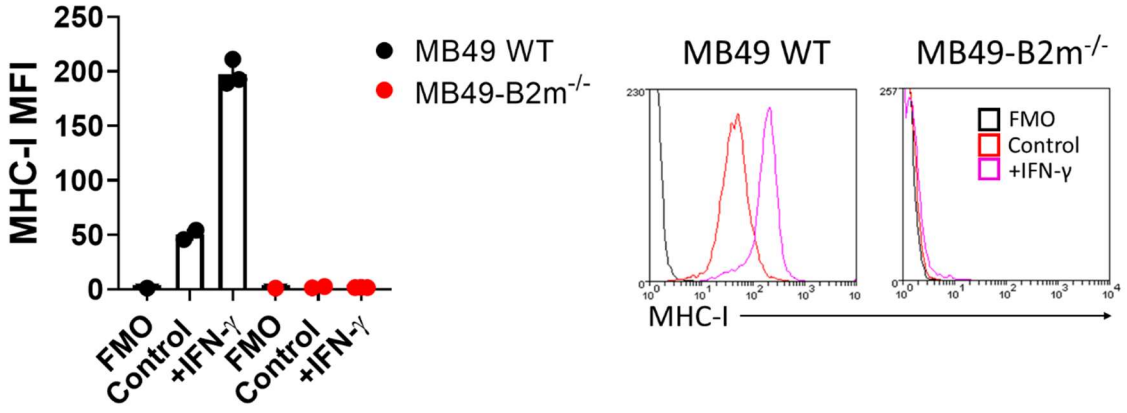

Figure 39. Flow cytometry analysis of MHC-I (H2-K^b) expression by parental or B2m$^{-/-}$ MB49 cells.

Survival follow-up showed that mice bearing MB49-B2m$^{-/-}$ bladder tumors succumbed earlier to tumor burden than mice bearing parental MB49 tumors (Figure 40), meaning that recognition of tumor cells via MHC-I by CD8$^+$ T cells plays an important role in the control of tumor growth in the bladder in the absence of treatment. Interestingly, intravesical MTBVAC treatment extended the survival of mice bearing B2m$^{-/-}$ tumors, but to a much lesser extent than in MHC-I sufficient tumors. Since MB49 tumors lacking MHC-I should be more susceptible to NK cell mediated attack, this result suggests that intravesical MTBVAC could be enhancing the antitumor function of NK cells or other innate immune cells but that it is not enough to achieve long term responses, for which CD8$^+$ T cells are needed.

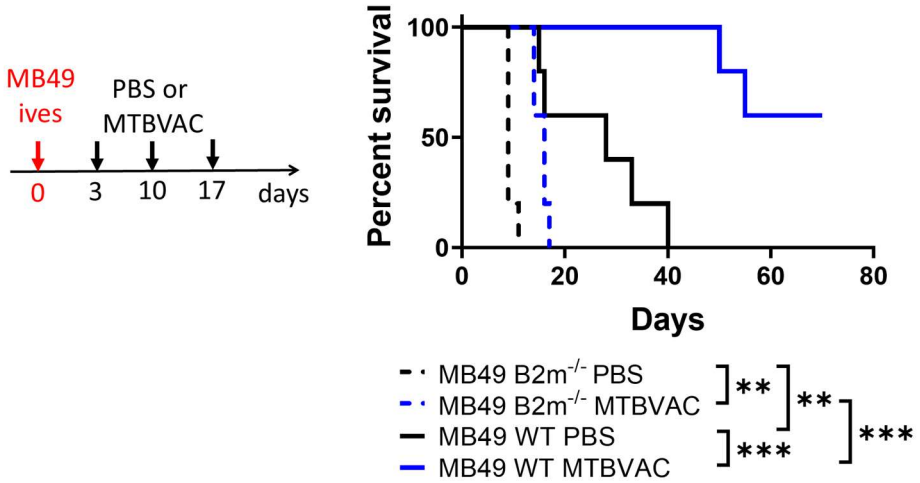

Figure 40. Survival of mice implanted with WT or B2m$^{-/-}$ MB49 cells in the bladder and treated with intravesical PBS or MTBVAC following the indicated schedule. *n* = 7 mice per group, from one experiment.

4.7.4 Intravesical MTBVAC treatment upregulates MHC-I and MHC-II in the bladder *in vivo* by an IFN-γ dependent mechanism

Next, we wanted to test whether intravesical bacterial treatment was favoring tumor cell recognition by $CD8^+$ T cells. For this, we made use of GFP-expressing MB49 cells, which allowed us to specifically analyze MB49 cells in tumor digests by flow cytometry, as shown in Figure 41 with non-fluorescent MB49 tumors as a control.

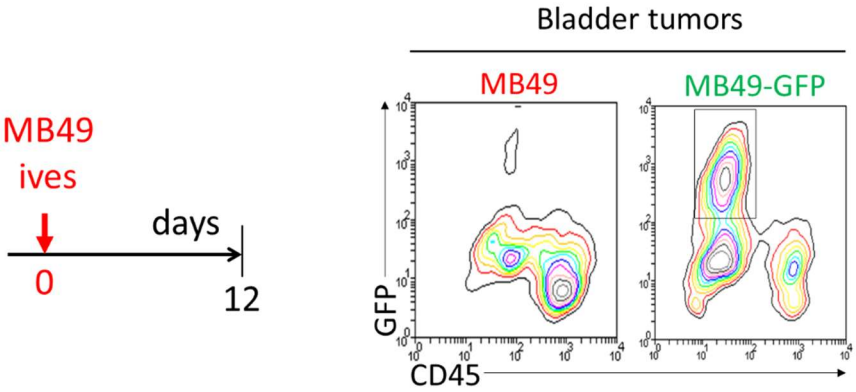

Figure 41. Mice were implanted with either parental MB49 or GFP-expressing MB49 cells orthotopically in the bladder and tumors were analyzed by flow cytometry at day 12. Shown are representative contour pltos for the identification of GFP-expressing tumor cells. Representative of *n* = 6 mice/group.

In the following experiments, we decided to analyze bladder tumors by flow cytometry at day 12 post tumor cell inoculation (Figure 42A). We chose this timepoint because it allowed us to perform two intravesical treatments before analysis and, most importantly, because it was a timepoint in which tumors were still present in treated mice, which was important to avoid performing the analysis after the tumor had already regressed. Even though bladder tumors were still evident in treated mice at day 12, they were already smaller in weight compared with untreated mice but still bigger than naïve bladders (Figure 42B), demonstrating an antitumoral effect that later would translate in the improved survival observed in previous experiments.

Analysis of digested bladder tumors by flow cytometry revealed that intravesical MTBVAC upregulated MHC-I in the surface of GFP^+ $CD45^-$ tumor cells (Figure 42D). We wondered whether this effect was mediated by IFN-γ, since MHC-I and MHC-II expression in MB49 cells increases when exposed to this cytokine *in vitro* (Figure 42C). The increase in MHC-I expression in tumor cells caused by intravesical treatment *in vivo* was completely

abrogated in Ifnγ$^{-/-}$ mice (Figure 42D), showing that modulation of MHC-I expression was not due to a direct interaction of the bacteria with tumor cells, but to an indirect mechanism mediated by immune cell-derived IFN-γ. Depletion experiments performed in the next sections (described later on) revealed that CD4^{+} and CD8^{+} T lymphocytes, both well-known IFN-γ-producing cells, were needed for MHC-I upregulation on tumor cells after bacterial immunotherapy (Figure 43B), with CD4^{+} T cells appearing as the most important subset. Altogether, these results reflect that bacterial immunotherapy drives MHC-I upregulation on the tumor cell surface in an IFN-γ- dependent manner, an event that might be crucial to enhance tumor cell recognition by CD8^{+} T cells.

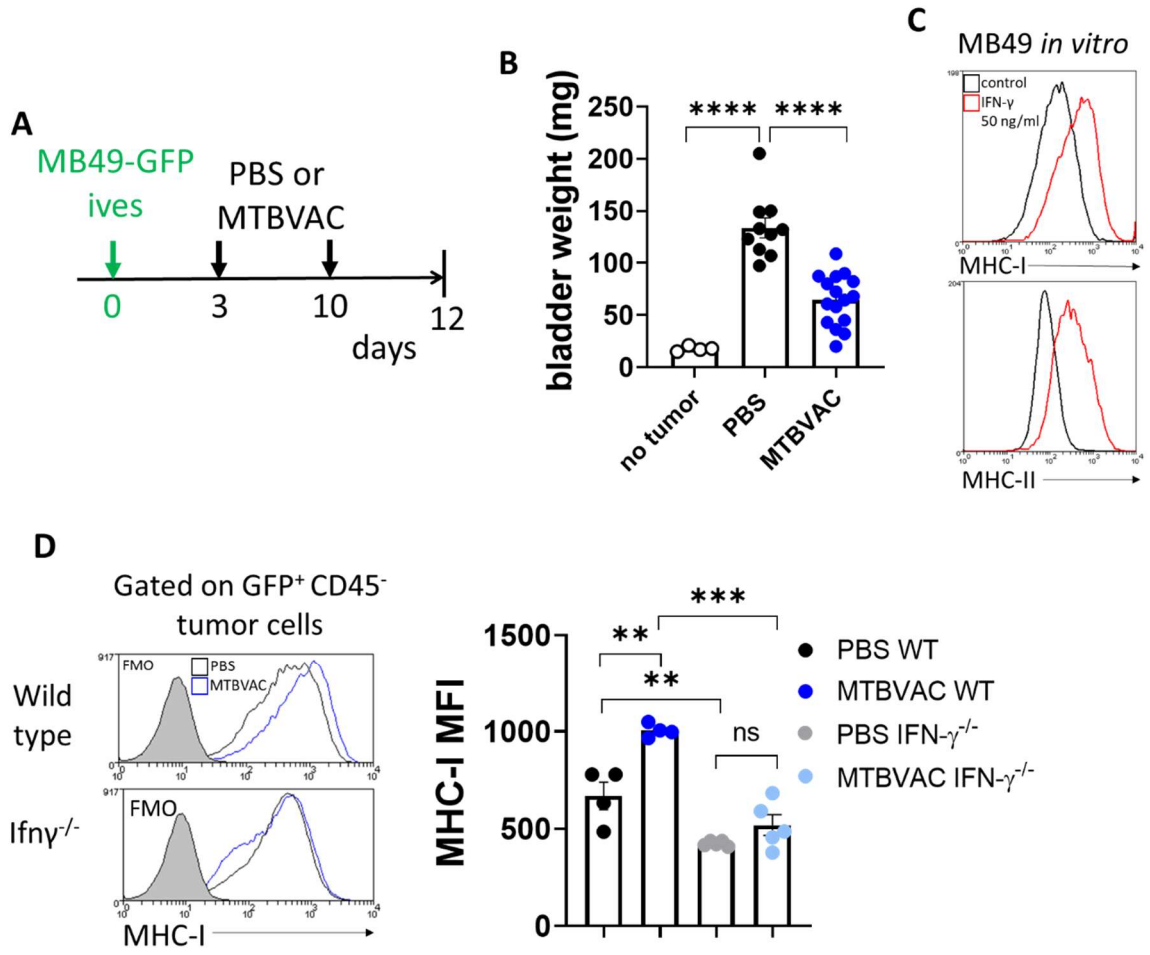

Figure 42. Mice were treated as summarized in (A). (B) Bladder tumor weights at day 12, *n* = 10-15 mice/group, from 2 independent experiments. (C) Expression of MHC-I (H2-K^{b}) and MHC-II by MB49 cells upon *in vitro* exposure to IFN-γ for 24 h. (D) Representative contour plots and quantification of MHC-I expression by tumor cells *in vivo* in different groups of mice treated as shown in (A), *n* = 4 – 5 mice/group, representative of two independent experiments.

Further analysis of tumor digests revealed that intravesical MTBVAC also upregulated MHC-II expression both in tumor and $CD45^+$ immune cells in an IFN-γ dependent fashion (Figure 43C,D), which could favor tumor cell recognition by $CD4^+$ T cells as well as enhance antigen presentation to $CD4^+$ T cells by APCs such as macrophages, B cells or DCs.

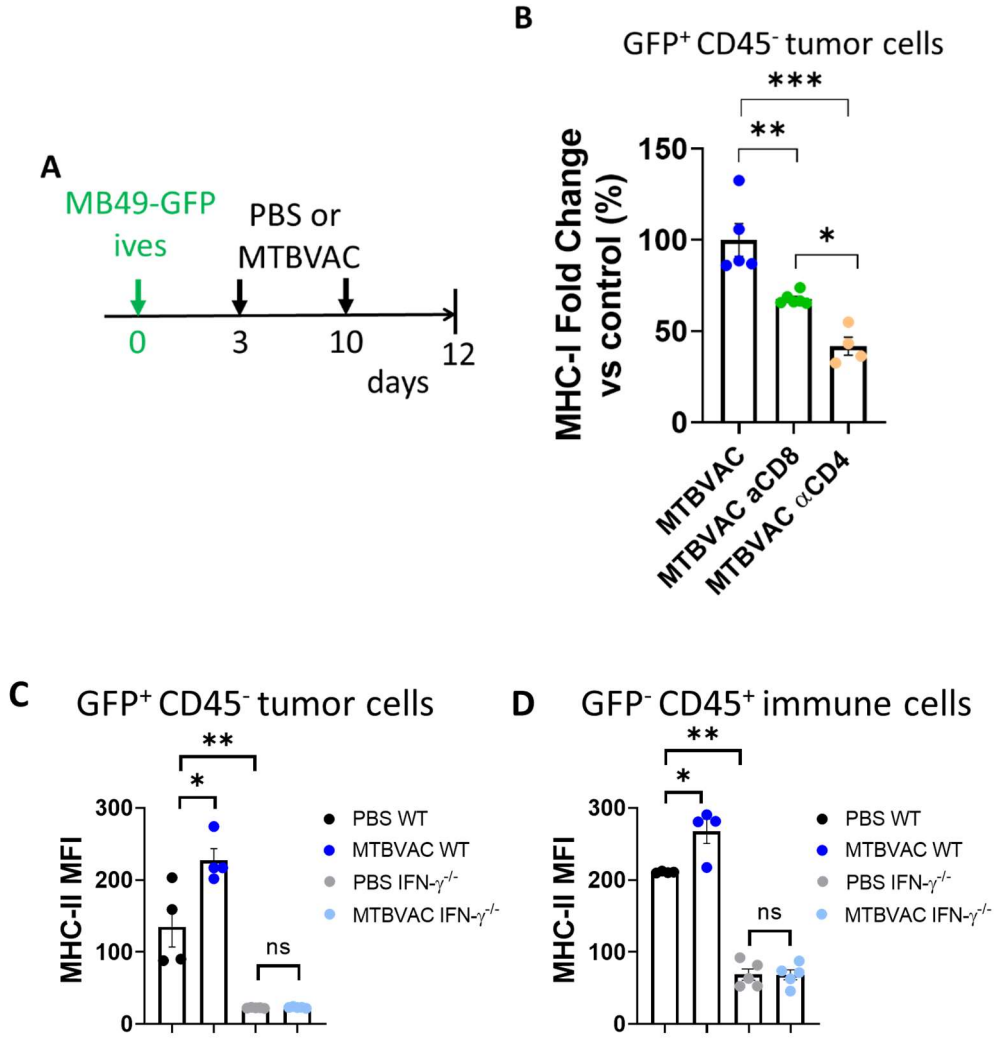

Figure 43. Mouse were treated as shown in (A). (B) MHC-I expression (normalized to levels of the MTBVAC group) by tumor cells *in vivo* in different groups of mice, *n* = 4-6 mice/group, from one experiment. (C) Expression of MHC-II tumor cells and immune cells (D) *in vivo*, *n* = 4-5 mice/group, from one experiment.

4.7.5 Intravesical delivery of bacteria induces a tumor-specific immune response

Next, we focused on studying whether intravesical MTBVAC treatment stimulated tumor-specific adaptive immune responses, similarly to other immunotherapies such as checkpoint blockade or therapeutic cancer vaccines[398,399]. Currently, it is a matter of debate whether bacterial immunotherapy for bladder cancer works by stimulating antitumor innate immunity[400], or whether it relies on bacterial-specific adaptive immune responses[340] or on improving tumor-specific responses[401].

In order to study tumor-specific responses in the MB49 model, we chose to evaluate the response to endogenous tumor antigens, avoiding artificial overexpression of proteins such as ovoalbumin (OVA). We took advantage of the fact that MB49 cells are of male origin and express antigens contained in the HY chromosome, which are immune reactive when implanted on female hosts[402]. T-cell epitopes derived from the HY chromosome have been described, and $CD4^+$ and $CD8^+$ T cells specific for these epitopes (Dby for CD4 and Uty for CD8) recognize and eliminate MB49 cells *in vitro*[403]. Another antigen commonly used in tumor immunology is the p15E immunodominant MHC-I antigen from the AKR/Gross murine leukemia virus (MuLV)[404,405], an endogenous retrovirus which is present in some murine cancer cell lines, such as MB49, B16-F10, LLC or MC38[406–408]. Concretely, the KSPWFTTL (p15E) peptide is known to drive H2-K^b-restricted T-cell responses against C57BL/6-derived tumors[405].

Therefore, we implanted mice with MB49 bladder tumors and evaluated the immune response against these antigens by ELISpot, consisting in overnight incubation of splenocytes in the presence of the described peptides for the detection of antigen-specific IFN-γ secreting colonies (spots) of T cells. Of note, IFN-γ spots obtained in the absence of antigen stimulation were subtracted to those obtained in the presence of antigen to obtain the number of antigen-specific IFN-γ spots.

Our results showed that MB49 bladder tumors elicited spleen $CD8^+$ T cell responses to the Uty and p15E peptides and $CD4^+$ T cell responses to the Dby peptide, whereas spots were not detected when splenocytes from non-tumor bearing (naïve) mice were used (Figure 44), validating our method. As a control, splenocytes from mouse bearing MB49 tumors did not respond to the OVA-derived OT-I peptide for $CD8^+$ T cells (Figure 44).

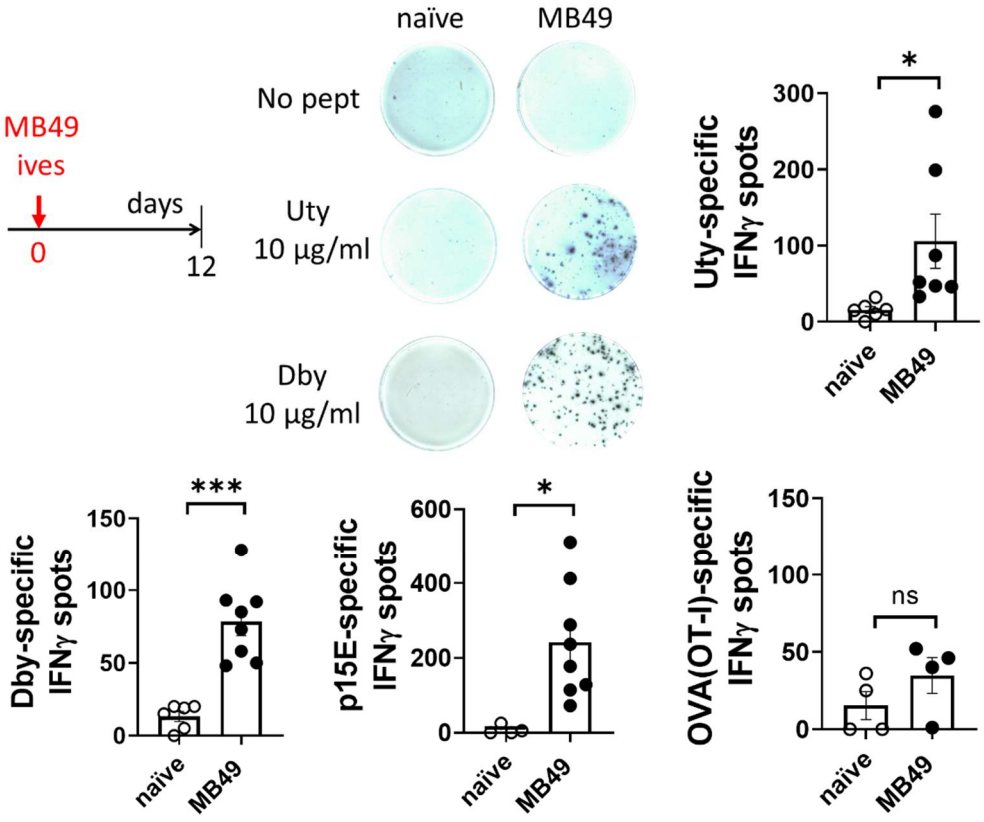

Figure 44. Mice were orthotopically implanted with MB49 tumor cells in the bladder. At day 12, splenocytes were obtained and incubated overnight with the indicated peptides to quantify IFN-γ producing colonies by ELISpot. *n* = 4-8 mice/group, from two independent experiments.

Next, we evaluated antigen-specific responses in mice bearing bladder tumors receiving intravesical bacterial treatment (Figure 45). ELISpot assay revealed that intravesical MTBVAC elicited superior Uty, Dby and p15E-specific T cell responses in comparison to PBS or BCG-treated mice (Figure 45), which concurs with the improved survival observed in mice receiving intravesical MTBVAC. These results evidence that intravesical MTBVAC treatment stimulates tumor antigen-specific adaptive immunity in MB49 tumor bearing mice.

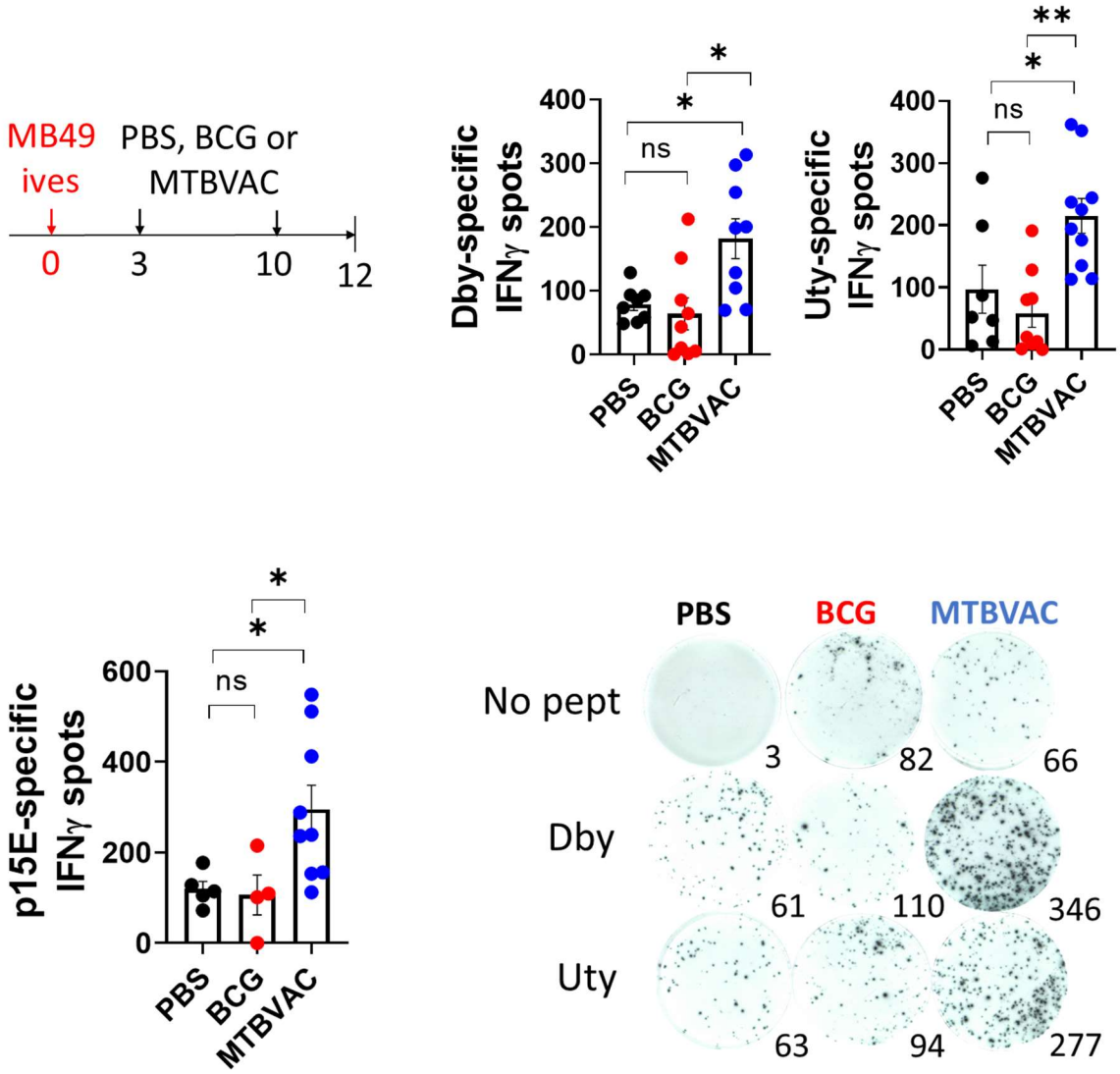

Figure 45. Mice were orthotopically implanted with MB49 tumor cells in the bladder and treated as shown in the Figure. At day 12, splenocytes were obtained and incubated overnight with the indicated peptides to quantify IFN-γ producing colonies by ELISpot. *n* = 4-10 mice/group, from two independent experiments.

Next, to test the functionality tumor-specific T cells, we performed *in vitro* killing assays with splenocytes isolated from bladder tumor bearing mice against luciferin-expressing MB49 cells (Figure 46). Our results revealed that splenocytes coming from mice treated with MTBVAC were more cytotoxic towards MB49 cells compared with splenocytes coming from untreated mice (Figure 46). Importantly, this enhanced cytotoxicity was abolished when $CD8^+$ T cells were depleted during the treatment course (Figure 46). This result corroborated that cytotoxicity was driven by $CD8^+$ T cells, and further demonstrates that intravesical MTBVAC enhances tumor-specific immune responses systemically.

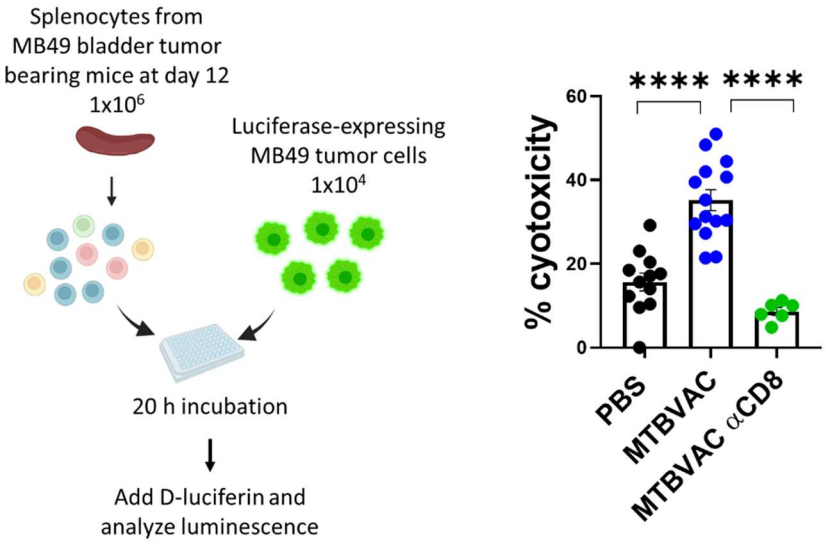

Figure 46. Mice were treated as in Figure 45. A group received antiCD8 depleting antibodies at day 2 and 9. At day 12, splenocytes were obtained and seeded over luciferase-expressing MB49 cells at a 100:1 E:T ratio. After 20 h, luminescence was measured and % cytotoxicity calculated in reference to control wells incubated without splenocytes. *n* = 6-14 mice/group, from two independent experiments.

As a third method of testing induction of tumor-specific immune responses, we used mice from survival experiments which originally rejected their MB49 bladder tumors after receiving intravesical MTBVAC treatment and survived until the 70-day experimental endpoint (Figure 47). We performed a secondary challenge with MB49 cells in a distal location, the flank, in survivors and naïve mice as control. Follow-up of tumor growth revealed that tumors progressed normally in naïve mice but regressed in all survivors, which evidences the generation of tumor-specific immune memory in these mice. To determine whether memory responses were driven by T cells, we depleted $CD4^+$ and $CD8^+$ T cells in a group of survivors before the secondary challenge. T cell depletion completely prevented the rejection of a secondary tumor graft in survivor mice (Figure 47).

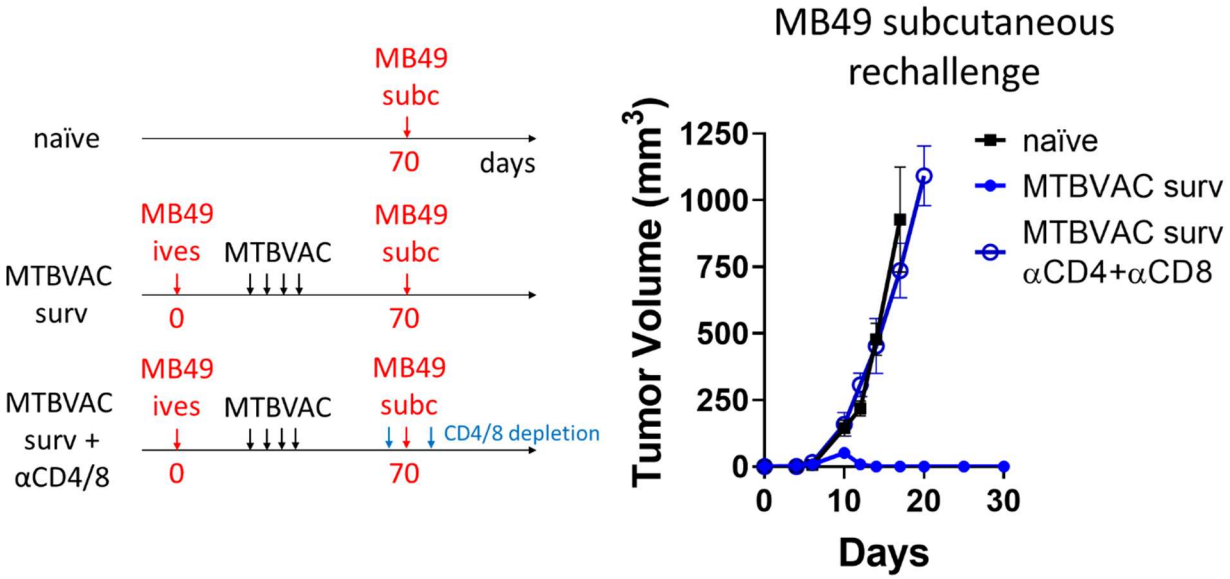

Figure 47. Analysis of MB49 subcutaneous tumor growth in mice treated as shown in the Figure. *n* = 5 mice/group, from one experiment.

To strengthen our results, we used another cohort of survivor mice and performed secondary challenges with MB49 cells in one flank and non-antigenically related B16-F10 cells in the contralateral flank. As expected, both tumors grew in naïve mice, whereas in survivors only MB49 tumors were rejected, further evidencing the generation of immune memory against antigens contained in MB49 tumors (Figure 48).

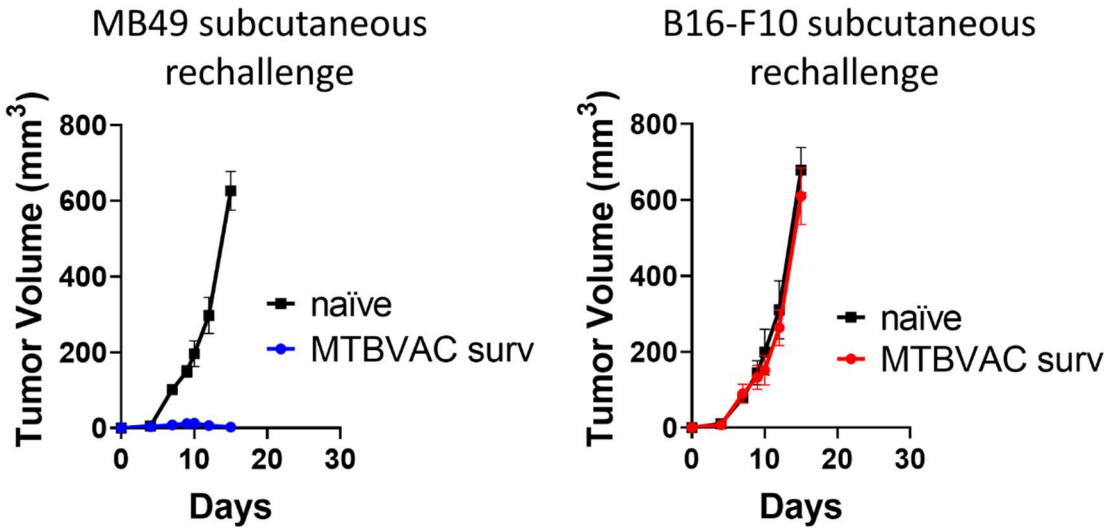

Figure 48. Analysis of MB49 and contralateral B16-F10 subcutaneous tumor growth in naïve or MB49 survivor mice. *n* = 6 mice/group, from one experiment.

As MB49 cells inoculated by the intravenous route metastasize to the lungs[409], we also tested whether MB49-bladder tumor survivors could reject an intravenous secondary challenge with MB49 cells (Figure 49). We found that survivor mice rejected the intravenous MB49 rechallenge, as no apparent lung tumor nodules were found 60 days after the secondary challenge (Figure 49). In stark contrast, naïve mice quickly succumbed (median survival = 11 days) due to tumor burden in the lung, showing that immune memory generated by bacterial immunotherapy was also effective against disseminated metastatic disease.

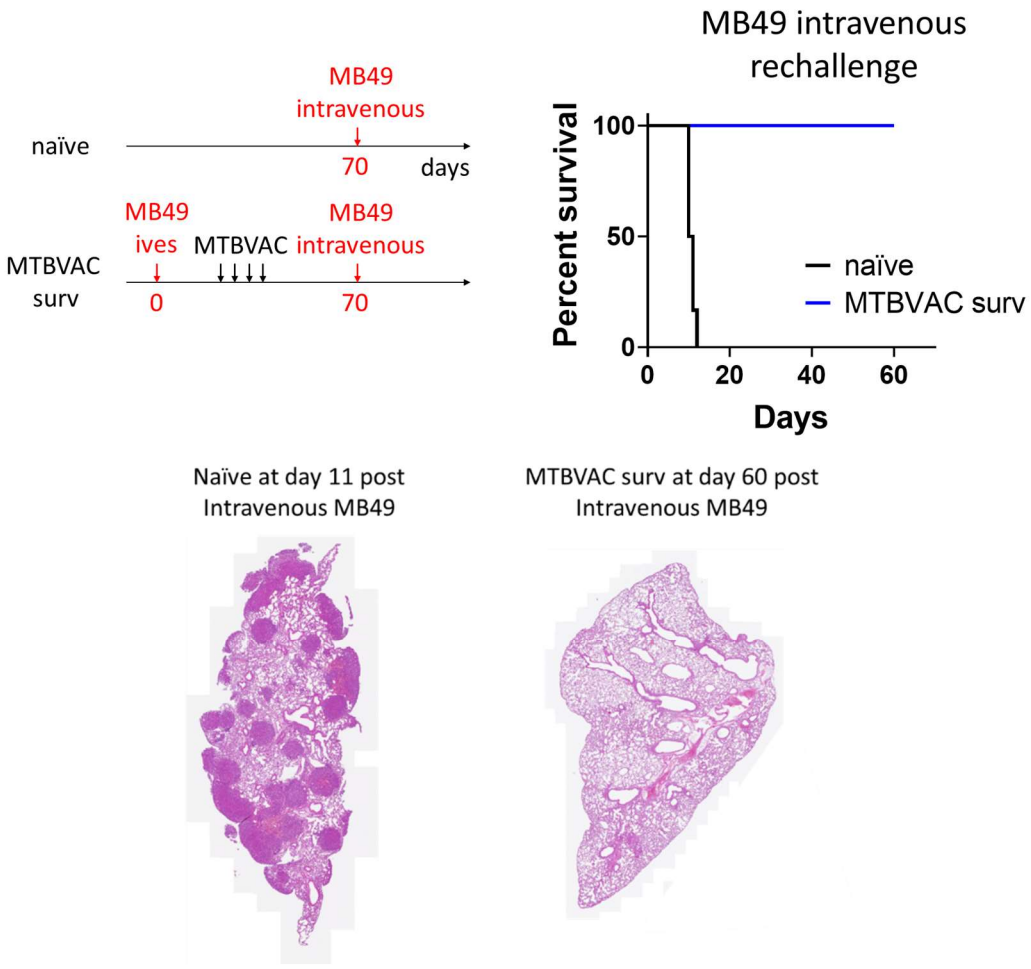

Figure 49. Survival of mice naïve or MB49 survivor mice inoculated with MB49 cells intravenously. Shown are representative images of the lungs after H&E staining from one mice per group. *n* = 6 mice/group, from one experiment.

Finally, we tested whether the tumor-specific memory response relied on MHC-I recognition of the tumor by $CD8^+$ T cells. For this, we rechallenged MB49-bladder tumor survivors with MB49-*B2m*$^{-/-}$ cells in the flank. Unexpectedly, MHC-I deficient MB49

tumors were still rejected in 4 out of 5 survivors, whereas they progressed normally in naïve mice (Figure 50). This result suggested that memory $CD4^+$ T cells were sufficient for driving tumor rejection upon a secondary graft in the absence of $CD8^+$ T cell-mediated recognition of tumor cells. We further confirmed this hypothesis by depleting $CD4^+$ T cells before the secondary challenge with MHC-I deficient tumor cells, which completely abrogated tumor rejection in 3 out of 3 mice tested. Surprisingly, NK cell depletion during rechallenge in survivor mice similarly abolished tumor rejection in 3 out of 3 mice (Figure 50), suggesting that the tumor-specific memory $CD4^+$ T cells functioned by stimulating NK cell mediated killing of tumor cells.

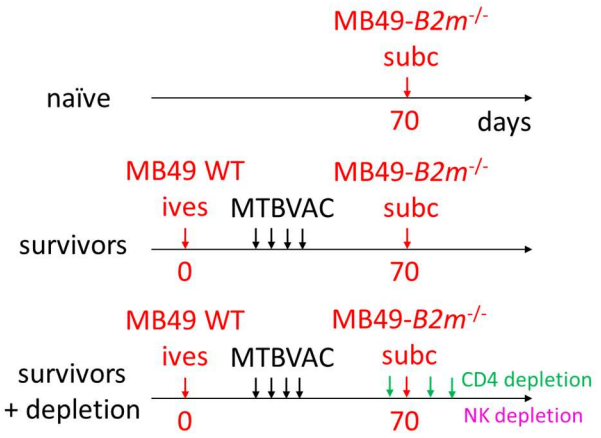

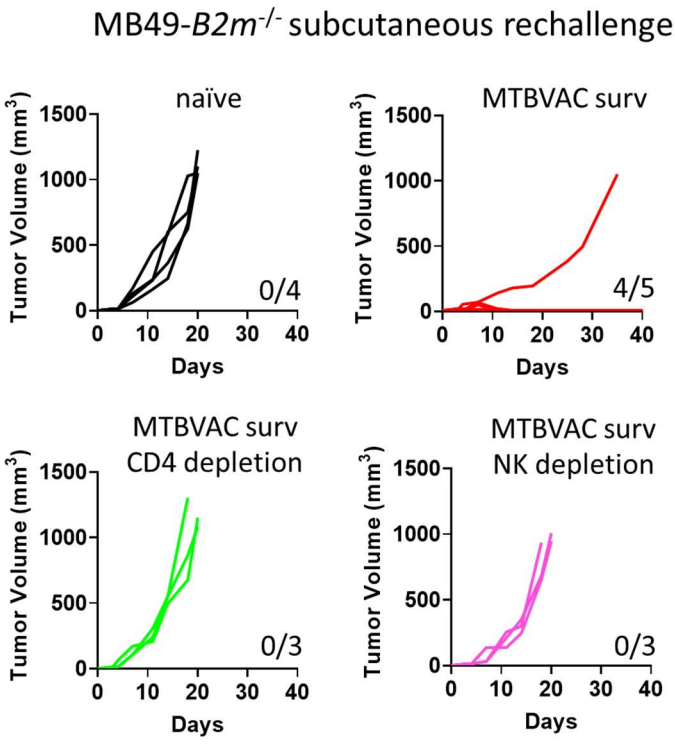

Figure 50. Analysis of B2m$^{-/-}$ MB49 subcutaneous tumor growth in mice treated as shown in the Figure. *n* = 3-5 mice/group, from one experiment.

4.7.6 Requirement of CD4$^+$ and CD8$^+$ T cells for bacterial immunotherapy

Considering that intravesical MTBVAC stimulated tumor-specific T cell responses, in this section we depleted separately CD8$^+$ or CD4$^+$ T lymphocytes during the course of intravesical treatments to test the contribution of these cells to the antitumoral effect (Figure 51A).

First, we observed that bladder weights were significantly higher in CD8$^+$ and specially in CD4$^+$ T cell-depleted mice compared with controls at day 12 post tumor cell inoculation (Figure 51B), underscoring the importance of adaptive immunity for MTBVAC therapeutic effect. Additionally, depletion studies revealed that both CD8$^+$ T-cell infiltration into bladder tumors as well as Uty and p15E-specific CD8$^+$ T cell responses were abrogated in the absence of CD4$^+$ T cells (Figure 51C,D,E). However, the Dby-specific response mediated by CD4$^+$ T cells was still present in CD8$^+$ depleted mice (Figure 51F), suggesting that the initiation of tumor-specific CD4$^+$ responses is independent of CD8$^+$ T cells.

Collectively, these results suggested that intravesical MTBVAC potentiates tumor-specific CD4$^+$ T cell responses, which are necessary for the priming of tumor-specific CD8$^+$ T cells and their infiltration into MB49 bladder tumors.

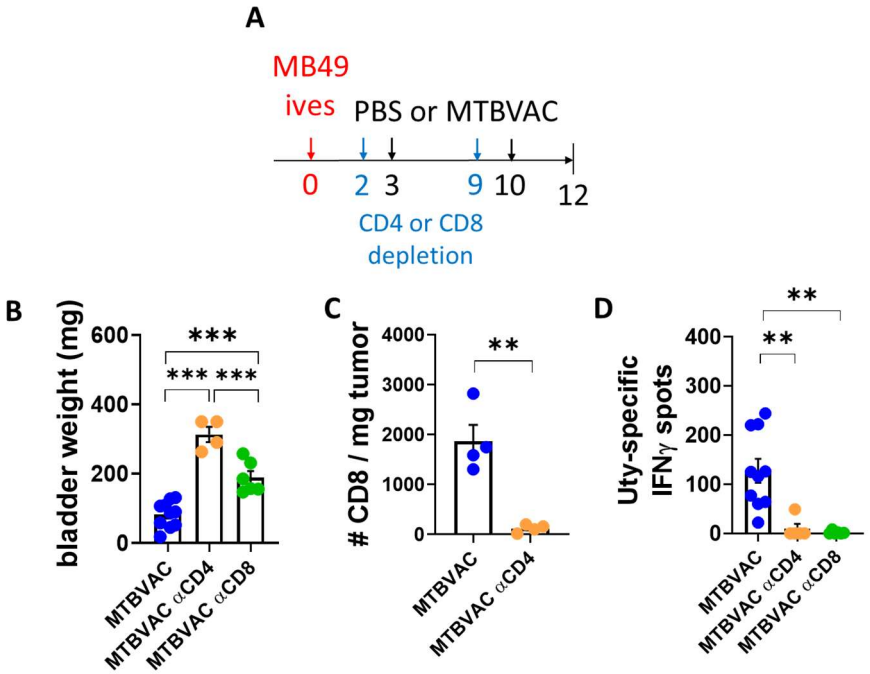

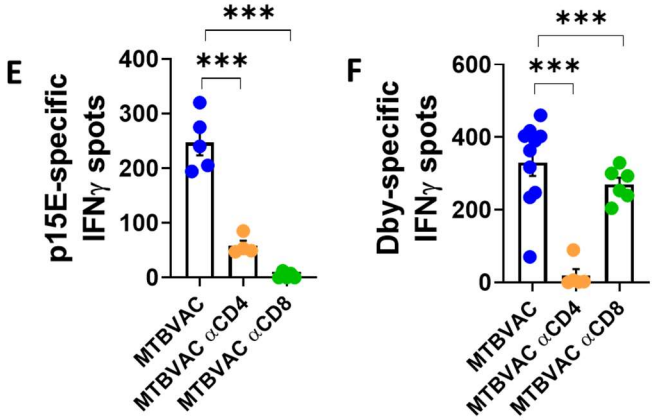

Figure 51. (A) Mice were implanted orthotopically with MB49 cells in the bladder and treated with MTBVAC at days 3 and 10. Two groups received CD4 or CD8 depleting antibodies at days 2 and 9. (B) Bladder tumor weights at day 12. (C) Quantification by flow cytometry of the absolute number of $CD8^+$ T cells per mg of tumor. (D,E,F) IFN-γ ELISpot using splenocytes of the indicated groups of mice incubated with Uty, p15E or Dby tumor-specific peptides overnight. *n* = 4-8 mice/group, from two experiments.

Next, we focused on the myeloid cell compartment, finding that intravesical MTBVAC treatment increased iNOS expression in bladder $CD11b^+$ $CD64^+$ macrophages compared to PBS controls (Figure 52). Increased iNOS expression in macrophages has been associated with success of αCTLA4 + αPD-L1 immunotherapy and was attributed to $CD4^+$ T cell-derived IFN-γ[80,410]. In a similar manner, $CD4^+$ T cell depletion during intravesical treatment abrogated the observed increase in $iNOS^+$ macrophages (Figure 52).

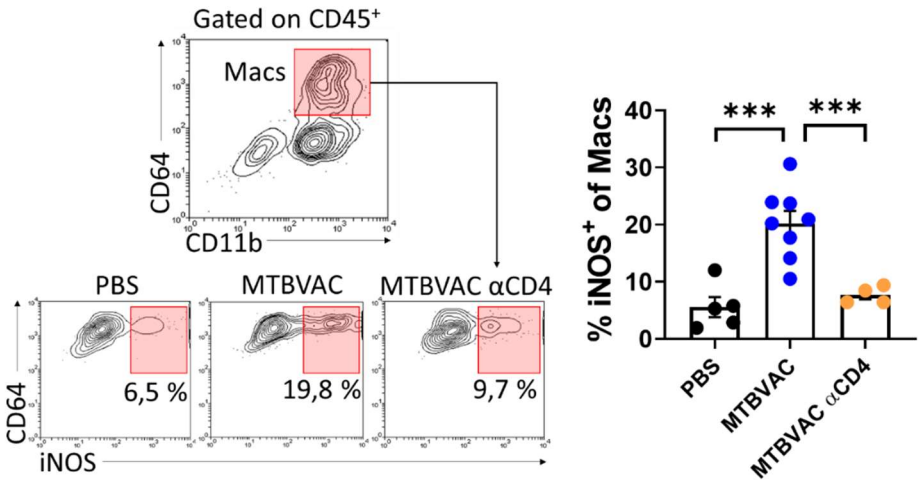

Figure 52. Mice were treated as in Figure 51. At day 12, macrophages were analyzed in bladder tumors by flow cytometry. Shown are representative contour plots and quantification of iNOS expression by macrophages infiltrating bladder tumors, *n* = 4-8 mice/group, pooled from two experiments.

We next assessed whether intravesical MTBVAC treatment caused phenotypical alterations within the tumor-infiltrating T cell compartment.

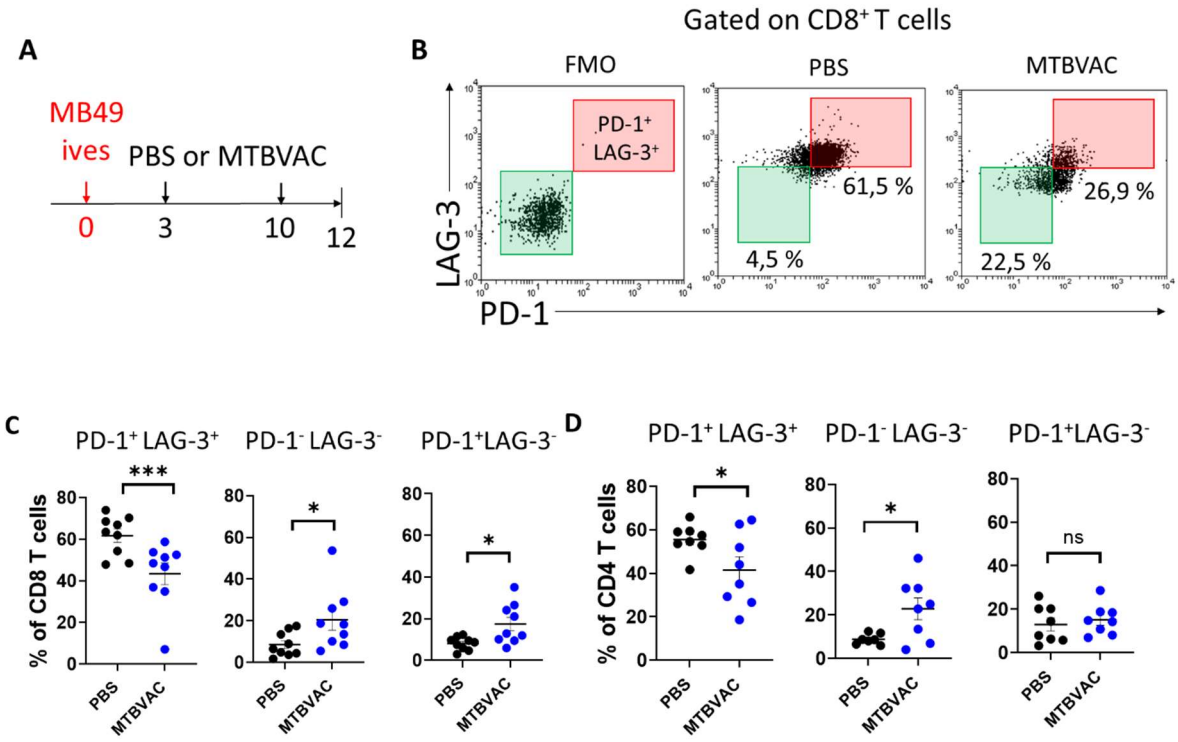

Figure 53. Mice were treated as shown in (A). At day 12, expression of PD-1 and LAG-3 in bladder TILs was analyzed by flow cytometry. Shown are representative contour plots and quantification for *n* = 8 mice/group, from two experiments.

Analysis of bladder tumors at day 12 revealed a significant reduction in the proportion of $CD8^+$ T cells expressing the inhibitory receptors PD-1 and LAG-3 in the MTBVAC group (Figure 53B,C), a phenotype associated with T-cell exhaustion[411]. Interestingly, a reduction in the PD-1^+ LAG-3^+ exhaustion signature was also observed in $CD4^+$ T cells (Figure 53D).

To determine whether reduced exhaustion levels correlated with improved functionality, we stimulated bladder tumor single cell suspensions *ex vivo* with PMA and ionomycin to detect cytokine expressing T cells. A higher proportion of tumor-infiltrating $CD8^+$ and $CD4^+$ T cells expressed IFN-γ in mice receiving intravesical MTBVAC (Figure 54A,B), which demonstrates improved functionality of these cells. Moreover, a higher proportion of tumor-infiltrating $CD4^+$ T cells expressed the costimulatory ligand ICOS in mice receiving intravesical MTBVAC (Figure 54C), a marker which delineates a $CD4^+$ subset with enhanced effector function, cytokine secretion and activation[412–414]. Of note, not only T cells were stimulated, since NK cells also secreted higher levels IFN-γ when stimulated

with PMA and ionomycin in treated mice compared to controls (Figure 54D), evidencing widespread stimulation of antitumor immunity by bacterial therapy.

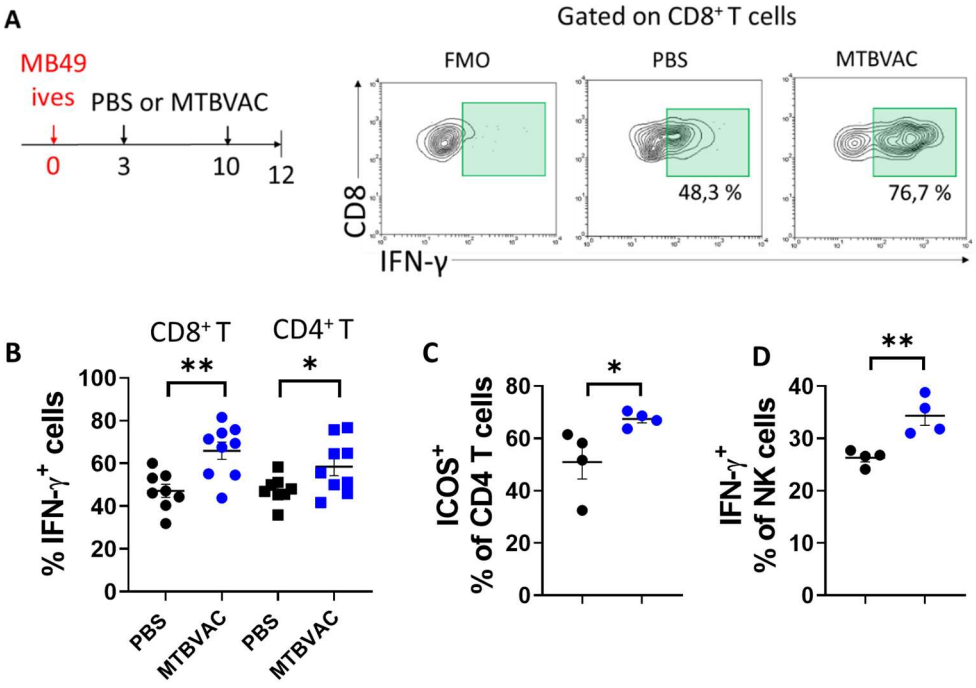

Figure 54. Mice were treated as shown in (A). IFN-γ and ICOS expression in distinct cellular subsets was analyzed by flow cytometry. *n* = 8 mice/group, from two experiments (IFN-γ in T cells) and *n* = 4 mice/group from one experiment (ICOS in CD4⁺ T cells and IFN-γ in NK cells)

4.7.7 Involvement of type 1 conventional Dendritic Cells in the mechanism of action of bacterial immunotherapy for bladder cancer

cDC1s are responsible for the processing and cross-presentation of tumor antigens and are essential for the priming of tumor-specific $CD4^+$ and $CD8^+$ T cell responses[72,79,415]. Given that MTBVAC intravesical treatment enhanced tumor-specific immunity, we wondered whether cDC1s play a role in driving bacterial immunotherapy efficacy for bladder cancer, which to our knowledge has never been studied.

First, we identified cDC1s in the bladder by flow cytometry 12 days after tumor cell inoculation and distinguished them from cDC2s by expression of XCR1 and not SIRPα, (Figure 55). As expected, $XCR1^+$ $SIRP\alpha^-$ cDC1s were selectively absent in bladder tumors from $Batf3^{-/-}$ which selectively lack this cellular subset[73].

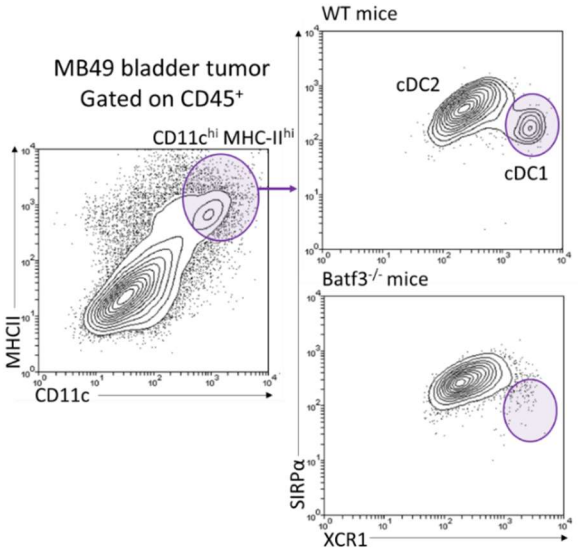

Figure 55. Flow cytometry analysis of cDC1s in MB49 orthotopic bladder tumors of wild-type (WT) and Batf3$^{-/-}$ mice. Shown are representative contour plots of n = 5 mice/group.

Flow cytometry analysis of bladder tumors at day 12 revealed that intravesical MTBVAC recruited cDC1s to the tumor site (Figure 56), and cDC1s from treated mice expressed higher levels of the costimulatory molecule CD86 in the tumor and of CD86 and the receptor CD40 in the bdLNs (Figure 56), evidencing higher activation status and T cell stimulatory potential.

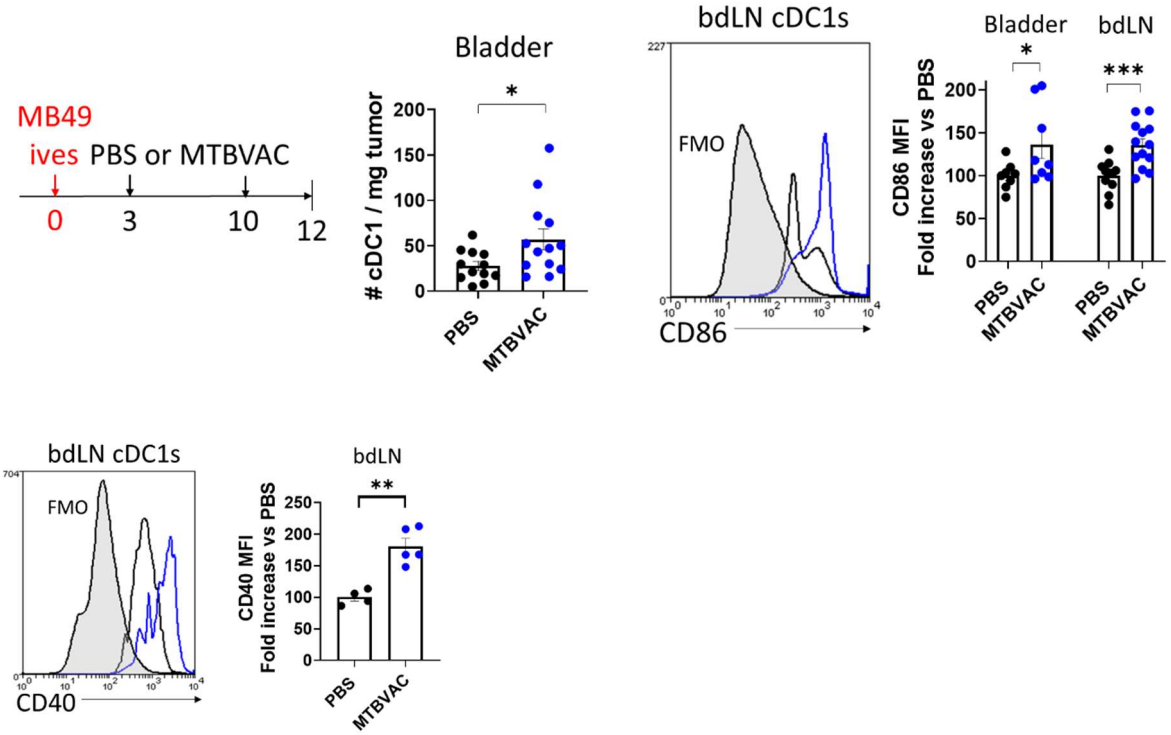

Figure 56. Mice were treated as shown in the Figure. Absolute numbers of cDC1s per mg of tumor and expression of CD40 and CD86 were analyzed by flow cytometry in bladder tumors and/or bladder draining LNs.

Next, we wondered whether MTBVAC treatment was favoring cDC1 upload with tumor-associated material to drive improved priming of tumor-specific T cells in the bdLN. To test this, we inoculated mice with ZsGreen-expressing MB49 cells to identify immune cells that had engulfed tumor-associated material. ZsGreen, unlike GFP, maintains its green fluorescence (wavelength emission peak: 509 nm) within intracellular compartments following phagocytosis, allowing us to track cells that have ingested fluorescent tumor-associated material[416,417]. We focused on tumor draining LNs, where antigen presentation to T cells occurs, and found that ZsGreen positivity was restricted mainly to the cDC1 and cDC2 compartment (Figure 57). Importantly, our results showed that a higher percentage of bdLN cDC1s contained ZsGreen in mice which received intravesical MTBVAC treatment.

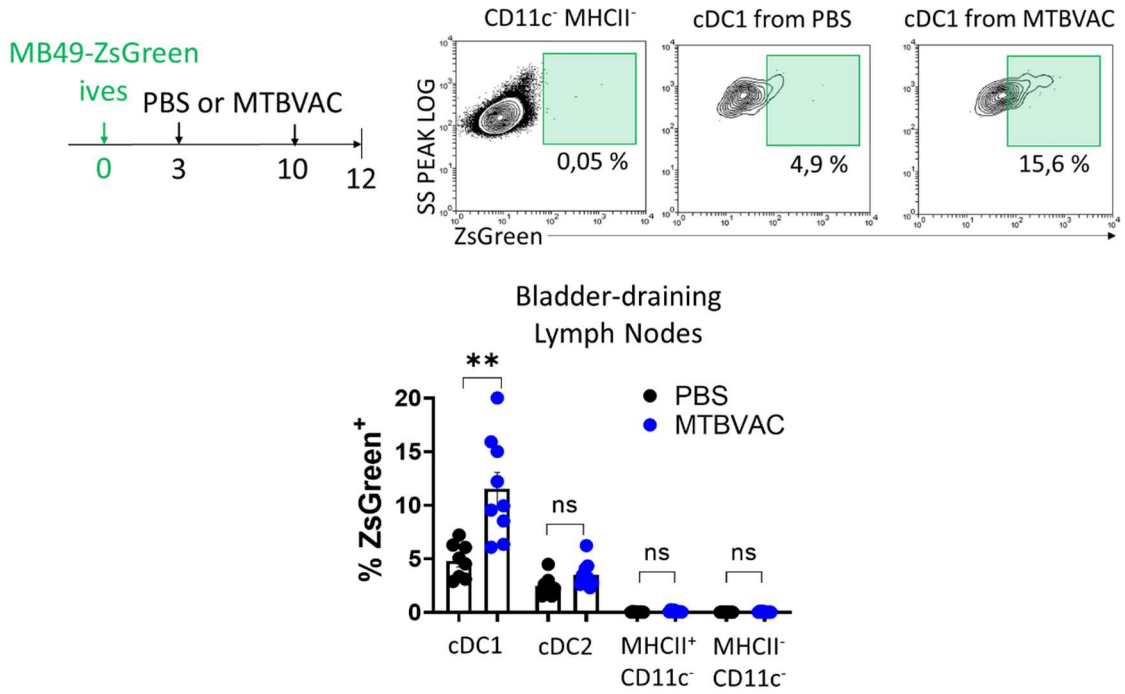

Figure 57. Mice were implanted orthotopically with ZsGreen-expressing MB49 cells and treated as shown in the Figure. At day 12, ZsGreen expression by distinct cellular subsets in the bdLN was analayzed by flow cytometry. *n* = 8 mice/group, pooled from two experiments.

Altogether, these findings suggested that intravesical MTBVAC favoured the migration of tumor-antigen loaded and activated cDC1s from the tumor to the bdLNs, which could

explain the improved tumor-specific responses observed in treated mice. A plausible explanation could be that MTBVAC is mediating tumor-cell death in the bladder by stimulation of innate immune cells such as NK cells or macrophages, providing immunogenic tumor cell debris to cDC1s, although this hypothesis merits further investigation.

To confirm a functional role for cDC1s in driving the therapeutic response to MTBVAC, we evaluated the survival of Batf3$^{-/-}$ mice bearing MB49 bladder tumors. MTBVAC antitumor effect was completely abrogated in Batf3$^{-/-}$ mice, in contrast to WT (Figure 58A), and these animals presented significantly higher bladder weights at day 12 after tumor cell inoculation compared with MTBVAC-treated WT mice (Figure 58B). Of note, untreated Batf3$^{-/-}$ mice succumbed earlier to tumor burden than untreated WT mice (Figure 58A), meaning that cDC1s are needed for spontaneous immune responses against MB49 bladder tumors.

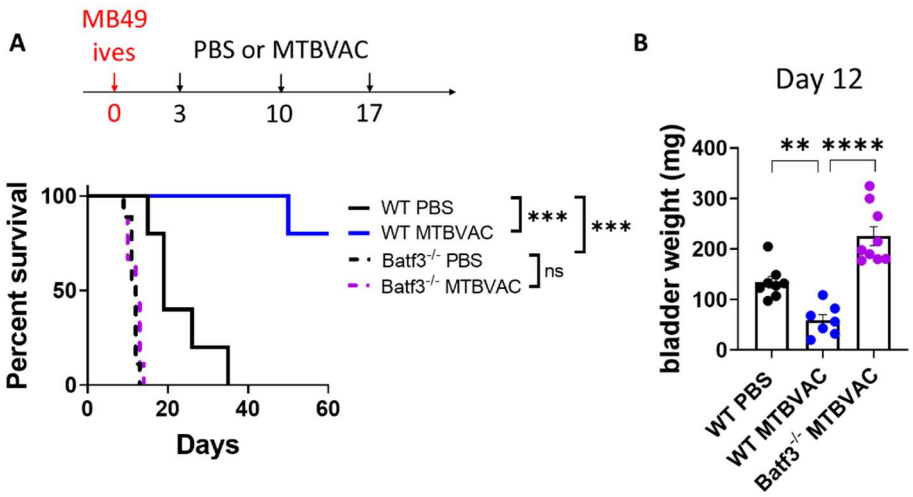

Figure 58. WT or Batf3-deficient mice were implanted orthotopically with MB49 cells in the bladder. (A) Follow-up of mice survival, *n* = 10 mice/group, from two independent experiments. (B) In separate experiments, bladder weights were measured at day 12, *n* = 7-9 mice/group, from two independent experiments.

We further analysed MB49 bladder tumors from mice lacking cDC1s (Figure 59A), finding that Batf3 deficiency abrogated MTBVAC-induced recruitment of CD8^{+} T cells (Figure 59B). Since we described that MTBVAC enhanced tumor-specific immune responses, we evaluated the response to the tumor antigens Uty and Dby in splenocytes by ELISpot and found that lack of cDC1s completely abrogated Dby, Uty and p15E-specific responses (Figure 59C,D,E). Finally, we also measured MHC-I expression on MB49 tumor cells from

the bladders of Batf3$^{-/-}$ mice, finding that its upregulation driven by intravesical MTBVAC was precluded when cDC1s were absent (Figure 59F). Lastly, improved *in vitro* cytotoxicity against MB49 cells was abolished when splenocytes from MTBVAC-treated Batf3$^{-/-}$ mice were used (Figure 59G).

Altogether these results show that Batf3-dependent cDC1s are essential for the recruitment of CD8^{+} T cells to the bladder, for the induction of CD4^{+} and CD8^{+} tumor-specific responses and for the resulting MHC-I upregulation on tumor cells, all of them driven by intravesical MTBVAC treatment. Consequently, treatment efficacy was abrogated in mice lacking cDC1s, meaning that absence of tumor-specific responses translates into loss of tumor growth control in the bladder.

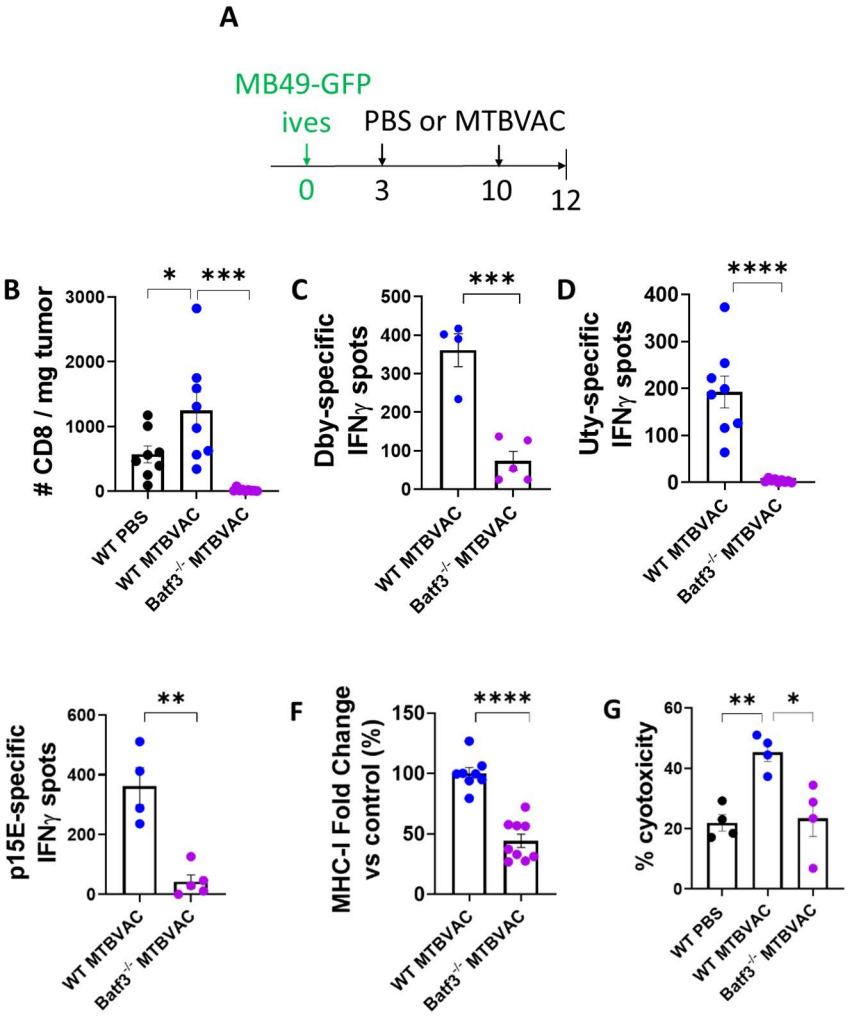

Figure 59. Mice were treated as shown in (A). (B) At day 12, absolute numbers of CD8^{+} T cells infiltrating bladder tumors were analyzed by flow cytometry. (C,D,E) ELISpot analysis of IFN-γ production by splenocytes following overnight incubation with the indicated peptides. (F) MHC-I

expression (fold-change vs WT MTBVAC group) by tumor cells *in vivo*. (G) Splenocyte-mediated cytotoxicity against luciferase-expressing MB49 cells *in vitro*. *n* = 4 (one experiment) or *n* = 8 (two independent experiments) mice/group, depending on the figure.

4.7.8 Combination of intravesical MTBVAC and systemic anti-PD-L1 checkpoint blockade induces efficient antitumor immunity

In previous sections we demonstrated the ability of intravesical MTBVAC to induce therapeutic responses in a setting of low tumor burden, since intravesical treatment was started at day 3 after tumor cell implantation. At this timepoint, there still was not overt outgrowth of tumors into the bladder lumen, but small tumors could be spotted in the epithelial layer (Figure 60). Importantly, at day 3 there are not visible signs of hematuria. MB49 bladder tumors quickly progressed, and at day 6 substantial growth into the bladder lumen and invasion of the lamina propria but not of the muscle layer can be observed (Figure 60). At the same time, hematuria starts to be apparent in mice around the day 6 timepoint, concurring with the tumor growth observed.

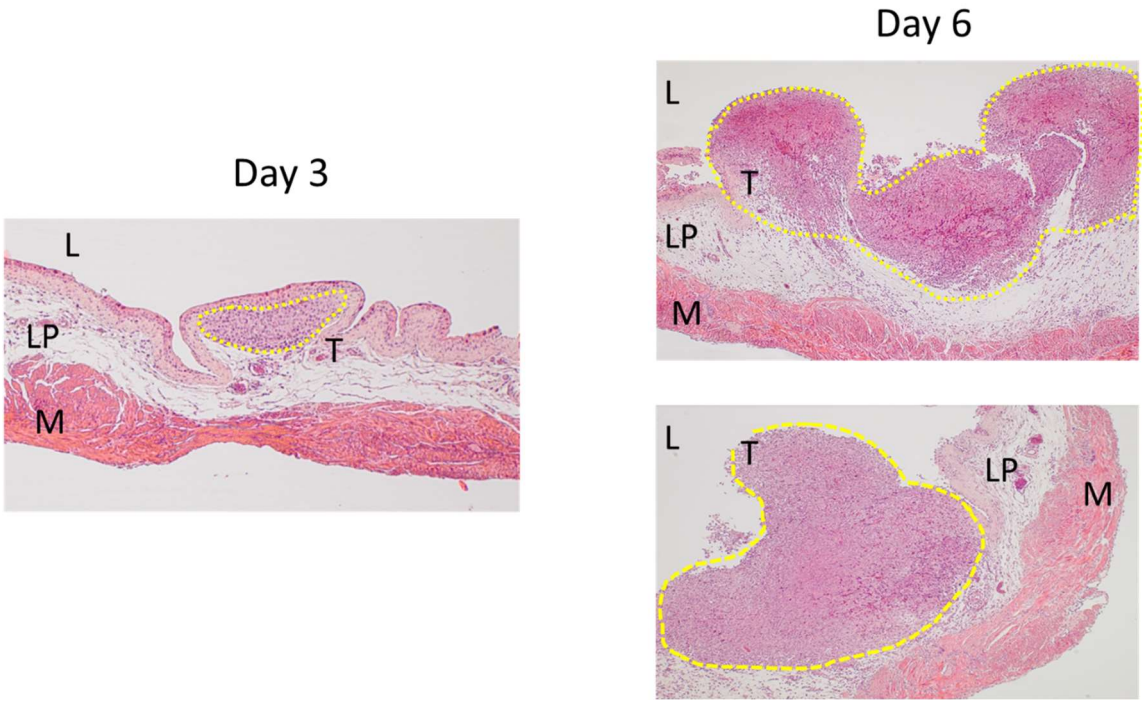

Figure 60. H&E staining of bladder tumors at day 3 or 6 post MB49 tumor cell inoculation. Tumor area is outlined in yellow. L : lumen, T : tumor, LP : lamina propria, M : muscularis. Images are representative of *n* = 3 mice/timepoint.

Therefore, in this section we wanted to test intravesical MTBVAC in already stablished, advanced bladder tumors, by starting treatments at day 6 after tumor implantation, modelling a high tumor burden scenario. As we expected this tumor to be difficult to treat, and since it is a promising strategy for both muscle and non-muscle invasive bladder cancer in the clinic, we also wanted to test the combination of intravesical bacterial therapy with systemic PD-L1 blocking antibodies.

Several observations led us to devise this strategy. First, flow cytometry analysis of MB49-GFP tumor-bearing mice revealed that both $CD45^{-}$ GFP^{+} (tumor cells) and $CD45^{+}$ SSC^{hi} (mostly myeloid cells) compartments showed PD-L1 upregulation after intravesical MTBVAC treatment. Using mice lacking IFN-γ, we found that PD-L1 upregulation was completely reliant on host IFNγ, since PD-L1 upregulation by intravesical MTBVAC was completely abrogated in the absence of this cytokine (Figure 61 and Figure 62). Cell depletion studies and use of $Batf3^{-/-}$ mice revealed that the upregulation of PD-L1 on tumor and immune cells caused by intravesical treatment depended on $CD4^{+}$ T cells and Batf3-dependent cDC1s, but not on $CD8^{+}$ T cells (Figure 61 and 62).

This result indicated that, as was the case with MHC-I, it is the immune system that drives enhanced PD-L1 expression in the bladder TME in response to intravesical treatment. Overall, we hypothesize that IFN-γ-secreting $CD4^{+}$ T cells primed by cDC1s are responsible for driving PD-L1 upregulation in the TME, which could be hindering the therapeutic potential of the treatment.

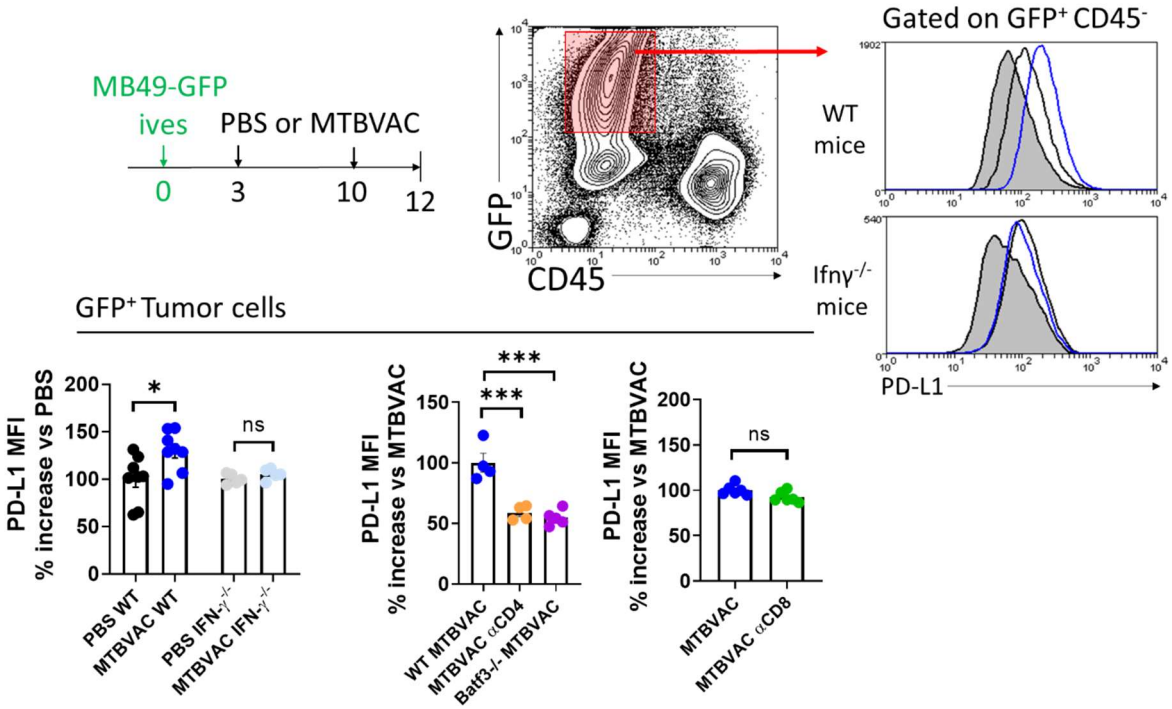

Figure 61. Mice were treated as indicated in the Figure and PD-L1 expression levels in tumor cells was assessed by flow cytometry.

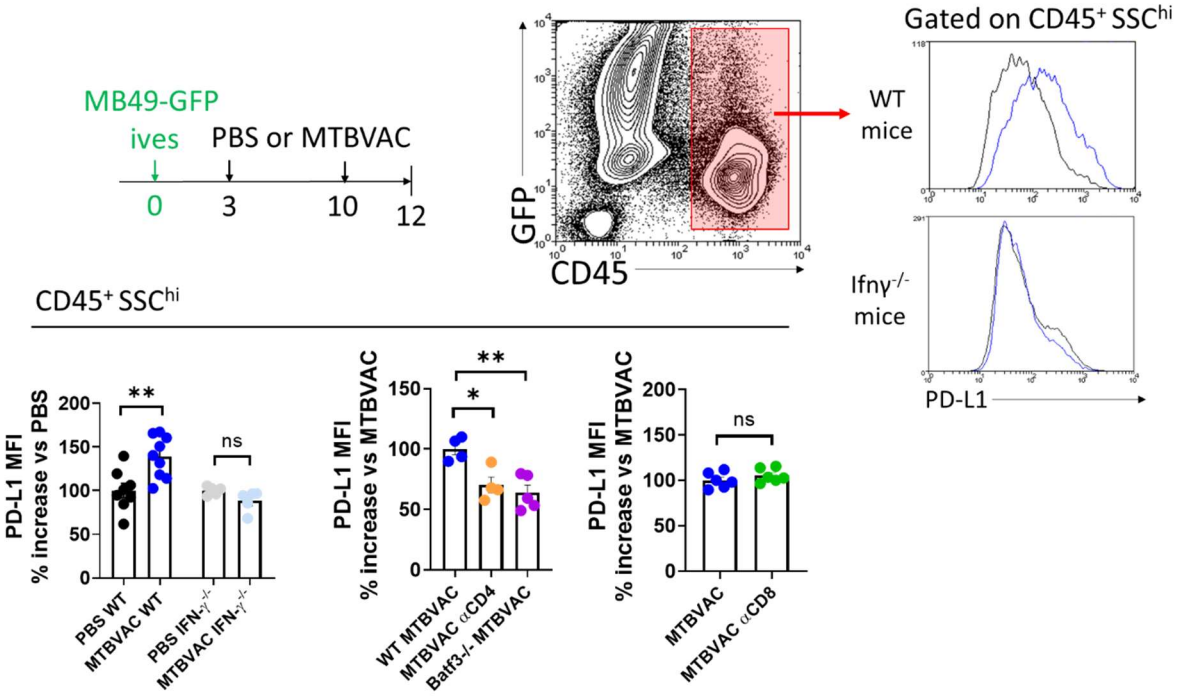

Figure 62. Mice were treated as indicated in the Figure and PD-L1 expression levels in immune cells was assessed by flow cytometry.

Therefore, we tested the combination of intravesical bacterial treatments with PD-L1 blockade administered systemically in the MB49 orthotopic bladder cancer model. We decided to start PD-L1 treatment at day 11 (Figure 64), around the timepoint in which we

observed PD-L1 upregulation in the bladder following intravesical treatment. Intravesical treatments were initiated at day 6 post tumor cell inoculation and continued once every week for a total of 6 (Figure 64).

Use of luciferase-expressing MB49 cells allowed us to quantify tumor-burden in mice by luminescence measurement (performed in two of the three experiments shown in the survival graph) at day 6, confirming homogeneous tumor-burden between groups before the start of the treatments (Figure 63). Luminescence measurements were discontinued after day 6 since they involved mouse anesthesia, which in our hands could lead to the death of mice during the procedure because of their weakened state when bearing bladder tumors.

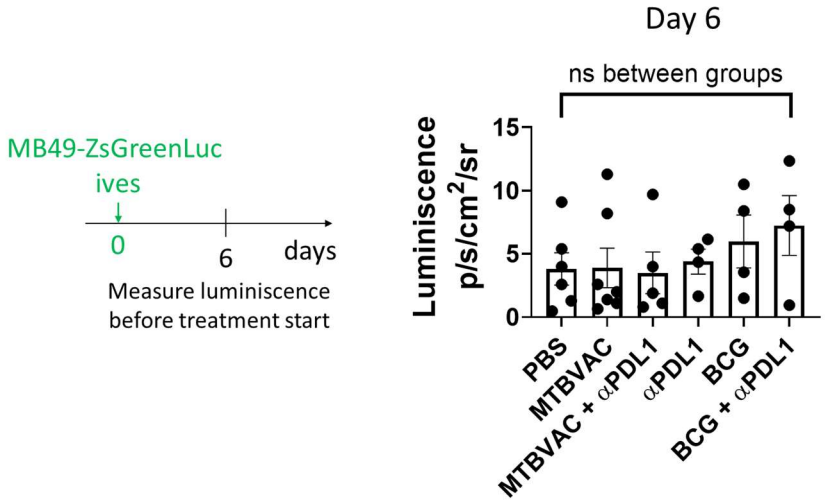

Figure 63. Mice were inoculated with ZsGreen/luciferase-expressing MB49 cells in the bladder and luminescence was analyzed on day 6, following administration of D-luciferin.

Follow-up of mice revealed that intravesical MTBVAC given as monotherapy was successful in driving tumor regression in this treatment setting, with 9 out of 15 mice found tumor-free by macroscopic visualization and histological analysis at day 70 post tumor cell inoculation (Figure 64). Strikingly, combination of intravesical MTBVAC with systemic αPD-L1 induced complete tumor rejection in all mice tested across the three independent experiments conducted (14 out of 14), significantly improving MTBVAC given as a monotherapy. In stark contrast, intravesical BCG or αPD-L1 alone did not provide any survival advantage compared to control PBS. However, the BCG + αPDL1 combination performed significantly better than PBS or BCG alone, although substantially lower than MTBVAC + αPDL1 and comparable to MTBVAC alone (Figure 64).

These results evidence that intravesical MTBVAC treatment can eradicate established bladder tumors in addition to being effective in a lower tumor burden scenario, such as when treatment was started at day 3 post tumor cell inoculation. Additionally, our data suggests that intravesical bacterial therapy can be improved by combination with systemic PD-L1 blockade.

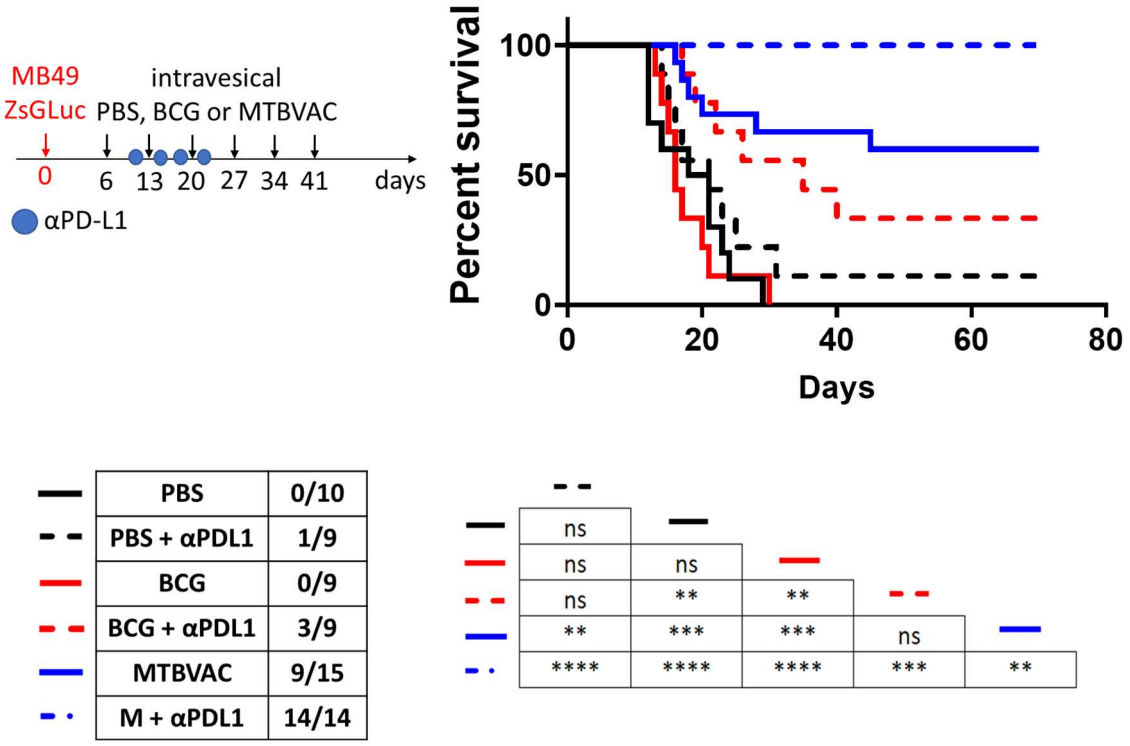

Figure 64. Mice were implanted with MB49-ZsGLuc bladder tumors and treated as indicated in the Figure. Mice were followed-up for survival until day 70. *n* = 9-15 mice/group, from three independent experiments.

Lastly, a reasonable concern for intravesical MTBVAC translation to the clinic would be the safety of the treatment. Safety of MTBVAC administered intradermally has already been shown in clinical trials[346], but intravesical inoculation is a new application for which safety must be proven first in preclinical studies. As a first approximation, we evaluated bacterial load in the bladder and bdLNs of mice which survived MB49 bladder tumors after six weekly MTBVAC intravesical treatments. Out of five mice analyzed at day 90 after tumor cell inoculation (50 days after the last intravesical treatment), we could not culture any bacilli from the bladder or bdLNs, which are the organs most exposed to bacteria. Although this evidences that MTBVAC does not persist in the host for a long time after

intravesical instillation in tumor-bearing mice, additional safety studies are warranted, such as bacterial load evaluation in other organs, histopathological analysis and inoculation in immune-deficient mice.

4.8 Resistance of bladder tumors to bacterial immunotherapy involves upregulation of IFN-γ-stimulated genes

During survival experiments we observed that some mice which received intravesical MTBVAC treatment showed initial apparent regression of their bladder tumor, evidenced by absence of palpable tumor and no visible hematuria. Some of these mice developed long term remissions, with no tumor outgrowth at later stages and no visible tumors upon necropsy at the day 70 experimental endpoint. However, some mice relapsed, and tumors reappeared between 30- and 50-days post tumor cell implantation. We isolated one of these tumors, which arose at day 50 after tumor inoculation, and established a cell line from it which we called Res50. We initially hypothesized that this cell line could be resistant to intravesical MTBVAC treatment representing a common scenario in the clinic, in which a high proportion of tumors are refractory to treatment, and that it would allow us to study mechanisms of resistance to this type of immunotherapy.

Therefore, we implanted Res50 tumors orthotopically and treated them with MTBVAC starting at day 3. We corroborated that Res50 tumors were resistant to intravesical therapy in contrast to MB49 parental tumors (Figure 65). Interestingly, Res50 tumors did not grow faster than parental MB49 in the absence of treatment, evidencing that differences only arose under pressure exerted by treatment. Thus, we generated a bladder cancer cell line which generated tumors resistant to intravesical MTBVAC treatment.

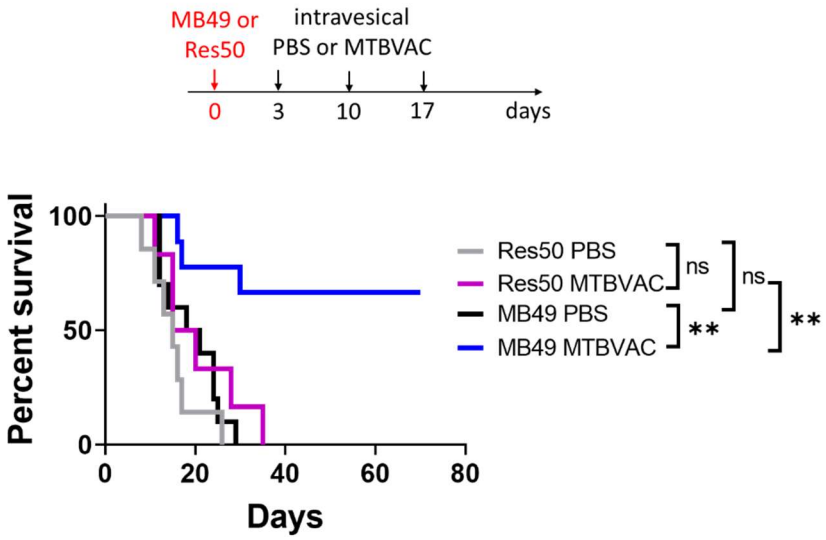

Figure 65. Mice were implanted orthotopically with MB49 or Res50 bladder tumors and treated as indicated in the Figure. Mice were followed-up for survival until day 70. *n* = 6 mice/group, from one experiment.

Resistance to immunotherapy can arise due to immunoediting, which involves the selection of clones that have lost expression of immunogenic neoantigens and thus are less prone to be recognized by $CD8^+$ T cells[418]. Although we did not compare neoantigen expression between MB49 and Res50 tumor cells, we thought that loss of immunogenicity would have made Res50 cells to grow more aggressively than parental MB49 in the absence of treatment as with $B2m^{-/-}$ MB49 tumors, but this was not the case (Figure 65). Instead, differences between the two tumors only became apparent when treatments were administered.

Another mechanism of tumor resistance to immunotherapy is loss of MHC-I expression due to mutations on the antigen presentation machinery, which hinders recognition of tumor cells by $CD8^+$ T cells[419–421]. Additionally, mutations in the tumor-intrinsic IFN sensing pathway (such as Jak1, Ifngr, Ifnar or Stat1 mutations)[420,422], can also preclude upregulation of MHC-I following IFN sensing, which we have shown to be a key step in the mechanism of action of bacterial immunotherapy. Therefore, to check whether Res50 had developed defects in the antigen presentation machinery or IFN sensing we exposed them to IFN-γ or IFN-α *in vitro* and analyzed IFN-stimulated genes such as MHC-I, MHC-II, PD-L1 and Qa-1^b (a NKG2A/C/E ligand), and LGALS9 (a TIM-3 ligand). Surprisingly, we found that Res50 cells expressed higher basal MHC-I levels than parental MB49, and this difference was still observed when cells were exposed to either type of IFN for 24 h (Figure 66).

Surprised by the fact that tumor cells with very high MHC-I expression were resistant to bacterial immunotherapy, we analyzed other IFN stimulated genes which can inhibit $CD8^+$ T cell function. For instance, basal expression of PD-L1 did not differ between both cell lines (Figure 66). However, after IFN-γ or α exposure, Res50 upregulated PD-L1 to higher levels than parental MB49 cells (Figure 66).

Although MHC-II expression on tumor cells can make them amenable to $CD4^+$ T cell targeting, it can also function as an inhibitory ligand for T cells upon ligation of LAG-3[423]. In MB49 and Res50 cells only IFN-γ but not IFN-α exposure increased MHC-II expression (Figure 66). As with PD-L1, Res50 upregulated MHC-II to a higher extent than parental MB49 cells after incubation with IFN-γ, although basal levels did not differ between both cell lines (Figure 66).

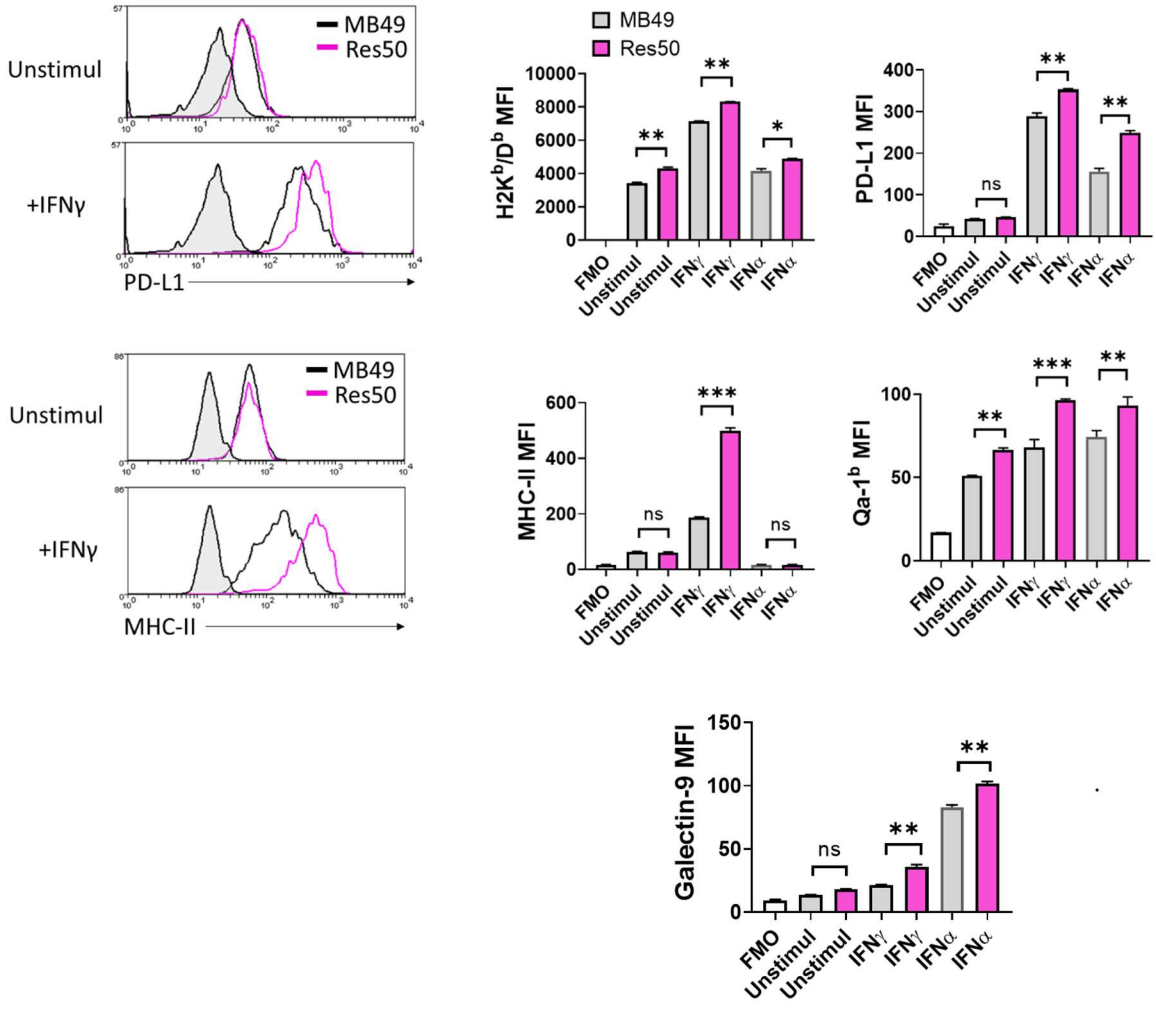

Figure 66. Flow cytometry analysis of the expression of different surface markers by MB49 and

Res50 tumor cells *in vitro* either unstimulated or stimulated for 24 h with 50 ng ml^{-1} of IFNα or IFNγ. Results shown are pooled from two independent experiments run in triplicates.

The human HLA-E homolog Qa-1^b is a non-classical MHC molecule which binds the NK and $CD8^+$ T cell inhibitory receptor CD94/NKG2A. We found that parental MB49 cells expressed detectable levels of surface Qa-1^b and upregulated it in response to IFN-α or γ, as expected (Figure 66). Interestingly, Res50 cells expressed higher levels of this inhibitory molecule in basal conditions and when stimulated with IFN (Figure 66), similarly to that observed for MHC-I.

Lastly, Galectin9 (LGALS9), an inhibitory ligand Tim-3 on $CD8^+$ T cells[424], was also found elevated in Res50 cells over MB49 cells, both in untreated and treated conditions (Figure 66). Of note, the expression of this molecule was preferentially induced by IFN-α.

Altogether, these results suggest that Res50 cells have a more active IFN sensing pathway which leads to enhanced expression of IFN-induced inhibitory ligands such as PD-L1, Qa-1, MHC-II or LGALS9, which could explain their resistance to intravesical bacterial immunotherapy with MTBVAC. It will be interesting to test in the future whether therapeutic blockade of this inhibitory ligands (antiLAG-3, antiNKG2A, antiTIM-3) could sensitize these resistant tumors to intravesical immunotherapy with MTBVAC.

4.9 Discussion

Intravesical BCG, one of the first cancer immunotherapies approved by the FDA, has been the gold-standard therapy against NMIBC for more than four decades. Despite its success, there is a wide margin for improvement and the mechanism of action of this treatment remains incompletely understood, both from the point of view of the bacterial determinants of protection and the host immunological mechanisms.

This treatment fails in up to 50% of patients, considering recurrence episodes and treatment withdrawals due to severe adverse events, representing approximately 10% of cases.[425] Around 70% of the patients who suffer recurrence episodes following BCG treatment undergo progression to T2 muscle-invasive disease, with radical cystectomy being the only therapeutic option in the clinical practice[426]. Moreover, BCG is not a unique strain but a diverse family of substrains with genetic heterogeneity. As a result, there are phenotypical differences among BCG substrains with respect to antigenicity and reactogenicity[294,427]. In

fact, some studies have reported differences between the BCG strains Connaught and Tice in preventing NMIBC recurrence and progression[293,375]. In this regard, MTBVAC represents a well-characterized vaccine strain which would eliminate the need to use BCG strains differing in efficacy. Importantly, use of MTBVAC for bladder cancer treatment might allow a reduction of the bacterial dose and/or number of instillations, which could lower the incidence of adverse effects which are produced currently by BCG[428]. Therefore, it will be interesting to determine the antitumoral efficacy of decreasing doses of MTBVAC in bladder tumor-bearing mice and compare it with the standard dose of BCG.

It is believed that close contact between BCG and the bladder epithelium is needed to achieve an optimal therapeutic effect in bladder cancer[429]. Indeed, blocking of BCG attachment to the bladder *in vivo* using fibronectin-directed antibodies impaired treatment efficacy in mouse models[385]. A lower antitumoral potency of heat-killed BCG has also been reported[430], suggesting that bacteria do not bind passively to bladder epithelium, but that instead they actively execute this process. Several studies have hypothesized that BCG infects bladder tumor cells *in vivo*, and that this is a key step in order to achieve an antitumoral effect[317,431]. As a response to BCG infection, tumor cells would release proinflammatory cytokines which would in turn activate the immune system[284,432]. In addition, it has been proposed that BCG-infected tumor cells express BCG derived antigens in MHC that may be targeted by BCG-specific T cells[432]. However, these hypotheses rely mostly on *in vitro* experiments, and definitive prove that BCG infects tumor cells *in vivo* is lacking, both in humans and mouse models[295]. In the mentioned studies, bladder tumor cells seeded in a 2D monolayer *in vitro* were exposed to high MOIs of BCG for as long as 24 hours. This allows bacteria to enter in contact with tumor cells simply by gravity force, and most likely does not accurately reflect the environment that BCG encounters in the bladder following an intravesical instillation which is maintained in the bladder for only 2 hours. Indeed, some studies found that in urine samples from patients undergoing intravesical BCG treatment analyzed by TEM, it was mostly leukocytes that harbored BCG, while there was no evidence of BCG phagocytosis by epithelial or tumor cells[433]. This was also observed recently by the group of Dr. Mar Valés by TEM analysis of urine samples from patients receiving intravesical BCG (personal communication).

Here, we propose that mycobacteria delivered intravesically into bladder tumors do not primarily infect epithelial or tumor cells, but are instead captured by phagocytic immune cells. Indeed, bladder macrophages ingest uropathogenic *E. coli* in mouse models and harbor more bacteria than DCs and other immune cell subsets, at least at early timepoints[434,435]. Here, we detected fluorescent MTBVAC bacilli in macrophages, neutrophils, monocytes and DCs, although only a single timepoint was analyzed, so future studies will be needed to determine the kinetics of infected populations over time. An interesting scenario would be that a first bacterial instillation "primes" bladder tissue by inducing the recruitment of phagocyte immune cells, which would facilitate internalization of mycobacteria in subsequent instillations. Indeed, in patients, the proinflammatory response measured in the urine was boosted following the 6th BCG instillation when compared to the first one, which is reminiscent of a trained innate immunity mechanism[436]. In our experiment involving MTBVAC-infected immune cell populations in bladder tumors, we could not discern whether the observed infected cell populations were a result of the first instillation (day 3), the second (day 10, two hours before euthanasia) or a combination of both, so additional experiments are needed to determine the effect of a first instillation in subsequent instillations and whether immune cell populations are durably infected by mycobacteria. Most importantly, it remains to be studied whether infection of immune cells in bladder tumors by mycobacteria truly influences the development of antitumor responses, especially since few cells were found infected. In our work, a higher number of bacteria in bladder tumors and lymph nodes concurred with stronger recruitment of immune cells to the bladder and overall improved antitumor responses, suggesting that increased bacterial load drives enhanced stimulation of the immune system.

Indirect evidence from other groups also suggested that bladder DCs can indeed be infected by BCG bacilli, since they were able to present BCG-derived peptides to BCG-specific CD4^{+} T cells *ex vivo*[295]. Most importantly, BCG and MTBVAC bacilli can be readily detected in bladder draining lymph nodes, which implies uptake by DCs in the bladder TME and migration to lymph nodes. An interesting possibility would be that DCs harboring mycobacteria have an enhanced maturation status and/or ability to migrate to the LN. We did not evaluate whether immune cells harboring mycobacteria in the bladder TME had an increased immunostimulatory phenotype in comparison to non-infected, although previous work from our laboratory showed that both infected and non-infected alveolar macrophages

are activated by BCG in the lung following pulmonary vaccination[264], meaning that upon infection, macrophage derived cytokines can alter surrounding populations.

Results shown here evidenced that MTBVAC has an intrinsic better ability to colonize the bladder epithelium compared with BCG, in a process that seems to be mediated by the proteins ESAT6 and CFP10. These two proteins, which are described to be secreted as an heterodimer, have been extensively studied in *M. tuberculosis* and are key virulence factors and immunodominant antigens[437]. Importantly, BCG does not express ESAT6/CFP10, while MTBVAC does. We have not yet characterized the molecular mechanisms by which ESAT6/CFP10 mediates bacterial attachment to the bladder epithelium, but previous studies suggested a role for these proteins in *M. tuberculosis* attachment to lung epithelial cells through the extracellular matrix protein laminin[392] or to airway microfold cells through the scavenger receptor B1[438]. Thus, we could speculate that mycobacteria-expressing ESAT6/CFP10 could be better fitted to adhere to the bladder epithelium through laminin or the scavenger receptor B1 in a similar manner as the described in the lung, or to other still unknown ligands. Importantly, both laminin and the scavenger receptor B1 are present in bladder tissue, with an augmented expression associated with bladder cancer development[439–441]. Conceivably, improved adherence to the bladder epithelium increases the chances of bacteria to be internalized by a professional phagocyte, which could explain the higher capacity of MTBVAC to colonize bladder tissue over BCG. Indeed, deletion of ESAT6/CFP10 proteins does not compromise the ability of MTBVAC to infect BMDMs or to survive inside them (data from our laboratory, not shown), but it does influence colonization of bladder tissue. However, ESAT6/CFP10 are not the only proteins involved in bacterial adherence to epithelium, so another plausible explanation is that the lack of these factors alters the expression or secretion of other proteins involved in colonization of the host. Moreover, there are more proteins expressed in MTBVAC and not in BCG that could be mediating these effects, although loss of ESAT6/CFP10 in MTBVAC almost completely abrogates the observed phenotype.

Interestingly, it has recently been shown that artificial overexpression of a mannose-binding protein (FimH) in BCG enhanced adhesion to the bladder epithelium and colonization of the bladder TME and consequently improved therapeutic responses in the orthotopic MB49 model[442]. This study and ours independently show that modulating the

ability of a bacteria to colonize the bladder TME can boost their antitumor efficacy upon intravesical inoculation.

Our results demonstrate that intravesical bacterial therapy triggers a tumor-specific response, and lack of therapeutic efficacy in Perf$^{-/-}$ and Rag1$^{-/-}$ mice suggested that the cytotoxic activity of CD8$^+$ T cells might be ultimately responsible for treatment success, a conclusion that is supported by the absence of therapy induced long-term responses in mice bearing MHC-I deficient bladder tumors. Importantly, rechallenge experiments evidence that therapy-induced tumor-specific immune memory driven by T cells is durable and functional against both localized and disseminated tumor cell rechallenge, even in the case of MHC-I loss.

Previous studies have reported that MHC-II neoantigens and tumor-specific CD4$^+$ T cells are required for efficient antitumor immunity and response to checkpoint blockade in mouse models[80]. In this regard, here we describe that bacterial immunotherapy enhances the CD4 tumor-specific response, and that CD4$^+$ T-cell depletion completely abrogates the CD8 tumor-specific response and the vaccine therapeutic effect. More studies are needed to elucidate mechanisms by which CD4$^+$ T cells prime the CD8+ response, but it is likely that the CD40/CD40L axis could have a role, since previous work identified that CD40 agonists eliminated bladder tumors by inducing a CTL response[204], and CD40 expression in cDC1s is needed for the rejection of immunogenic tumors in mice[79]. Moreover, CD4$^+$ T cell-secreted IFN-γ can upregulate MHC-I on tumor cells but could also have antiproliferative effects[25], or enhance tumor cell sensitivity to cell death-inducing stimuli such as tumor necrosis factor (TNF) or Fas. Critically, we found that cDC1s were completely required for priming tumor specific CD4$^+$ T cells, which agrees with recent reports[79]. Alternatively, CD4$^+$ T cell could be killing tumor cells by themselves, as cytotoxic subsets of CD4$^+$ T cells have been found specifically in human bladder tumors[443].

It is interesting to note that in a recent study genetic deletion of MHC-II in MB49 cells did not affect their growth rate when orthotopically implanted in the bladder in comparison to parental WT MB49 cells. Moreover, although intravesical BCG antitumor effect in this model is very limited, as is our case, response of bladder tumors to treatment was unaffected by tumor cell MHC-II deletion[342]. Although we would need to confirm this using intravesical MTBVAC, which properly rejects MB49 WT tumors, this result would suggest

that activation of $CD4^+$ T cells in the TME by intravesical bacteria is not driven by MHC-II presentation of tumor antigens by the tumor cells themselves, but by antigen presenting immune cells in the TME.

Our work in $Batf3^{-/-}$ mice unequivocally shows that cDC1s are needed for the enhanced priming of tumor-specific $CD4^+$ and $CD8^+$ responses during MTBVAC therapy, as well as for the infiltration of $CD8^+$ T cells into the TME. This DC subset is essential in cancer immunosurveillance and is also required for the response to other immunotherapies such as checkpoint blockade or αCD40[204,444]. Bacterial immunotherapy induced activation of cDC1s, based on CD86 and CD40 expression, and favored the capacity of this cellular subset to acquire tumor-derived material and deliver it to the bdLNs, where antigen presentation and induction of tumor-specific responses are expected to occur. How does MTBVAC treatment facilitate the loading of cDC1s with tumor-associated material? We hypothesize that intravesical delivery of MTBVAC may activate innate immune effector mechanisms such as macrophages or NK cells at an early stage in the bladder TME, which would induce tumor cell death and the initial release of tumor antigens. However, this needs to be formally tested and the early events following bacterial instillations merit further investigation. In any case, released tumor-associated material would then be acquired by cDC1s, responsible for priming tumor-specific T cells in the bdLN. Conceivably, influx of $CD4^+$ and $CD8^+$ into the bladder TME could be facilitated by a proinflammatory cytokine and chemokine milieu established in response to bacterial infection. Importantly, this mechanism might be further boosted by subsequent rounds of intravesical instillations in a self-sustaining manner. What has become clear is that for bacterial immunotherapy to be effective, tumor-specific adaptive immune responses are indispensable, and innate immune effectors cannot drive tumor rejection by themselves, at least in this specific model.

Since no model is perfect, it would be desirable to extend our findings in MB49 tumors to other bladder cancer models, such as those consisting in implantation of MBT-2 bladder cancer cell lines in C3H mice, adding the advantage of using a genetically different mouse strain, or the N-butyl-N-(4-hydroxybutyl)-nitrosamine (BBN) carcinogen-driven model of bladder cancer, which more faithfully models human bladder cancer. Indeed, a recent study which analyzed the transcriptome of tumor cell lines derived from an $Upk3a\text{-}Cre^{ERT2}$; $Trp53^{L/L}$; $Pten^{L/L}$; $Rosa26^{LSL\text{-}Luc}$ (UPPL) genetically driven mouse model of bladder cancer

or from the BBN model, found that they better modelled human bladder cancer than the widely used MB49 tumor cells, which appeared to resemble fibroblast-like cells having undergone epithelial-to-mesenchymal transition, and not epithelial cells[445].

Our work shows that MTBVAC drives the rejection of fully established bladder tumors in which intravesical BCG is completely ineffective, suggesting that this improved version of bacterial therapy might be efficient against BCG-unresponsive tumors, for which few therapeutic options exist besides radical cystectomy. Critically, the antitumoral effect of MTBVAC was greatly improved by the systemic administration of PD-L1 blocking antibodies. Of note, intravesical MTBVAC drove PD-L1 upregulation both in tumor and immune cells, which represents a mechanism of adaptive resistance to immunotherapy. Several studies have correlated high levels of PD-L1 expression in tumor infiltrating immune cells with a better response to checkpoint blockade immunotherapy[446], since it is a biomarker of a functional ongoing antitumor immune response that can be boosted by blocking this axis. Indeed, it has been shown that IFN-γ produced by $CD8^+$ T cells upregulates immunosuppressive mechanisms driven by indoleamine-2,3-dioxygenase (IDO) and PD-L1 in the tumor microenvironment[155]. Our data suggest that the higher level of PD-L1 expression found on tumor-infiltrating immune cells is a consequence of enhanced IFN-γ production induced by bacterial treatment, and therefore it could be acting as surrogate marker of the vaccine-induced antitumoral response and sensitizing the tumor to checkpoint blockade immunotherapy.

Contrary to our results, a previous study using the orthotopic MB49 model found that treatment with antiPD-L1 in monotherapy did favor tumor control, and combination with intravesical BCG did not further extend mice survival. However, in our experiments we did not find a therapeutic effect of PD-L1 blockade when given as a monotherapy. This could be explained by their use of a fully human antiPDL1 IgG1 antibody (Avelumab), whereas we used the rat 10F.2H11 clone, which is an IgG2. Therefore, antibody-dependent cytotoxicity (ADCC) towards PD-L1 expressing MB49 cells or PD-L1 immunoregulatory myeloid cells could conceivably happen in their model and not in ours, since IgG2s display much lower affinity for Fcγ receptors compared to IgG1s[447]. Of note, human IgGs can bind mouse Fcγ receptors and trigger ADCC[448]. Anyway, we found that PD-L1 blockade improved intravesical bacterial therapy in our experimental settings, and in our case, this

can be fully ascribed to blockade of the PD-1/PD-L1 immunosuppresive axis and not to ADCC mechanisms. Supporting our findings, other groups have recently found working with mouse models that adaptive resistance of MB49 tumors to a novel bacterial minicell-based oncolytic agent given by the intravesical route was due to enhanced PD-L1 expression in the TME of treated mice, and this was circumvented by treatment combination with systemic antiPD-L1 (in this case the rat 10F.2H11 clone), which was less effective when given alone[449]. This study, in conjunction with our work, indicate that PD-L1 blockade works best when an antitumor immune response has already been ignited by intravesical treatment with bacteria, at least in our experimental settings. Therefore, our results suggest that the combination of intravesical bacteria with immune checkpoint blockade could highly benefit both BCG-naïve and BCG-unresponsive NMIBC patients, something which is currently being evaluated in numerous clinical trials.

Altogether, our results expand our understanding about how intravesical delivery of live-attenuated mycobacterial vaccines achieve immune system activation and tumor rejection. In addition, we describe for the first time the bacterial proteins ESAT6 and CFP10 as determinants of intravesical bacterial immunotherapy efficacy against bladder tumors. Our findings could be helpful in the future to develop more effective bacterial-based treatments against bladder cancer, either based on *M. tuberculosis* attenuated strains or improved versions of BCG and provide a rationale for further evaluation of intravesical MTBVAC for NMIBC treatment in clinical trials, both alone and in combination with PD-L1 checkpoint blockade.

4.10 Conclusions

1. Weekly intravesical delivery of MTBVAC into the bladders of MB49 tumor bearing mice yields improved therapeutic responses compared to BCG, the current gold-standard for NMIBC treatment.

2. We identify the proteins ESAT6 and CFP10, which are absent in BCG, as key mediators of bladder tissue colonization by MTBVAC, driving enhanced immune cell recruitment and improved antitumor responses.

3. Our data suggest that following intravesical inoculation of BCG or MTBVAC into tumor-bearing mice, bacteria are internalized mostly by immune myeloid cells and not epithelial or tumor cells

4. We found that intravesical MTBVAC therapy functioned by enhancing cDC1-dependent priming of both tumor-specific $CD4^+$ and $CD8^+$ T cells and their recruitment into the bladder TME.

5. MTBVAC therapy favored MHC-I upregulation in tumor cells, facilitating their recognition by $CD8^+$ T cells, but also drove increased expression of the immunoregulatory molecule PD-L1 by a mechanism involving IFN-γ secretion by T cells.

6. Evidencing that PD-L1 upregulation represented an adaptive mechanism of resistance to bacterial immunotherapy, therapeutic administration of PD-L1 blocking antibodies greatly boosted the efficacy of intravesical BCG and MTBVAC in MB49 tumor-bearing mice.

7. Isolation of a regressing bladder tumor revealed that resistance to bacterial immunotherapy can arise via the upregulation of IFN-induced immune regulatory molecules in tumor cells, and will allow us to study whether blocking this pathways could aid in the treatment of bacterial immunotherapy-resistant tumors.

Chapter 2

Intravenous delivery of BCG to the lung enables antitumor immunity

5.1 Chapter introduction

More than one century ago, Raymond Pearl observed a correlation between presence of lung tuberculosis lesions and lower ratios of cancer in autopsies[209,210]. As described in the general introduction, based on these findings researchers hypothesized during the subsequent decades that the attenuated mycobacterium BCG could be used as an anticancer therapy[230,231,450]. However, after conducting different clinical trials for several types of tumors, including leukemia, prostate, gastric or lung cancer, only the application of BCG for bladder tumors succeeded[226], becoming one of the first immunotherapies approved by FDA in 1990. Indeed, more than four decades later, intravesical BCG is still a first-line therapy against non-muscle invasive bladder cancer (NMIBC), as we have seen in the previous section.

Generally, it is well-accepted that contact of BCG with the tumor tissue is necessary for antitumoral effect[284]. This may be the reason why BCG has only found success for the treatment of human melanoma and bladder cancer, the only two types of cancer in which it is used nowadays. Intralesional administration in melanoma and intravesical in bladder cancer clearly allow BCG to enter in contact with the tumor and its surrounding environment. Although clinical application of BCG in other cancers given by the intradermal route has been explored, it was generally not very successful[451]. Therefore, we hypothesized that for BCG to effective in other tumor types, such as lung cancer, it would require a route of administration allowing contact of the bacteria with the tumor-bearing organ.

Three different discoveries led as to experimentally test the intravenous route of administration of BCG for cancer treatment. First, in 1959 Lloyd Old described that mice vaccinated with BCG by the intravenous route were almost completely resistant to subcutaneous transplantation of three different syngeneic tumors, although in this work BCG was administered before tumor inoculation[221]. More recently, Seder *et al.* showed that intravenous BCG vaccination prevented *M. tuberculosis* infection in rhesus macaques with a much higher efficacy than BCG given by other routes such as intradermal, aerosolized, or even both at the same time[218]. Importantly, intravenous BCG vaccination allowed colonization of the lung by the bacteria, which is a prior desirable for cancer treatment. In the third place, intravenous BCG administration alters the hematopoietic stem cells

compartment, leading to the generation of trained macrophages with enhanced responses to secondary stimuli, such as *M. tuberculosis*. Although we did not know whether this mechanism would also play an important role in a cancer-related scenario, the potential generation of immune-stimulatory myeloid cells is a priori a desirable event for the development of efficient antitumor immune responses.

Since an active area of research in the laboratory is mucosal vaccination for the prevention of tuberculosis infection[264], our initial idea consisted in testing whether mucosal (intranasal) vaccination with BCG would prevent experimental metastasis of tumor cells to the lung, which we found it did. This idea evolved into a more therapeutic approach, as we observed that intranasal treatment with BCG could also delay tumor growth in the lung even when it was administered after tumor cell inoculation. Next, for the reasons given above, we went on to test treatment with BCG given by the intravenous route, which resulted surprisingly effective in three different mouse models. Lastly, given the success of this therapeutic approach, we focused on studying the immunological mechanism of action behind its effectiveness.

5.2 Prophylactic vaccination with live-attenuated mycobacteria prevents metastasis to the lung

As a first approximation, we vaccinated mice with 10^6 CFUs by the intranasal (inBCG) or subcutaneous (scBCG) route. One month later, mice were challenged intravenously with B16-F10 melanoma cells, which generate metastatic tumor nodules in the lungs of mice, and counted tumor foci at day 15.

We found that inBCG or inMTBVAC reduced the number of lung metastases at day 15 when compared to controls given PBS, whereas scBCG did not. We performed the same experiment but vaccinating mice three months before the B16-F10 challenge and obtained similar results (Figure 67). These preliminary results meant that vaccination with live-attenuated mycobacteria can prevent experimental metastasis to the lung, and that colonization of the target organ by the bacteria is needed for this effect.

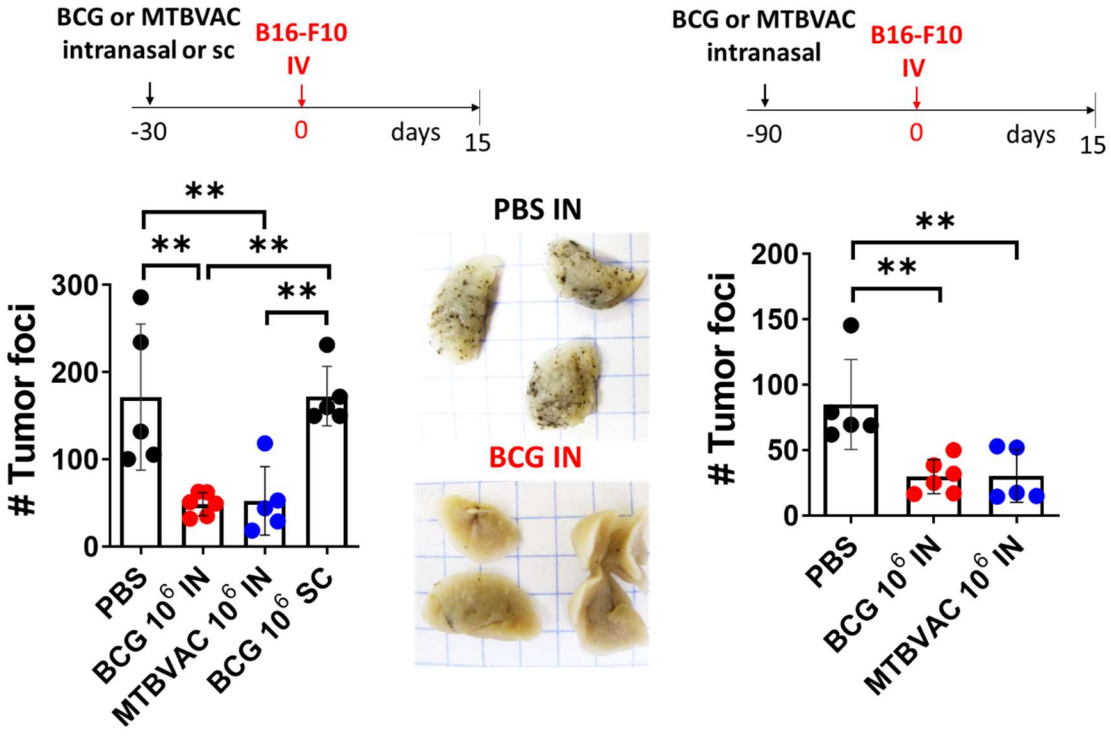

Figure 67. Mice were vaccinated either intranasally or subcutaneously 30 or 90 days before tumor challenge. 15 days after intravenous inoculation of $1{,}5x10^5$ B16-F10 tumor cells, lung metastases (tumor foci) were counted by visual inspection by two researchers and the mean was used. *n* = 5-6 mice/group, from one experiment.

5.3 Mouse models of tumors growing in the lung for survival experiments

Although the prevention of lung metastasis by BCG administration was an interesting finding, we thought that it would be more clinically relevant to test BCG in a therapeutic scenario, that is, after the tumor is established in the lungs. Therefore, we abandoned the previous line of research and focused on studying BCG efficacy against tumors growing in the lung when administered after tumor cell inoculation.

Additionally, in the following experiments we decided to evaluate mouse survival instead of just counting lung metastases at a given day. This way, we would also evaluate the health status of the mouse, including weight loss, appearance (hunched posture, ruffled fur, pale mucous membranes, dehydration), quality and frequency of breathing and general behavior (lethargy, response to stimuli), which we used as criteria for the application of humane endpoint.

We first titrated the B16-F10 inoculum dose for survival experiments, finding that a dose of $5x10^4$ best suited us to avoid mice dying too early for the vaccine to make an effect and to avoid long survival experiments or less than a 100 % tumor take (Figure 68A).

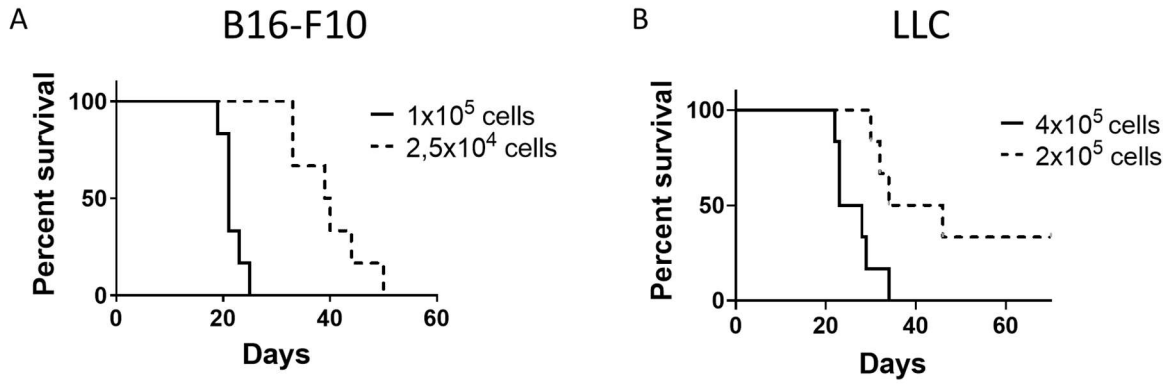

Figure 68. Survival of mice inoculated with different doses of B16-F10 melanoma cells (A) or LLC lung adenocarcinoma cells (B) by the intravenous route. *n* = 6 mice/group, from one experiment.

We also did this with LLC tumor cells, which generate orthotopic lung tumors when administered intravenously[452], choosing a dose of $4x10^5$ cells since the lower $2x10^5$ dose did not allow for a 100 % tumor take (Figure 68B).

As a third lung cancer model, we initially wanted to test BCG in a GEM mouse model of lung adenocarcinoma based on Cre recombinase-inducible expression of a mutated allele of Kras ($Kras^{LSLG12Vgeo}$). Injection of tamoxifen into this mouse strain drives expression of Cre recombinase in all tissues, therefore we had problems with tumors arising in other organs than the lungs, which complicated the interpretation of results from survival experiments. Additionally, in our hands tumorigenesis in this model was very slow, with mice starting to show symptoms 1 year after the induction of Cre recombinase expression. To overcome these issues, we established a cell line from a lung tumor arising in one of these mice with the objective of generating a faster and less cumbersome lung cancer model.

As shown in Figure 69, 8 months after tamoxifen injection into Ubc-Cre-ERT2; $Kras^{LSLG12V\beta Geo}$ mice, we euthanized a mouse and observed presence of tumor nodules in the lungs. This tumor nodules were excised, homogenized and plated on Petri dishes. After 2 weeks of incubation, we observed tumor cell growth and subcultivated the cells for 3 more passages, establishing a cell line which we named KC8. Since Ubc-Cre-ERT2; $Kras^{LSLG12V\beta Geo}$ mice came of a mixed genetic background, we checked whether transplanted KC8 cells were tumorigenic after transplantation into C57BL/6 mice (Figure 69).

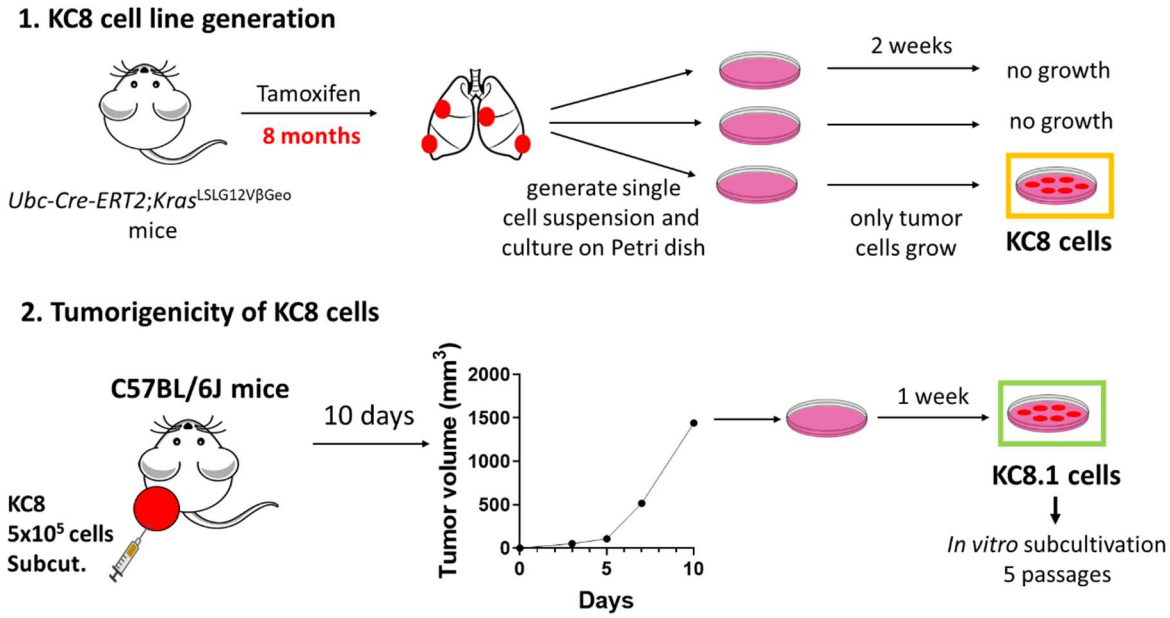

Figure 69. Schematic depiction of KC8.1 lung adenocarcinoma cell line generation.

We further isolated this growing tumor and established a cell line from it which we named KC8.1. Next, we confirmed that KC8.1 cells were tumorigenic when transplanted subcutaneously into C57BL/6 mice. To generate orthotopic lung adenocarcinomas, we first tried intratracheal inoculation of KC8.1 cells, although we did not manage to generate lung tumors with this method. However, intravenous delivery of KC8.1 cells did originate lung orthotopic tumors (Figure 70). Titration of the number of cells inoculated revealed a clear dose-dependent decrease in mice survival (Figure 70).

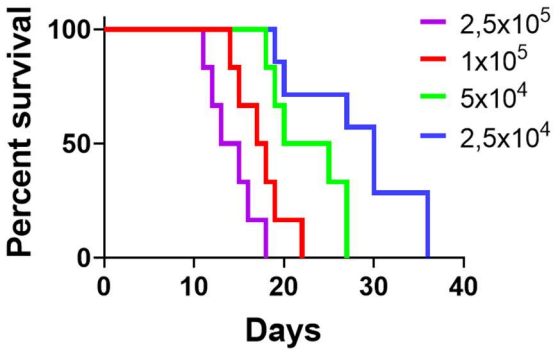

Extrapulmonary metastases

Cell number	Lung	Subcutaneous	Pleural cavity	Lymph Node	Cervical/urethral
$2,5x10^5$	6/6	0/6	0/6	0/6	0/6
$1x10^5$	6/6	3/6	3/6	3/6	0/6
$5x10^4$	6/6	6/6	5/6	5/6	2/6

Figure 70. Survival of mice inoculated with different doses of KC8.1 lung adenocarcinoma cells by the intravenous route and frequency of metastases in distinct anatomical locations observed by visual inspection. *n* = 6 mice/group, from one experiment.

Additionally, with lower inoculum doses, such as $1x10^5$ or $5x10^4$, increased mice survival allowed metastatic outgrowth to become apparent in other organs than the lung (Figure 70). Upon necropsy after following humane endpoint criteria, tumor nodules in the lung were observed in all cases across all doses assayed. However, in the $1x10^5$ group tumors were also observed in the pleural cavity (in 50 % of the mice), also known as malignant pleural effusions, something which has been described for other Kras mutant lung adenocarcinoma cell lines and was dependent on mutated Kras expression[453]. We also observed the generation of subcutaneous tumors in the neck in 3 out of 6 mice inoculated with $1x10^5$ KC8.1 tumor cells, as well as in the mediastinal lymph node. With a smaller dose of $5x10^4$,

the incidence of tumors appearing in the described locations increased to almost a 100 %, and metastases also appeared in the cervical/urethral region in 2 out of 6 mice (Figure 70).

With these results in mind, in the following experiments we chose to work with an intermediate dose of $1x10^5$ KC8.1 cells, taking into consideration for survival experiments that metastases can appear in locations other than the lungs. Since at higher doses ($2,5x10^5$) of KC8.1 cells metastases in other regions did not appear and mice quickly succumbed due to tumor burden in the lung (Figure 70), we hypothesized that extrapulmonary metastases could originate from primary lung tumor nodules, although this asseveration needs further research.

5.4 The route of administration of BCG influences its efficacy against lung tumors in a therapeutic scenario

Once we had the models optimized, we went on to test different routes of BCG administration to treat tumor bearing mice. We decided to treat mice 7 days after tumor cell inoculation, since we confirmed that at this timepoint both B16-F10 and LLC tumors were already established in the lungs when analyzed by histological analysis (Figure 71 and 72).

As expected, untreated B16-F10 and LLC lung tumors progressively grew when analyzed at later timepoints (Figure 71 and 72). Of note, we observed that B16-F10 cells tended to form smaller tumor nodules but more numerous, whereas LLC cells formed bigger tumor nodules. For example, we can observe 7 small tumor nodules in a representative fraction of the lung of a mice inoculated with B16-F10 and analyzed at day 7 (Figure 71), whereas with LLC inoculation we could observe 8 nodules at day 7 throughout the whole lung. We additionally confirmed establishment of live tumor cells in the lung at day by luminescence analysis using luciferase-expressing B16-F10 cells and D-luciferin injection into tumor-bearing mice (Figure 73).

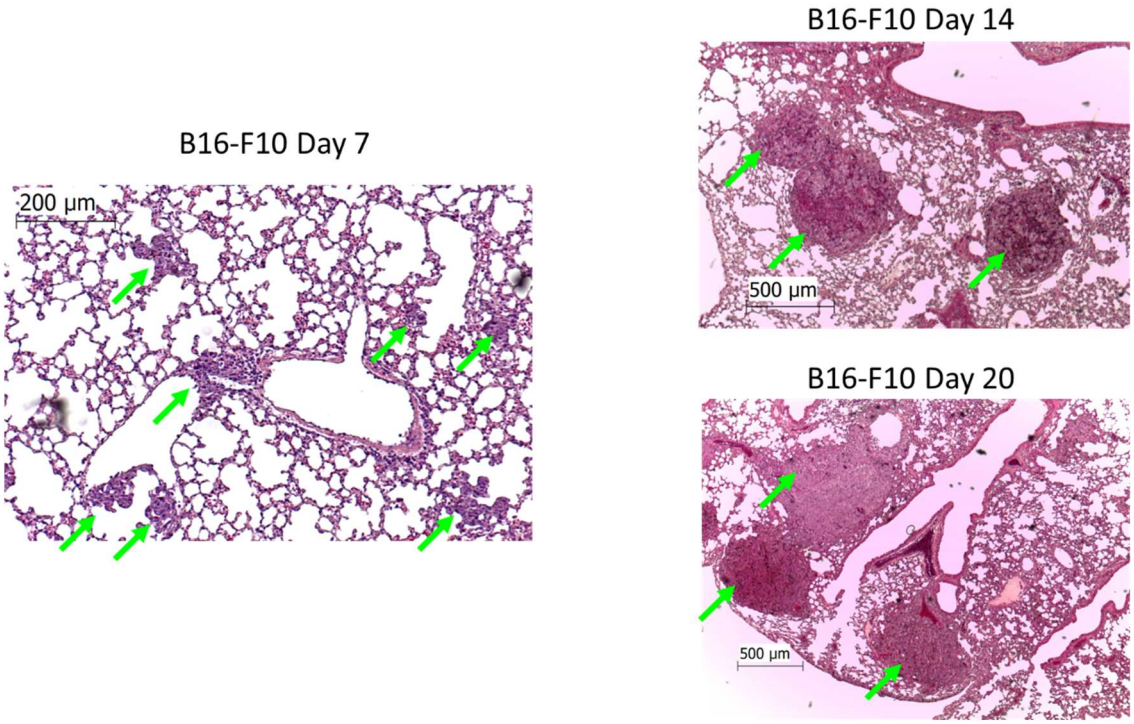

Figure 71. H&E staining of B16-F10 lung tumor nodules at days 7, 14 and 20. Representative of n = 3 mice/timepoint. Lung tumor nodules are pointed by green arrows.

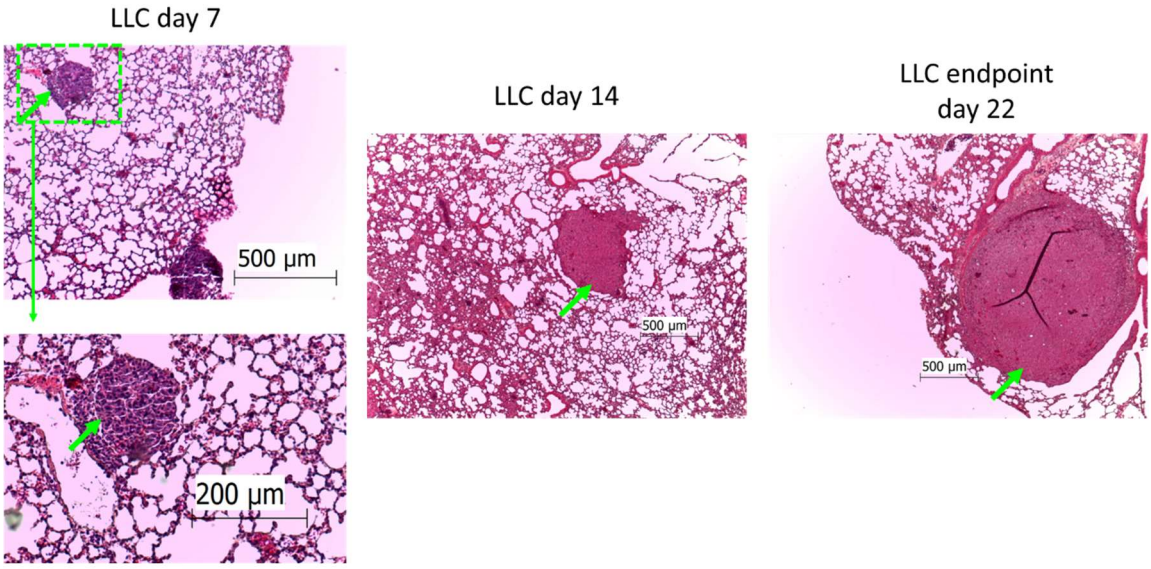

Figure 72. H&E staining of LLC tumor nodules at days 7, 14 and 22. Representative of n = 3 mice/timepoint. Lung tumor nodules are pointed by green arrows.

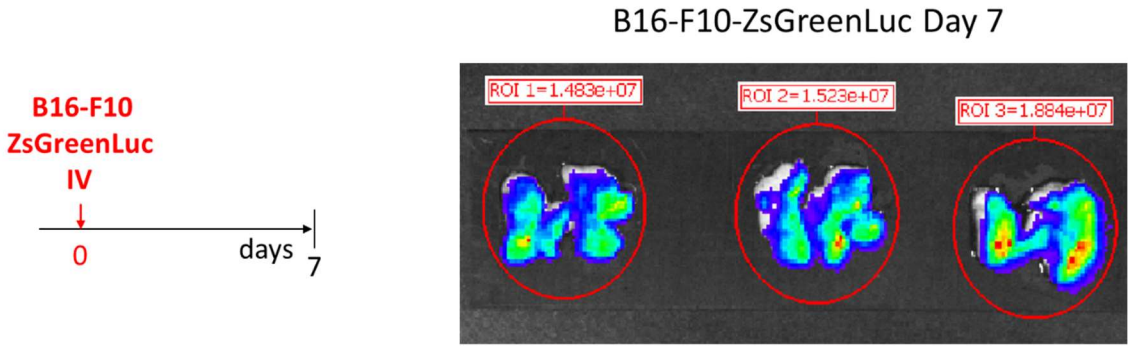

Figure 73. Luminescence analysis of lungs bearing luciferase-expressing B16-F10 tumors at day 7 post tumor cell inoculation. *n* = 3 mice.

In addition to inBCG and traditional scBCG vaccine administration routes for treatment of lung tumor-bearing mice, we also included the intravenous (ivBCG), since recently published work indicated that ivBCG was very effective in preventing tuberculosis infection in the lung in mouse and macaque models by inducing both a strong pulmonary T cell response and altering myelopoiesis in the bone marrow to generate trained immunostimulatory macrophages[218,260], which we considered *a priori* desirable events for inducing efficient antitumor responses.

We found that both inBCG and ivBCG were effective in slowing tumor growth in the B16-F10 model, while scBCG was completely ineffective (Figure 74), confirming our hypothesis that contact of BCG with the organ bearing the tumor, the lung in this case, is needed for its antitumoral effect. Indeed, ivBCG and inBCG routes of administration have been described to cause lung colonization for several weeks in mice and macaques[218,454].

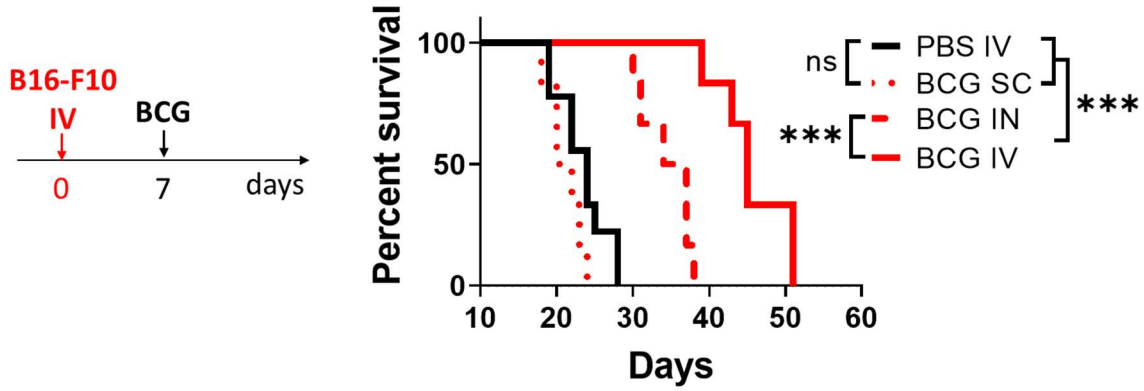

Figure 74. Survival of mice inoculated intravenously with B16-F10 cells and treated with 10^6 CFUs of BCG Pasteur either subcutaneously (SC), intranasally (IN) or intravenously (IV). PBS given IV was used as a control. *n* = 6 mice/group. ns: not significant, ****P*<0.001, log-rank (Mantel-Cox) test.

Interestingly, although both routes achieve colonization of the lungs, ivBCG was more successful at slowing tumor growth, increasing the median survival of mice from 35 days in inBCG to 45 days in the ivBCG group. These results suggest that the route of administration of BCG is critical for its antitumoral effect in a therapeutic scenario, and we identify the iv route as the most potent for the treatment of B16-F10 lung metastases.

Although detailed analysis of immune cell populations in the lungs of tumor-bearing mice are shown in later sections, here I will make a parenthesis to explain the superior efficacy of ivBCG compared to inBCG. For this, we generated mice with B16-F10 lung metastases, treated them with inBCG or ivBCG at day 7, and analyzed lung immune cell populations by flow cytometry at day 20. First, we incubated lung single cell suspensions overnight with a variety of stimuli and added brefeldin A for the last 4 h to detect IFN-γ producing cells. Even in unstimulated conditions, a higher fraction of lung $CD8^+$ and $CD4^+$ T cells secreted IFN-γ in ivBCG compared to inBCG mice. ivBCG also triggered a stronger PPD-specific response than inBCG, meaning that the iv route of administration achieves a more robust BCG-specific immune response in the lung than the in (Figure 75). After polyclonal restimulation with αCD3/CD28, both T cell subsets also produced more IFN-γ in ivBCG mice compared to inBCG (Figure 75). Overall, these results suggest that ivBCG induces a higher activation status of T cells in the lung than inBCG.

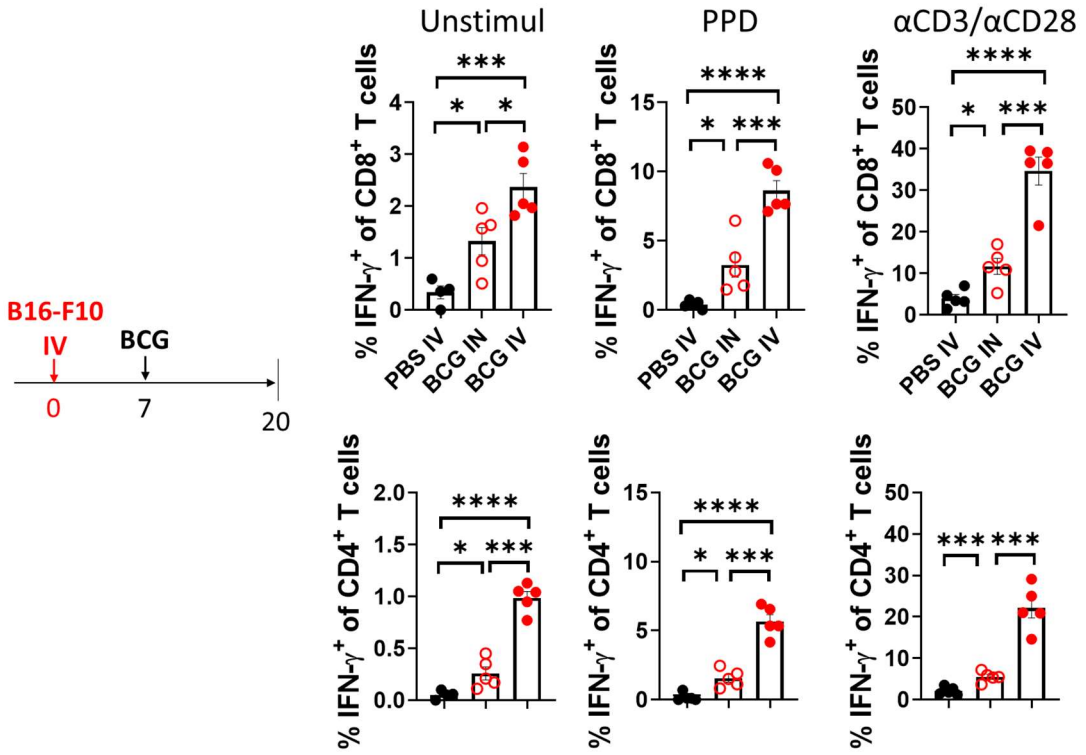

Figure 75. Mice were inoculated intravenously with B16-F10 cells, treated at day 7 with PBS or BCG Pasteur and lungs analysed by flow cytometry at day 20. Single cell suspensions were unstimulated, stimulated with 10 µg ml^{-1} of protein purified derivative (PPD) or stimulated with plate bound antiCD3 and soluble antiCD28 antibodies for 6 h in the presence of Brefeldin A. Proportions of cell subsets expressing IFN-γ are shown. *n* = 5 mice/group, from one experiment.

Analysis of lung cDC1s revealed that only ivBCG induced higher levels of the costimulatory molecule CD86 in the surface of these cells. Additionally, ivBCG and not inBCG changed the phenotype of $CD4^+$ T cells to a more pronounced Th1 profile, with higher T-bet expression and lower GATA3 (Figure 76). Finally, ivBCG also enhanced the cytotoxic profile of lung $CD8^+$ T cells, evidenced by a higher percentage expressing Granzyme B (Figure 76). Overall, we show that ivBCG promotes the antitumoral profile of lung immune cells to a higher extent than inBCG, which concurs with its enhanced efficacy against B16-F10 lung metastases in a therapeutic scenario.

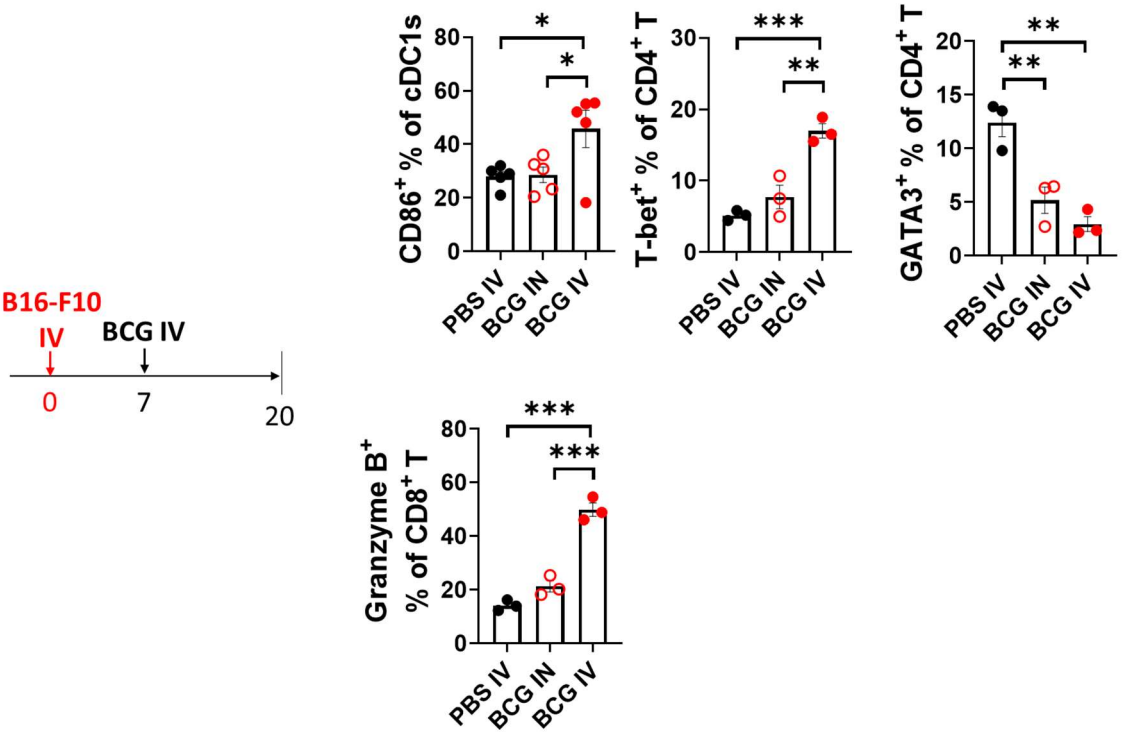

Figure 76. Lungs of mice treated as in Figure 75 were analyzed by flow cytometry. Frequencies of distinct cell populations expressing different markers are shown. *n* = 3-5 mice/group, from one experiment.

Next, we wondered whether live BCG is needed for achieving antitumoral effect in this experimental setup, as has been described for its use in bladder cancer[430,455]. We treated B16-F10 tumor bearing mice with 10^7 CFUs of BCG previously heat-killed by the intravenous route and observed no survival benefit compared to controls, in contrast with 10^6 CFUs of live BCG (Figure 77). Therefore, active colonization of the lung by live BCG is needed for optimal antitumoral efficacy.

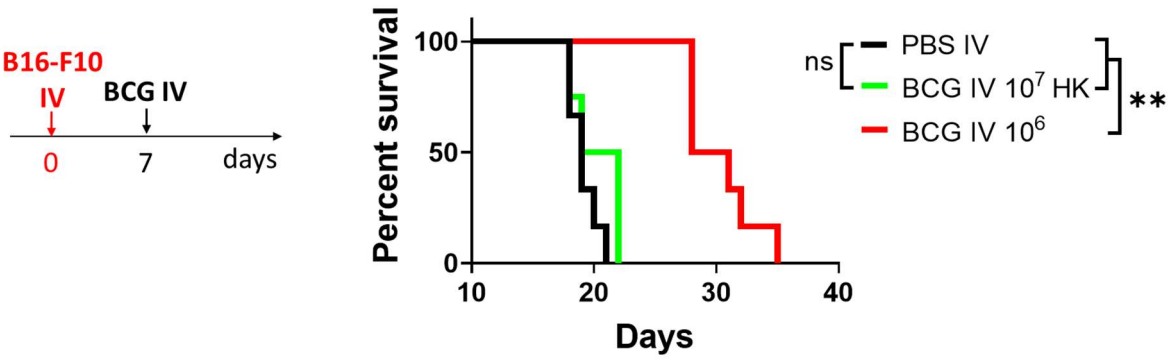

Figure 77. Survival of mice inoculated intravenously with B16-F10 cells and treated intravenously with 10^6 CFUs of BCG Pasteur or 10^7 CFUs of BCG Pasteur previously heat-killed (HK). *n* = 6 mice/group, from one experiment.

We additionally wondered whether modifying the dose of ivBCG could affect it efficacy, aiming to find the lowest dose with the maximum antitumoral effect to minimize potential side-effects resulting from the administration of a live bacteria by the intravenous route. We found that a dose of 10^5 CFUs of BCG did slow tumor growth compared to control PBS, but to a much lesser extent than the 10^6 dose (Figure 78). However, further increasing the dose by ten-fold (10^7) did not improve treatment efficacy (Figure 78). Therefore, we chose 10^6 CFUs as the lowest dose with the highest antitumor activity and used it for the remaining experiments.

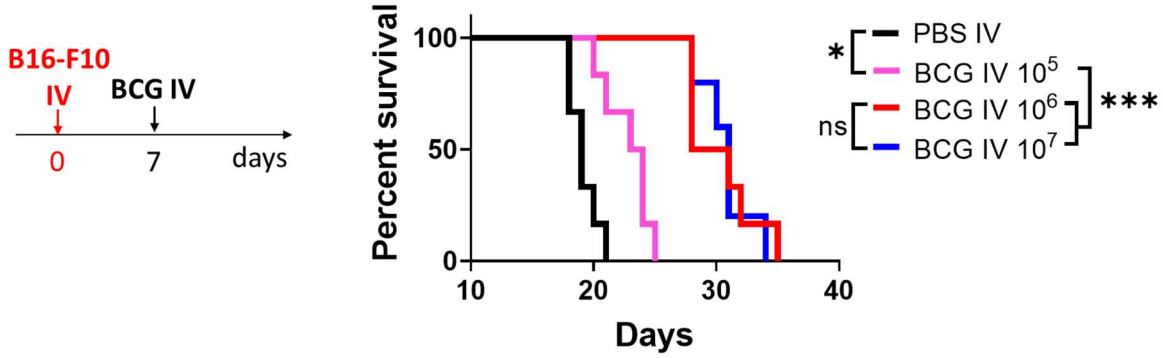

Figure 78. Survival of mice inoculated intravenously with B16-F10 cells and treated with different doses of BCG by the IV route. *n* = 6 mice/group, from one experiment.

We performed additional experiments to confirm the antitumoral effect of 10^6 CFUs of ivBCG, and found consistent results across three independent experiments, confirming the survival benefit conferred by BCG in this context (Figure 79A). We also performed two experiments in which mice were euthanized at day 20 post tumor cell inoculation and found reduced number of tumor foci in the lungs of ivBCG treated mice compared to controls (Figure 79B). This result meant that the therapeutic effect of ivBCG was already apparent at day 20, two weeks after treatment administration.

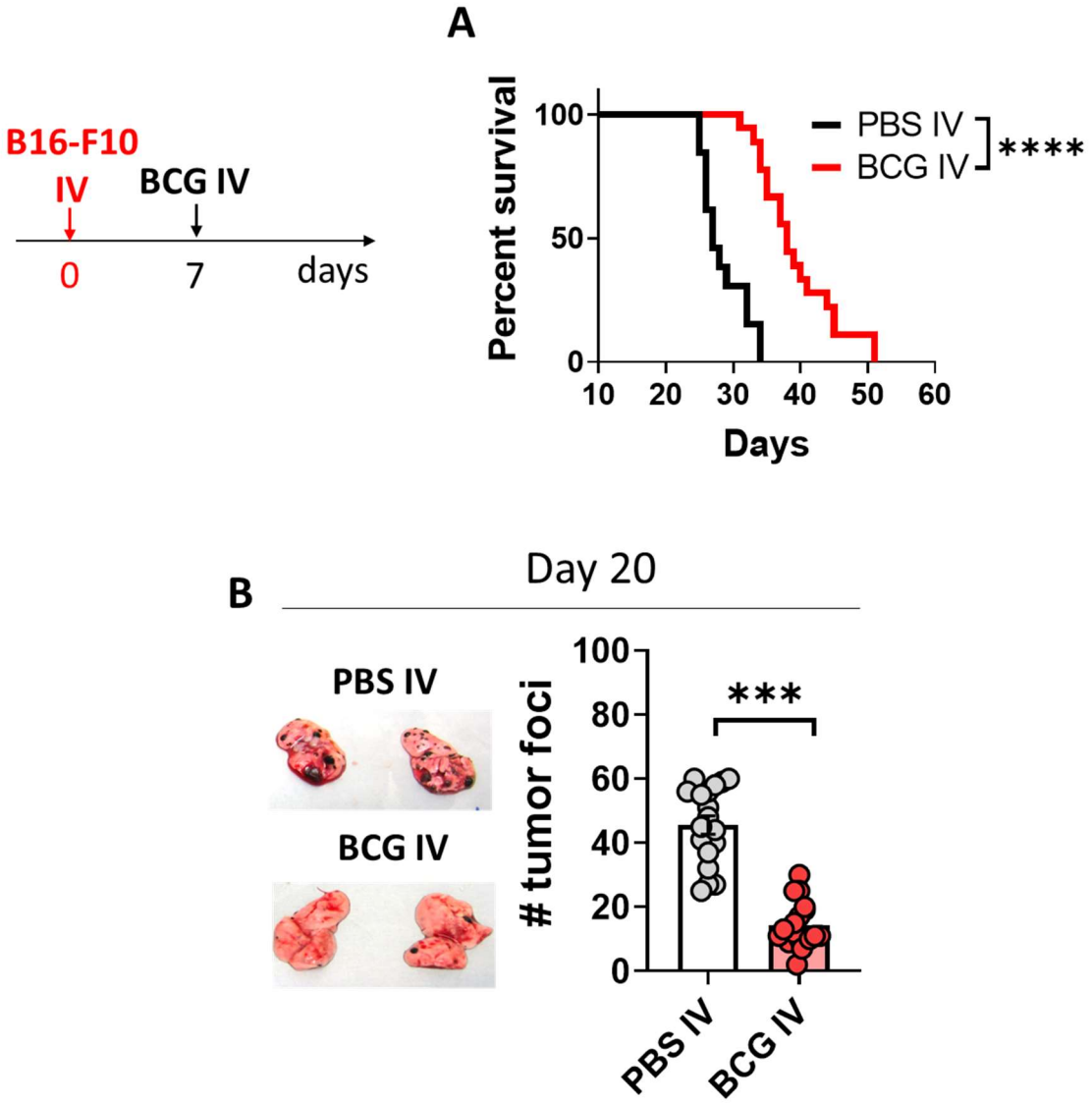

Figure 79. (A) Survival of mice inoculated intravenously with B16-F10 cells and treated with ivBCG at day 7, *n* = 12 mice/group, from two independent experiments. (B) Number of tumor foci in the lungs counted by visual inspection at day 20 post tumor cell inoculation, *n* = 18 mice/group, from three independent experiments.

5.5 Contribution of the adaptive immune system to the therapeutic effect of intravenous BCG

Having observed a therapeutic effect of ivBCG in the context of B16-F10 metastases growing in the lung, we next studied the mechanism of action behind the antitumoral effect. Taking into consideration that we have described that intravesical bacterial immunotherapy for bladder cancer relies on IFN-γ, perforin and the adaptive immune system, we also tested their contribution in this system. First, we inoculated Rag1$^{-/-}$ mice, which lack T and B

cells, with B16-F10 cells intravenously. Surprisingly, we found that in this mouse strain B16-F10 tumors do not grow in the lung and mice survived indefinitely, although they grew when inoculated subcutaneously (data not shown). This had already been described in the literature[456], and was attributed to a population of lung $CD8^+$ Tregs which suppressed NK cell activity, which is crucial for the control of B16-F10 lung metastases[457]. We did not further pursue this line of research, although in future experiments it prevented us to use $Rag1^{-/-}$ mice to test the specific contribution of innate immune cells to the antitumoral effect provided by ivBCG in the B16-F10 and LLC models (similarly, LLC lung tumors did not grow in $Rag1^{-/-}$ mice).

Next, we inoculated $Ifn\gamma^{-/-}$ mice with B16-F10 cells, treated them with ivBCG at day 7 and evaluated survival. Mice lacking expression of IFN-γ, which is a central cytokine in the orchestration of antitumor immune cell responses, did not benefit from ivBCG treatment (Figure 80A), suggesting that antitumoral effect is based on the stimulation of the immune system, rather than bacteria being cytotoxic to tumor cells themselves. We performed the same experiment using mice lacking perforin, which similarly to $Ifn\gamma^{-/-}$ mice, did not benefit from treatment (Figure 80B). These results mean that ivBCG treatment functions by enhancing immune cell responses against the tumor, relying on IFN-γ to orchestrate antitumor immunity and the cytotoxic effector perforin to kill tumor cells.

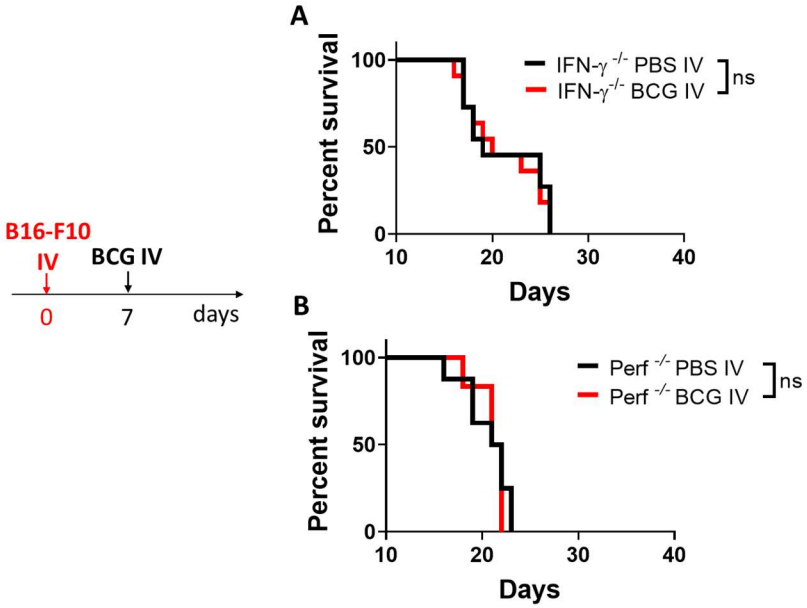

Figure 80. Survival of $Ifn\gamma^{-/-}$ (A) or $Perf^{-/-}$ (B) mice inoculated intravenously with B16-F10 cells and treated with ivBCG at day 7. *n* = 12 mice/group in A and B, from two independent experiments.

Next, we made use of mice lacking TLR4. Survival analysis in this mice strain revealed that ivBCG treatment against B16-F10 lung metastases was still effective in the absence of TLR4 (Figure 81), suggesting that TLR4-mediated sensing of BCG is not required for antitumor efficacy in this model. This result contrasts with MTBVAC intravesical therapy for bladder cancer, where TLR4 was needed for antitumor effect (Chapter 1, section 4.5), suggesting differences in the antitumor immune response between the lung and the bladder.

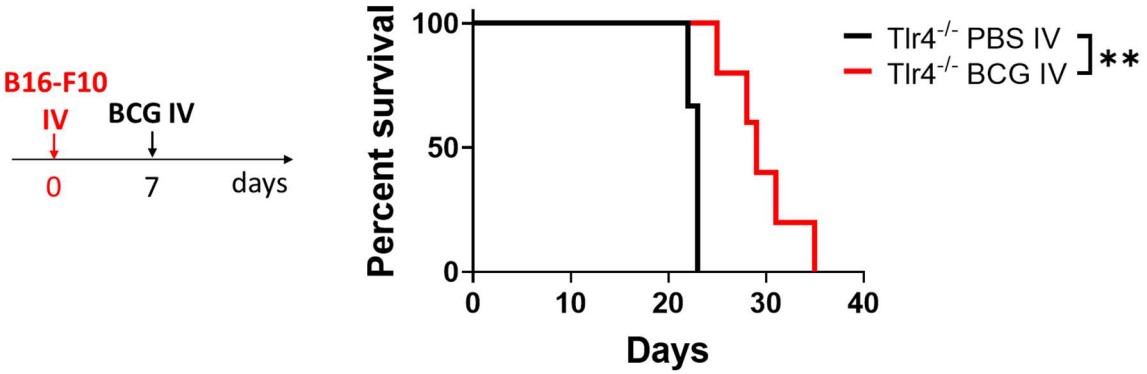

Figure 81. Survival of $Tlr4^{-/-}$ mice inoculated intravenously with B16-F10 cells and treated with ivBCG at day 7, *n* = 6 mice/group, from one experiment.

Since IFN-γ and perforin are two effector molecules used by the adaptive immune system (also by NK cells) to control tumor growth, and in our bladder cancer model we had observed that bacterial immunotherapy worked by enhancing adaptive immunity, we hypothesized that in this model T cells could be responsible for driving ivBCG therapeutic effect. To test this, we separately depleted $CD4^+$ and $CD8^+$ T cells in mice bearing B16-F10 tumors and treated with ivBCG (Figure 82).

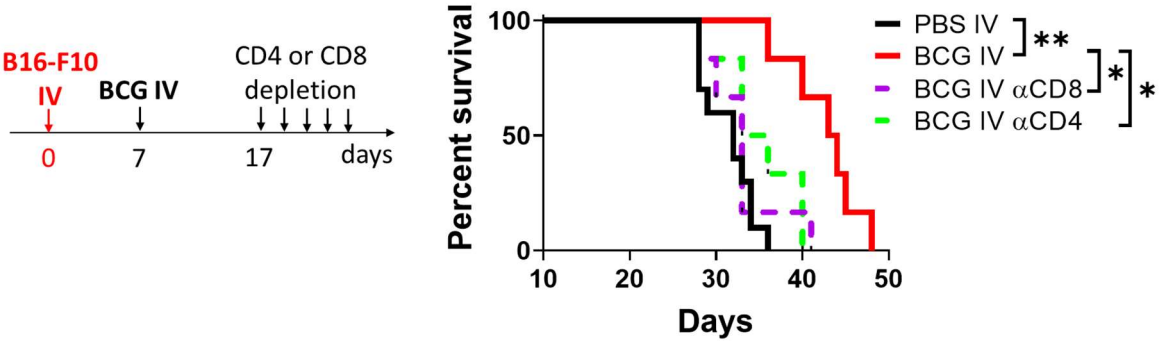

Figure 82. Survival of mice inoculated intravenously with B16-F10 cells, treated with ivBCG and depleted of $CD4^+$ or $CD8^+$ T cells from day 17 until endpoint. *n* = 6 mice/group, from one experiment.

We observed that depletion of either $CD4^+$ or $CD8^+$ abrogated the survival benefit observed in non-depleted ivBCG mice (Figure 82), meaning that both T cell subsets were required for treatment efficacy and suggesting that ivBCG functions by enhancing T-cell mediated antitumor immunity.

To further test this hypothesis, we analyzed T cells in the lungs of B16-F10 tumor bearing mice by flow cytometry. Analysis was performed at day 20, since at this timepoint we already observe a therapeutic effect of ivBCG (Figure 79).

First, we observed higher absolute numbers of $CD8^+$ T cells but not $CD4^+$ in the lungs of ivBCG compared to control mice (Figure 83).

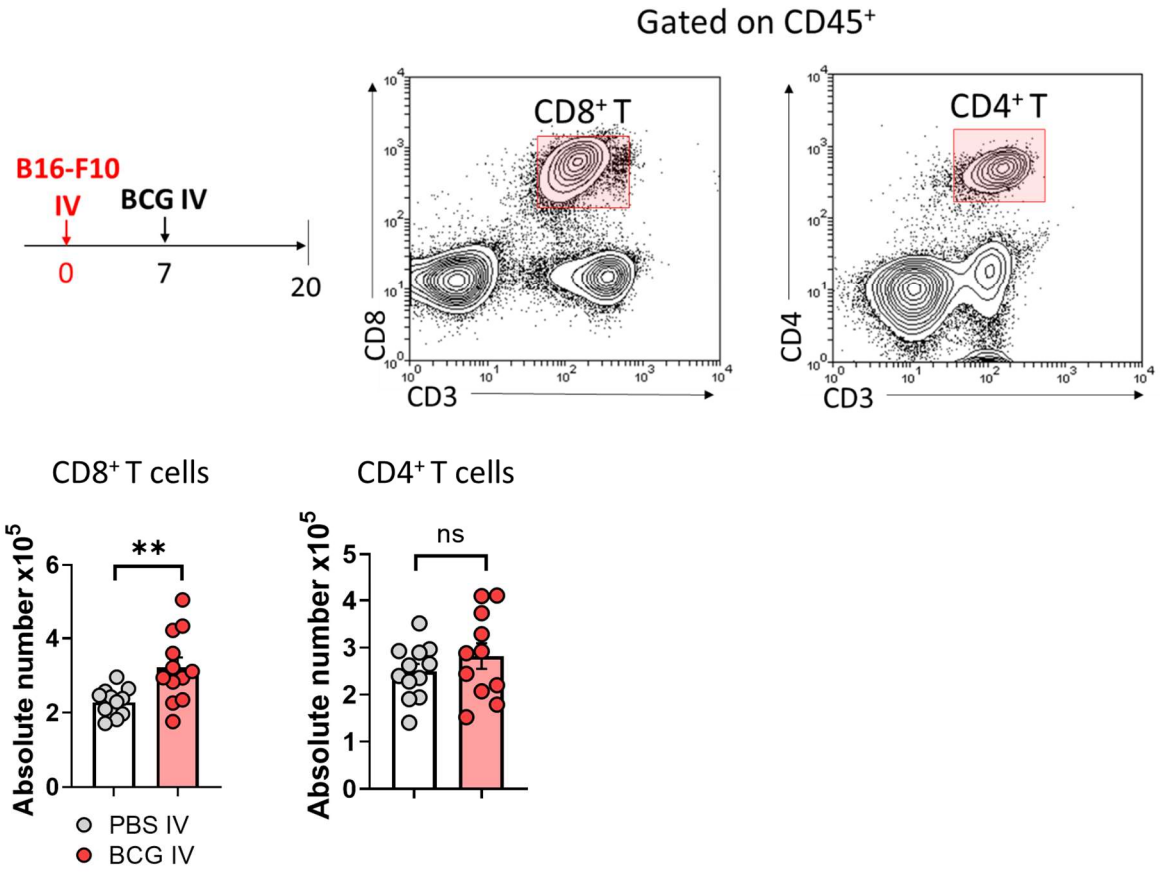

Figure 83. Mice were treated as indicated in the Figure and lungs processed and analysed by flow cytometry. Representative contour plots for $CD8^+$ and $CD4^+$ T cell identification and absolute numbers are shown. *n* = 12 mice/group, from two independent experiments.

Next, we incubated lung single cell suspensions with αCD3 and αCD28 stimulating antibodies in the presence of Brefeldin A to evaluate cytokine secretion by T cells. A higher percentage of $CD4^+$ and $CD8^+$ T cells secreted IFN-γ in ivBCG mice compared to controls

(Figure 84), suggesting improved effector function. We also analyzed the secretion of the proinflammatory cytokine TNF and, surprisingly, a lesser percentage of both T cell subsets secreted this cytokine in ivBCG mice compared to controls (Figure 84). Interestingly, although TNF secretion by immune cells can induce tumor cell death[458,459], it can also promote tumor growth[460] and immune cell dysfunction or event death[461,462] in the context of antitumor immunity.

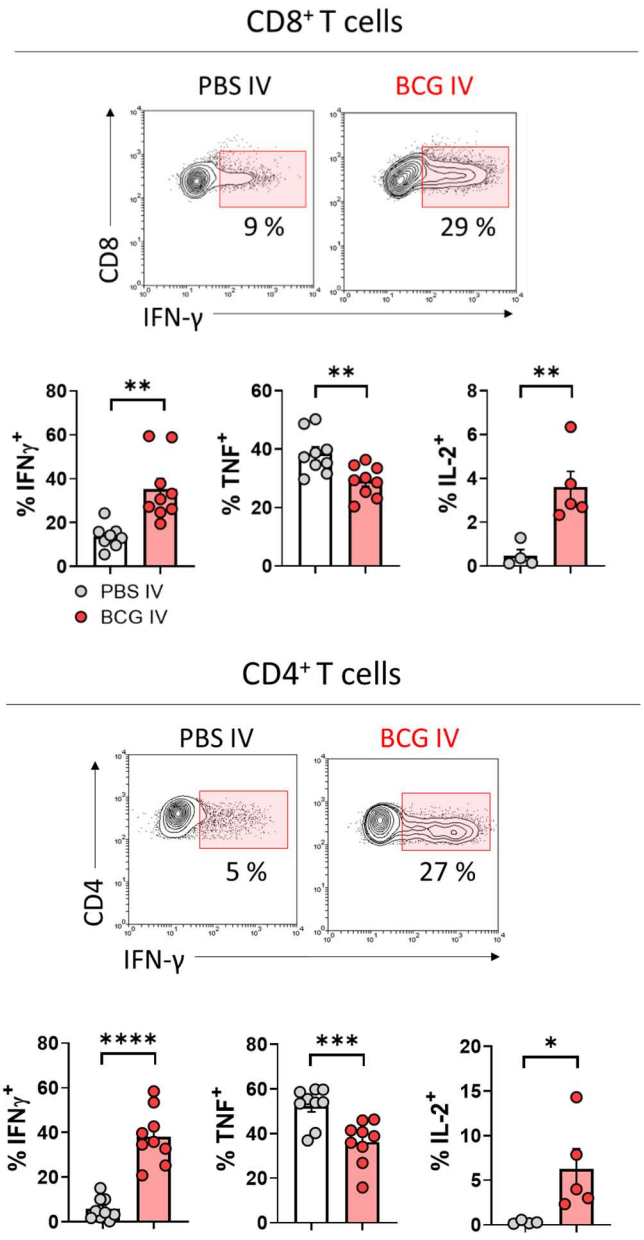

Figure 84. Mice were treated as in Figure 83. Lung cell suspensions were stimulated *ex vivo* and cytokine expression determined by intracellular staining in T cells. Shown are representative

contour plots for IFN-γ and quantification for IFN-γ, TNF and IL-2. *n* = 9 mice/group for IFN-γ and TNF (two independent experiments) and *n* = 5 for IL-2, one experiment.

We found a higher percentage of lung CD4$^+$ and CD8$^+$ T cells secreting IL-2 in ivBCG mice, with almost negligible IL-2 expression in T cells from control mice (Figure 84). IL-2 is a polyfunctional cytokine which induces T cell proliferation[463], and a high CD4/IL-2 signature in melanoma tumors has been associated with immunotherapy success[464]. Therefore, enhanced IL-2 secretion observed in ivBCG treated mice may be favoring the proliferation of T cells and their acquisition of cytotoxic and effector function.

T cells from tumor-bearing mice were further analyzed and we observed that lung CD8$^+$ T cells from untreated mice expressed high levels of T cell factor 1 (TCF1) and low levels T-cell immunoglobulin and mucin-domain containing-3 (TIM-3). This phenotype has been described to be specifically acquired by T cells in tumors growing in the lung in contrast to subcutaneous tumors and is characterized by a lack of acquisition of effector function[465]. ivBCG treatment shifted CD8$^+$ T cell phenotype, with a marked TCF1 downregulation and concomitant TIM-3 upregulation, consistent with differentiation into effector T cells, also evidenced by improved IFN-γ and IL-2 expression upon restimulation as well as acquisition of Killer Cell Lectin Like Receptor G1 (KLRG1) expression (Figure 84 and 85).

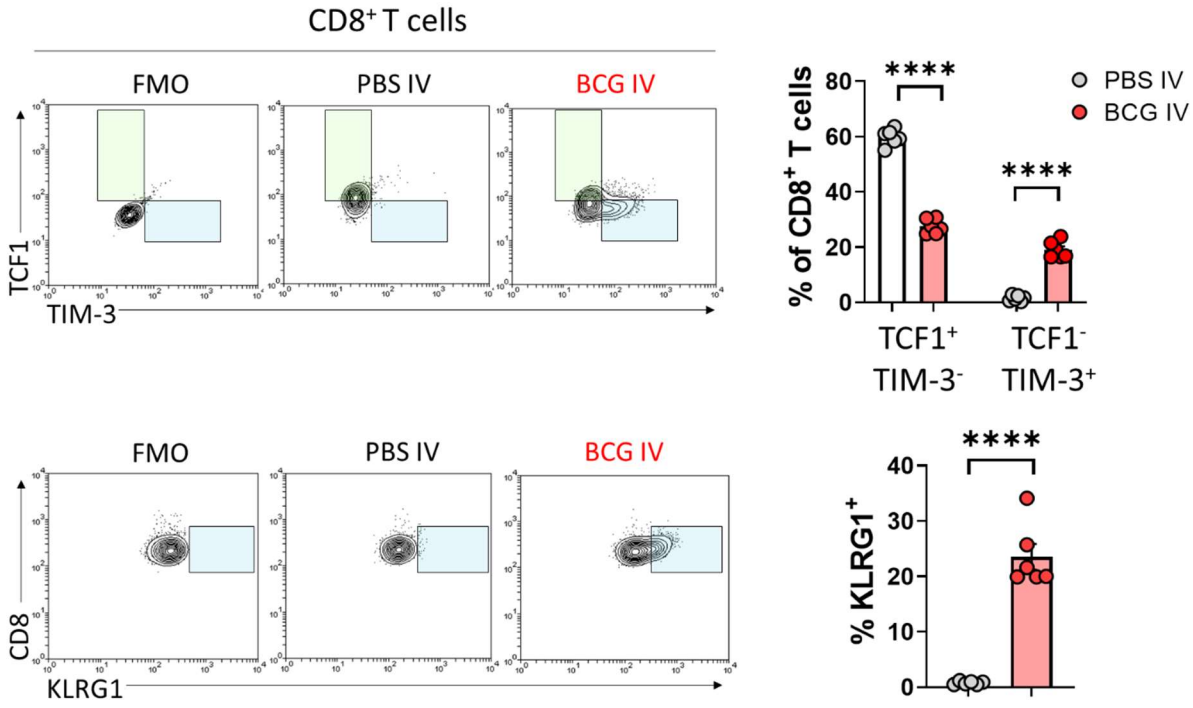

Figure 85. Mice were treated as in Figure 83. Lung cell suspensions were stained and TCF1, TIM-2

and KLRG1 expression analyzed in CD8$^+$ T cells. Shown are representative contour plots and quantification. *n* = 6 mice/group, from one experiment.

Next, we set out to analyze specifically T cells that had infiltrated lung tissue in B16-F10 tumor bearing mice, following a similar schedule than in the last Figure. For this, we administered intravenously a PerCP-Vio700-labeled CD45-directed antibody just before euthanasia, which allowed us to discern between immune cells circulating in the vasculature (CD45 IV$^+$) and immune cells that have infiltrated lung tissue, which are protected from labeling (CD45 IV$^-$), an experimental approach which has already been described[466].

First, an increase in the absolute number of CD4$^+$ and CD8$^+$ T cells infiltrated in the lung (CD45 IV$^-$) could be observed in ivBCG bearing B16-F10 lung tumors (Figure 86).

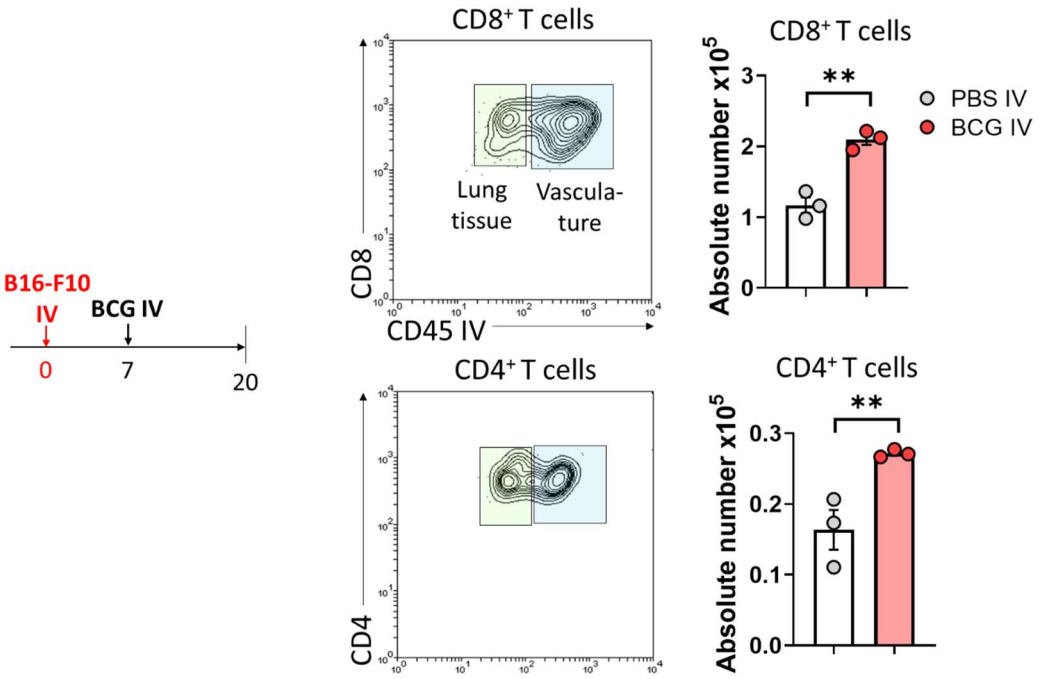

Figure 86. Mice were treated as in Figure 83 and given antiCD45-PerCP-Vio700 antibodies intravenously before euthanasia. Processed lung single cell suspensions were subsequently stained for flow cytometry analysis. Shown are representative contour plots of tissue-infiltrating (CD45 IV$^-$) and vasculature (CD45 IV$^+$) T cells, and absolute numbers of CD45 IV$^-$ CD8$^+$ and CD4$^+$ T cells. *n* = 3 mice/group, from one experiment.

Further phenotypic analysis revealed that a higher percentage of CD8$^+$ T cells infiltrating lung tissue from ivBCG mice expressed Granzyme B compared to controls (Figure 87), suggesting a higher cytotoxic potential. Of note, very few lung-infiltrating CD8$^+$ T cells

(around 5 %) expressed Granzyme B in untreated mice, again suggesting weak priming of effector function in the absence of treatment, something which has already been described specifically for tumors growing in the lung[465]. In agreement with this result, we found a higher percentage of infiltrated $CD8^+$ T cells expressing the activation marker CD69 in ivBCG compared to untreated mice (Figure 87). Again, few lung-infiltrating $CD8^+$ T cells were activated in untreated mice bearing B16-F10 tumors (Figure 87).

Focusing on the lung-infiltrating $CD4^+$ compartment, ivBCG skewed the phenotype of this cells into a Th1 type, with higher expression of T-bet and decreased expression of GATA3 (Figure 87). Importantly, Th1-like $CD4^+$ T cells have been described to facilitate antitumor immunity by enabling $CD8^+$ T cell mediated cytotoxicity[467,468]. Indeed, we observed that $CD4^+$ T cells were needed for ivBCG antitumoral effect in a previous experiment (Figure 87).

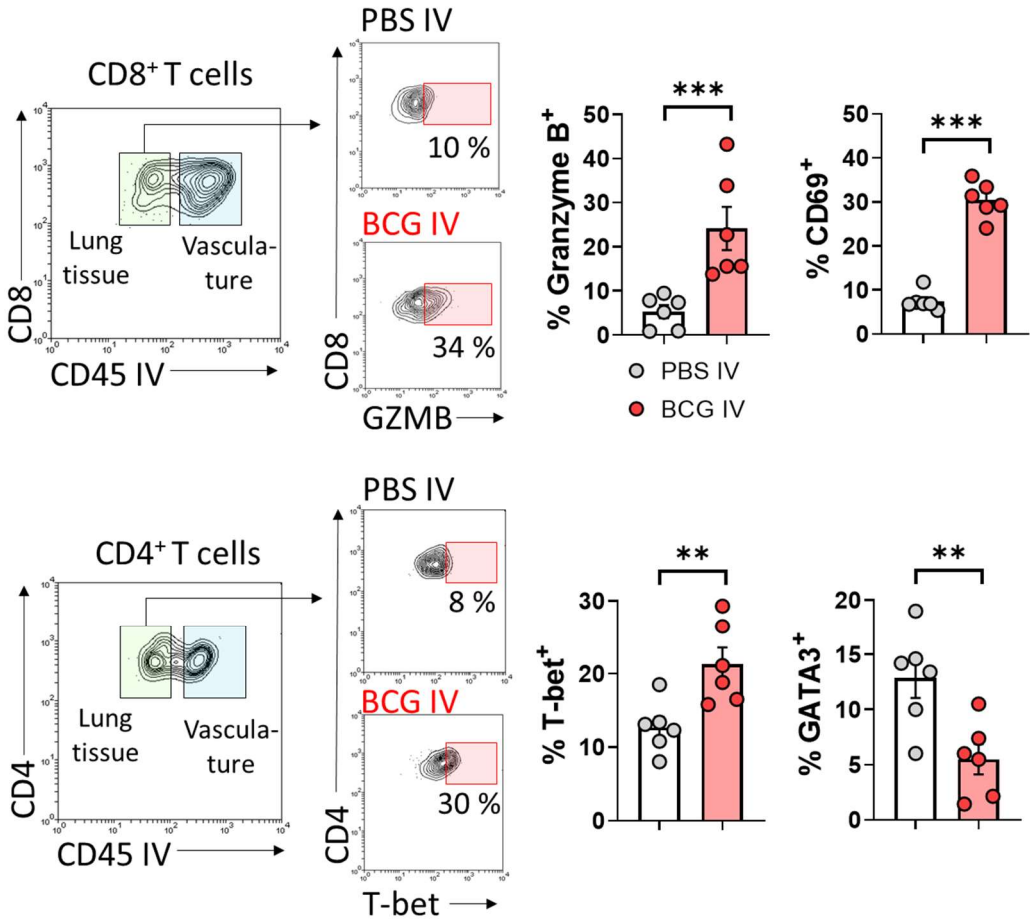

Figure 87. Mice were treated as in Figure 83. Shown are representative contours for discerning lung-infiltrating from intravascular T cells and analysis of Granzyme B, CD69, T-bet and GATA3

expression in lung-infiltrating (CD45 IV$^-$) T cell subsets. *n* = 6 mice/group, from two independent experiments.

With this tool available, next we examined differences between T cells infiltrating lung tissue and T cells in the vasculature, to determine whether the infiltration of T cells into the lung TME changes their phenotype and/or functionality. Surprisingly, we observed that Granzyme B expression by CD8$^+$ T cells was reduced when they entered tumor-bearing lung tissue compared to in vasculature (Figure 88) both in untreated and ivBCG mice, although Granzyme B expression was always higher in the latter group. Similarly, less lung infiltrating CD4$^+$ T cells expressed T-bet compared to circulating, although in ivBCG T-bet expression was higher in both subsets (Figure 88). These results suggest that the immunosuppressive TME alters the functionality of recruited CD4$^+$ and CD8$^+$ T cells which have infiltrated the tissue, and that ivBCG partially overcomes this phenomenon by enhancing the antitumor function of both lung-infiltrating and circulating T cells.

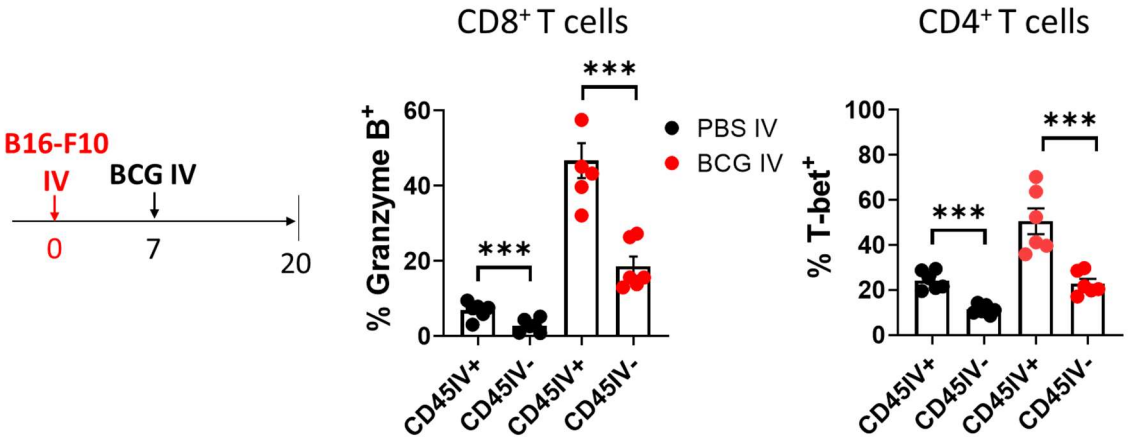

Figure 88. Differential expression of Granzyme B and T-bet by tissue-infiltrating (CD45 IV$^-$) and intravascular (CD45 IV$^+$) T cells. *n* = 6 mice/group, from two independent experiments.

5.6 Induction of a tumor-specific response in the lung

In the previous section we observed improved effector function of T cells in the lungs of ivBCG mice. Although we do not directly evaluate it, this T cell population would include both BCG-specific T cells and tumor-specific T cells. We wondered whether the antitumoral effect of BCG in our model was only due to the BCG-specific response or it also involved tumor-specific immunity. To study tumor-specific immunity we chose to work with B16-F10 cells engineered to express the glycoprotein epitope aminoacids 33-41

(gp33)[360], from the lymphocytic choriomeningitis mammarenavirus (LCMV), which allowed us to follow gp33-specific $CD8^+$ T cell responses. We devised different strategies to study the tumor-specific response, such as proliferation assays with peptide-loaded DCs, staining of gp33-specific $CD8^+$ T cells with dextramers, *in vitro* cytotoxicity assays with splenocytes isolated from tumor-bearing mice, and *in vivo* reconstitution of $Rag1^{-/-}$ with splenocytes from tumor-bearing mice.

In the first approximation, we performed a proliferation assay with lung single cell suspensions obtained from mice bearing B16-F10.gp33 tumors in the lung and treated or not with ivBCG. To induce proliferation of tumor-specific T cells, we used BMDCs generated from naïve mice loaded with gp33 peptide. To evaluate proliferation, prior to co-culture we stained lung-single cell suspensions with Cell Trace Violet (CTV) and co-incubated these cells with previously generated BMDCs from naïve mice loaded with gp33 or not, as a control (Figure 89A). After 72 h of incubation, we analyzed the $CD8^+$ T cells by flow cytometry, as proliferating cells progressively loose the CTV stain and its fluorescence intensity diminishes. When we compared the proliferation of $CD8^+$ T cells coming from either control mice or ivBCG mice, we observed that gp33-loaded DCs induced higher proliferation of $CD8^+$ T cells than non-loaded DCs, which evidences the presence of gp33-specific $CD8^+$ T cells in both groups (Figure 89B). However, a higher percentage of $CD8^+$ T cells proliferated in samples coming from ivBCG mice compared to control mice when cocultured with gp33-loaded DCs (Figure 89C). This result suggested that ivBCG was improving the $CD8^+$ T cell-mediated tumor-specific response.

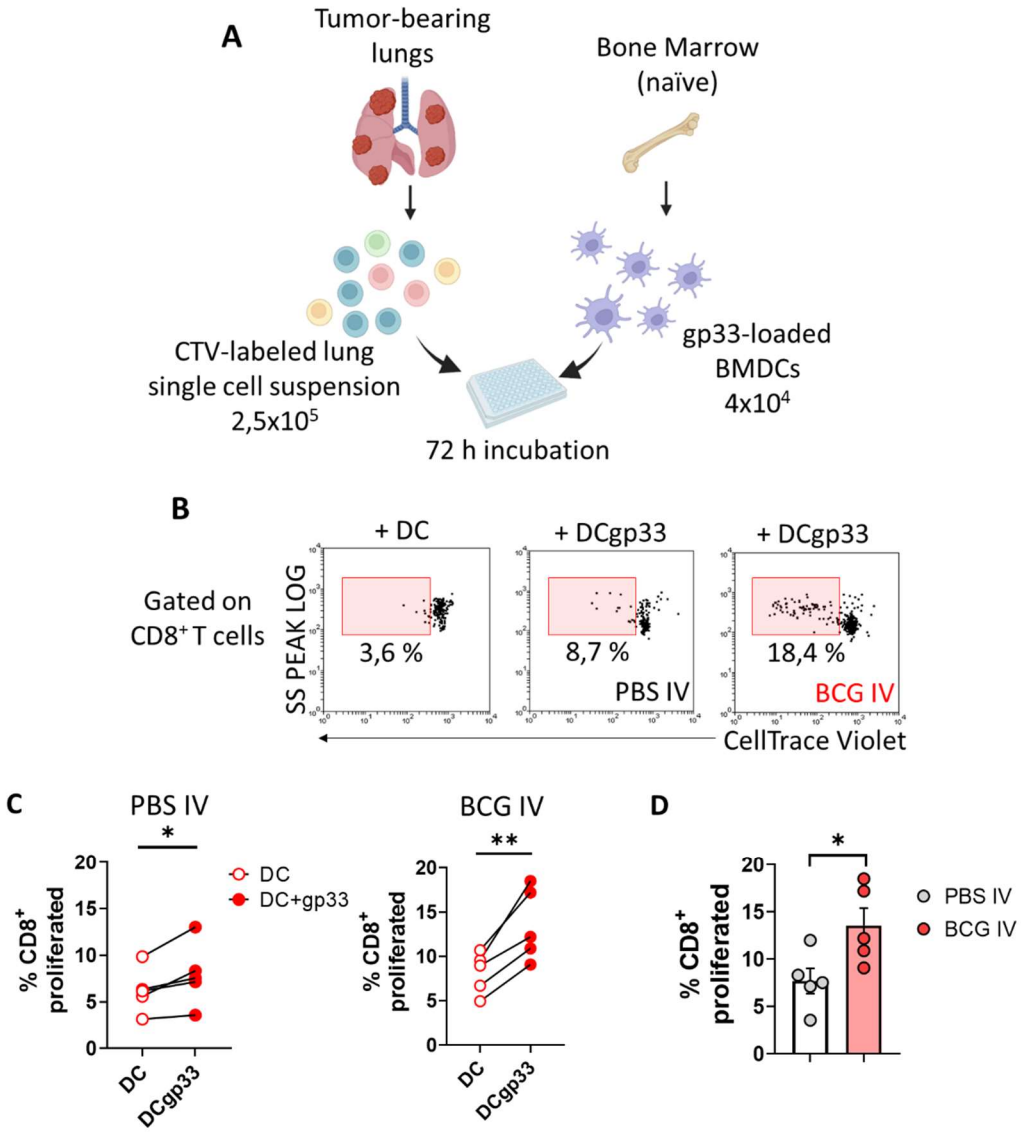

Figure 89. (A) Schematic depiction of experimental setup. (B) Representative dot plots of CellTrace Violet proliferation marker dilution in CD8⁺ T cells from 72 h cocultures with unloaded or gp33 peptide loaded DCs from PBS or BCG mice, and quantification (C). (D) Comparison of CD8⁺ T cell proliferation from PBS or BCG-treated mice after 72 h incubation with gp33-loaded BMDCs. *n* = 5 mice/group, from one experiment. CTV: Cell Trace Violet. BMDCs: Bone-marrow derived dendritic cells.

Given the complexity of the previous assay, we decided to validate these results with an alternative method. We stained lung single cell suspensions with gp33-specific dextramers, which are fluorochrome-conjugated polymers with gp33-peptide bound MHC-I molecules, which attach to the TCR of gp33-specific CD8⁺ T cells allowing detection by flow cytometry. Since the proportion of a clone specific for a given peptide is expected to be very small among the total population of CD8⁺ T cells, staining with dextramers is technically challenging because of unspecific binding. Therefore, we initially tested the

specificity of our gp33-dextramer staining protocol using splenocytes from LCMV-infected mice, where we expected to detect gp33-specific T cells more easily than in a tumor model (Figure 90). To evaluate gp33-dextramer staining, we gated on $CD44^+$ activated $CD8^+$ T cells to minimize unspecific staining, a common practice when performing tetramer or dextramer staining[469,470]. We obtained roughly 3.3 % of gp33-specific $CD8^+$ T cells in LCMV-infected mice splenocytes versus 0.5 % in naïve non-infected mice, indicating a low amount of unspecific staining. Therefore, we confirmed that our dextramer efficiently stained gp33-specific $CD8^+$ T cells.

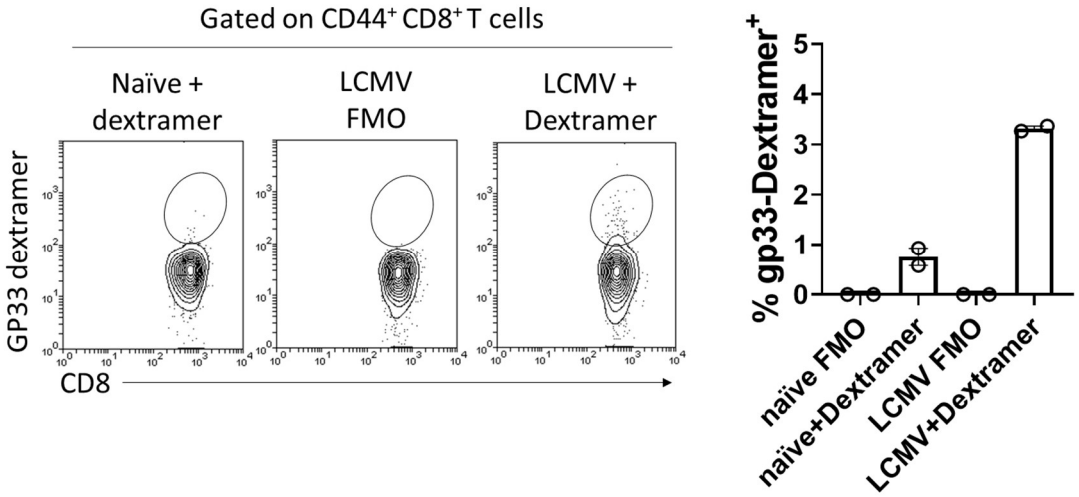

Figure 90. Mice were infected with 10^5 PFUs of LCMV or left uninfected (naïve). Seven days later, spleens were harvested and splenocytes stained with APC-conjugated gp33-specific dextramers and its expression was evaluated on $CD8^+$ T cells. Shown are representative contour plots and quantification of gp33-specific $CD8^+$ T cells among the total $CD8^+$ T cell population. *n* = 2 mice/group. FMO: fluorescence minus one.

Next, we analyzed the tumor-bearing lungs of mice bearing lung B16-F10.gp33 tumors. Dextramer staining revealed a higher percentage of gp33-specific $CD44^+$ $CD8^+$ T cells among total $CD8^+$ T cells in the lungs of mice which received ivBCG (Figure 91A), suggesting that treatment favors the induction of tumor-specific immunity.

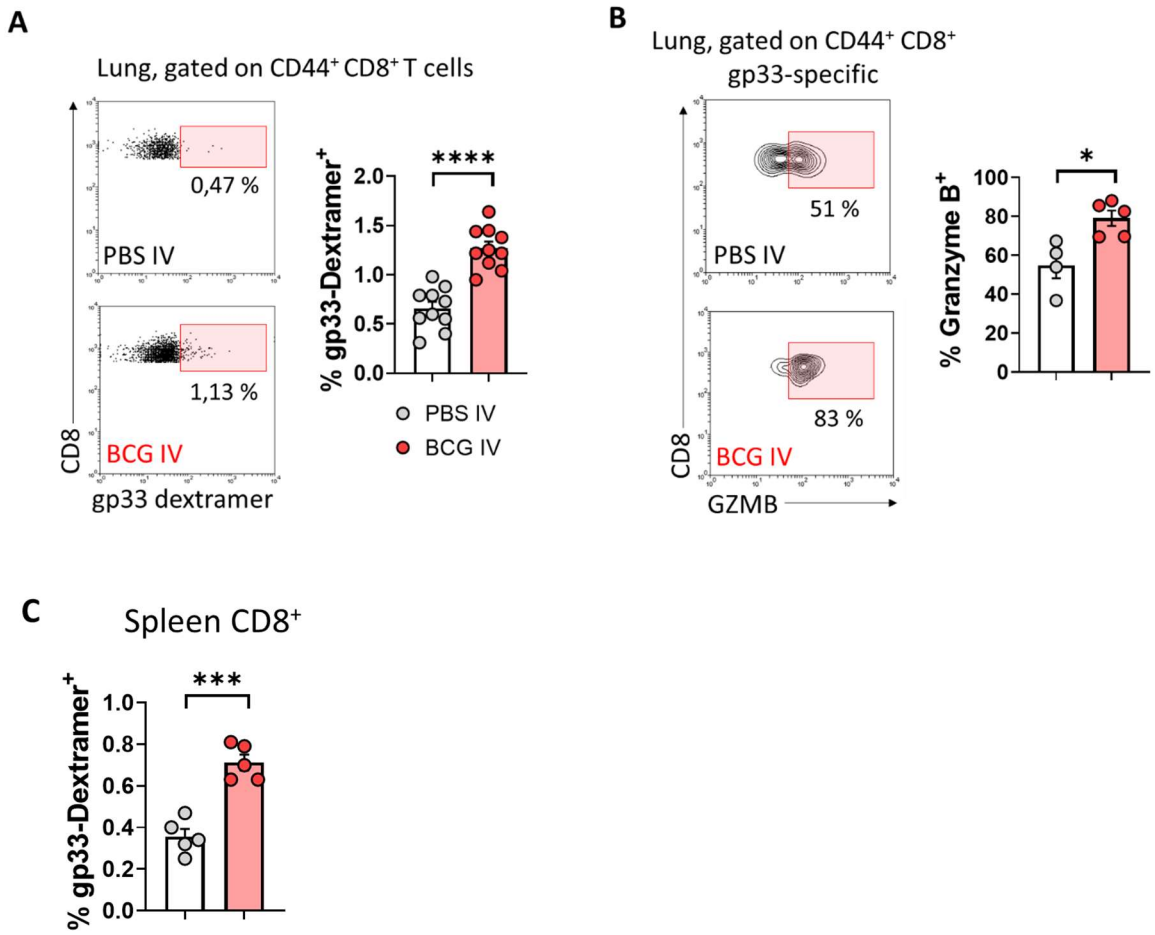

Figure 91. Mice were inoculated intravenously with gp33-expressing B16-F10 tumor cells and treated with PBS or BCG IV at day 7. At day 20, lungs and spleens were harvested and gp33-specific CD8$^+$ T cells were stained with dextramers. Shown are representative plots and quantification of gp33-specific CD44$^+$ CD8$^+$ T cells proportions among the total CD8$^+$ T cell population. *n* = 10 mice/group in (A) from two independent experiments, *n* = 4-5 in (B) and *n* = 5 in (C) from one experiment.

We further analyzed the phenotype of gp33-specific CD8$^+$ T cells, finding that around 50 % of gp33-specific CD8$^+$ T cells were positive for Granzyme B staining in the control PBS group versus 80 % for ivBCG mice (Figure 91B), which suggested that BCG treatment stimulated the cytotoxic function of tumor-specific T cells. In addition to identifying tumor-specific T cells at the tumor site, in one experiment we analyzed the induction of systemic tumor-specific immunity by staining gp33-specific T cells in the spleen. We observed that ivBCG also induced a higher percentage of gp33-specific T cells in the spleen, suggesting that tumor-specific immunity was generated systemically (Figure 91C).

Next, to functionally evaluate tumor-specific immune responses, we performed *in vitro* cytotoxicity assays with splenocytes isolated from tumor-bearing mice against tumor cells (Figure 92). Although it would have made more sense to perform these experiments with immune cells isolated from tumor-bearing lungs, isolation of T cells from the spleen is easier and yields a much higher number of cells, making these experiments easier to perform. However, in the future we plan to complement these experiments with $CD4^+$ or $CD8^+$ T cells isolated from the lungs of tumor-bearing mice. Importantly, we observed enhanced systemic tumor-specific immunity in ivBCG mice, so we thought that using splenocytes for these assays would be relevant. Luciferase-expressing tumor cells were used as targets so we could directly evaluate viability by analyzing luminescence after addition of luciferin to the wells. Although this method is technically less challenging than evaluating cell death by flow cytometry, it does not allow us to discern between cytotoxicity and growth inhibition of tumor cells.

As seen in Figure 92, splenocytes isolated from B16-F10.gp33 tumor bearing mice treated with ivBCG were more potent at inhibiting the growth of B16-F10-ZsGreenLuc cells after 20 h of co-culture compared to the IV PBS group. As a control, we used *a priori* non-antigenically related LLC-ZsGreenLuc cells as targets, which were not affected by splenocyte co-culture (Figure 92), confirming that we were evaluating antigen-specific responses. Of note, B16-F10 cells used in the *in vitro* assay did not express gp33, therefore immunity was generated against other endogenous tumor antigens.

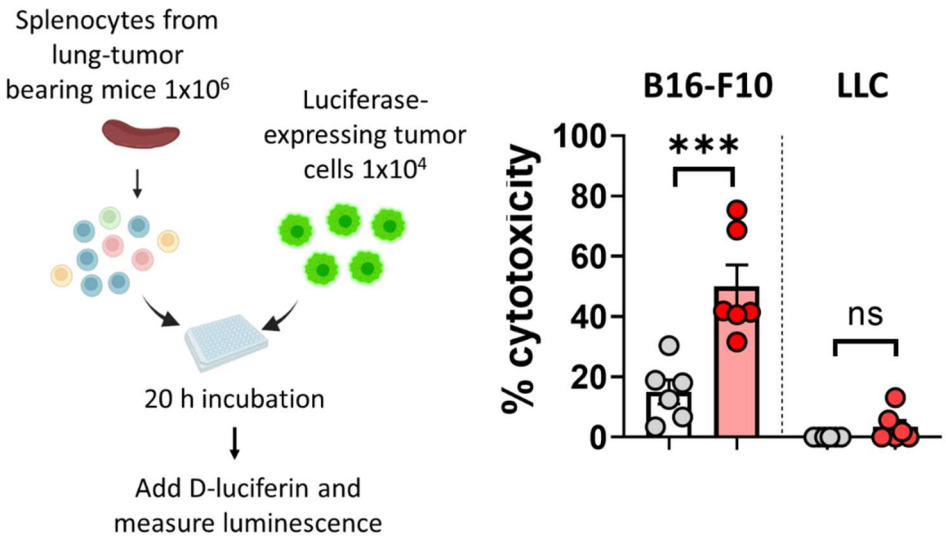

Figure 92. Mice were treated as in Figure 91, splenocytes isolated and seeded over luciferase-

expressing tumor cells at a 100:1 E:T ratio. 20 h later, luminescence was analyzed. Shown is a schematic depiction of experimental setup and quantification of cytotoxicity towards luciferase-expressing B16-F10 or LLC tumor cells. Percentage cytotoxicity was calculated in reference to the luminescence emitted by control wells with tumor cells cultured without effectors. *n* = 6 mice/group, from one experiment.

Lastly, to confirm that these *in vitro* experiments were relevant in an *in vivo* scenario, we reconstituted Rag1$^{-/-}$ mice with splenocytes coming from mice bearing lung B16-F10-gp33 tumors, treated or not with ivBCG at day 7 and euthanized at day 20, a timepoint in which we had observed enhanced gp33-specific responses in the spleen (Figure 93). As a control, a group of Rag1$^{-/-}$ mice was reconstituted with splenocytes coming from non-tumor bearing mice treated with ivBCG. 1 week after reconstitution, we subcutaneously inoculated B16-F10 tumor cells in reconstituted mice (Figure 93A). Follow-up of tumor growth revealed that B16-F10 tumors grew slower in mice reconstituted with splenocytes coming from ivBCG mice bearing B16-F10.gp33 tumors compared to untreated mice (Figure 93). We could attribute this phenomenon to tumor-specific responses and not just to the BCG-specific, since transplanted tumors grew faster in mice receiving splenocytes from non-tumor bearing mice treated with ivBCG, compared to tumor-bearing (Figure 93).

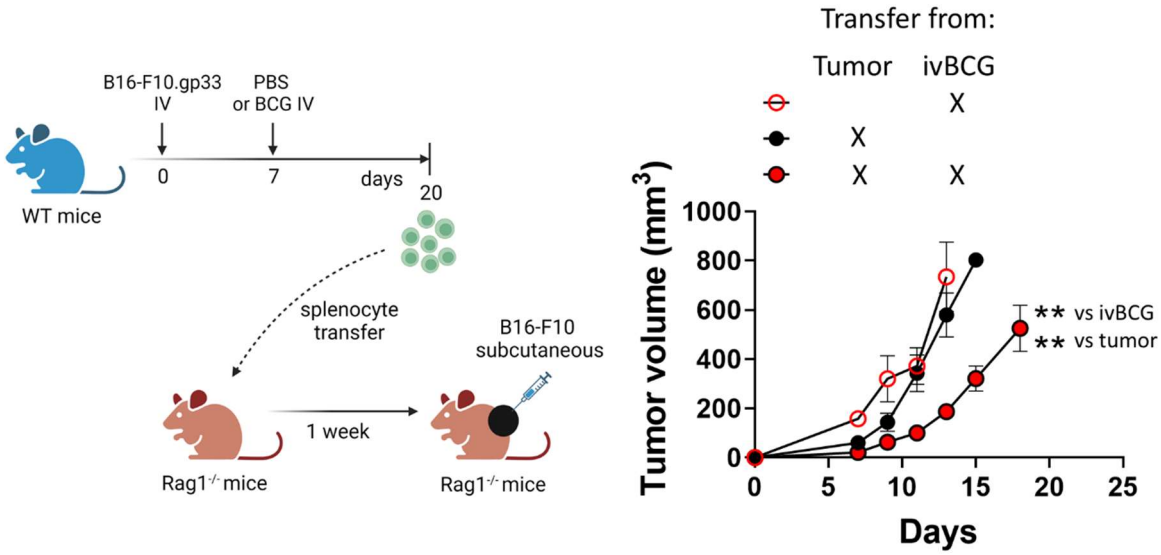

Figure 93. Schematic depiction of experimental setup. Shown in the graph is follow-up of B16-F10 tumor growth in Rag1$^{-/-}$ mice transferred with 10x10^6 splenocytes from the indicated sources, *n* = 6 mice/group, from one independent experiment. Source of splenocytes were pooled splenocytes from 6 mice for tumor-bearing mice and pooled splenocytes from 2 mice for non-tumor bearing ivBCG treated mice.

Altogether, our results allow us to propose that ivBCG treatment generates a systemic tumor-specific response against B16-F10 tumors growing in the lung, which leads to improved survival. Therefore, as is the case with antibody-based immunotherapies, chemotherapy and radiotherapy[471], bacterial immunotherapy can enhance adaptive immune responses against tumor antigens.

5.7 Contribution of Batf3-dependent dendritic cells

Immune responses against tumor antigens are initiated by Batf3-dependent cDC1s, which are specialized in the uptake of dead tumor-cell associated material and cross-priming of tumor-specific $CD8^+$ and $CD4^+$ T cells[79,415,472–474]. Furthermore, this cellular subset is required for the success of different types of immunotherapies[72,204,444,475]. More specifically, Batf3-dependent cDC1s are required for the control of B16-F10 lung metastases[476]. Therefore, in the next experiments we examined the role of cDC1s in the antitumoral effect of ivBCG against B16-F10 lung tumors.

First, we examined the phenotype of cDC1s in the lungs of B16-F10 tumor bearing mice at day 20, to determine whether ivBCG affected their phenotype. cDC1s in mice tissues are generally defined as $XCR1^+$ CD172a(Sirpα)[-477–479]. We identified cDC1s in the lungs of B16-F10 tumor bearing mice based on the expression of these markers (Figure 94).

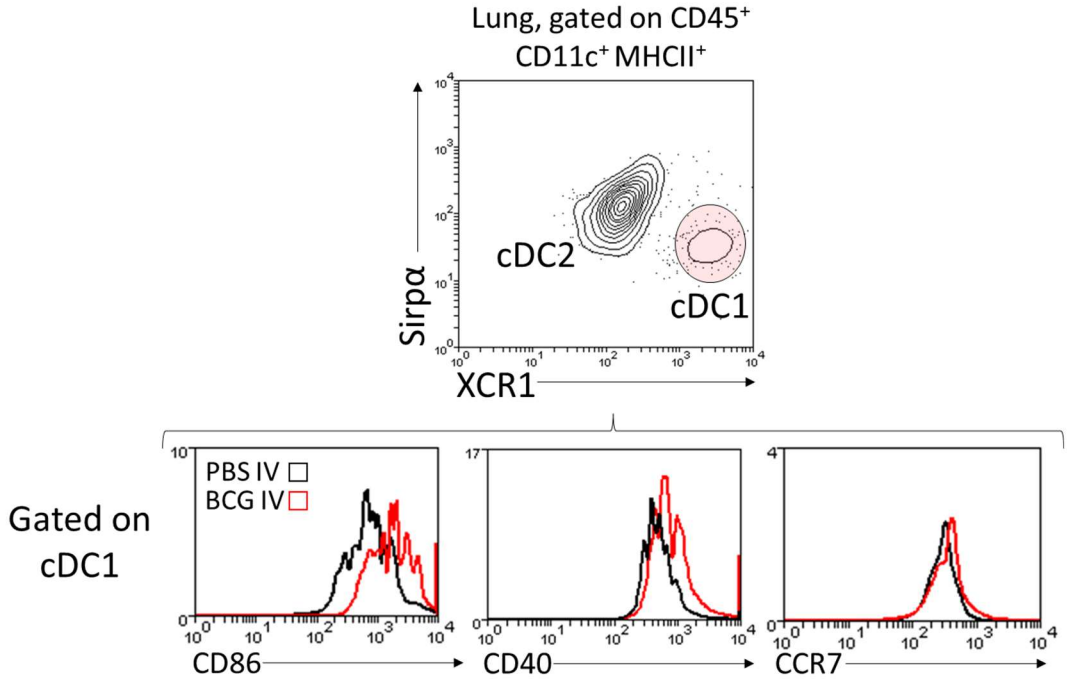

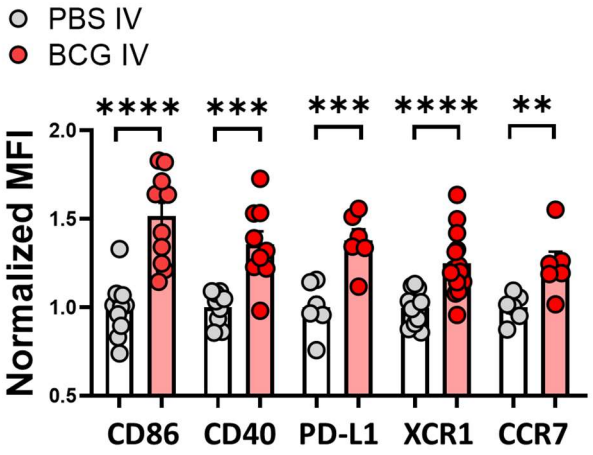

Figure 94. Mice were inoculated intravenously with B16-F10 cells and treated with PBS or BCG IV at day 7. At day 20, lungs were harvested and processed for flow cytometry analysis. Shown is a representative contour plot for cDC1 identification in the lung and representative histograms and quantification of different surface markers on cDC1s. Results are expressed as the fold increase in Mean Fluorescence Intensity (MFI) of a given marker in the ivBCG group vs the control PBS group. *n* = 10 mice/group for CD86, CD40 and XCR1 and *n* = 6 mice/group for PD-L1 and CCR7, from two independent experiments.

We found enhanced expression of the costimulatory proteins CD86 and CD40 on the surface of lung cDC1s, suggesting a higher activation status (Figure 94). XCR1, the receptor of the cDC1 chemoattractant XCL1, was also upregulated in mice undergoing treatment (Figure 94), which could facilitate cDC1 recruitment to the lungs. Indeed, triggering intratumoral XCL1 expression has been suggested as a mean to recruit cDC1s to the tumor bed, and tumors downregulate XCR1 expression on cDC1s by a PGE_2-dependent mechanism, hindering their recruitment[480]. Our results showed elevated PD-L1 expression on lung cDC1s of mice receiving ivBCG (Figure 94). Even though it could be a finding that evidence cDC1 activation and engagement of the IFN-γ signaling pathway on these cells, upregulation of PD-L1 on cDC1s may be negatively influencing T and NK cell function[160], although we will be discussing this in another chapter. Finally, we also found elevated CCR7 expression in cDC1s from ivBCG, which could facilitate their migration to regional lymph nodes.

Given that cDC1s take up tumor-associated material and migrate to the regional lymph nodes to prime adaptive immune responses, we also analyzed the phenotype of cDC1s in the lung-draining lymph node, known as the mediastinal lymph node (mLN), in tumor-bearing mice at day 20. Migratory DCs in the mLN are defined as $CD11c^{int}MHC\text{-}II^{hi}$, as opposed to resident DCs ($CD11c^{hi}MHC\text{-}II^{int}$)[79]. First, we observed higher abundance of

migratory cDC1s ($XCR1^+$ $Sirp\alpha^-$) in the mLN of ivBCG mice (Figure 95A), suggesting enhanced migration from the lung, which could be explained by their higher expression of CCR7 in the lung. Among total migratory cDCs, cDC1s were slightly more frequent in mice undergoing BCG treatment (Figure 95B), which could be explained by enhanced migration specifically of the cDC1 subset from the lung or due to a higher ability to proliferate or survive in the mLN. Additionally, we detected higher levels of CD86, CD40, XCR1 and PD-L1 in migratory cDC1s from mice undergoing BCG treatment (Figure 95C), which suggests that BCG-activated cDC1s in the tumor-bearing lung migrate to the mLN, where they could be priming T cell responses to a higher extent than in control untreated mice.

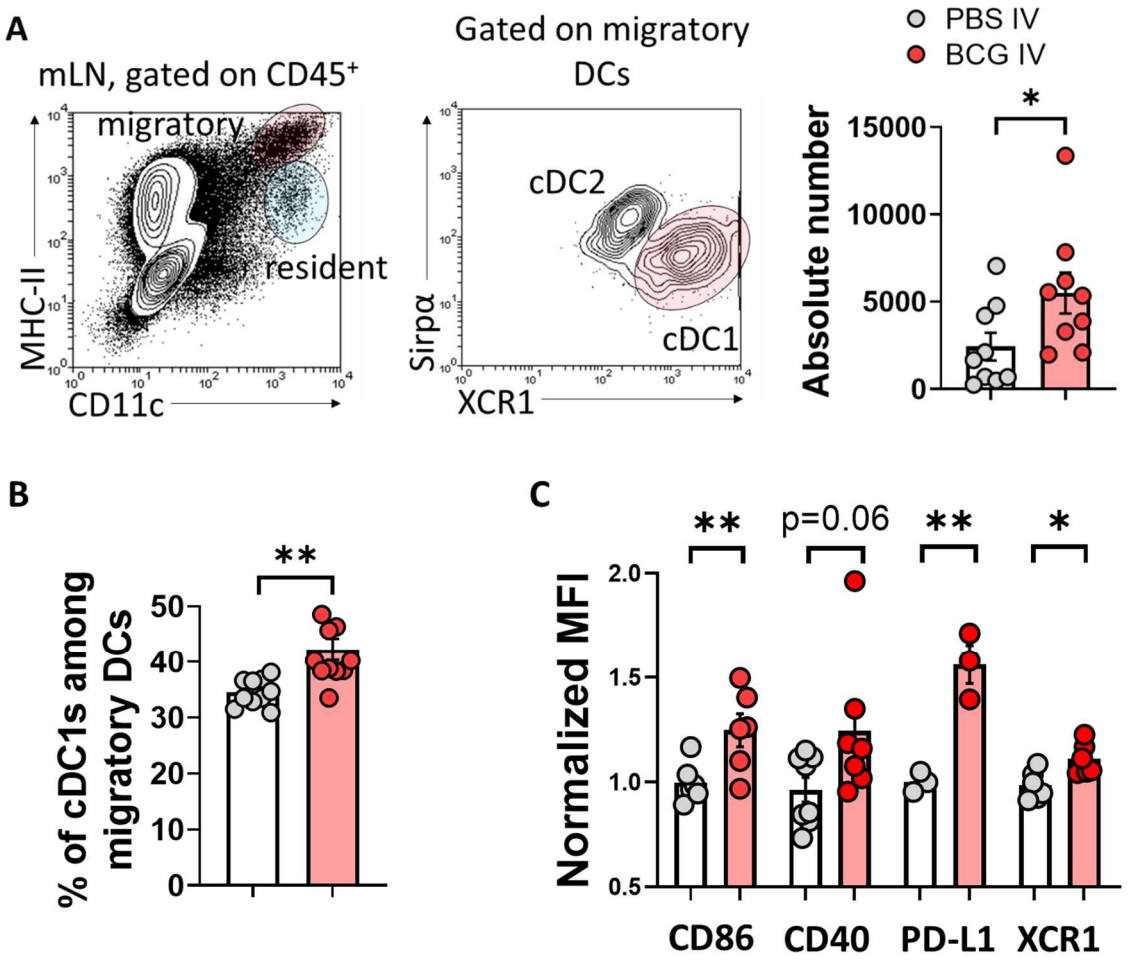

Figure 95. Mice were treated as in Figure 94. At day 20, lung-draining mediastinal lymph nodes (mLNs) was harvested and analyzed by flow cytometry. Shown is a representative contour plot for identification of migratory and resident DCs and for identification of migratory cDC1s (A). Graph in (A) depicts quantification of migratory cDC1s absolute numbers. (B) Quantification of cDC1

frequency among total migratory DCs. (C) Expression of distinct surface markers in migratory cDC1s. *n* = 9 mice/group (A,B), *n* = 6 mice/group (C), *n* = 3 mice/group (C,PD-L1).

Next, we wondered how early were cDC1s being activated in mice treated with ivBCG. For this, we performed a time course experiment in which we analyzed cDC1s in the lungs, mLNs and spleens of mice bearing lung B16-F10 tumors at days 11, 14 and 18 post-tumor cell inoculation (Figure 96). We observed dissimilar patterns for the different markers studied. PD-L1 was already upregulated in lung and spleen cDC1s as early as day 11 (Figure 96), four days after ivBCG administration. CD86 upregulation started to be apparent at day 14 in both lung and spleen, one week after treatment, whereas CD40 upregulation in both compartments was only observed at day 18 (Figure 96). In the mLN, although only the day 11 and 18 timepoints could be analyzed, our data show upregulation of the three markers at day 18 but not at day 11 (Figure 96).

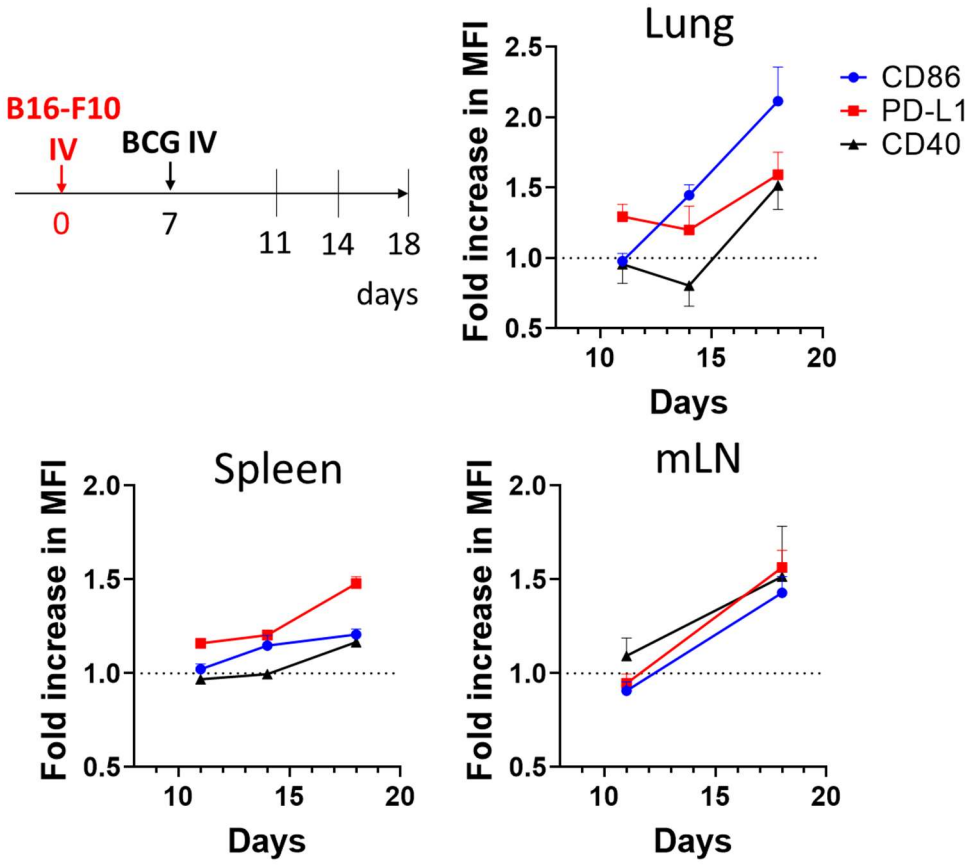

Figure 96. Mice were inoculated intravenously with B16-F10 cells and treated with IV PBS or BCG at day 7. Expression of CD86, PD-L1 and CD40 surface markers was analyzed on lung, spleen and mLN cDC1s at days 11, 14 and 18 post tumor cell inoculation by flow cytometry. Results are shown

as fold increase in MFI of a given marker in the ivBCG group versus the IV PBS group. *n* = 3 mice/group per timepoint.

Besides expression of costimulatory molecules, another relevant aspect of cDC1 biology is their privileged ability to secrete IL-12 in response to infection[481] and in tumors[475,482]. IL-12 is a cytokine with potent immune-stimulatory and antitumorigenic properties[483], such as inducing IFN-γ secretion by $CD4^+$ and $CD8^+$ T cells[484–486], increasing NK and $CD8^+$ T cell cytotoxicity[487] and reprogramming immune suppressive MDSCs into a T cell-stimulatory profile[488]. We hypothesized that ivBCG could be driving enhanced IL-12 production by cDC1s. Detection of IL-12 cytokine expression by flow cytometry is technically difficult and has been previously performed by *in vivo* administration of Brefeldin A[482] or using transgenic reporter mice[475]. As we did not have these tools available or set-up in our laboratory, we decided to perform *ex vivo* stimulation of lung single cell suspensions with low doses of LPS and IFN-γ in the presence of Brefeldin A to stimulate IL-12 secretion[489,490]. Although it is an artificial way of triggering cytokine secretion, we though it could give us an idea of the intrinsic ability of DCs to respond to stimuli, something they would conceivably be doing *in vivo* inside the tumor.

First, we noticed that we could only detect IL-12 production by DCs using LPS/IFN-γ stimulation, since we did not detect IL-12 in DCs from unstimulated lung single cell suspensions (Figure 97A).

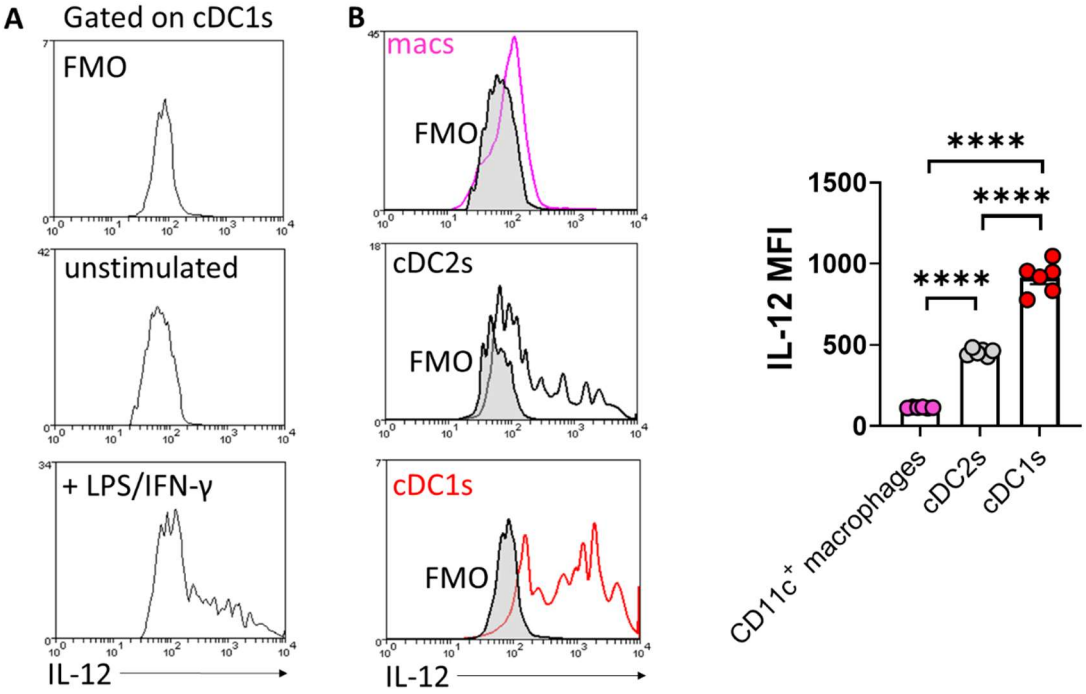

Figure 97. Mice were inoculated with B16-F10 cells intravenously and at day 20 lung single cell suspensions were stimulated *ex vivo* with LPS and IFN-γ in the presence of Brefeldin A for 4 h. Shown are representative histograms of IL-12 expression on cDC1s unstimulated or stimulated (A) and representative histograms and quantification of IL-12 expression by different subsets of cells (B). *n* = 6 mice/group, from one experiment.

Additionally, flow cytometry analysis showed that cDC1s were the prominent cell subset producing IL-12 in lung tumors after *ex vivo* restimulation, compared to cDC2s and non-DC CD11c^{+} macrophages (Figure 97B), which is in line with the existing literature[476,482]. This suggested that our *ex vivo* stimulation method could be a useful approximation for evaluating IL-12 production by immune cells infiltrating lung tumors.

Next, we analyzed IL-12 production in B16-F10 tumor bearing mice treated with ivBCG. Flow cytometry analysis of lung single cell suspensions revealed that ivBCG increased IL-12 cytokine expression only in DCs, but more markedly in the cDC1s subset, which was the prominent cell type producing this cytokine after *ex vivo* stimulation in both treated and untreated mice (Figure 98).

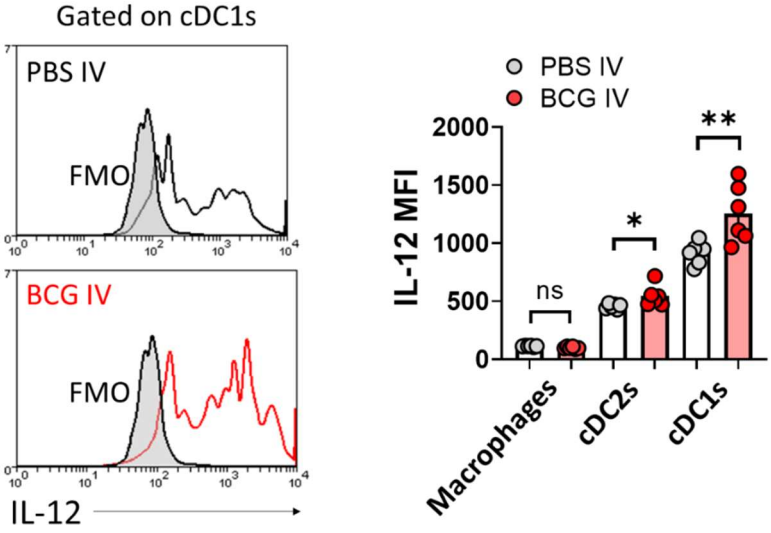

Figure 98. Mice were treated as in Figure 97. Shown are representative histograms and quantification of IL-12 expression by different subsets of cells from PBS or BCG-treated mice. *n* = 6 mice/group, from one experiment.

Altogether, these results suggested that administration of ivBCG promotes cDC1 activation in B16-F10 lung tumors, measured as expression of costimulatory molecules and IL-12. Given that this cellular subset is specialized in cross-presentation and initiation of tumor-specific responses, stimulation of cDC1 function might contribute to the antitumoral effect of ivBCG.

In the following experiments, we evaluated whether cDC1s are functionally required for BCG treatment efficacy. For this, we used mice lacking the transcription factor Batf3, which specifically lack this cellular subset[73]. First, we confirmed that cDC1s were absent from the lungs and mLN of this mice strain, with the additional aim of checking that we were correctly identifying them by flow cytometry. As expected, $XCR1^{+}$ $Sirp\alpha^{-}$ DCs were selectively absent in mice lacking Batf3, both in the lungs and mLN (Figure 99).

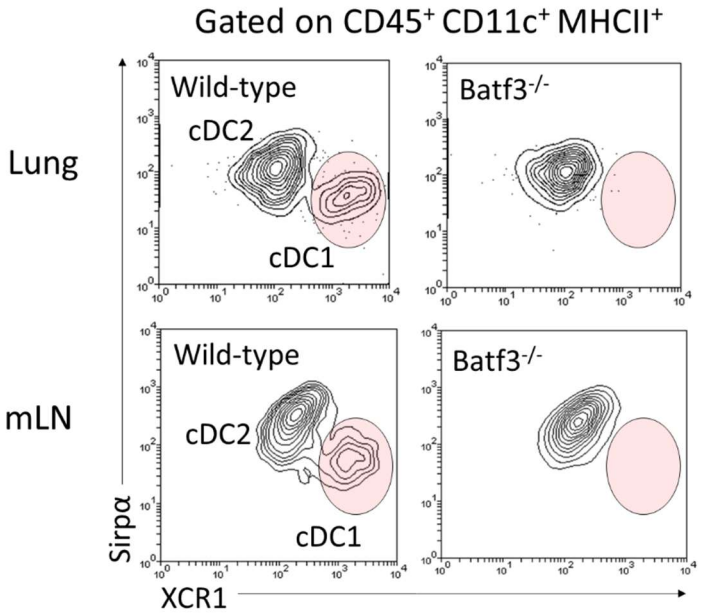

Figure 99. Flow cytometry identification of cDC1s in the lungs and mediastinal lymph node (mLN) of wild-type and Batf3$^{-/-}$ mice. Shown are representative contour plots of *n* = 2 mice/group.

Next, we inoculated WT and Batf3$^{-/-}$ mice with gp33-expressing B16-F10 tumor cells to evaluate tumor-specific responses (Figure 100A). Analysis at day 20 revealed that ivBCG did not reduce the number of visible tumor foci in the lung surface of Batf3$^{-/-}$ mice, in contrast to WT mice (Figure 100B), suggesting that cDC1s were required for efficacy. Flow cytometry analysis of the lung revealed that the infiltration of CD8^{+} T cells into the tumor-bearing lung triggered by ivBCG was abrogated in mice lacking cDC1s (Figure 100C), as well as their expression of Granzyme B (Figure 100D). Interestingly, CD8^{+} T cells from untreated Batf3$^{-/-}$ mice expressed less Granzyme B than in untreated WT mice (Figure 100D), implying that Batf3-dependent cDC1s prime cytotoxic CD8^{+} T cells against lung tumors in the absence of treatment. Interestingly, our data showed that the induction of a Th1 phenotype in CD4^{+} T cells, marked by higher T-bet expression and lower GATA3, did not rely on Batf3-dependent cDC1s (Figure 100E), which suggests that other APCs are responsible for driving this phenotype.

Along with the previous analysis, we also examined gp33-tumor specific responses. We found that the enhancement of gp33-specific CD8^{+} T cell responses by ivBCG was completely abolished in Batf3$^{-/-}$ mice (Figure 101A,B). Moreover, splenocytes isolated from mice lacking cDC1s and bearing B16-F10.gp33 tumors did not display cytotoxicity

against B16-F10 cells *in vitro*, in stark contrast with splenocytes isolated from WT ivBCG mice (Figure 101C).

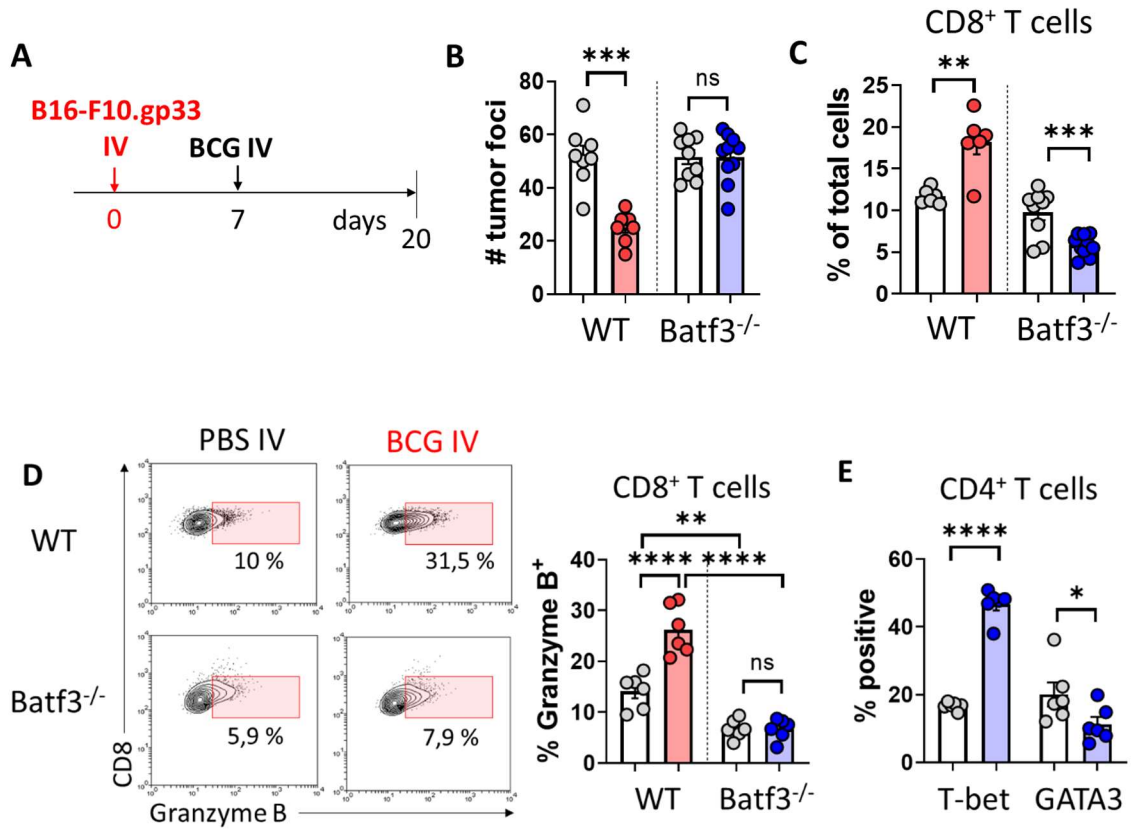

Figure 100. Mice were treated as shown in (A). At day 20 tumor foci were counted by visual inspection (B) and lung single cell suspensions were analyzed by flow cytometry (C,D,E). Shown are representative contour plots (D) and quantification. *n* = 6-10 mice/group, from two independent experiments except (E).

Altogether, these results show that cDC1s participate in ivBCG-driven recruitment of $CD8^+$ T cells, their acquisition of a cytotoxic phenotype and in the enhancement of tumor-specific responses.

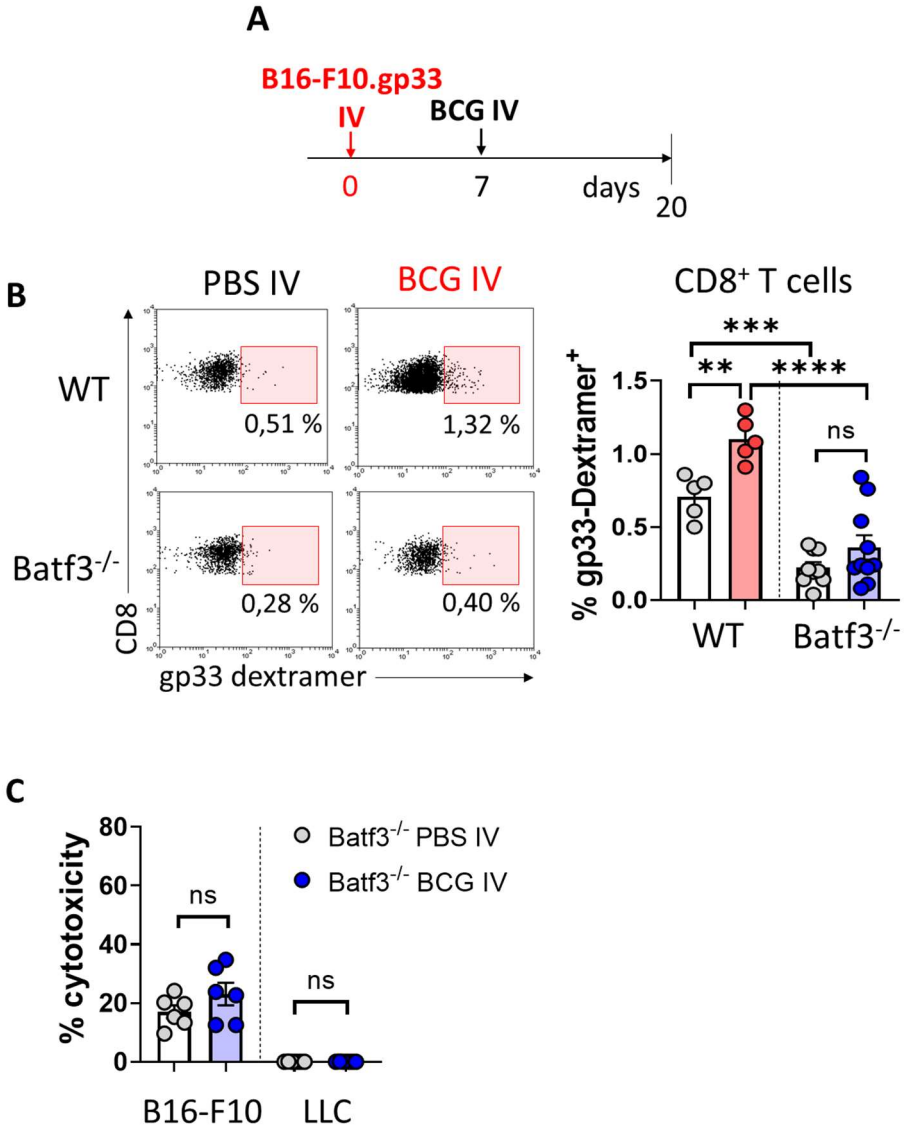

Figure 101. Mice were treated as shown in (A), and at day 20 lung single cell suspensions were analyzed by flow cytometry. Shown are representative dot plots for gp33-specific $CD8^+$ T cell identification and quantification (B) for n = 6-10 mice/group, from two independent experiments. (C) Splenocytes from $Batf3^{-/-}$ mice were isolated and incubated with luciferase-expressing B16-F10 or LLC tumor cells *in vitro* for 20 h and cytotoxicity measured by luminiescence analysis for n = 6 mice/group, from one experiment.

Finally, we evaluated the survival of $Batf3^{-/-}$ mice inoculated with B16-F10. BCG treatment was completely ineffective in mice lacking Batf3 (Figure 102), which corroborates an indispensable role of cDC1s in driving BCG therapeutic efficacy in this model.

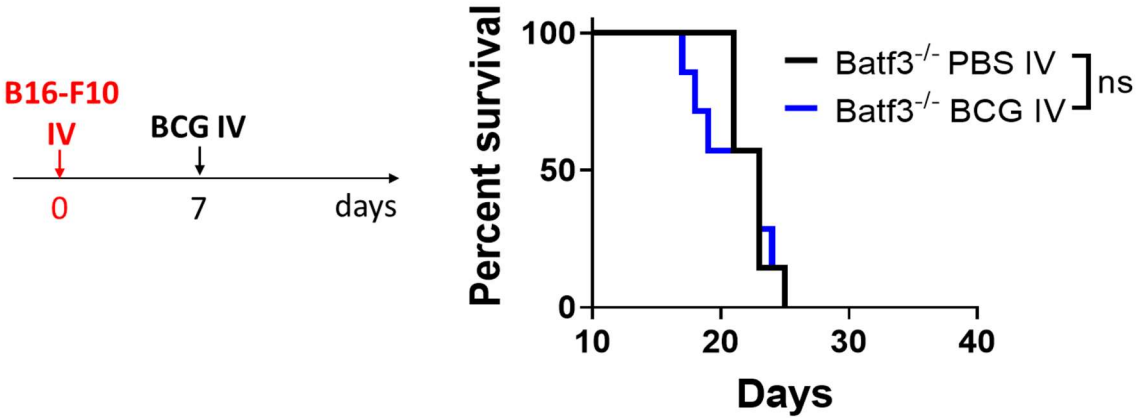

Figure 102. Survival of Batf3$^{-/-}$ mice inoculated intravenously with B16-F10 cells and treated with PBS or BCG IV. *n* = 7 mice/group, from two independent experiments.

5.8 Intravenous BCG stimulates lung NK cells

NK cells have a prominent role in the control of disseminated tumor cells and metastasis[124], being specifically required for the control of B16-F10 lung metastases[476,491,492]. In addition, BCG can activate human NK cells *in vitro*[327,493] and *in vivo*[494,495], and these innate immune cells have been shown to be indispensable for intravesical BCG immunotherapy in mouse models of bladder cancer[332]. Taking into consideration these findings, we wondered whether NK cells participated in the antitumoral immune response triggered by ivBCG.

First, we analyzed NK cells in the lungs of B16-F10 tumor-bearing mice at day 20 (Figure 103A). Lung NK cells were defined by flow cytometry as CD45^{+} CD3^{-} NKp46^{+} CD49b^{+} cells (Figure 103B). Our data indicated that ivBCG recruited NK cells to the tumor-bearing lung, evidenced by a higher percentage among CD45^{+} immune cells and higher absolute numbers (Figure 103B). Further analysis of their phenotype revealed that a higher percentage of NK cells expressed Granzyme B when receiving ivBCG treatment (Figure 103C), as well as increased CD11b expression (Figure 103D), a marker of mature NK cells which display a more cytotoxic phenotye[496].

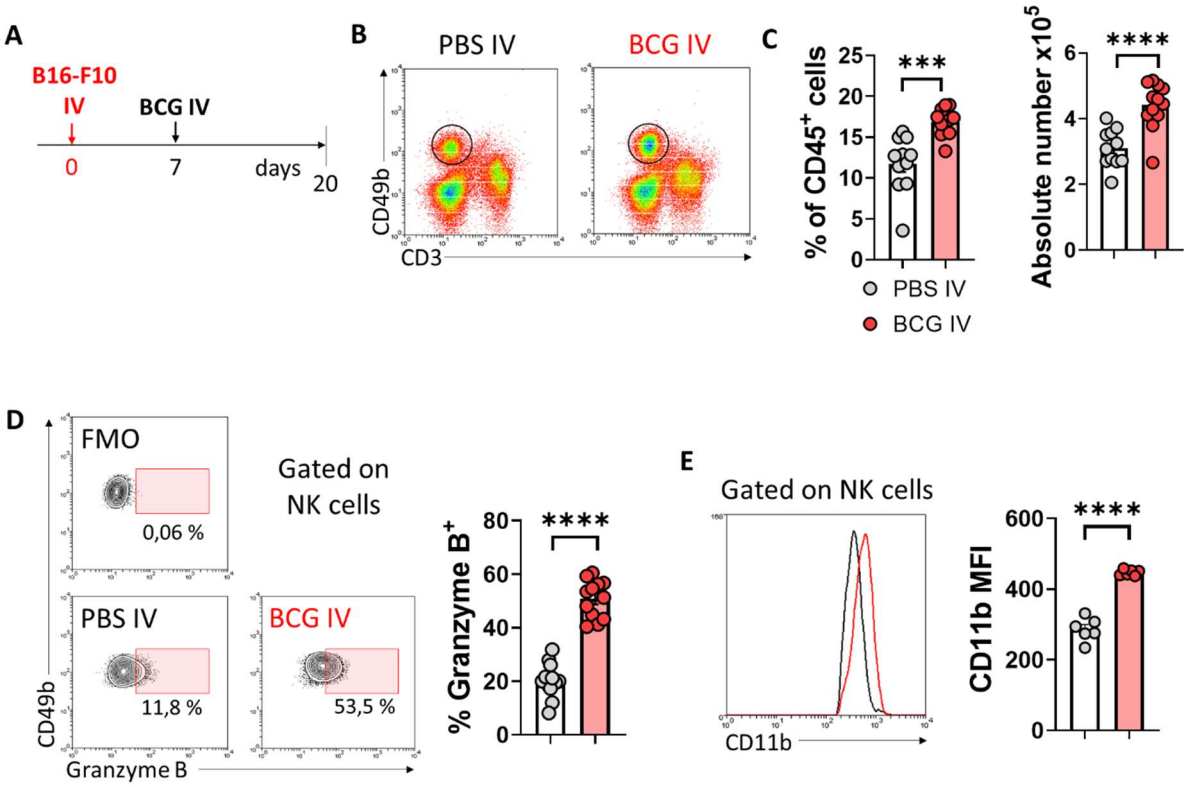

Figure 103. Mice were treated as shown in (A). NK cells identified in the lung by flow cytometry (B) and their absolute numbers and frequencies analyzed (B,C), *n* = 12 mice/group, from two independent experiments. (D) Representative contour plots of intracellular Granzyme B expression in NK cells and quantification for *n* = 12 mice/group. (E) Expression of CD11b by lung NK cells, *n* = 6 mice/group, one experiment.

Next, we stimulated lung single cell suspensions *in vitro* with plate bound αNK1.1 antibodies[497,498] to detect IFN-γ and CD107a expression by NK cells. To detect actively degranulating cells, FITC-conjugated CD107a antibody was added during i*n vitro* stimulation, in the presence of Brefeldin A the last 3 h of the assay. Indeed, αNK1.1 stimulation increased NK cell degranulation, measured as percentage of cells expressing CD107a (Figure 104A). Our results revealed that *ex vivo* stimulated NK cells from ivBCG mice expressed more CD107a and IFN-γ when compared to controls (Figure 104B), suggesting a higher activation status. Interestingly, we observed that among total NK cells in the lung, those which were $CD11b^{hi}$ expressed two-fold more IFN-γ and CD107a than their $CD11b^{lo}$ counterparts (Figure 104C), confirming that high CD11b expression delineates a higher maturation status of NK cells and correlates with greater cytotoxic potential.

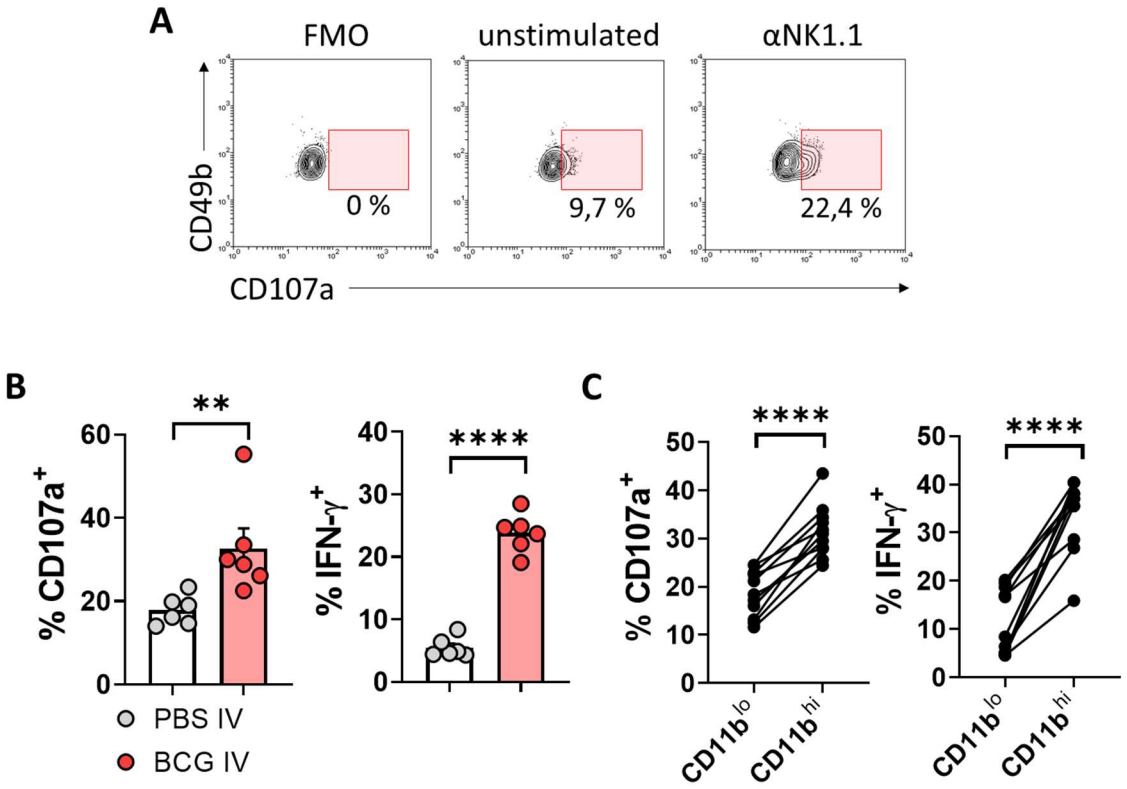

Figure 104. Mice were treated as in Figure 103. (A) Representative contour plots of CD107a expression by NK cells in lung single cell suspensions left either unstimulated or stimulated *ex vivo* with plate bound antiNK1.1 for 4 h in the presence of Brefeldin A the last 3 h. (B) Quantification of CD107a and intracellular IFN-γ by lung NK cells following ex vivo restimulation, *n* = 6 mice/group, from one experiment. (C) Differential expression of activation markers by $CD11b^{hi}$ and $CD11b^{lo}$ NK cell subsets.

We also wondered whether ivBCG differentially stimulated circulating conventional NK cells (cNKs) and lung-tissue resident NK cells (trNKs). In humans and mice, trNK cells can be identified by expression of CD49a and usually co-express CD69 and CD103, accounting for approximately 15 % of lung NK cells[499–501]. In B16-F10 lung tumor-bearing mice, approximately 14,5 % of NK cells expressed the tissue-residence marker CD49a (Figure 105A). Further analysis revealed that ivBCG stimulated both cNKs and trNKs to a comparable extent (Figure 105B,C). Additionally, we found no differences in IFN-γ and Granzyme B expression between trNK and cNK cells in the untreated setting. Therefore, ivBCG can stimulate both circulating cNK and lung trNK cells.

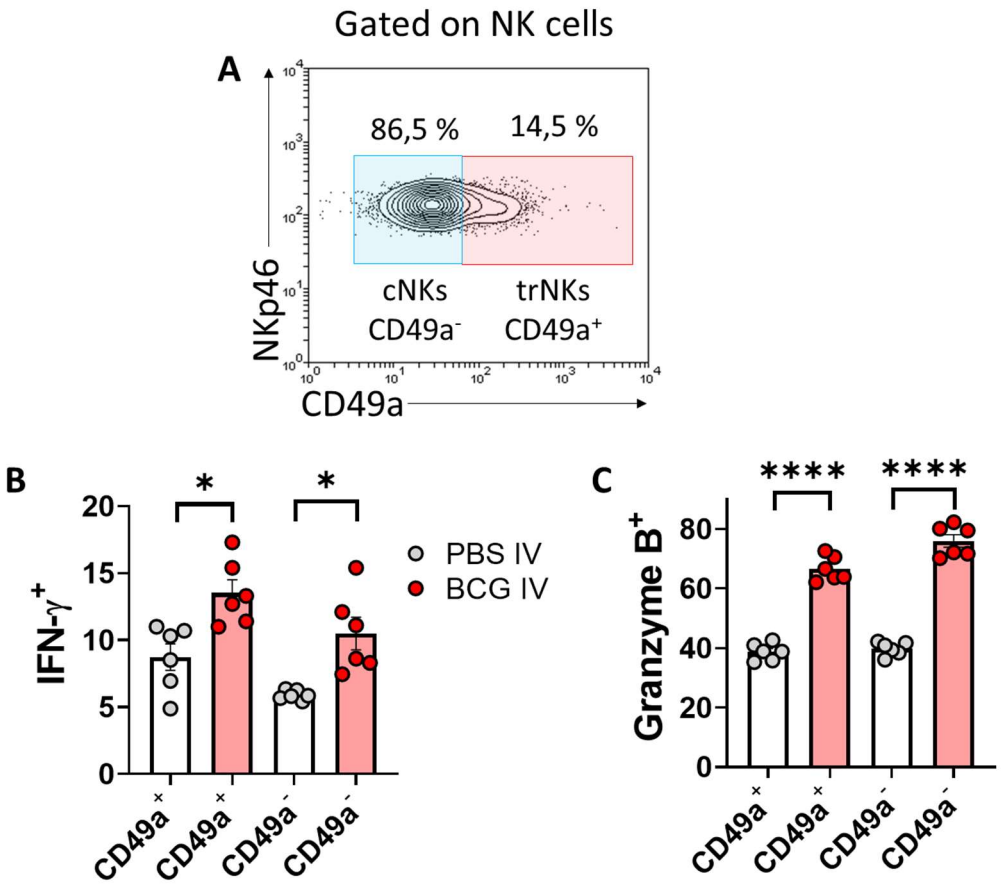

Figure 105. Mice were treated as in Figure 103. (A) Representative contour plot for discerning conventional NK cells (cNKs) and tissue-resident (trNKs), and average proportions for *n* = 6 mice/group. Quantification of IFN-γ (B) and Granzyme B (C) expression by cNKs and trNKs, *n* = 6 mice/group, one experiment.

As another means of measuring specifically the phenotype of NK cells that have infiltrated the tumor-bearing lung, we administered labeled antiCD45 antibodies before euthanasia to discern circulating and lung-infiltrating populations (Figure 106). Although performed with only three mice per group, we observed that BCG treatment increased the absolute numbers of NK cells in lung tissue. Moreover, infiltrated NK cells expressed more Granzyme B in mice which had received ivBCG treatment (Figure 106).

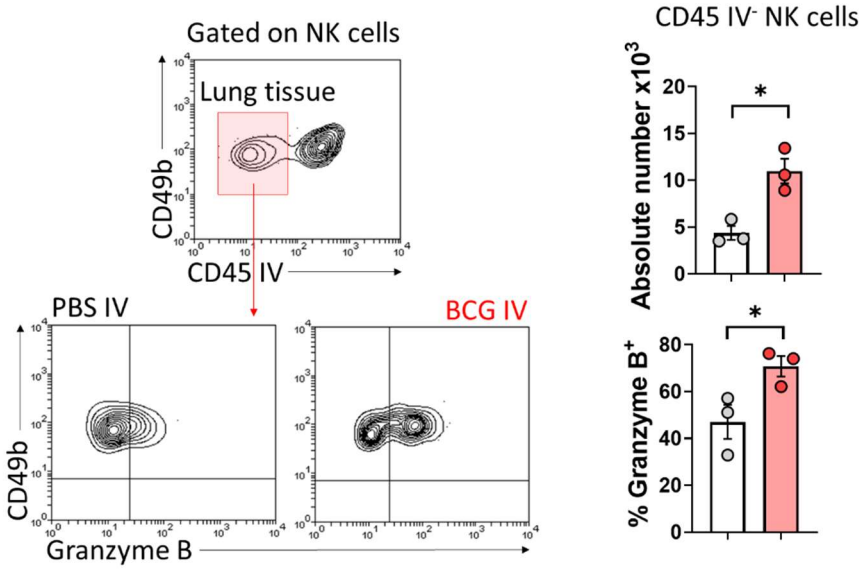

Figure 106. Mice were treated as in Figure 103. Shown are representative contour plots for discerning lung tissue and circulating NK cells, based on intravenous staining with an antiCD45 antibody. Absolute number of lung-resident NK cells and Granzyme B expression in this population was measured. *n* = 3 mice/group, one experiment.

Next, we set out to test the cytotoxic potential of BCG-stimulated NK cells *in vitro* against target syngeneic B16-F10 cells. We engineered a B16-F10 cell line lacking MHC-I by CRISPR/Cas9-mediated disruption of the β_2-microglobulin gene (B16-F10-*B2m*$^{-/-}$), which completely abrogated MHC-I expression even when incubated with IFN-γ for 24 h (Figure 107). This B16-F10 cell line lacking MHC-I would conceivably be more susceptible to NK cell-mediated attack since MHC-I is an inhibitory ligand for these cells[502].

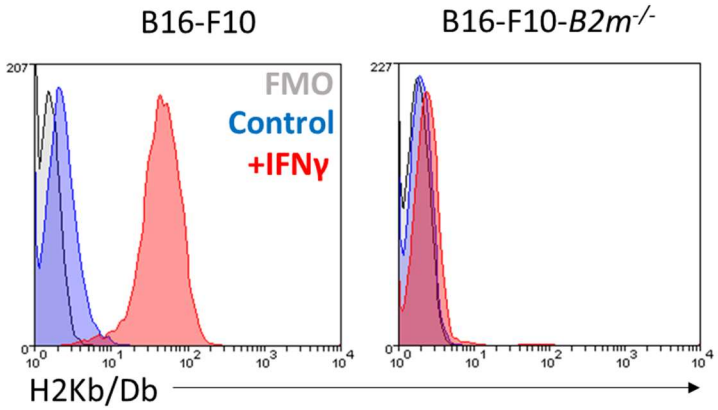

Figure 107. H2K^b/D^b expression by B16-F10 parental and B16-F10-*B2m*$^{-/-}$ tumor cells *in vitro*. Grey: FMO, Blue: control, Red: + IFN-γ (50 ng ml^{-1} 24 h).

NK cells were isolated from the spleens of mice by magnetic isolation with CD49b microbeads, with a purity of the resulting population of approximately 60 % across all the

experiments performed. Ideally, we would have wanted to isolate NK cells from lung tumors for testing their cytotoxic function, but the number of NK cells we could obtain from this tissue would be much lower compared to the spleen, a common organ for isolating NK cells for cytotoxic assays. Importantly, ivBCG colonizes the spleen as well as the lungs[218,454], so we thought ivBCG-stimulated spleen NK cells could function as a proxy for BCG-stimulated lung NK cells.

Isolated NK cell cytotoxicity was evaluated against parental B16-F10 cells and B16-F10 lacking MHC-I (B16-F10-*B2m*$^{-/-}$). Tumor cells were labeled before adding NK cells at different effector to target (E:T) ratios, and after 20 h tumor cell death was tracked by flow cytometry. As seen in Figure 108A, NK cells from ivBCG mice displayed enhanced cytotoxicity towards B16-F10-*B2m*$^{-/-}$ cells than NK cells from control mice at the E:T ratios tested (Figure 108), evidenced by a five-fold higher proportion of tumor cells undergoing cell death (AnnexinV^{+} 7-AAD^{-}) and already dead (AnnexinV^{+} 7-AAD^{+}). As expected, parental MHC-I sufficient B16-F10 cells were more resistant to NK cell cytotoxicity in the same conditions, although significantly higher cytotoxicity of NK cells coming from ivBCG mice was observed at the higher 5 to 1 E:T ratio (Figure 108).

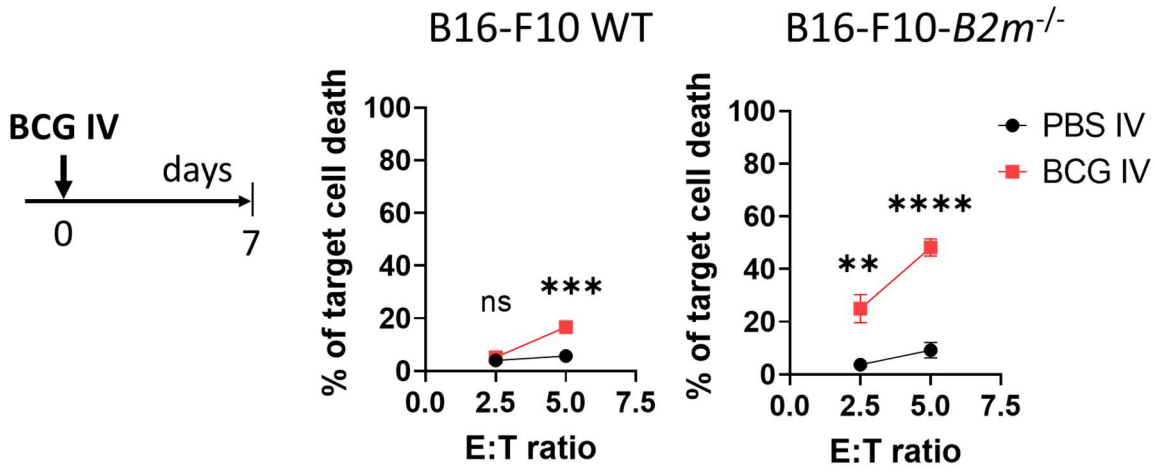

Figure 108. *In vitro* NK cell cytotoxicity against B16-F10 tumor cells was tested. Cell death markers were analyzed in the CTV labeled target population. In each experiment, conditions were run in triplicates and average values were used for analysis. Shown are results from two independent experiments. For each experiment, NK cells were isolated from pooled splenocytes coming from 2 mice per condition (either PBS or BCG IV-treated mice).

To validate our findings *in vivo*, we inoculated mice intravenously with MHC-I deficient B16-F10 cells to determine whether stimulation of NK cell activity by ivBCG could slow

tumor growth in the lung, since they would completely avoid direct recognition by $CD8^+$ T cells. We observed that ivBCG significantly improved mouse survival in WT mice, suggesting that stimulated NK cells could be contributing to the control of MHC-I deficient tumors (Figure 109). To extend our findings, we evaluated the survival of mice lacking perforin bearing MHC-I deficient B16-F10 tumors. As shown in figure 109, ivBCG did not extend survival in mice lacking perforin, further suggesting that the perforin-mediated cytotoxic function of NK cells could be driving the efficacy of ivBCG in this model, since MHC-I deficient tumors should be resistant to perforin-mediated $CD8^+$ T cell attack.

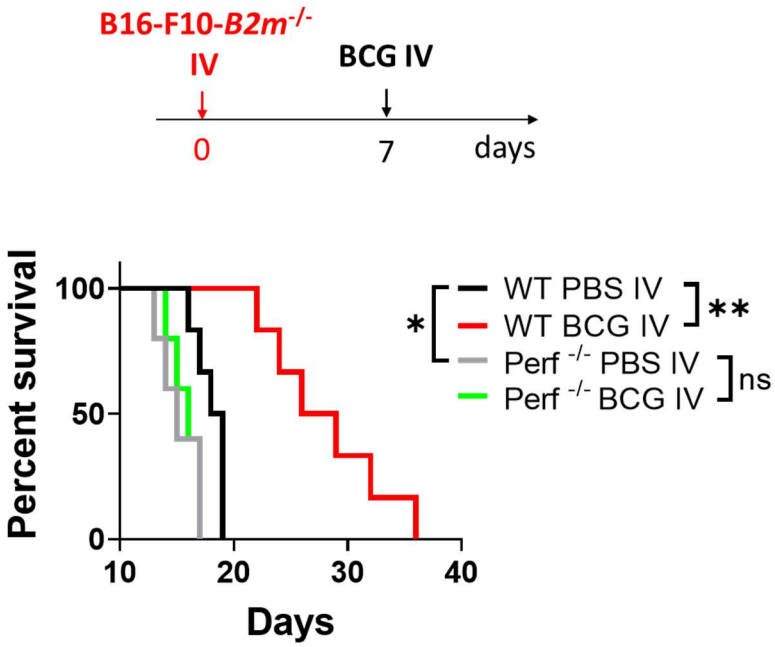

Figure 109. Survival of wild-type (WT) or perforin deficient (Perf $^{-/-}$) mice inoculated intravenously with MHC-I deficient B16-F10 cells and treated with BCG or PBS at day 7. *n* = 6 mice/group, one experiment.

5.9 BCG-stimulated NK cells recruit dendritic cells to the tumor bed and enhance adaptive immune responses

Next, we hypothesized that NK cells could be acting upstream of tumor-specific adaptive immune cells to mediate tumor growth control after BCG treatment. Concretely, as NK cells rapidly respond to stimuli, we thought that BCG-activated NK cells could be favoring the development of tumor-specific adaptive immune responses, which are indeed required for the efficacy of ivBCG against MHC-I sufficient B16-F10 tumors as we showed in the $CD4^+$ and $CD8^+$ T cell depletion experiments.

First, we tested whether NK cells were also required for the antitumoral effect of ivBCG against MHC-I sufficient B16-F10 lung tumors. For this, we depleted them by bi-weekly administration of αNK1.1 antibody, starting just before ivBCG treatment and until day 20 (Figure 110) to eliminate any contribution of BCG-stimulated NK cells to antitumor immunity. We also included a group of mice treated with ivBCG and depleted NK cells from day 16 to endpoint (Figure 110), to test whether NK cells were also required in later stages of tumor development.

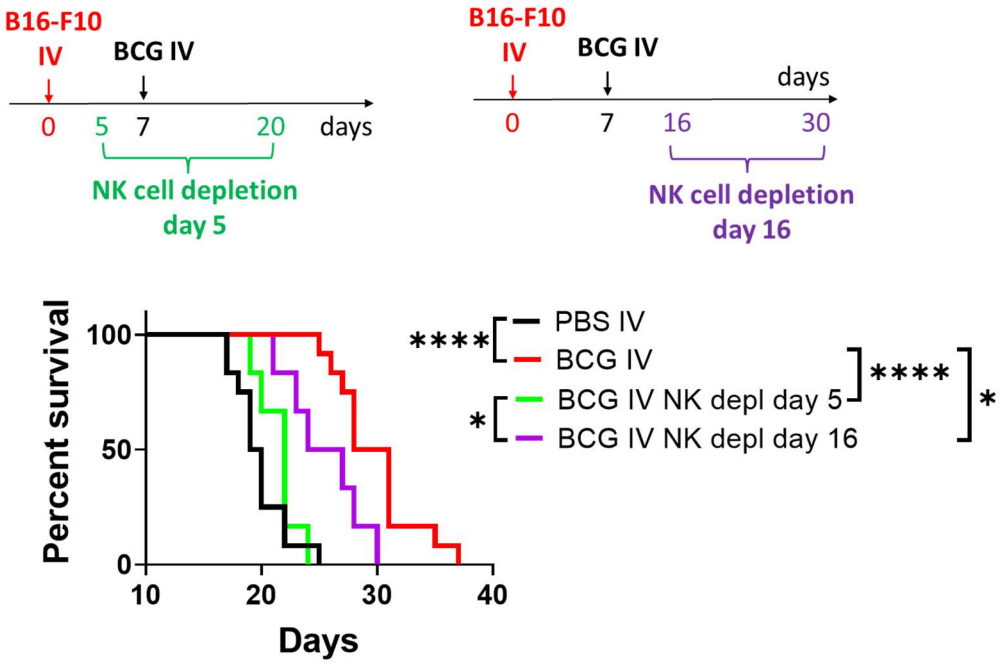

Figure 110. Survival of mice inoculated intravenously with B16-F10 cells, treated with BCG and depleted of NK cells following the schedules shown. *n* = 6 mice/group, one experiment.

Our results revealed that NK cells are required for ivBCG efficacy both during early and late stages of tumor growth in the lung, as NK cell depletion in both settings significantly shortened mice survival in comparison to treated non-depleted mice (Figure 110). However, NK cells appeared to be most important in early stages, since mice undergoing NK cell depletion from days 16 to 30 survived longer than mice undergoing early NK cell depletion, from days 5 to 20 (Figure 110). Thus, we confirm that ivBCG efficacy depends on the presence of NK cells, which are specially required around the time of treatment administration, in early stages of tumor growth.

Next, to unravel the role of NK cells in driving ivBCG treatment success, we similarly depleted them in B16-F10.gp33 tumor bearing mice undergoing ivBCG treatment from days 5 to 20 and analyzed immune responses at day 20 (Figure 111A).

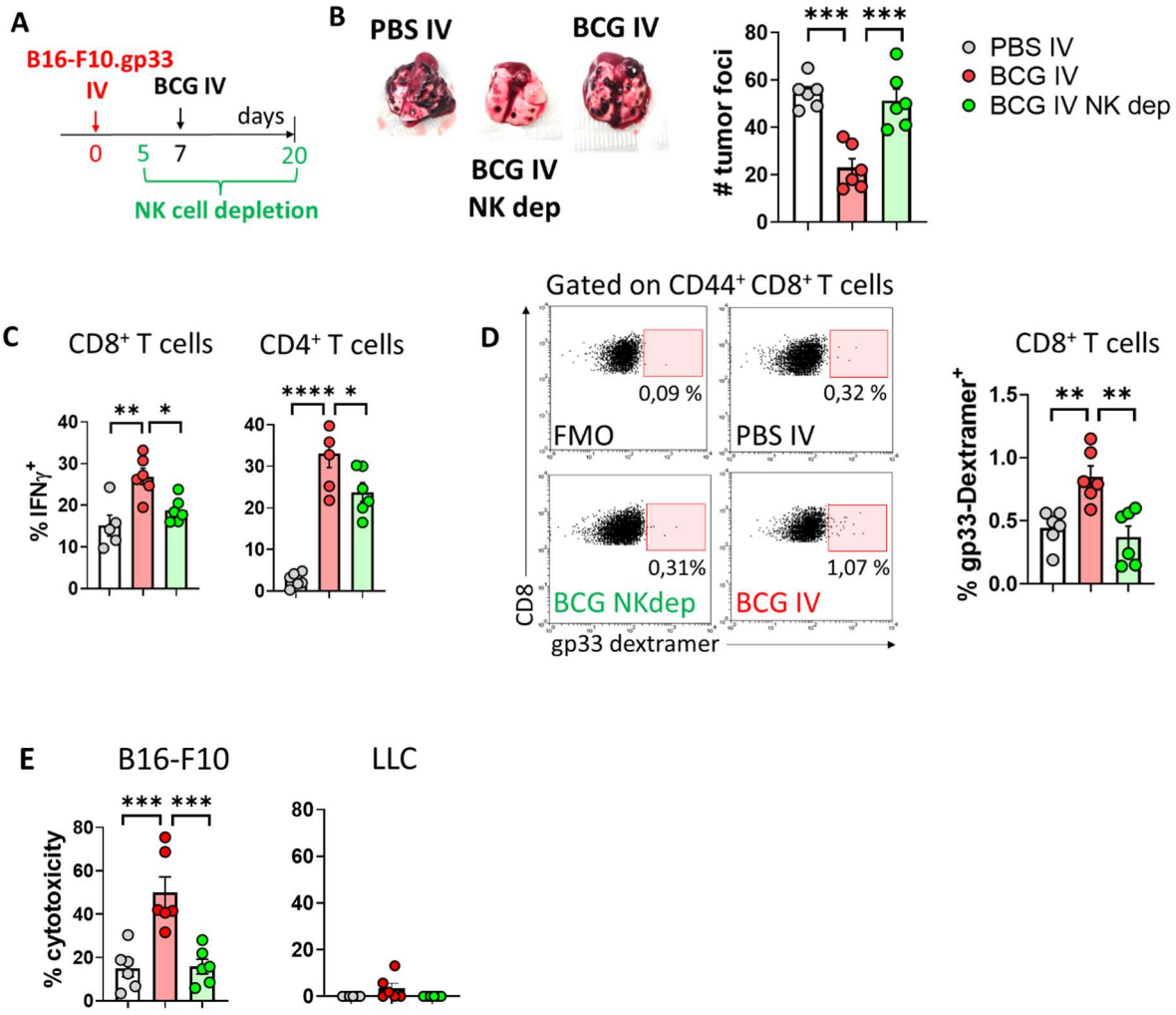

Figure 111. Mice were inoculated intravenously with gp33-expressing B16-F10 cells, treated with ivBCG and NK cell-depleted as shown in (A). (B) Representative images and number of tumor foci in the lungs counted by visual inspection. (C) Expression of IFN-γ by T cells following ex vivo restimulation. (D) Representative dot plots for gp33-specific $CD8^+$ T cells identification and quantification. (E) Cytotoxicity assay using splenocytes at a 100:1 E:T ratio towards luciferase-expressing B16-F10 and LLC cells. *n* = 6 mice/group, one experiment.

Confirming the results obtained in the NK depletion survival experiment, BCG ability to reduce visible B16-F10 tumor foci in the lung was abolished in the absence of NK cells (Figure 111B). Next, we analyzed lung T cell function by flow cytometry. After stimulation with αCD3/αCD28 antibodies, the enhanced IFN-γ expression by lung $CD4^+$ and $CD8^+$ T cells observed in BCG-treated mice was partially lost when NK cells were depleted (Figure

111C). This result suggested that NK cells mediate the improvement of T cell responses in the lung driven by ivBCG. Focusing on tumor-specific responses, ivBCG no longer improved gp33-specific responses in the lung when NK cells were depleted (Figure 111D). To further validate this finding, we performed *in vitro* killing assays with splenocytes isolated from these mice and found that NK cell depletion completely abrogated the improvement of B16-F10-specific cytotoxicity by ivBCG (Figure 111E). Altogether, these results suggested that BCG-stimulated NK cells participate in the generation of tumor-specific adaptive immune responses in the lung.

Next, we wondered whether NK cell perforin-mediated cytotoxic activity was needed for the generation of adaptive immune responses. For this, although ideally we would have used mice with NK cell-restricted deletion of perforin, we did not have this tool available so we used standard perforin knock-out mice. Therefore, in the following experiments we cannot rule out a contribution of T cell perforin-mediated cytotoxicity to the observed effects.

We analyzed the lungs of $Perf^{-/-}$ mice inoculated intravenously with B16-F10.gp33 cells, either untreated or treated with ivBCG (Figure 112A). Confirming the results of the survival experiments conducted with this mouse strain, ivBCG did not reduce tumor burden in the lung at day 20 in the absence of host perforin expression (Figure 112A). Concurring with this lack of efficacy, ivBCG no longer enhanced gp33-tumor specific $CD8^+$ T cell responses in the lung in the absence of host perforin (Figure 112B), neither *in vitro* splenocyte-mediated cytotoxicity against B16-F10 tumor cells (Figure 112C). However, we still observed enhanced IFN-γ secretion by $CD4^+$ and $CD8^+$ T cells of ivBCG mice in the absence of perforin, meaning that stimulation of T cell function did not rely on perforin.

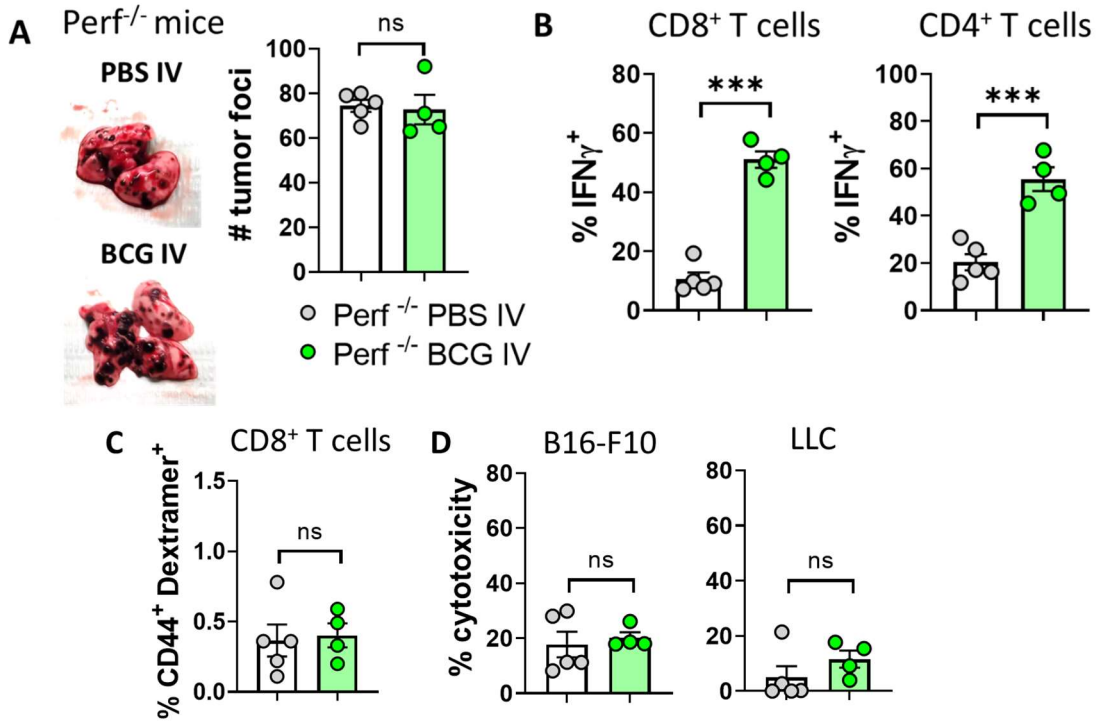

Figure 112. Perforin deficient mice (Perf$^{-/-}$) were inoculated intravenously with gp33-expressing B16-F10 cells and treated with PBS or BCG at day 7. (A) Representative images and quantification of visible tumor foci in the lungs at day 20. (B) Expression of IFN-γ by T cell subsets following ex vivo restimulation. (C) Frequency of gp33-speciifc CD44^{+} CD8^{+} T cells among the total CD8^{+} population in the lungs. (D) Splenocyte cytotoxicity towards target luciferase-expressing B16-F10 or LLC tumor cells at a 100:1 effector to target ratio. *n* = 4-5 mice/group, one experiment.

Tumor cell killing is not the only role that NK cells can carry out in the context of antitumor immunity. They have also been described to be responsible for cDC1 recruitment to the tumor bed[127,128,503], therefore orchestrating the initiation of adaptive immune responses.

Here, we hypothesized that BCG-stimulated NK cells could also be favoring cDC1 recruitment to lung tumors. To test this, we analyzed cDC1s in the lungs of B16-F10.gp33 tumor-bearing mice. Our data revealed that ivBCG augmented cDC1 numbers in the tumor-bearing lung, measured as percentage among CD45^{+} cells, as absolute counts or as percentage among DCs (Figure 113). Interestingly, NK cell depletion in ivBCG mice completely abolished this effect (Figure 113), meaning that ivBCG-driven recruitment of cDC1s is mediated by NK cells.

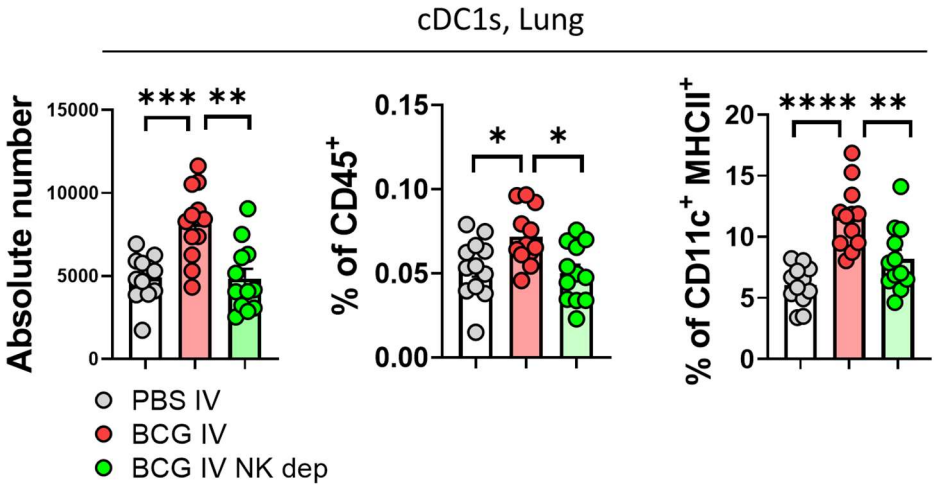

Figure 113. Mice were inoculated intravenously with B16-F10 cells and treated with PBS or BCG at day 7. A group received NK1.1 depleting antibodies from days 5 to 20. At day 20, lung cDC1s were quantified by flow cytometry. *n* = 12 mice/group, from two independent experiments.

Next, we wondered the mechanism by which BCG-stimulated NK cells were recruiting cDC1 to the tumor-bearing lung. NK cells have been described to recruit cDC1s by secreting the chemoattractant factors CCL5 and XCL1[127]. Therefore, we first analyzed CCL5 expression in the tumor-bearing lung by intracellular staining. This chemokine was mostly secreted by NK cells, evidenced both by a higher MFI of CCL5 in these cells and a higher percentage of the population secreting it compared to $CD3^+$ T cells. Lung $CD3^+$ T cells also secreted CCL5, although to a lesser extent than NK cells (Figure 114).

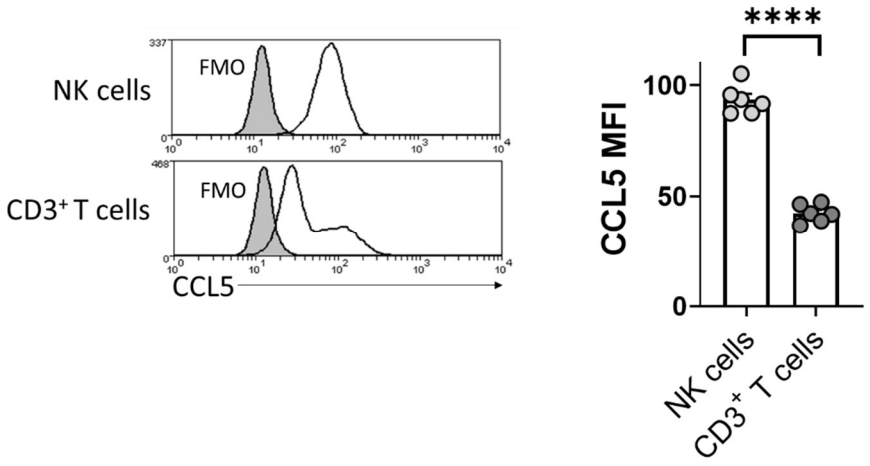

Figure 114. Representative histograms and quantification of intracellular CCL5 expression by NK and $CD3^+$ T cells in the lungs of B16-F10 tumor bearing mice at day 20. *n* = 6 mice, from one experiment.

Further analysis revealed that BCG treatment increased the percentage of NK cells secreting CCL5 in the lungs of tumor-bearing mice, as well as the MFI of CCL5 in this

population (Figure 115A). Of note, BCG treatment also increased CCL5 expression by $CD8^+$ T cells (Figure 115), although both the proportion of cells expressing it and the MFI was lower compared to the NK cell population. Altogether, these results reveal a mechanism by which ivBCG stimulates CCL5 expression by NK and $CD8^+$ T cells in the tumor-bearing lung, which could drive the NK cell-dependent recruitment of cDC1s.

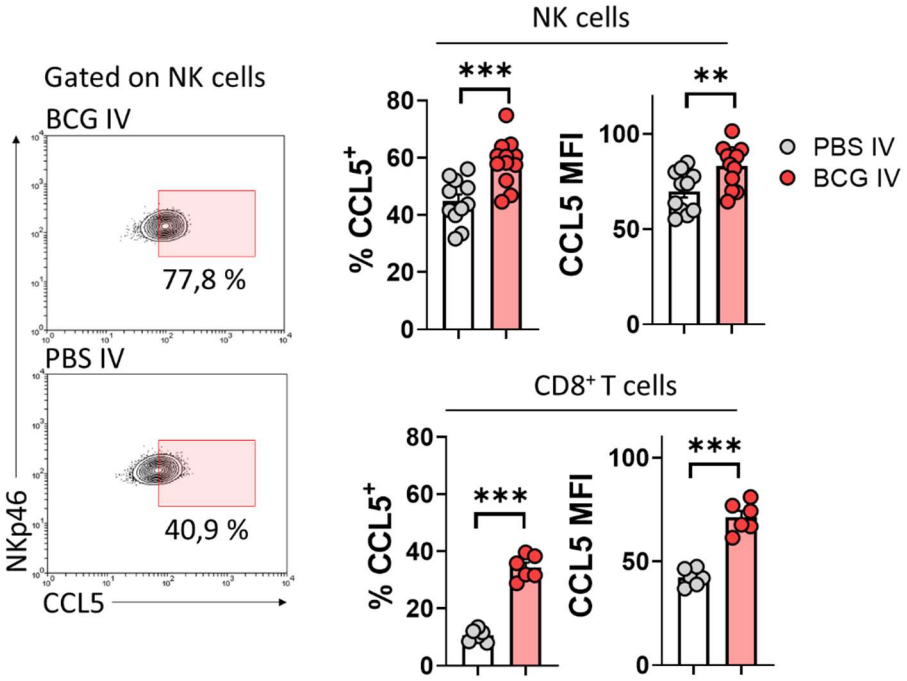

Figure 115. Analysis of CCL5 expression by NK and $CD8^+$ T cells in the lungs of B16-F10 tumor bearing mice treated with IV BCG or PBS as a control. *n* = 12 mice/group for NK cells, two independent experiments, or *n* = 6 mice/group for $CD8^+$ T cells.

Since trNK cells have been shown to be specifically responsible for upregulating CCL5 secretion in tumors following IL-12 treatment[503], we evaluated the ability of lung cNKs and trNKs to express CCL5 following ivBCG. In our model, both cNK and trNK responded similarly to ivBCG regarding CCL5 expression (Figure 116)

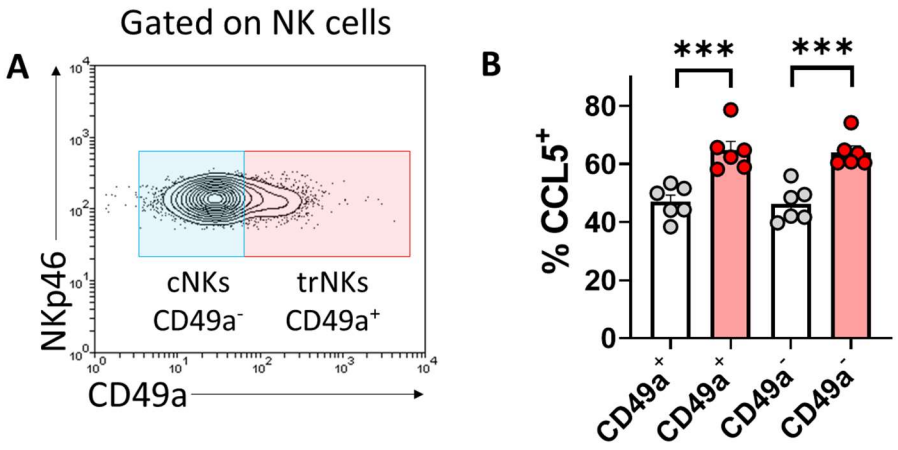

.

Figure 116. Mice were treated as in Figure 115. Analysis of intracellular CCL5 expression by cNKs or trNKs, *n* = 6 mice/group.

Next, we analysed CCL5 protein levels in homogenates of B16-F10 tumor-bearing lungs by ELISA, finding that ivBCG treatment increased CCL5 concentration in lung tissue, confirming flow cytometry data (Figure 117). Interestingly, although we observed that $CD8^+$ T cells also increased CCL5 expression following ivBCG, NK cell depletion in decreased CCL5 protein levels to those of control PBS (Figure 117), evidencing that the main source of CCL5 in response to BCG treatment are NK cells. Determination of other critical cytokines for antitumor responses revealed that BCG treatment increased both IL-12 and IFN-γ protein levels in lung tissue in comparison to untreated mice, while NK cell depletion slightly reverted (non-significantly) this effect for IL-12 and had no effect in the case of IFN-γ (Figure 117).

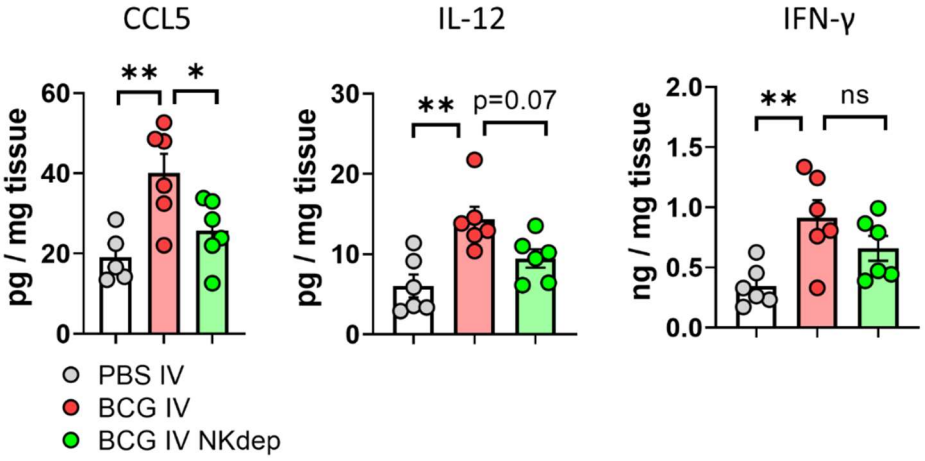

Figure 117. Mice were treated as in Figure 113, and a group received NK1.1 depleting antibodies from days 5 to 20. At day 20, protein levels of CCL5, IL-12 and IFN-γ were measured in lung tissue homogenates.

Next, we interrogated the TGCA RNA-seq database using the GEPIA2 tool[504] to determine whether these observations could be translated to human lung adenocarcinoma. Using an optimized NK cell signature[505], we found that abundance of NK cells correlated with that of cDC1s. Concomitantly, a strong correlation between CCL5 transcript levels and the NK cell signature was observed, as well as between CCL5 transcripts and cDC1s. Interestingly, transcript levels of XCL1, another cytokine involved in NK cell-mediated recruitment of cDC1s[127], did not correlate with the abundance of cDC1 transcripts, at least in lung adenocarcinoma patients (Figure 118). Finally, as previously described, levels of FLT3LG positively correlated with cDC1 abundance[128].

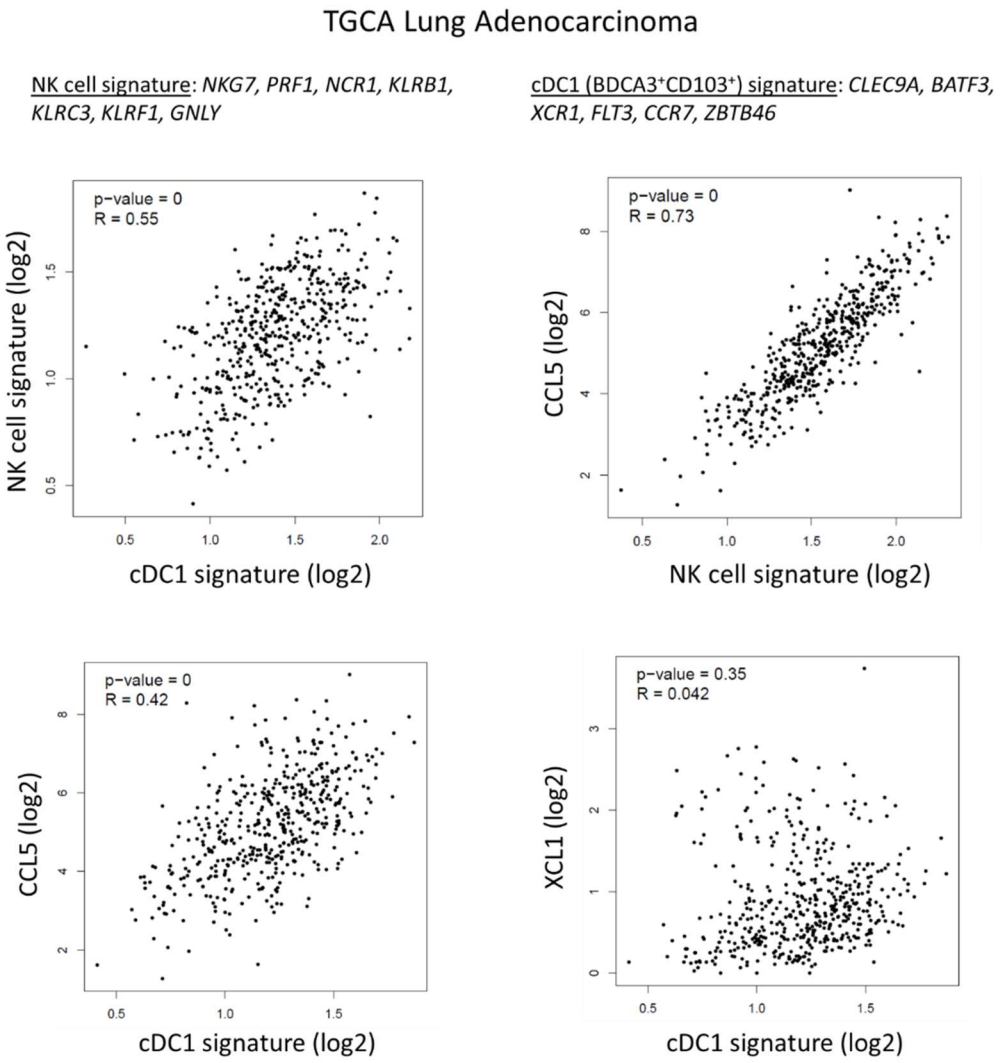

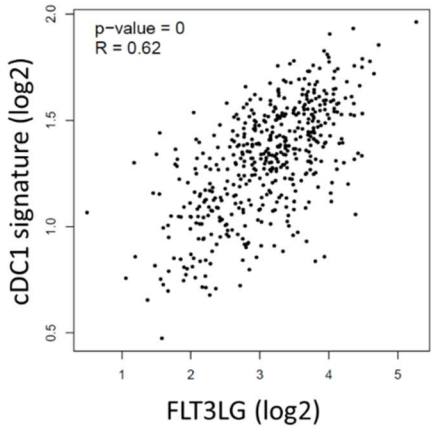

Figure 118. Correlation between distinct transcripts abundance in lung adenocarcinoma specimens analyzed by RNA-seq. *Made using the GEPIA2 tool, data from the TGCA RNA-seq databse*.

Considering our results, we hypothesized that the ability of NK cells to promote tumor-specific adaptive immune responses could rely on a mechanism involving both killing of tumor cells and CCL5-mediated recruitment of cDC1s, which in turn acquire tumor-associated material and cross-prime tumor-specific T cells in the lung-draining mLN.

In an attempt to experimentally test this idea, we generated ZsGreen-expressing B16-F10 lung tumors, since the fluorescent protein ZsGreen, unlike GFP, maintains its fluorescence within intracellular compartments following phagocytosis, allowing us to track cells that have ingested tumor-associated material[416,417].

In a preliminary experiment, we confirmed that we could detect cells carrying tumor-associated material by flow cytometry by comparing mice inoculated with ZsGreen expressing B16-F10 cells with mice inoculated with parental B16-F10 cells. Flow cytometry analysis of lung tissue revealed that cDC1s, cDC2s, alveolar macrophages, monocytes/macrophages and neutrophils acquired green fluorescence in contrast to control B16-F10 tumors (Figure 119), which validated our ability to detect fluorescent tumor-associated material in phagocytic cell subsets. As expected, non-phagocytic cell subsets such us lymphocytes did not acquire ZsGreen associated fluorescence in mice inoculated with B16-F10-ZsGreen cells, consistent with their inability to mediate tumor-associated cell debris phagocytosis (Figure 119).

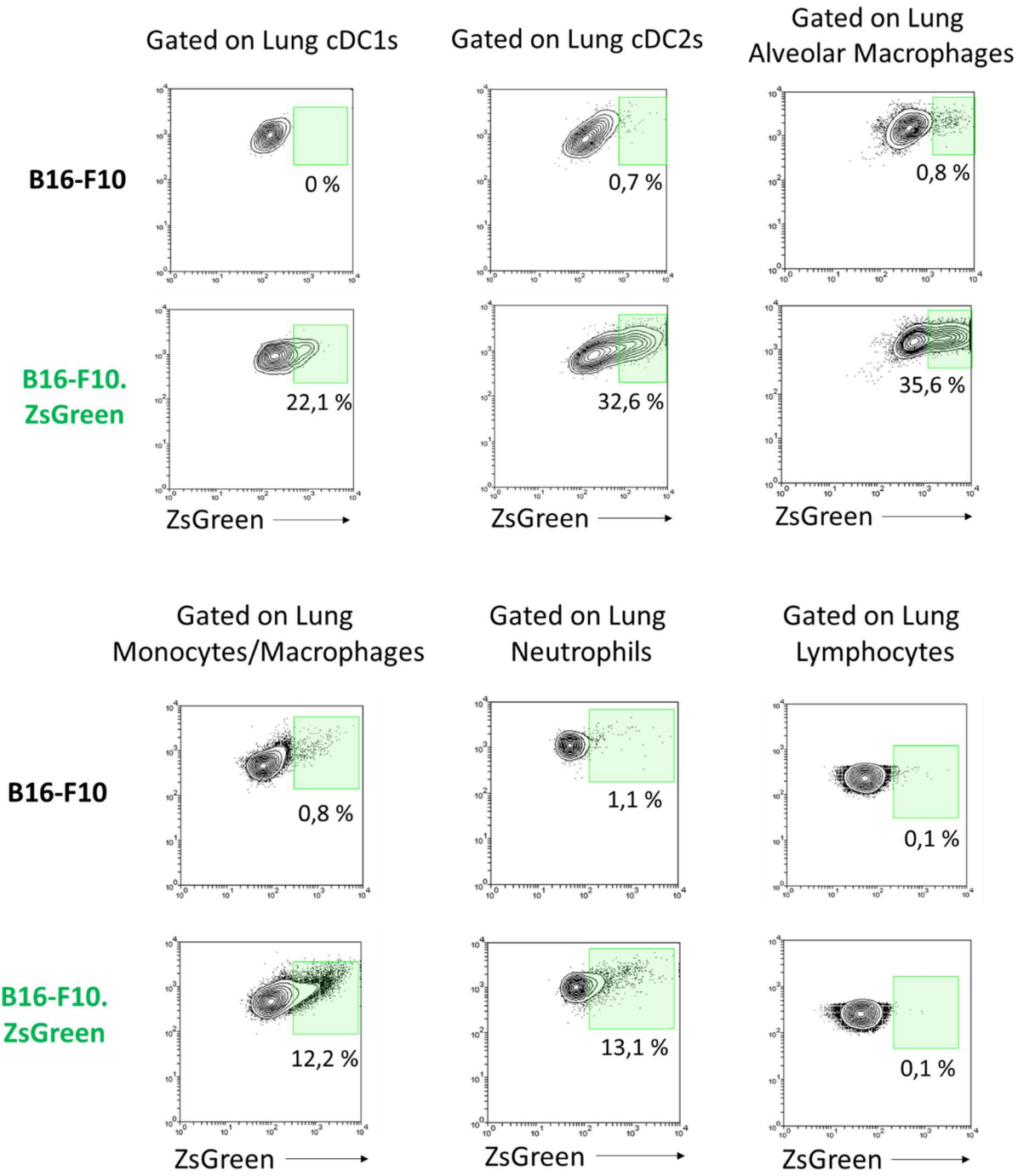

Figure 119. Representative contour plots of ZsGreen expression in distinct cellular compartments from the lungs of B16-F10 or B16-F10-ZsGreen tumor bearing mice at day 20. Plots are representative of *n* = 3 mice/group.

Next, we checked if we could detect cells carrying tumor-associated material in the lung-draining mLN. A fraction of cDC1s and cDC2s from mice bearing fluorescent B16-F10 tumors acquired ZsGreen expression when compared to mice inoculated with parental B16-F10 cells, consistent with the ability of DCs to acquire tumor-associated material and

migrate to the lymph nodes. As a control, CD11c$^-$ MHCII$^-$ cells in the mLN, which would mostly comprise T and B cells, did not acquire ZsGreen expression (Figure 120).

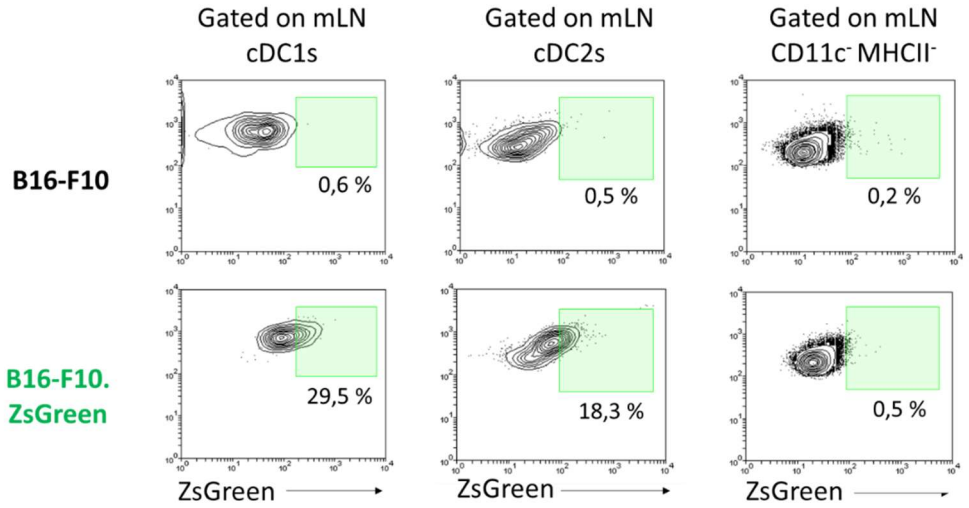

Figure 120. Representative contour plots of ZsGreen expression in distinct cellular compartments from the lung-draining mLN of B16-F10 or B16-F10-ZsGreen lung tumor bearing mice at day 20. Plots are representative of *n* = 3 mice/group.

Therefore, we corroborated that our model allowed us to track DCs that have ingested tumor cell derived material in the lung and travelled to the mLN. Of note, the percentages of DCs carrying tumor-associated material in the mLNs in our experimental conditions are comparable to that observed by other groups using intravenous inoculation of KP lung adenocarcinoma cells (20-40% for cDC1 and 5-20% for cDC2)[506].

Further analysis revealed that migratory cDC1s in the mLN expressed higher levels of ZsGreen compared to their resident counterparts and to migratory cDC2s, at least at the timepoint analyzed (Figure 121), which is consistent with their specialized ability to take up tumor antigen and migrate from the tumor to the draining mLN. Of note, resident cDC1s and cDC2s still expressed more ZsGreen than lymphocytes (Figure 121), which worked as negative controls. This could be due to antigen transfer of tumor proteins between different DC subsets in the LN, which has been described[416].

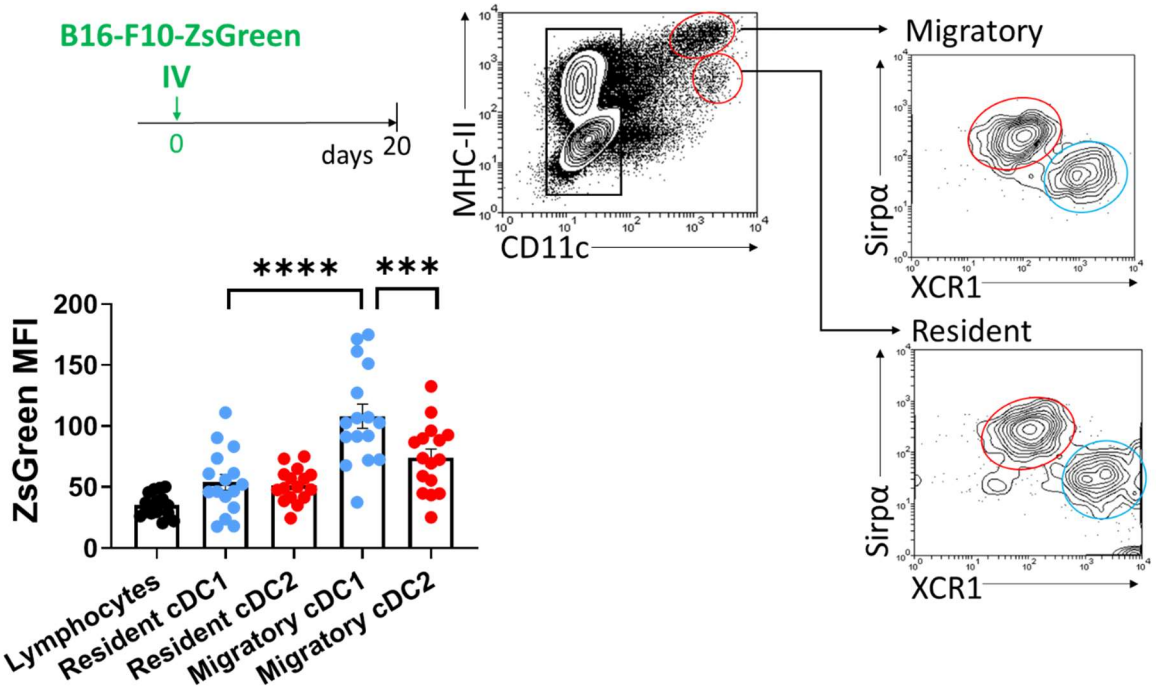

Figure 121. Mice were treated as shown in the Figure. At day 20, lung-draining mLNs were processed and analyzed by flow cytometry. Shown are representative contour plots for defining distinct migratory and resident DC subsets, and quantification of ZsGreen expression in them. *n* = 15 mice/group, one experiment.

Of note, migratory cDC1s also expressed higher levels of CD40 and CD86 than their resident counterparts in the mLN (Figure 122), which indicates higher potential to prime T cell responses.

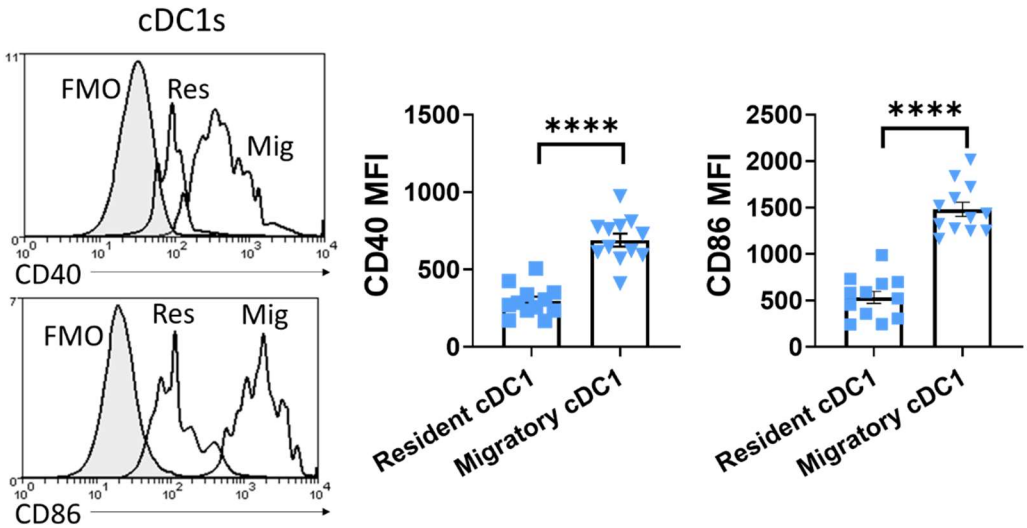

Figure 122. Mice were treated as in Figure 121. At day 20, expression of CD40 and CD86 in distinct cDC1 subsets in the lung-draining mLN was analyzed by flow cytometry. Shown are representative

histogram plots and quantification for 12 mice/group, from two independent experiments. FMO: fluorescence minus one.

Interestingly, migratory cDC1s in the lung-draining mLN expressed higher surface CD40 protein than cDC1s from the spleen or the lung (Figure 123), highlighting their privileged ability to prime tumor-specific T cells in this anatomical compartment, since CD40 expression specifically by cDC1s is required for their licensing, priming of tumor-specific T cells and subsequent rejection of transplanted immunogenic tumors[78,79].

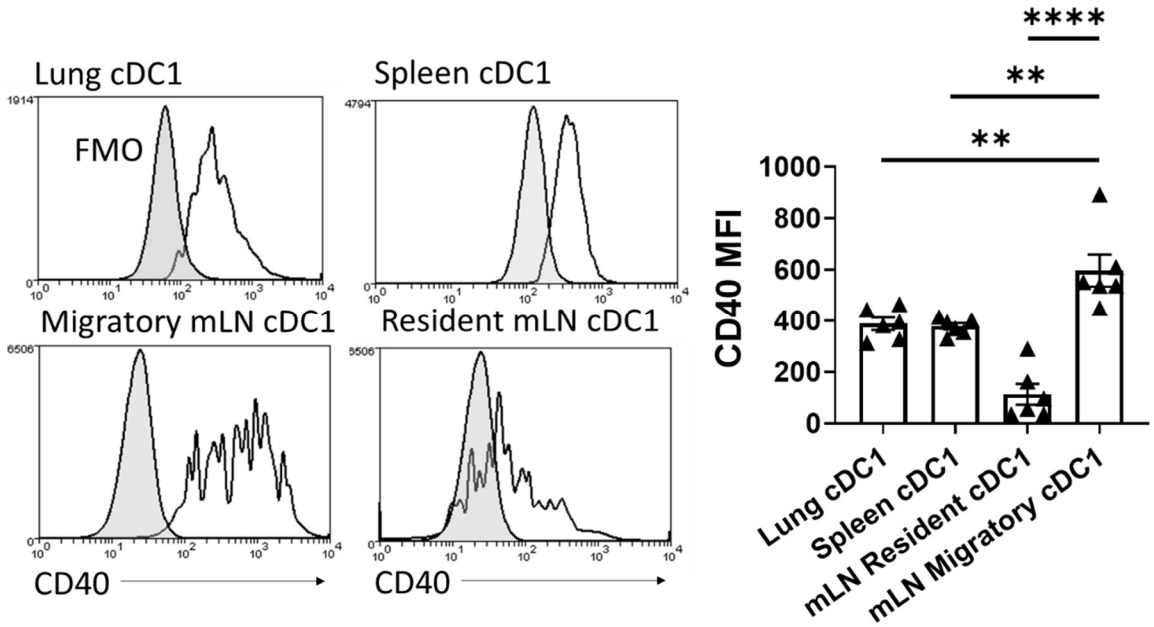

Figure 123. Mice were treated as in Figure 121. At day 20, CD40 expression in cDC1s from distinct anatomical compartments was measured. Shown are representative histogram plots and quantification for *n* = 6 mice/group, from one experiment. FMO: fluorescence minus one.

Then, to test our hypothesis, we measured ZsGreen expression in mLN migratory cDC1s from mice bearing B16-F10-ZsGreen lung tumors and treated or not with BCG. Flow cytometry analysis revealed that BCG treatment increased both the fraction of migratory cDC1s carrying tumor-associated material and the MFI of ZsGreen in these cells (Figure 124). Interestingly, NK cell depletion from days 5 to 20 reverted the increased ZsGreen fluorescence observed in migratory cDC1s, suggesting that they were responsible for this effect (Figure 124).

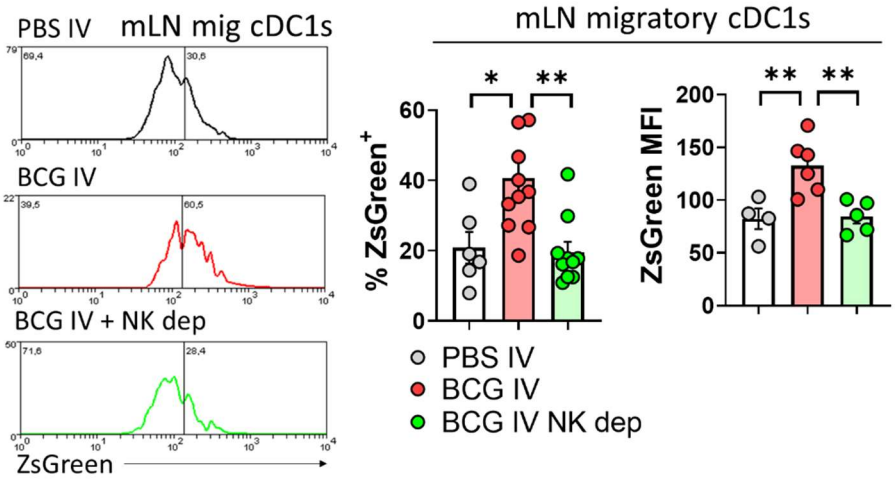

Figure 124. Mice were inoculated intravenously with ZsGreen expressing B16-F10 tumor cells and treated with PBS or BCG at day 7. A group received antiNK1.1 depleting antibodies from day 5 to 20. At day 20, lung-draining mLNs were processed and analyzed by flow cytometry. Shown are representative plots of ZsGreen expression in migratory cDC1s and quantification for *n* = 6-10 mice/group, from 2 independent experiments.

We thought that increased ZsGreen positivity in mLN cDC1s from mice undergoing treatment could be either due to enhanced killing of tumor cells by NK cells and subsequent phagocytosis of tumor cell-derived debris, or to enhanced migration of loaded cDC1s to the mLN, since inflammatory conditions trigger DC maturation and migration.

In an attempt to address this question, we also evaluated ZsGreen expression by cDC1s in the tumor-bearing lungs. Flow cytometry analysis revealed that cDC1s in the tumor-bearing lung displayed enhanced loading with fluorescent tumor-associated material in mice undergoing BCG treatment, again in a NK-cell dependent manner (Figure 125), showing that cDC1s from treated mice already contain more tumor-associated material in the lungs before migrating to the draining lymph nodes.

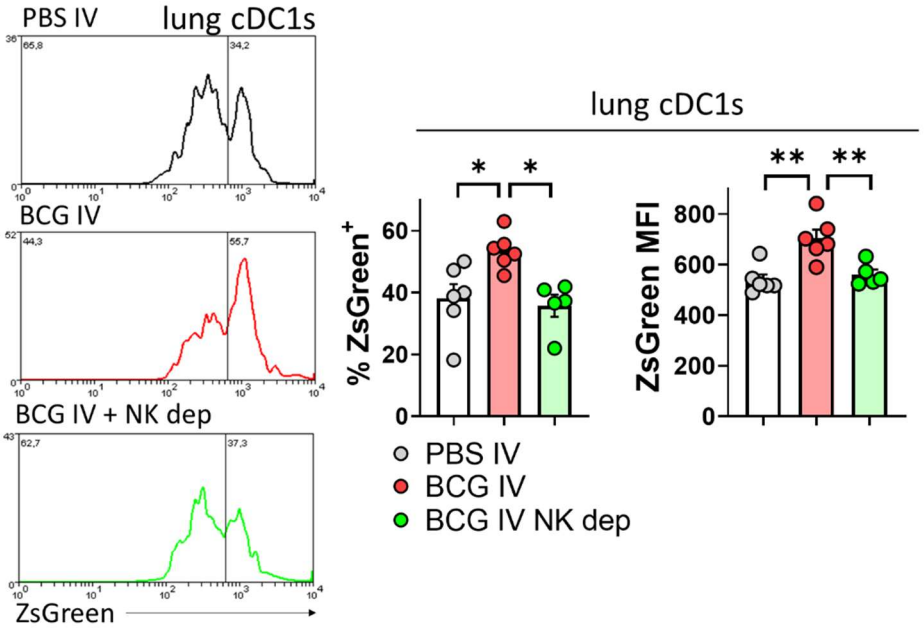

Figure 125. Mice were treated as in Figure 124. At day 20, lungs were processed and analyzed by flow cytometry. Shown are representative plots of ZsGreen expression in cDC1s and quantification for *n* = 6 mice/group, from one experiment.

Considering our results, we wondered whether the enhanced loading of cDC1s with tumor-associated material observed in ivBCG mice was linked to NK cell cytotoxic activity. To test this, we grew B16-F10-ZsGreen tumors in mice lacking perforin and measured ZsGreen expression in mLN migratoy cDC1s. Our data revealed that ivBCG did not increase the amount of fluorescent tumor-associated material carried by cDC1s in the lung-draining mLN in the absence of host perforin expression (Figure 126). This result suggested that immune cell perforin-mediated cytotoxicity towards tumor cells is needed for the enhanced loading of cDC1s with tumor-associated material.

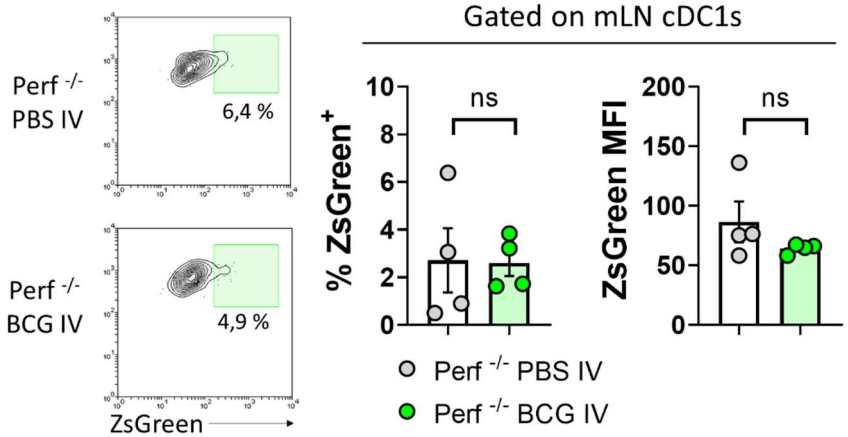

Figure 126. Perforin deficient mice were treated as in Figure 124. At day 20, lung-draining mLNs

were processed and analyzed by flow cytometry. Shown are representative contour plots of ZsGreen expression in cDC1s and quantification for *n* = 4 mice/group, from one experiment.

Next, we tried to corroborate *in vivo* that ivBCG was inducing tumor cell death via stimulation of NK cells. We took advantage of B16-F10-ZsGreen cells and identified them in the lungs by flow cytometry based on ZsGreen expression and lack of CD45 (Figure 127).

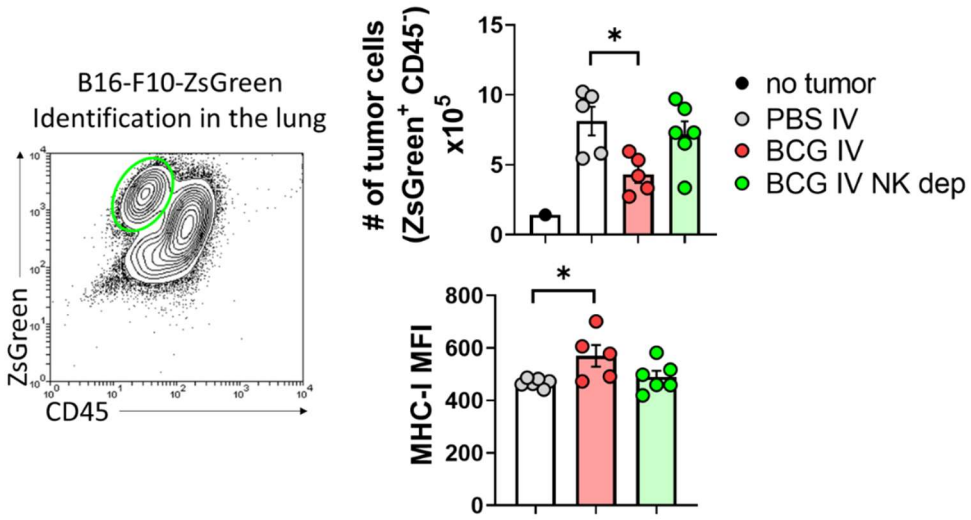

Figure 127. Mice were treated as in Figure 124. At day 20, lungs were processed for flow cytometry analysis. Shown is a representative contour plot for ZsGreen$^+$ tumor cell identification in the lungs, and quantification of absolute numbers of tumor cells and of MHC-I expression by these cells. *n* = 5-6 mice/group, from one experiment.

Flow cytometry analysis revealed that ivBCG significantly reduced the total number of ZsGreen$^+$ tumor cells in the lungs compared to untreated mice, meaning that BCG treatment effectively reduced tumor burden at day 20. Although differences did not reach statistical significance, there was a trend for increased tumor burden in NK-depleted mice treated with BCG (Figure 127). Interestingly, BCG treatment upregulated MHC-I expression on tumor cells at day 20 (Figure 127), which could make them more amenable to targeting by CD8$^+$ T cells at a timepoint in which NK cells start to be less crucial than in early stages of tumor growth. NK cells did not seem to play a clear role in tumor cell MHC-I upregulation. (Figure 127).

Then, we also analyzed cleaved-caspase expression 3 in ZsGreen$^+$ CD45$^-$ tumor cells, finding that BCG treatment moderately increased the percentage of tumor cells staining positive for active caspase-3 (Figure 128), a marker of apoptotic cell death. NK cell

depletion reverted this phenomenon, implicating BCG-stimulated NK cells in tumor cell death to provide tumor-associated material to cDC1s.

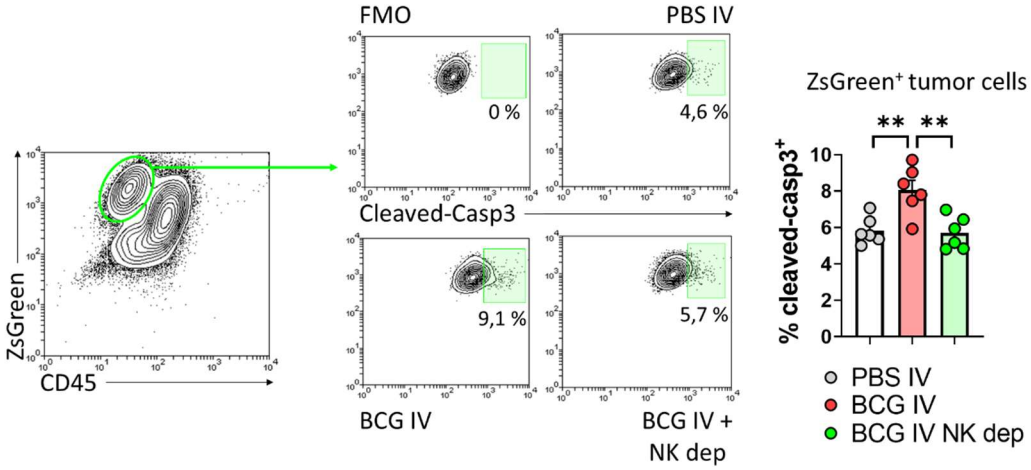

Figure 128. Mice were treated as in Figure 124. Shown are representative contour plots and quantification of cleaved-caspase 3 expression by ZsGreen⁺ tumor cells. *n* = 6 mice/group, from one experiment.

The crosstalk between NK cells and cDC1s in the TME is not limited to CCL5 or XCL1-mediated recruitment of cDC1s to the tumor bed, as NK cells can also influence the maturation status and functionality of cDC1s by secreting cytokines such as IFN-γ, FLT3LG or GM-CSF[507]. To determine whether BCG-stimulated NK cells were affecting cDC1 function within the tumor, we evaluated IL-12 production by cDC1s in B16-F10 tumor-bearing mice undergoing NK cell depletion. We found that NK cell depletion abrogated increased IL-12 production by cDC1s in mice receiving BCG treatment, therefore also implicating NK cells in the modulation of cDC1 functionality in the tumor (Figure 129).

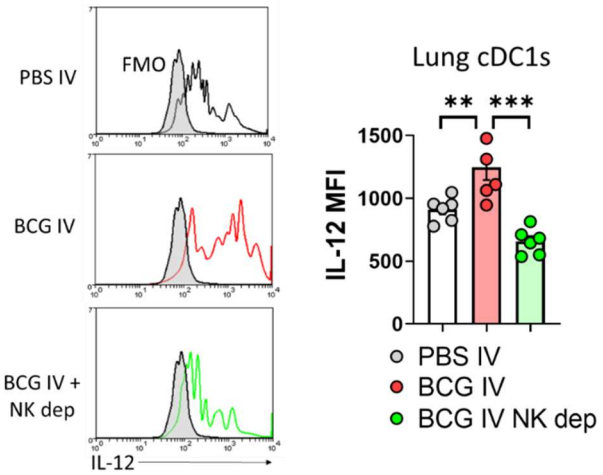

Figure 129. Mice were treated as in Figure 124. At day 20, lungs were processed, and single cell suspensions were stimulated ex vivo for analysis of IL-12 expression. Shown are representative plots and quantification of IL-12 expression by lung cDC1s. *n* = 6 mice/group, from one experiment.

Altogether, these results allowed us to further explain the mechanism by which ivBCG improves tumor-specific adaptive immune responses against tumors growing in the lung. We show that NK cell perforin-mediated cytotoxicity, critically stimulated by BCG treatment, provokes initial tumor cell death and provides tumor cell debris to cDC1s. Additionally, NK cells recruit cDC1s to the tumor-bearing lung by a CCL5-dependent mechanism and contribute to IL-12 secretion by these cells, further stimulating adaptive immunity. Consequently, ivBCG increases the amount of cDC1s bearing tumor-associated material in the lung-draining mLN, conceivably promoting antigen cross-presentation and improving tumor-specific T cell responses, which would then travel to the tumor and take the relay from NK cells.

5.10 An early role for lung $CD4^+$ and $CD8^+$ T cells in stimulating NK cell function

Next, we wanted to study the mechanism by which ivBCG enhances NK cell function in the tumor-bearing lung. Specifically, our first question to answer was whether BCG directly activates NK cells, which can indeed sense virus and bacteria via TLR or other PRRs[508], or whether it is an immune cell-dependent mechanism.

Since IFN-γ is a key cytokine in the orchestration of innate and adaptive immune responses[509], we first tested whether NK cells were normally activated in lung tumors from mice lacking this molecule. Flow cytometry analysis of the lung at day 20 revealed that both NK cell recruitment and activation triggered by ivBCG were completely abrogated in mice lacking IFN-γ (Figure 130B-D). Concurrently, BCG treatment did not enhance gp33-specific $CD8^+$ T cell responses in $IFN\gamma^{-/-}$ mice (Figure 130E). These results evidence that activation of lung NK cells by ivBCG is mediated by a mechanism relying on host IFN-γ expression. This finding was surprising taking into consideration that NK cell activation has been described to rely prominently in other cytokines such as IL-2, IL-18, IL-12, IL-15 or type I IFN.

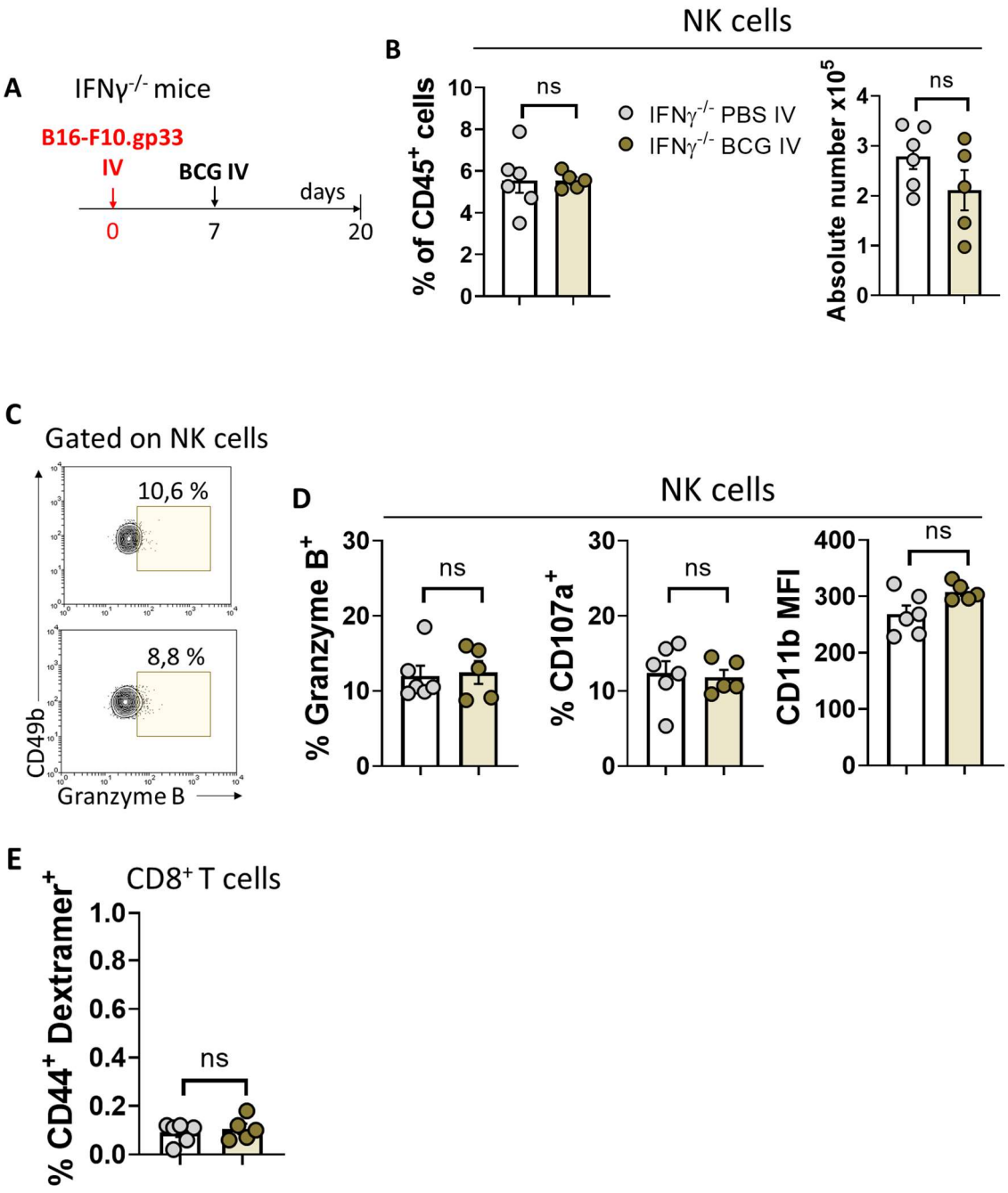

Figure 130. IFN-γ$^{-/-}$ mice were inoculated intravenously with gp33-expressing B16-F10 cells and treated with either IV PBS or BCG at day 7 (A). At day 20, single cell suspensions were generated from the tumor-bearing lungs and analysed by flow cytometry. (B) Quantification of NK cell absolute numbers and proportions in the lung. (C, B) Representative contour plot and expression of Granzyme B, CD107a and CD11b in NK cells. (E) Quantification of gp33-specific CD44$^+$ CD8$^+$ T cells among the total population of CD8$^+$ T cells. *n* = 5-6 mice/group, from one experiment.

The next logical step was to determine the source of IFN-γ for NK cell stimulation. Since BCG is an intracellular (attenuated) bacteria, it is mostly targeted by an adaptive immune response involving IFN-γ secretion, which stimulates the bactericidal activity of

macrophages, where mycobacteria usually reside[510]. Therefore, attenuated mycobacteria such as BCG are known to be potent inducers of IFN-γ secretion mostly by BCG-specific $CD4^+$ but also $CD8^+$ T cells[511].

We wondered whether an initial BCG-specific T cell response in the lung was the responsible of mediating NK cell activation. For this, we separately depleted $CD4^+$ and $CD8^+$ T cells early during ivBCG and until endpoint (days 5 to 20) in B16-F10.gp33 tumor-bearing mice and examined immune responses in the lung at day 20 (Figure 131A). We must consider that depletion eliminated both BCG-specific and tumor-specific T cells, making it impossible to discern their differential contribution in this context.

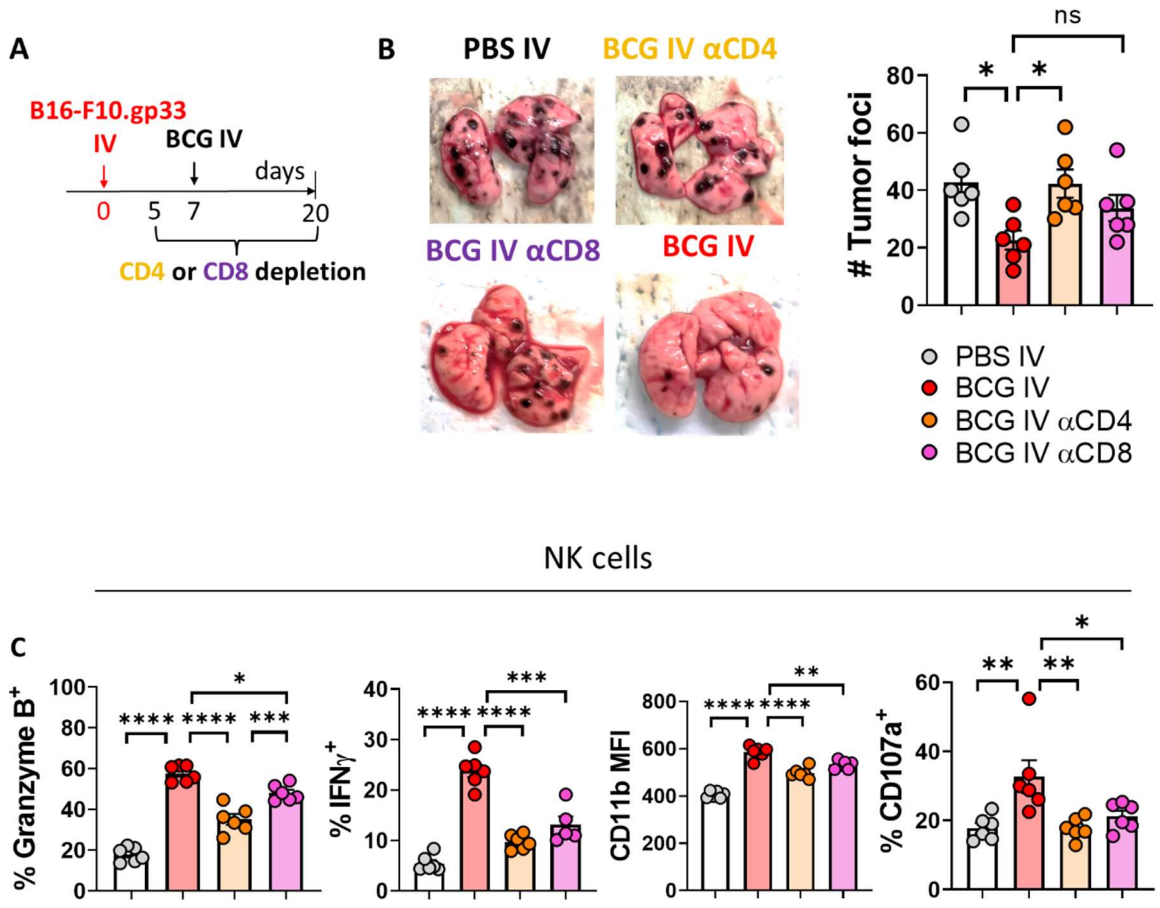

Figure 131. WT mice were treated as shown in (A). At day 20, tumor foci in the lung were counted by visual inspection and representative images are shown (B). Lungs were further processed for flow cytometry analysis. (C) Analysis of different activation markers on lung NK cells. *n* = 6 mice/group, from one experiment.

Visual inspection of lung metastases at day 20 revealed that depletion of $CD4^+$ T cells abrogated the protective effect of ivBCG, whereas early $CD8^+$ T cell depletion showed a

non-significant trend for increased tumor burden compared to non-depleted ivBCG mice, (Figure 131B).

Flow cytometry analysis of lung NK cell phenotype (Granzyme B, IFN-γ, CD107a and CD11b expression) revealed that early depletion of either $CD4^+$ or $CD8^+$ T cells reverted the increased functionality of these cells observed in non-depleted ivBCG mice (Figure 131C), suggesting that T cells are needed for optimal NK cell activation by ivBCG. Interestingly, we previously showed that NK cell depletion also reduced T cell functionality (Figure 111), suggesting an activation feedback loop between NK cells and T cells.

Next, we focused on T cell functionality in the lungs of these mice, to assess whether the absence of the $CD4^+$ T cell subset could affect the activity of $CD8^+$ T cells in the context of ivBCG, or vice versa. Surprisingly, depletion of $CD4^+$ diminished IFN-γ production by $CD8^+$ after αCD3/CD28 restimulation (Figure 132B), and the same phenomenon was observed the other way around: absence of $CD8^+$ T cells reduced IFN-γ expression by $CD4^+$ T cells (Figure 132B). Therefore, our data suggest a positive feedback loop mechanism by which either T cell subset, conceivably in response to BCG treatment, stimulates the functionality of the other T cell subset in a bystander activation fashion. Furthermore, we show that $CD4^+$ T cells were necessary for the generation of tumor-specific responses, since $CD4^+$ depletion abrogated the generation of gp33-specific $CD8^+$ T cells (Figure 132C). Finally, as another metric of $CD8^+$ function, $CD4^+$ depletion diminished the cytotoxic potential of $CD8^+$ T cells measured as expression of Granzyme B (Figure 132D).

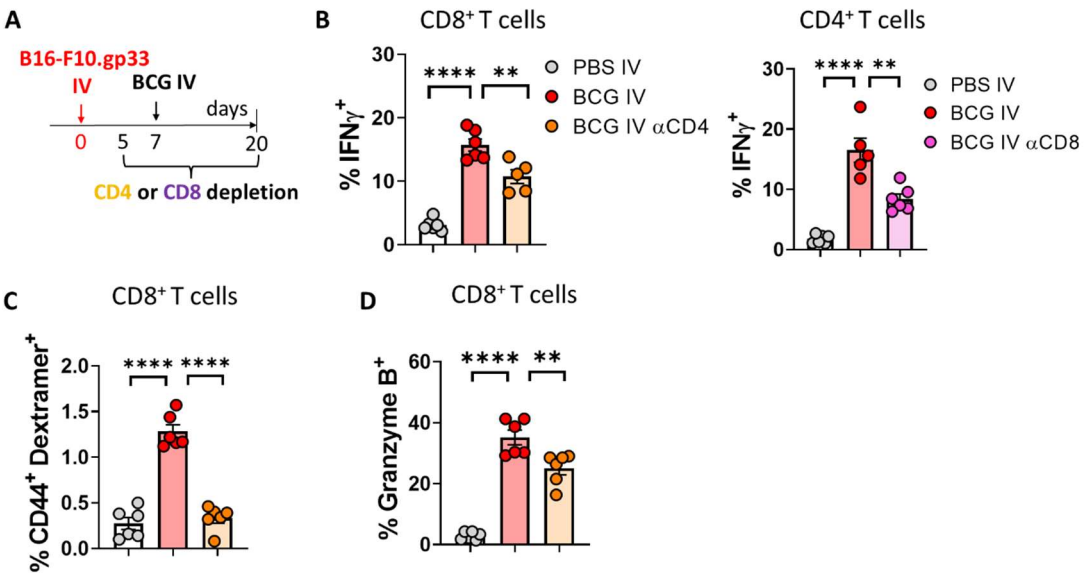

Figure 132. WT mice were treated as in (A). At day 20, lungs were processed for flow cytometry analysis. (B,C) Quantification of IFN-γ expression by T cells following ex vivo restimulation. (C) Quantification of gp33-specific $CD44^+$ $CD8^+$ T cells among the total population of $CD8^+$ T cells. (D) Granzyme B expression by $CD8^+$ T cells. *n* = 6 mice/group, from one experiment.

Finally, we performed an *in vitro* cytotoxicity assay using splenocytes isolated from these mice against B16-F10 cells, and found that both $CD4^+$ and $CD8^+$ depletion abrogated the enhanced tumor-specific cytotoxicity induced by splenocytes isolated from non-depleted ivBCG mice (Figure 133), underscoring the requirement of both T cell subsets for successful antitumor efficacy in this model.

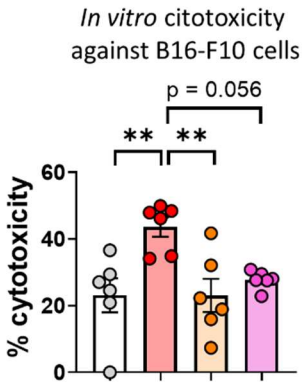

Figure 133. WT mice were treated as Figure 132. At day 20, spleens were processed and splenocytes seeded over luciferase-expressing B16-F10 cells at a 100:1 ratio. After 20 h, luminescence was analysed and % cytotoxicity calculated in reference to control wells cultured without effector cells. *n* = 6 mice/group, from one experiment

As we pointed out before, our $CD4^+$ and $CD8^+$ T cell depletion experiments did not allow us to discern the contribution of BCG-specific T cells versus tumor-specific T cells to the stimulation of NK cell activity. To test this, we used $Batf3^{-/-}$ mice (Figure 134A), which cannot mount tumor-specific responses due to lack of cross-presenting cDC1s. We first wondered whether lung T cells from $Batf3^{-/-}$ mice could respond to ivBCG, and found that BCG administration in these mice still stimulated IFN-γ secretion by both T cell subsets although to a lesser extent than on WT mice, especially for $CD8^+$ T cells (Figure 134B). This finding suggests that the immune response to BCG relies only partially on Batf3-dependent cDC1s. To confirm that the BCG-specific T cell response is still present in $Batf3^{-/-}$ mice, we isolated the splenocytes from these mice and stimulated them *in vitro* with protein purified derivative (PPD, or also called tuberculin, which contains mycobacterial proteins). As can be observed in Figure 134C, the BCG-specific response, measured as

IFN-γ secretion following 72 h of incubation with PPD, was equally present in WT and Batf3$^{-/-}$ mice treated with ivBCG.

Therefore, we had a model in which tumor-specific responses are abrogated but BCG-specific responses are still partially present. In this context, we evaluated NK cell activation status in the lung and found that their functionality was still enhanced by ivBCG in Batf3$^{-/-}$ mice (Figure 134C).

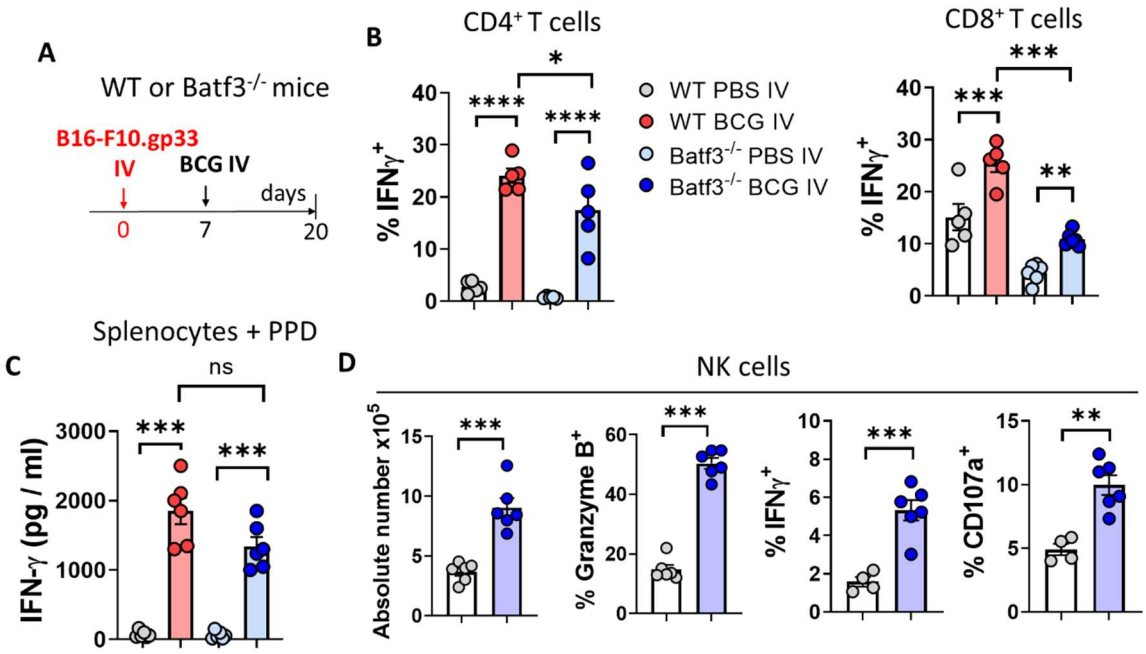

Figure 134. WT or Batf3$^{-/-}$ were treated as shown in (A). (B) At day 20, lung single cell suspensions were stimulated *ex vivo* with antiCD3/CD28 and IFN-γ expression in T cells was analyzed by flow cytometry. (C) At day 20, spleen single cell suspensions were stimulated *ex vivo* for 72 h with PPD and IFN-γ was analyzed by ELISA in the supernatant. (D) NK cells were analyzed only in Batf3$^{-/-}$ mice. *n* = 6 mice/group, from one experiment.

Furthermore, to functionally test NK cell antitumor activity in the absence of cDC1s, we challenged Batf3$^{-/-}$ mice intravenously with MHC-I deficient B16-F10 tumor cells, which are susceptible to NK cells but avoid CD8^{+} T cell recognition. BCG treatment in this scenario extended mice survival (Figure 135), further suggesting that NK cell tumoricidal activity is still present in mice lacking cDC1s.

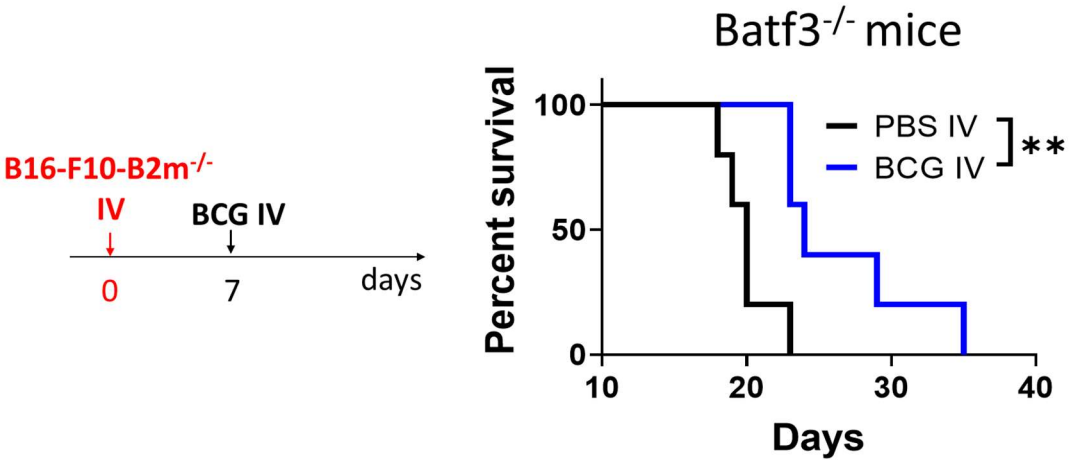

Figure 135. Survival of Batf3$^{-/-}$ mice bearing B16-F10-B2m$^{-/-}$ tumors in the lung and treated or not with BCG IV. *n* = 6 mice/group, from one experiment.

Collectively, our data indicates that neither cDC1s nor tumor-specific T cell responses are required for the stimulation of NK cells by ivBCG. Therefore, since T cells were still stimulated by ivBCG in Batf3$^{-/-}$ mice, we hypothesize that BCG-specific T cells are responsible for the stimulation of NK cell antitumor activity in the lungs, although further research is needed to validate these results.

5.11 Systemic BCG remodels the lung myeloid cell compartment

The literature shows that intranasal administration of BCG alters the phenotype of lung myeloid cells[264,512]. Furthermore, as already pointed out before, ivBCG reprograms BM hematopoiesis in mice, enhancing myelopoiesis at the cost of lymphopoiesis and inducing the generation of macrophages with a "trained" immune-stimulatory phenotype, which protected mice against *M. tuberculosis* infection[260]. There is ample literature describing modulation of macrophage activity by BCG, especially in the context of tuberculosis. In the field of tumor immunology, going back to 1973, it was hypothesized that BCG antitumor effects might be explained by the enhancement of the tumoricidal and phagocytic activity of macrophages[513]. Thus, considering the well-known influence of myeloid cells in tumor progression and modulation of immune responses[178], we set out to evaluate the effect of ivBCG on the lung myeloid cell compartment of B16-F10 tumor bearing mice (Figure 136).

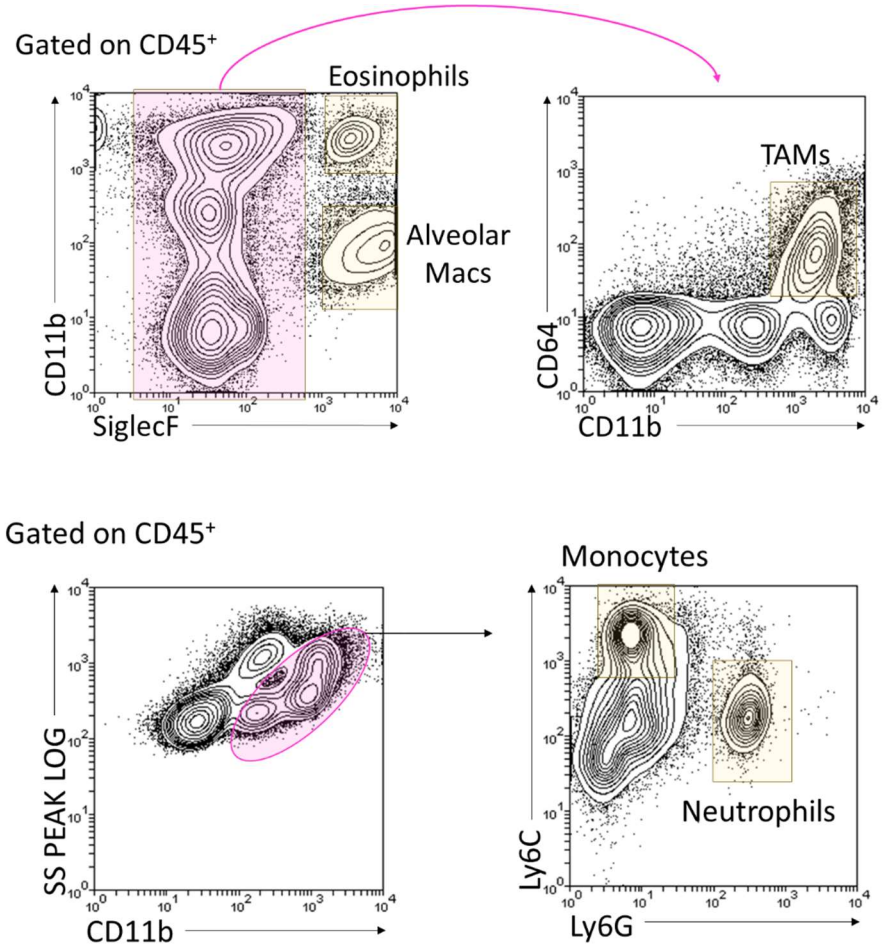

Figure 136. Flow cytometry analysis of the myeloid compartment of tumor bearing lungs at day 20 after challenge. Shown are representative contour plots for the dentification of different myeloid cell subsets.

Flow cytometry analysis of the lungs at day 20 revealed that ivBCG increased the number of tumor-associated macrophages (TAMs; $CD11b^{+}CD64^{+}$) and monocytes ($CD11b^{+}Ly6C^{+}Ly6G^{-}$) and decreased eosinophils ($CD11b^{+}$ $SiglecF^{+}$) and resident alveolar macrophages (AMs; $CD11b^{int}$ $SiglecF^{+}$), with no changes in neutrophil numbers ($CD11b^{+}$ $Ly6G^{+}Ly6C^{med}$) (Figure 137A). These findings were replicated when looking at cell population percentages among total $CD45^{+}$ immune cells (Figure 137B).

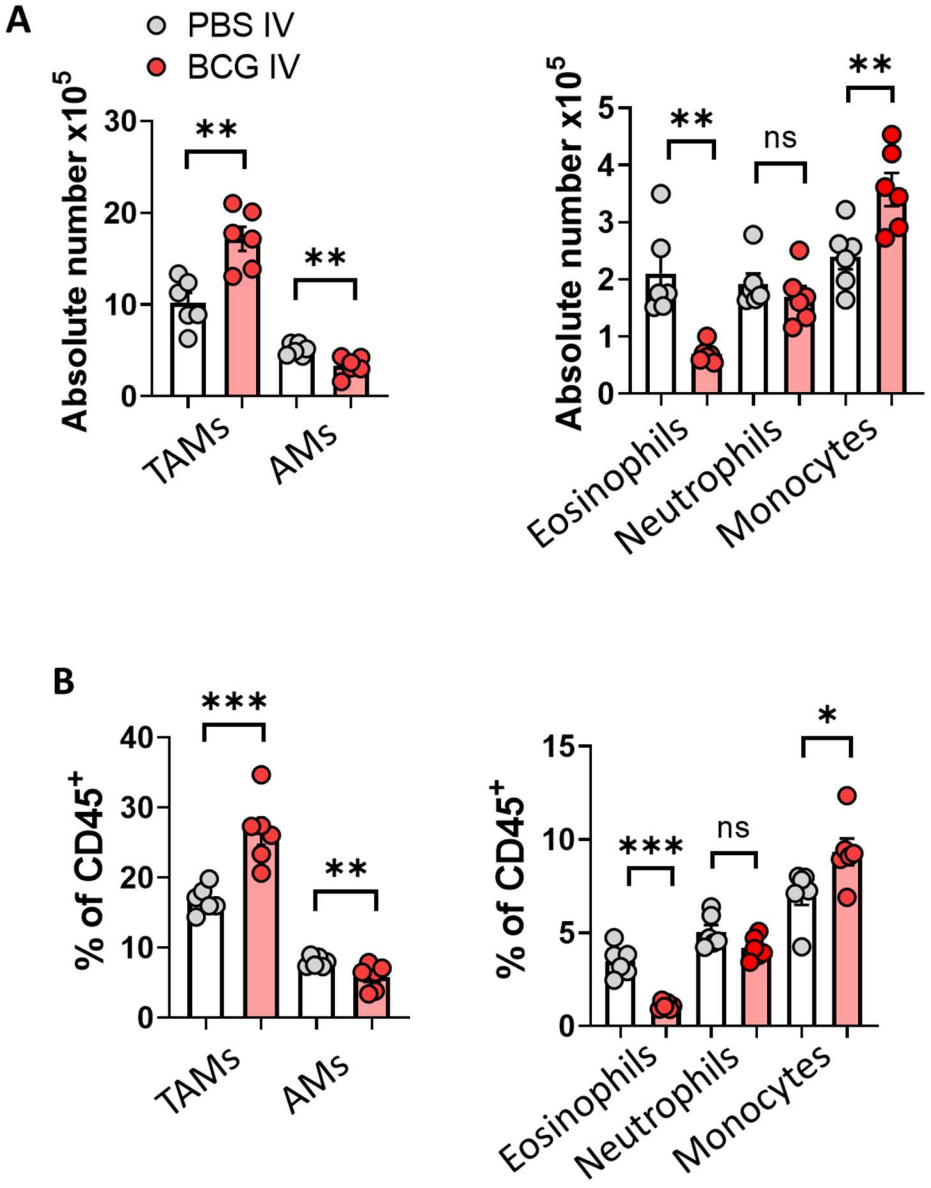

Figure 137. WT mice were inoculated with B16-F10 intravenously and treated or not with BCG IV at day 7. At day 20, lung single cell suspensions were analyzed by flow cytometry. Absolute numbers of different myeloid populations in the tumor-bearing lungs (A) or proportions among total CD45$^+$ immune cells (B). *n* = 6 mice/group, from one experiment.

Of note, the ability of BCG to reduce lung eosinophil numbers was specifically dependent on NK cells and CD4$^+$ T cells, as depletion of these cellular subsets partially abrogated the eosinophil reduction observed in non-depleted ivBCG mice (Figure 138A). Recruitment of macrophages followed a similar trend, as NK cell and CD4$^+$ T cell depletion (but not CD8$^+$) diminished macrophage numbers in the lungs of BCG-treated mice (Figure 138B).

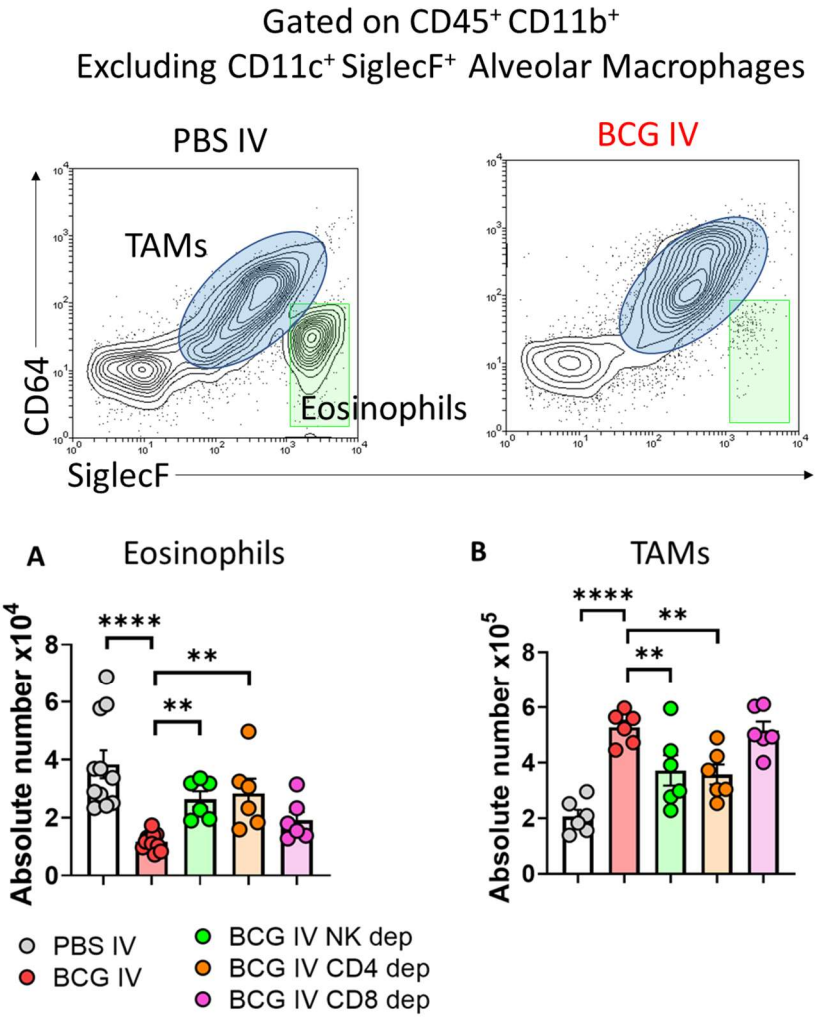

Figure 138. Representative contour plots and quantification of absolute numbers of eosinophils and TAMs by flow cytometry in different groups of mice bearing B16-F10 lung tumors. *n* = 6 mice/group, from one experiment.

We were intrigued by the increase in the CD11b$^+$ CD64$^+$ TAM population, which most likely encompasses a continuum from recruited monocytes to differentiated TAMs, as well as TAMs originating from resident interstitial populations, something which has been described for TC-1 and LLC lung tumors in mice[514]. Since we did not have the tools to study the developmental origin of TAMs in response to BCG treatment, we instead focused on analysing their phenotype, and found that ivBCG dramatically shifted TAMs away from a "M2-like" immune-suppressive phenotype (CD206$^+$ CD86$^-$) into a "M1-like" antitumoral phenotype (CD206$^-$ CD86$^+$) (Fig 139). This shift in macrophage phenotype could be mediating the increased NK and T-cell function observed in these mice, since alveolar macrophages and "M2-like" TAMs inhibit adaptive immunity and support tumor growth and spreading[482,515–517].

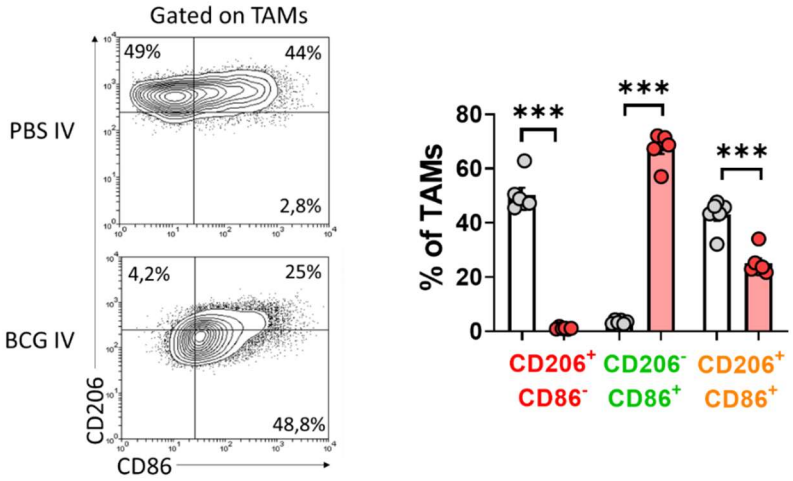

Figure 139. Mice were treated as in Figure 137. Expression of CD86 and CD206 was analysed in the CD11b$^+$ CD64$^+$ TAM population. *n* = 6 mice/group, from one experiment.

Next, we wondered which cells were responsible for ivBCG effect on TAMs. NK cell depletion during BCG treatment partially but not totally reverted the shift in macrophage phenotype (Figure 140), which indicates that BCG-activated NK cells can modulate TAM function in lung tumors but are not the solely responsible.

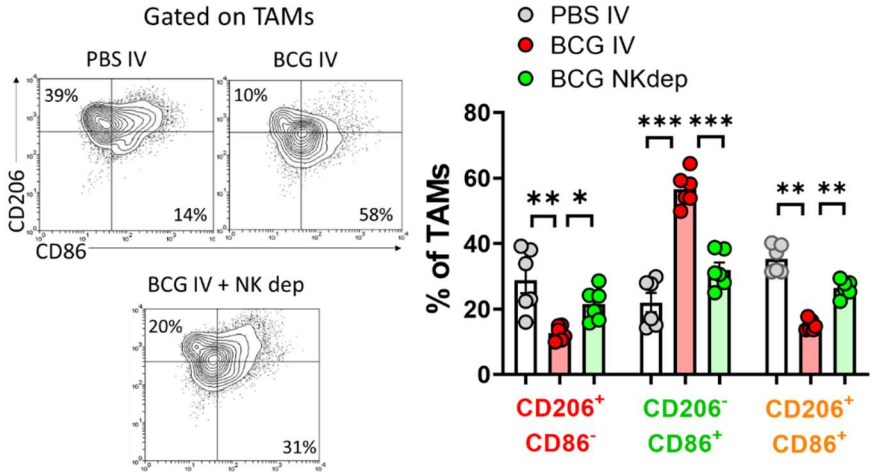

Figure 140. Expression of CD86 and CD206 was analyzed in the CD11b$^+$ CD64$^+$ TAM population of different groups of mice bearing B16-F10 lung tumors. *n* = 6 mice/group, from one experiment.

In a similar manner, CD4$^+$ and CD8$^+$ depletion in tumor-bearing mice revealed that T cells were also responsible of modulating macrophage phenotype in this context. Concretely, in mice lacking CD8$^+$ T cells and specially CD4$^+$ T cells, BCG treatment no longer shifted macrophage phenotype into an immune-stimulatory profile (Figure 141).

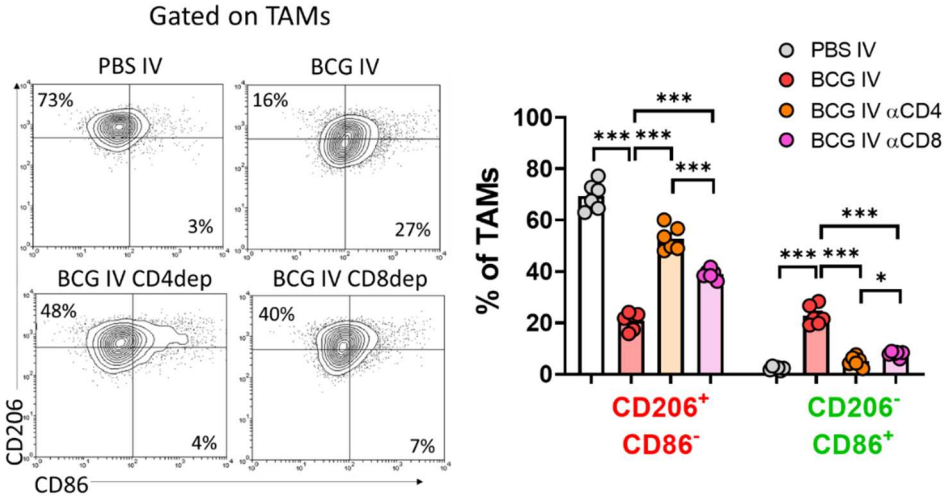

Figure 141. Expression of CD86 and CD206 was analyzed in the CD11b$^+$ CD64$^+$ TAM population of different groups of mice bearing B16-F10 lung tumors. *n* = 6 mice/group, from one experiment.

Use of Batf3$^{-/-}$ mice revealed that neither cDC1s nor tumor-specific T cells were influencing TAM phenotype, whereas lack of host IFN-γ completely abrogated BCG effect on TAM phenotype (Figure 142). Therefore, our data suggests that a coordinated mechanism involving NK cells, both T cell subtypes and IFN-γ drives TAM phenotype shift in our model. Most importantly, our results show that BCG bacilli by themselves are not capable of modulate TAM phenotype, but that this event is driven by the immune system. Most likely, this could be due to the fact that the observed effects rely on coordinated TLR (or other PRR)-mediated sensing of BCG and IFN-γ signalling in the macrophage.

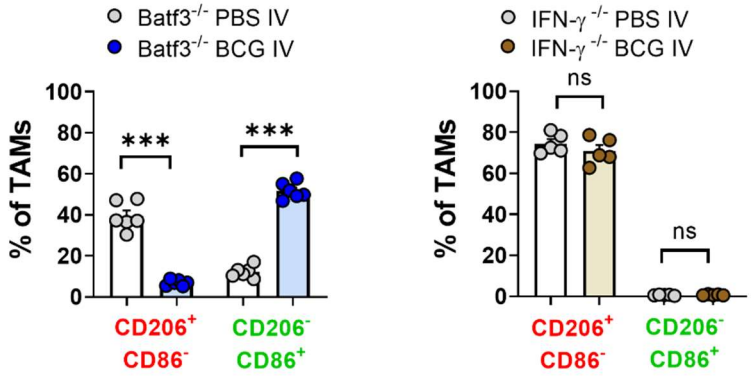

Figure 142. Expression of CD86 and CD206 was analysed in the CD11b$^+$ CD64$^+$ TAM population of different groups of mice bearing B16-F10 lung tumors. *n* = 5-6 mice/group, from one experiment.

Systemic BCG also increased the fraction of TAMs expressing iNOS (Fig 143A) and increased the percentage of MHCII$^+$ macrophages (Fig 143B), both markers of M1-like macrophages, again in an IFN-γ dependent manner (Figure 143C). Of note, enhanced iNOS

and decreased CD206 expression by TAMs is noted in regressing tumors from mice treated with antiPD-1/antiCTLA4 checkpoint blockade[410].

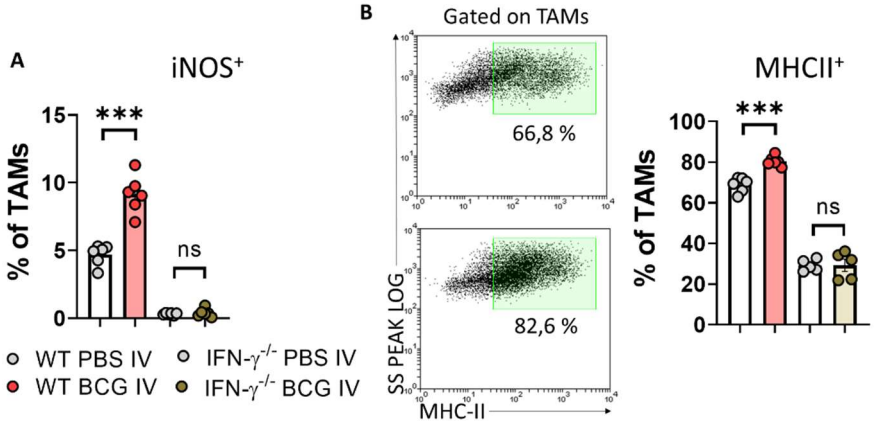

Figure 143. Representative dot plots and quantification of iNOS and MHC-II expression by TAMs in different groups of mice bearing B16-F10 lung tumors. *n* = 6 mice/group, from one experiment.

Next, we hypothesized that the strong immune response in the lung elicited by ivBCG could also be upregulating immunoregulatory mechanisms such as the PD-1/PD-L1 axis, which normally functions to limit autoimmunity but in cancer restrains the antitumor immune response. First, we evaluated PD-L1 expression in distinct lung cell compartments of tumor-bearing mice treated or not with ivBCG (Figure 144)

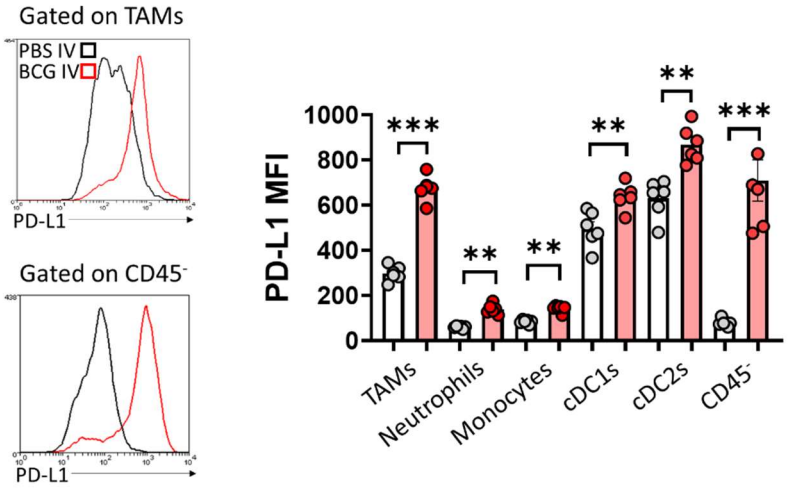

Figure 144. Representative histograms and quantification of PD-L1 expression by different cellular subsets in the lungs of mice bearing B16-F10 tumors. *n* = 6 mice/group, from one experiment.

Our data revealed a widespread BCG-induced increase in the expression of surface PD-L1 on different lung cellular subsets (Fig 144). On tumor-bearing untreated mice, PD-L1 was mostly expressed by DCs. However, upon BCG treatment, PD-L1 was significantly

upregulated in TAMs, neutrophils, monocytes and both DC subsets. Interestingly, PD-L1 was massively upregulated in the $CD45^-$ cell fraction (Figure 144), a heterogeneous population which probably comprises tumor cells, epithelial cell and fibroblasts, although we did not thoroughly characterize its composition.

Using IFN-$\gamma^{-/-}$ mice bearing B16-F10 tumors we observed that this phenotype was completely dependent on IFN-γ expression by the host (Fig 145), suggesting that PD-L1 upregulation on the lung is a consequence of the BCG-triggered inflammatory response.

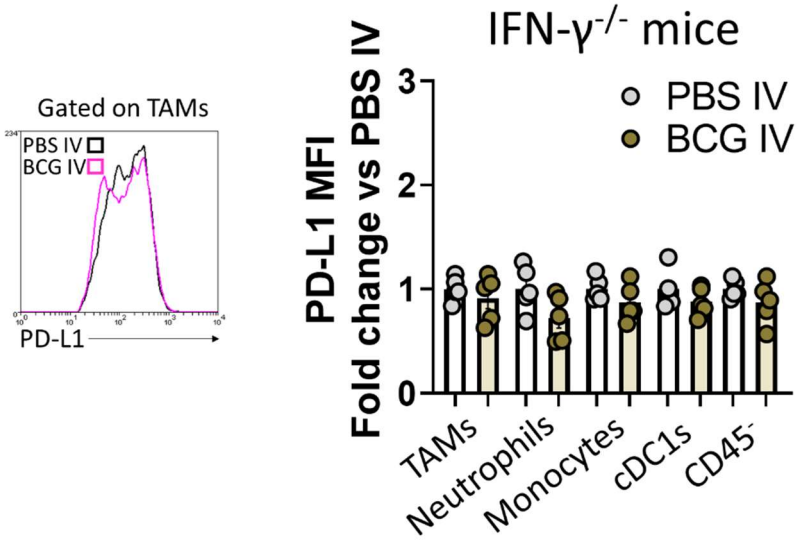

Figure 145. Representative histograms and quantification of PD-L1 expression by different cellular subsets in the lungs of IFN-$\gamma^{-/-}$ mice bearing B16-F10 tumors. *n* = 5-6 mice/group, from one experiment.

Not only was PD-L1 upregulated in the lung TME, but we also observed enhanced PD-L1 expression on DCs from the mLNs of tumor-bearing mice treated with ivBCG (Figure 146), Section 2.6). Therefore, the generation of adaptive immune responses could also be hindered by PD-L1 expression in the mLN.

In vivo depletion experiments during BCG treatment course (days 5-20) revealed that the prominent cellular subset responsible for PD-L1 upregulation on TAMs were $CD4^+$ T cells, as their depletion in BCG-treated mice almost completely diminished PD-L1 expression levels to that of PBS control mice (Figure 146). However, although to a lesser extent, $CD8^+$ and NK depletion in BCG-treated mice also partially reverted PD-L1 upregulation in TAMs (Figure 146).

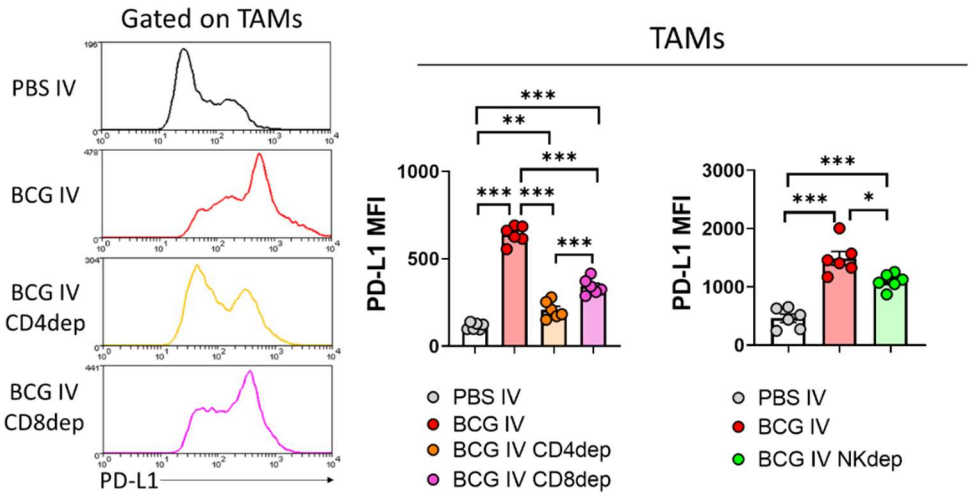

Figure 146. Representative histograms and quantification of PD-L1 expression by TAMs in the lungs of different groups of mice bearing B16-F10 tumors. *n* = 6 mice/group, from one experiment.

A similar pattern was observed when PD-L1 was analyzed on lung cDC1s (Figure 147).

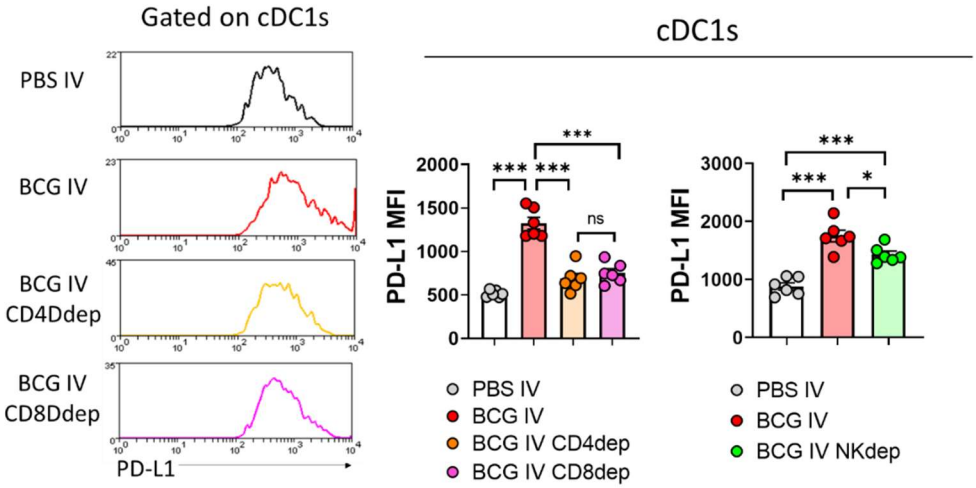

Figure 147. Representative histograms and quantification of PD-L1 expression by cDC1s in the lungs of different groups of mice bearing B16-F10 tumors. *n* = 6 mice/group, from one experiment.

Collectively, these findings made us explore the combination of therapeutic antibodies targeting PD-L1 with ivBCG treatment in mice bearing lung tumors, which we will describe in a separate section.

5.12 Efficacy of intravenous BCG in orthotopic lung tumors

We wanted to extend our findings using the B16-F10 lung metastasis model to a true model of orthotopic lung cancer, so we decided to use intravenous inoculation of Lewis Lung Carcinoma (LLC) cells, a *Kras*^{G12C}/*P53*^{WT} cell line which has been extensively used as a model of *Kras*-mutant NSCLC[453,518]. For the treatment of LLC-tumor bearing mice, we

used a similar experimental schedule as in the B16-F10 model, administrating ivBCG 7 days post tumor-cell inoculation. We first confirmed that at this timepoint LLC tumors were already established in the lungs by histological analysis, and as expected, untreated LLC lung tumors progressively grew when analysed at day 14 and until endpoint (Figure 72 Section 2.3).

First, we found that ivBCG treatment delayed the growth of LLC lung tumors, significantly improving the survival of tumor-bearing mice and delaying the onset of symptoms associated with growing lung tumors. As observed in the B16-F10 model, ivBCG efficacy was also dependent on IFN-γ, perforin and cDC1s, suggesting a similar mechanistic scenario (Figure 148). Moreover, ivBCG was also effective in MHC-I deficient LLC tumor-bearing mice, suggesting that BCG-activated NK cells could also be playing an important role against orthotopic lung tumors (Figure 148).

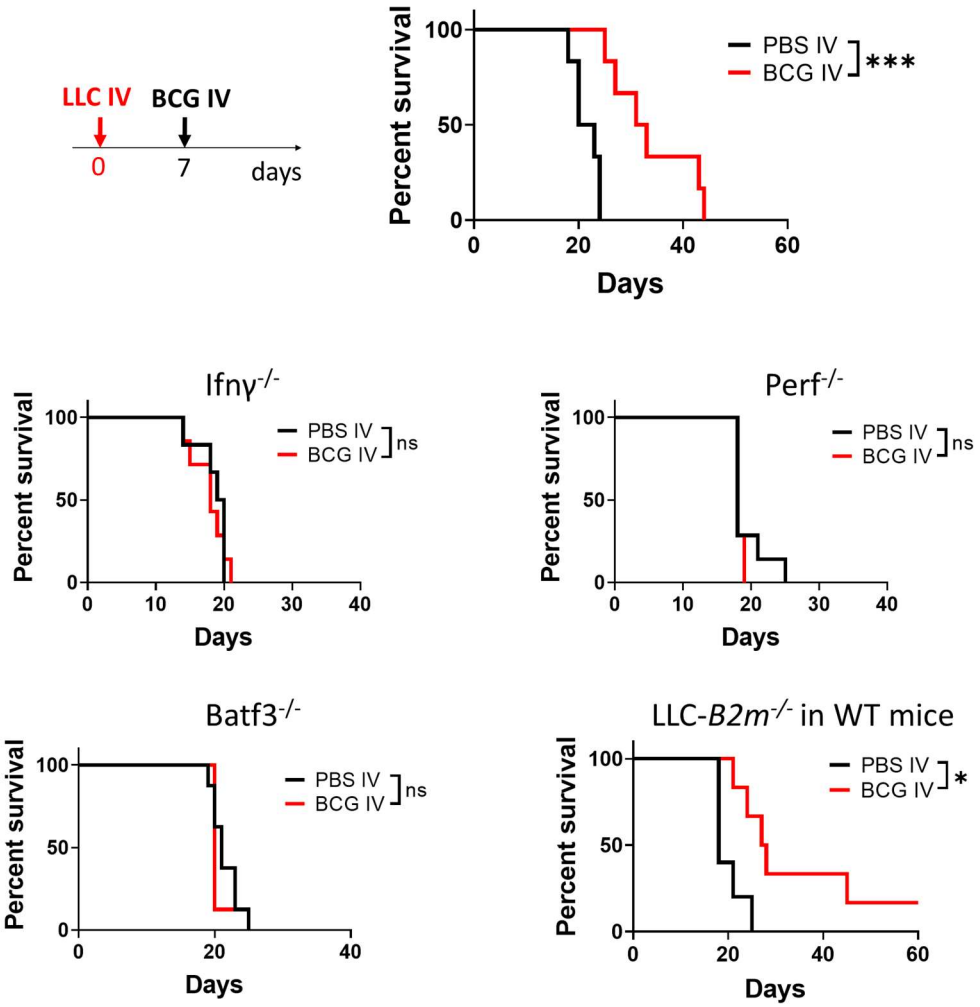

Figure 148. Survival analysis of different mice strains inoculated intravenously with parental or

MHC-I deficient LLC tumor cells and treated with either PBS or BCG at day 7. *n* = 12 mice/group for LLC in WT mice (from two independent experiments) and *n* = 6 mice/group for the rest, from one experiment.

5.13 Combination of intravenous BCG with immune checkpoint blockade extends mouse survival

Considering that BCG treatment induced widespread PD-L1 upregulation in the lung as a consequence of a robust immune response (Section 2.10), we hypothesized that blocking the PD-L1/PD-1 axis could further improve ivBCG given as a monotherapy. We chose to start treatment with PD-L1 blocking antibodies at day 17, around the time PD-L1 upregulation started to be apparent in the lung, and 4 bi-weekly doses of 200 µg were administered, a schedule commonly used in the literature.

First, in the B16-F10 lung metastasis model, addition of αPD-L1 treatment to ivBCG significantly extended mouse survival from a median of 40 days with ivBCG alone to 50 days (Figure 149). Interestingly, αPD-L1 treatment alone did not slow tumor growth in the B16-F10 model compared to control mice, which could be due to the fact that the treatment was started late or to an already described inefficacy of αPD-L1 against tumors growing in the lung[465,506,519].

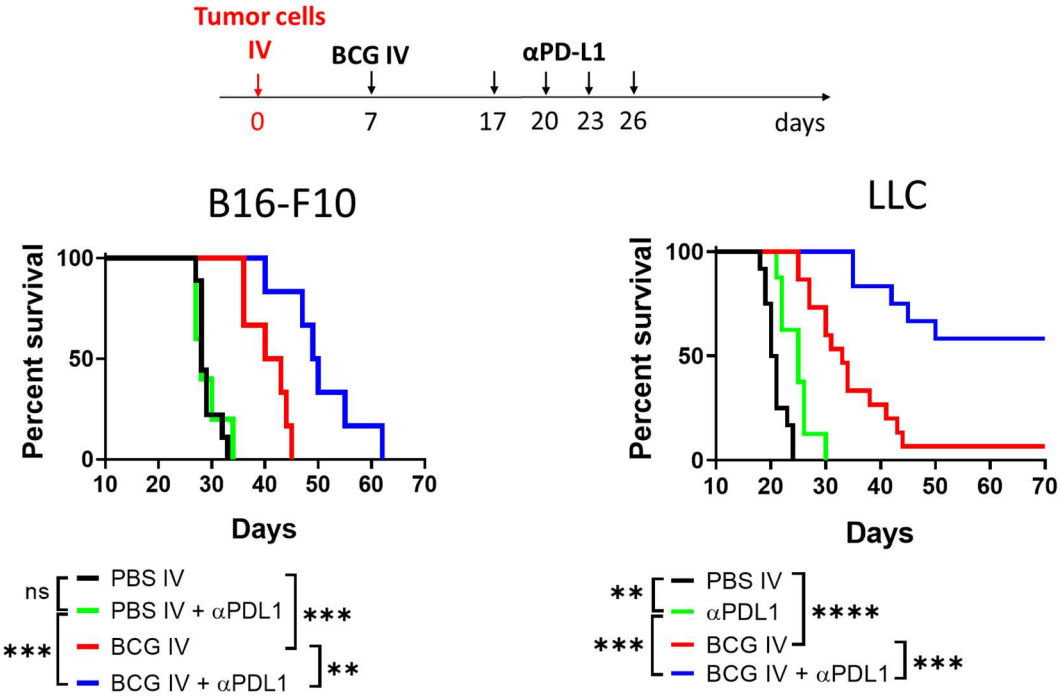

Figure 149. Survival of mice treated as shown in the figure. *n* = 6-9 mice/group for B16-F10, from one experiment, and *n* = 8-15 mice for LLC, from two independent experiments.

Next, we tested this improved therapeutic approach in LLC tumor bearing mice. The ivBCG + αPD-L1 combination displayed a strong antitumoral effect, with more than 50 % (7/12) of the mice surviving at the end of the follow-up (90 days). As expected, BCG treatment alone extended mice survival from a median of 20 days in the control group to 34 days, but to a much lesser extent than the treatment combination. In this model, αPD-L1 administration could slow tumor growth, although minimally (Figure 149). Of note, we confirmed that mice surviving at the end of the follow-up were apparently tumor-free by visual inspection and histological analysis, in stark contrast with control-treated mice at endpoint (Figure 150).

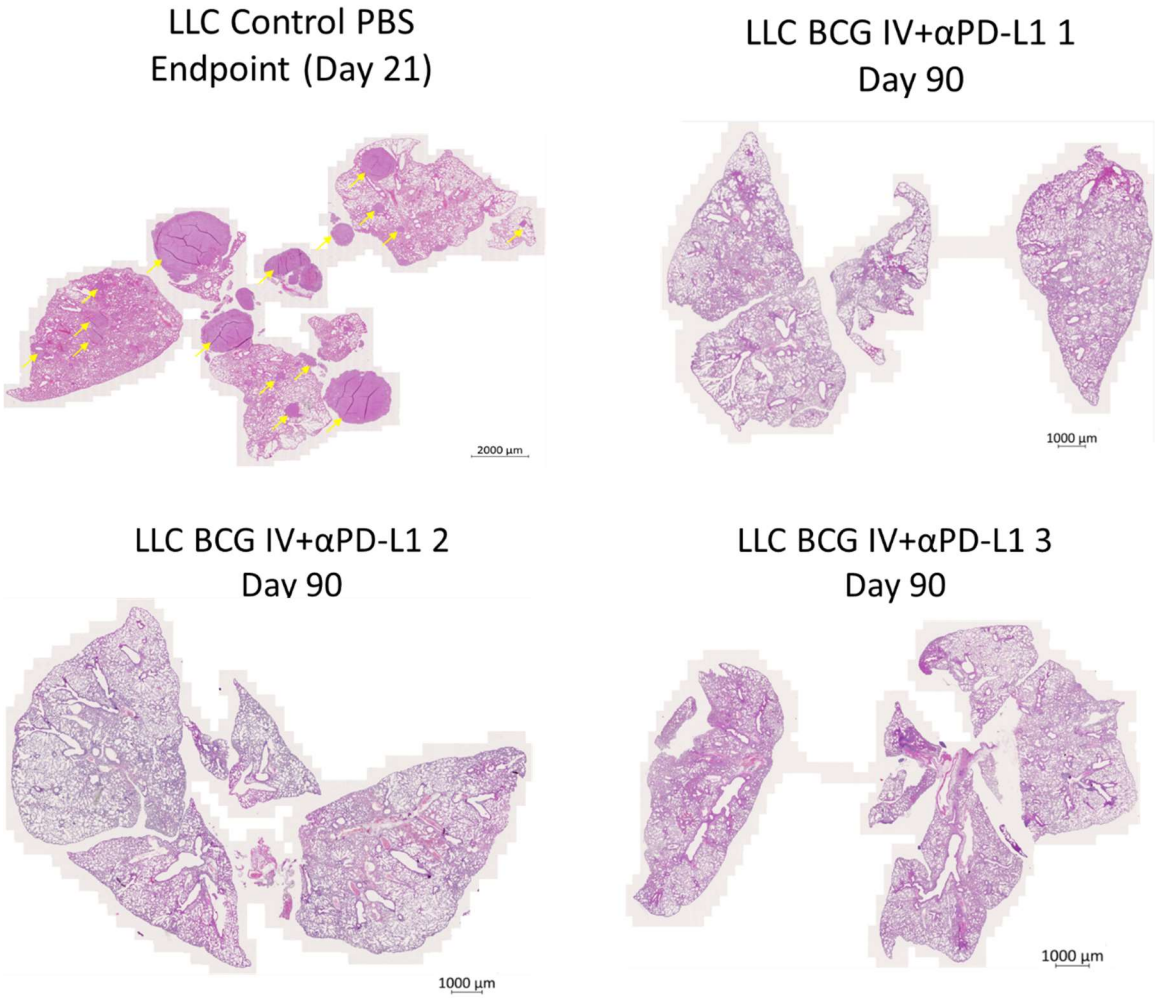

Figure 150. H&E staining of lungs from a representative LLC tumor-bearing mice at endpoint and three representative LLC survivors following combination therapy at day 90 post tumor cell inoculation (representative of *n* = 6 survivor mice). Yellow arrows indicate tumor nodules.

In the last sections we showed that ivBCG induced a tumor-specific immune response against B16-F10 cells growing in the lung. A common way to test the generation of tumor-

specific adaptive immune memory is to rechallenge mice which had rejected the primary tumor with the same tumor cell line. In the B16-F10 lung metastasis model, no mice survived the primary challenge, so we could not use this approximation. Taking advantage of the fact that BCG + αPD-L1 combination cured a considerable number of mice bearing LLC lung tumors, we rechallenged survivors subcutaneously with a high dose (10^6 cells) of LLC cells in the right flank and non-antigenically related B16-F10 cells in the left flank, to test the generation of immune memory against LLC tumor antigens (Figure 151). B16-F10 tumors grew normally with the same kinetics in naïve and LLC survivor mice, as expected (Figure 151). However, LLC tumors were rejected by LLC survivors and not by naïve mice (Figure 151). This result suggests that ivBCG + αPD-L1 combination induces a tumor-specific immune response against LLC tumor antigens which is durable in time and functionally capable of responding to a rechallenge in a different localization than the primary tumor, which would prevent tumor relapse.

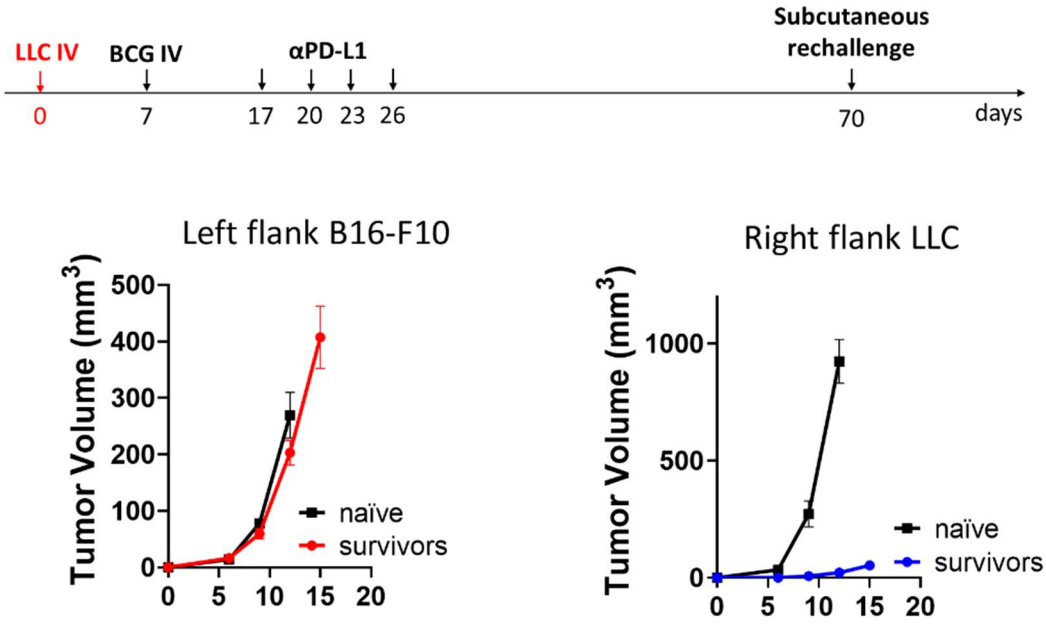

Figure 151. LLC survivor mice were rechallenged with 1x10^6 LLC or B16-F10 tumor cells in contralateral flanks. Tumor growth was followed for 15 days. *n* = 6 mice/group, from one experiment.

Lastly, we also evaluated the efficacy of ivBCG in the KC8.1 lung adenocarcinoma model we had developed. In contrast to B16-F10 and LLC lung tumors, ivBCG was ineffective against KC8.1 tumors, although we found a reduction in the number of extrapulmonary metastases that spontaneously originate in this model in mice receiving treatment (Figure

152). This result suggested that although ivBCG could not slow KC8.1 tumor growth in the lung, it precluded the dissemination of tumor cell to other organs.

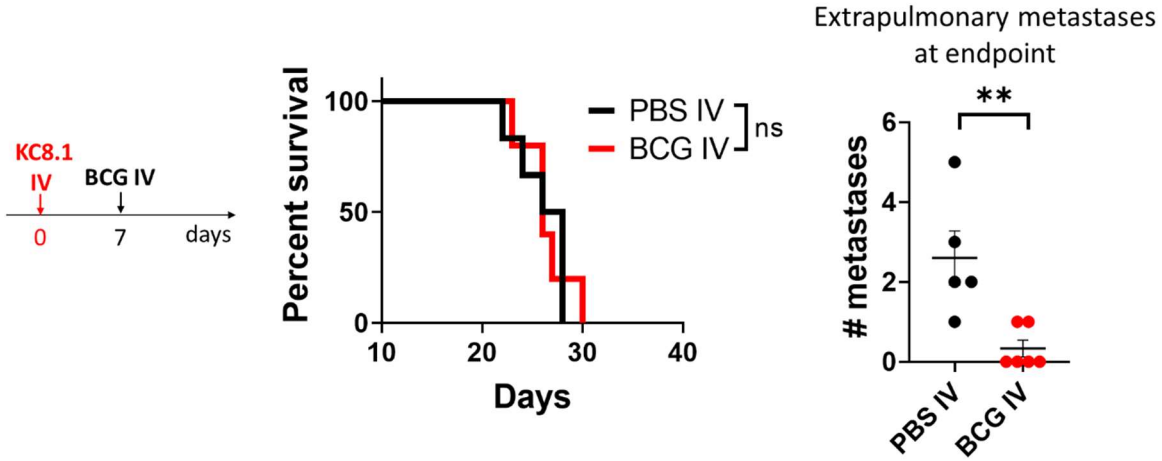

Figure 152. Survival of mice bearing KC8.1 lung adenocarcinoma tumors treated or not with BCG IV at day 5, and quantification of extrapulmonary metastases at endpoint. *n* = 5-6 mice/group, from one experiment.

Given the failure of ivBCG treatment in this model, we combined it with antiPD-L1 therapy following the schedule shown in Figure 153. Follow up of KC8.1 tumor bearing mice showed that only the combination of ivBCG and antiPD-L1 extended mouse survival, in contrast to either therapy alone, highlighting the ability of this therapeutic approach combination to treat resistant lung tumors.

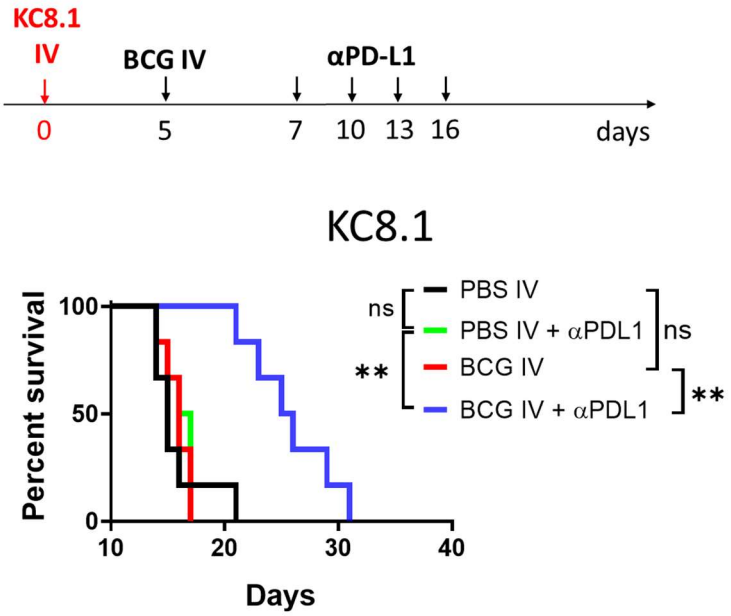

Figure 153. Survival of mice bearing KC8.1 lung adenocarcinoma tumors treated as shown in the Figure. *n* = 6 mice/group, from one experiment.

5.15 Immune checkpoint blockade boosts T and NK cell functionality in mice treated with intravenous BCG

Given its success when combined with ivBCG, we wondered which immune pathways were boosted by the addition of antiPD-L1 mAb treatment. For this, we generated lung B16-F10.gp33 tumors and analyzed them by flow cytometry at day 20 (control PBS and ivBCG groups) and at day 26 (ivBCG and ivBCG+αPD-L1 groups, Figure 154).

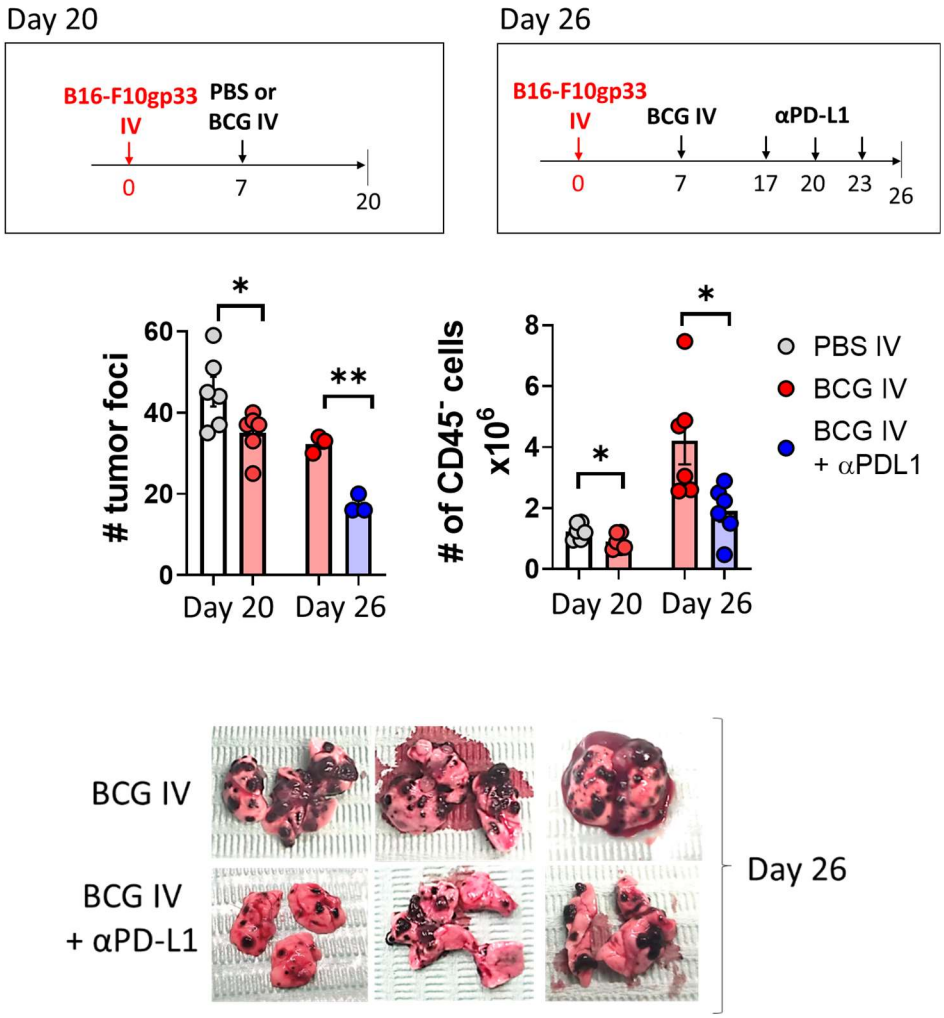

Figure 154. Mice were treated as indicated in the Figure. At day 20 or 26, lung tumor foci were counted by visual inspection, representative images are shown for day 26. Lungs were further processed for flow cytometry analysis and absolute number of $CD45^-$ in the lungs were enumerated. *n* = 6 mice/group, from one experiment.

Visual inspection of the lungs at day 20 revealed that ivBCG reduced the number of B16-F10 tumor foci compared to control PBS mice, as expected from previous experiments (Figure 154). At day 26, less B16-F10 tumor foci were found after three doses of αPD-L1

compared to mice receiving just ivBCG. Representative images of lungs are shown in the Figure 154. As a more unbiased way to measure tumor burden in the lungs, we enumerated the total number of $CD45^-$ non-immune cells, a population which probably includes more cells than just tumor cells. However, we thought that it could be used to quantify tumor burden since it is mainly tumor cells that proliferate along the duration of the experiment. We observed that this approximation correlated well with visual counting of tumor foci, since total $CD45^-$ cells were reduced by ivBCG treatment compared to control PBS at day 20, and by ivBCG + αPD-L1 compared to ivBCG alone at day 26 (Figure 154).

Next, we analyzed infiltrating immune cells by flow cytometry. Interestingly, after polyclonal *ex vivo* restimulation, $CD8^+$ and $CD4^+$ T cells from ivBCG mice produced even more IFN-γ at day 26 than at day 20, showing that the immune-stimulatory properties of BCG are durable, at least at the time point analyzed. Our results show that treatment combination further increased production of IFN-γ by $CD8^+$ T cells at day 26 compared to ivBCG alone, but not in the case of the CD4 fraction. Looking at IL-2, ivBCG increased its production at day 20 by both T cell subsets, and ivBCG+αPD-L1 further boosted IL-2 production by $CD4^+$ T cells at day 26 (Figure 155)

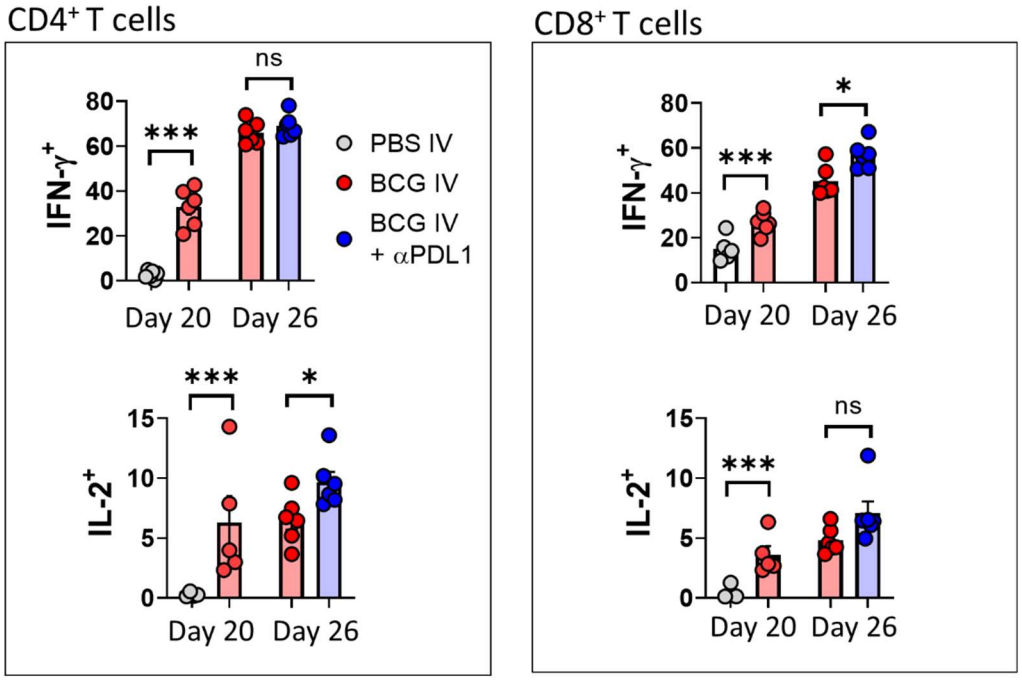

Figure 155. Mice were treated as in Figure 154 and lungs processed for flow cytometry analysis at days 20 or 26. T cells were restimulated *ex vivo* and expression of IFN-γ and IL-2 quantified. *n* = 6 mice/group, from one experiment.

Looking at tumor-specific immunity, we observed that although ivBCG increased proportions of gp33-specific CD44$^+$ CD8$^+$ T cells in the lungs at day 20, as expected, treatment combination did not further increase them at day 26 (Figure 156). Interestingly, looking at the bulk CD8$^+$ fraction, ivBCG increased the proportion of activated cells (CD44$^+$) at day 20 compared to control PBS (Figure 156). CD8$^+$ T cell activation induced by ivBCG was even stronger at day 26, with around 78 % of them expressing CD44 compared to 56 % at day 20. Addition of αPD-L1 further increased the number of activated CD8$^+$ T cells in the lungs at day 26 from 78 % in the ivBCG alone group to 92 % (Figure 156). These results could mean that although addition of αPD-L1 to ivBCG did not further generate gp33-specific CD8$^+$ T cells, it increased the functionality of existing tumor-specific clones.

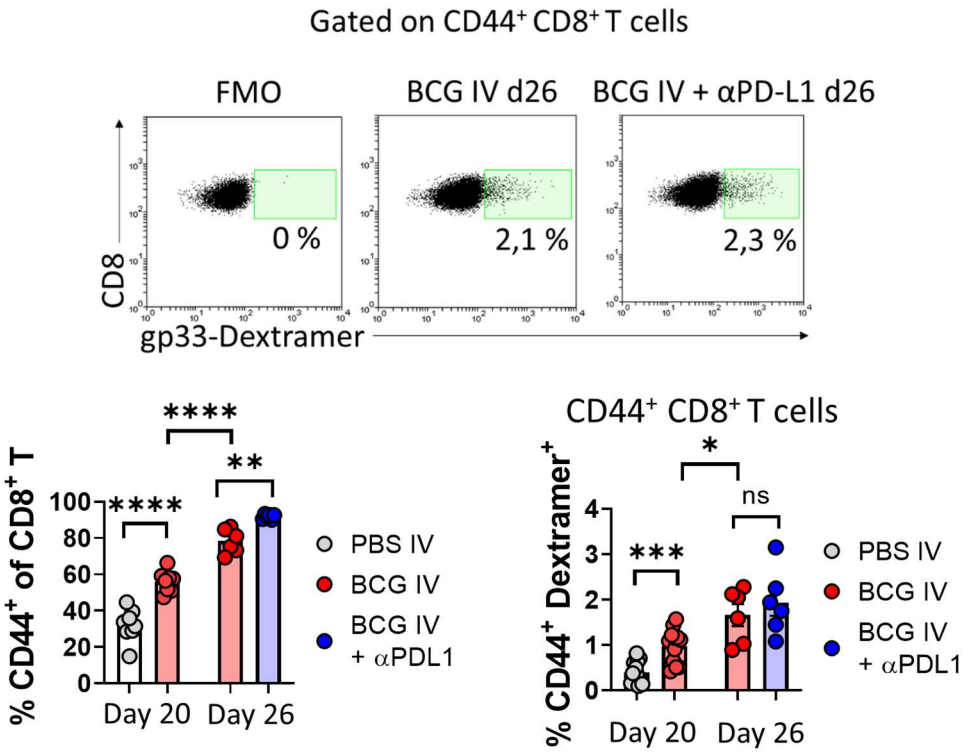

Figure 156. Mice were treated as in Figure 154 and lungs processed for flow cytometry analysis at days 20 or 26. Shown are representative dot plots for identification of gp33-specific CD44$^+$ CD8$^+$ T cells in the lungs and quantification of activated CD44$^+$ and CD44$^+$ gp33-specific populations among total CD8$^+$ T cells. *n* = 6 mice/group, from one experiment.

To further test this, we analyzed the phenotype of gp33 tumor-specific CD8$^+$ T cells and found that treatment combination led to a higher proportion of gp33-specific CD8$^+$ T cells expressing Granzyme B at day 26 compared to ivBCG alone, suggesting invigoration of

cytotoxic function by αPD-L1 treatment. Of note, not only gp33-specific $CD8^+$ T cells expressed more Granzyme B in mice undergoing combination treatment, but also the total $CD8^+$ population (Figure 157).

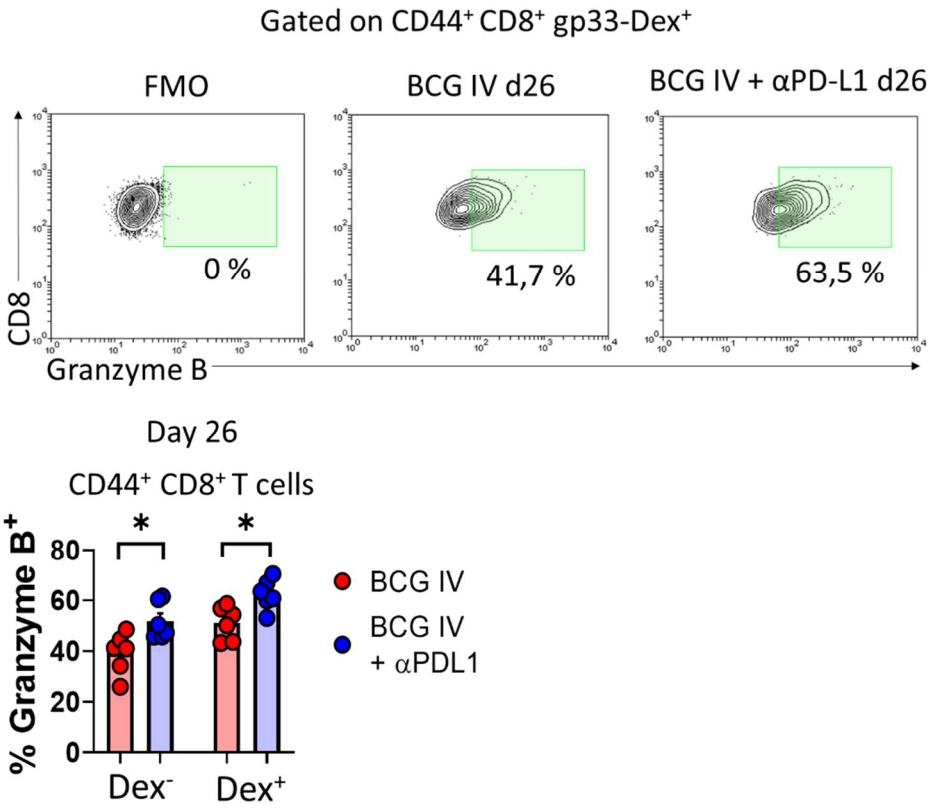

Figure 157. Mice were treated as in Figure 154 and lungs processed for flow cytometry analysis at day 26. Shown are representative dot plots of Granzyme B expression by gp33-specific $CD44^+$ $CD8^+$ T cells and quantification of Granzyme B expression in gp33-specific and bulk populations of $CD8^+$ T cells. *n* = 6 mice/group, from one experiment.

PD-1/PD-L1 axis blockade has also been described to alter NK cell function in preclinical mouse models of cancer[520], prompting us to evaluate lung NK cells after αPD-L1 treatment (Figure 158).

Following *ex vivo* restimulation with plate bound αNK1.1, at day 20 lung NK cells from ivBCG mice more readily degranulated ($CD107a^+$), as expected (Figure 158). At day 26, NK cells from ivBCG were less prone to degranulate, but combination with antiPD-L1 promoted degranulation following restimulation, compared to the ivBCG alone group (Figure 158). As observed in previous experiments, ivBCG stimulated IFN-γ expression by NK cells at day 20, and PD-L1 blockade further enhanced this effect at day 26 (Figure 158). However, when looking at Granzyme B in unstimulated NK cells at day 26, combination

with PD-L1 blockade did not enhance its expression compared to ivBCG alone. Altogether, these results suggest that PD-L1 blockade improves the ability of lung NK cells to respond to *ex vivo* restimulation in mice treated with ivBCG.

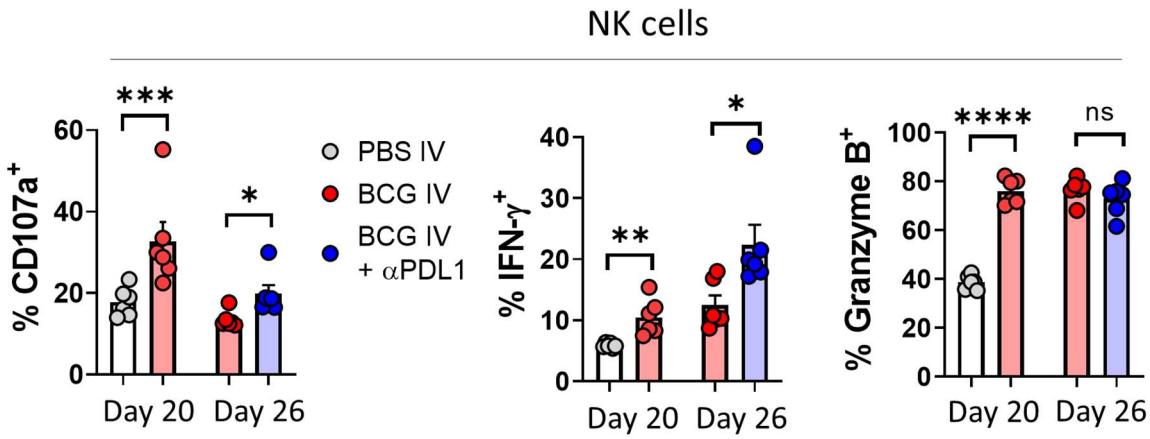

Figure 158. Mice were treated as in Figure 154 and lungs processed for flow cytometry analysis at days 20 or 26. Shown is quantification of the expression of different activations markers by NK cells in the lungs. *n* = 6 mice/group, from one experiment.

Lastly, using splenocytes isolated from tumor-bearing mice at day 26, we observed that combination treatment stimulated *in vitro* cytotoxicity towards B16-F10 cells, and also towards non-antigenically related LLC tumor cells, although to a lesser extent (Figure 159).

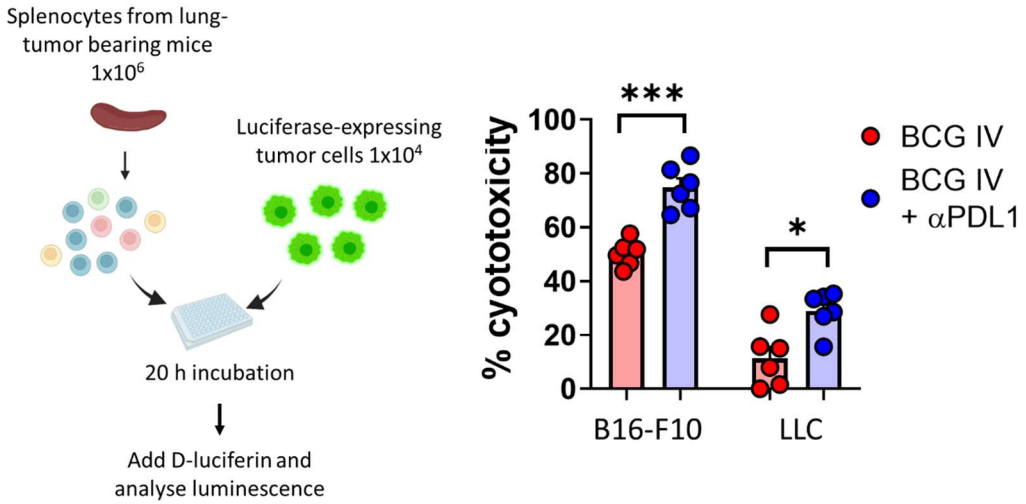

Figure 159. Mice were treated as in Figure 154 and at day 26 spleens were processed and splenocytes seeded over luciferase-expressing B16-F10 or LLC cells at a 100:1 ratio. After 20 h, cytotoxicity was evaluated by luminescence measurement. *n* = 6 mice/group, from one experiment.

Overall, we find that addition of PD-L1 blockade to ivBCG treatment further stimulates the functionality of T and NK cells in lung tumors, which concurs with the survival benefit conferred by the combination treatment compared to either of them alone.

5.16 Pre-existing BCG-specific immunity boosts the antitumoral effect of intravenous BCG

In previous sections we hypothesized that BCG-specific T cells induced by ivBCG treatment could be responsible of triggering NK cell activation and the subsequent immunological events which lead to lung tumor growth control. We wondered whether preexisting BCG-specific immunity would further boost ivBCG treatment, something which has already been demonstrated for intravesical treatment for bladder tumors and was attributed to accelerated recruitment of BCG-specific T cells to the tumor in pre-immunized mice[340]. Here, in a preliminary experiment, we found that ivBCG treatment was more effective in mice which were vaccinated subcutaneously with BCG 42 days prior to tumor cell inoculation compared to non-previously immunized mice (Figure 160). As expected, pre-vaccination with BCG without further BCG treatment was unable to slow tumor growth compared to PBS controls (Figure 160). Although further research is needed, this result strengthens our hypothesis that BCG-specific adaptive immunity has a role in driving tumor-specific responses, since accelerating or boosting it by previous immunization improves treatment efficacy.

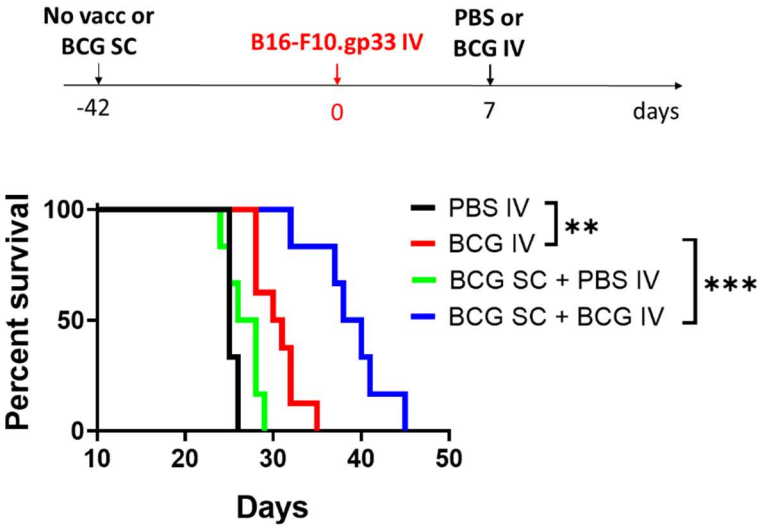

Figure 160. Mice were vaccinated subcutaneously with PBS as a control or 10^6 CFUs of BCG Pasteur 42 days before tumor challenge with intravenous B16-F10 tumor cells. Mice were further treated

by the intravenous route with PBS as a control or 10^6 CFUs of BCG Pasteur. *n* = 6 mice/group, from one experiment.

5.17 Discussion

Our results allow us to propose a tentative mechanism of action to explain the antitumor efficacy of ivBCG:

1) *Activation of NK cells and recruitment of cDC1s*

Although we do not formally demonstrate that BCG-specific T cells drive NK cell activation in the lung (1), our data is consistent with this hypothesis. First, $CD4^+$ or $CD8^+$ T cell depletion during ivBCG treatment partially abolished NK cell simulation, whereas NK cells were normally activated in $Batf3^{-/-}$ mice, which lack tumor-specific but can mount BCG-specific responses.

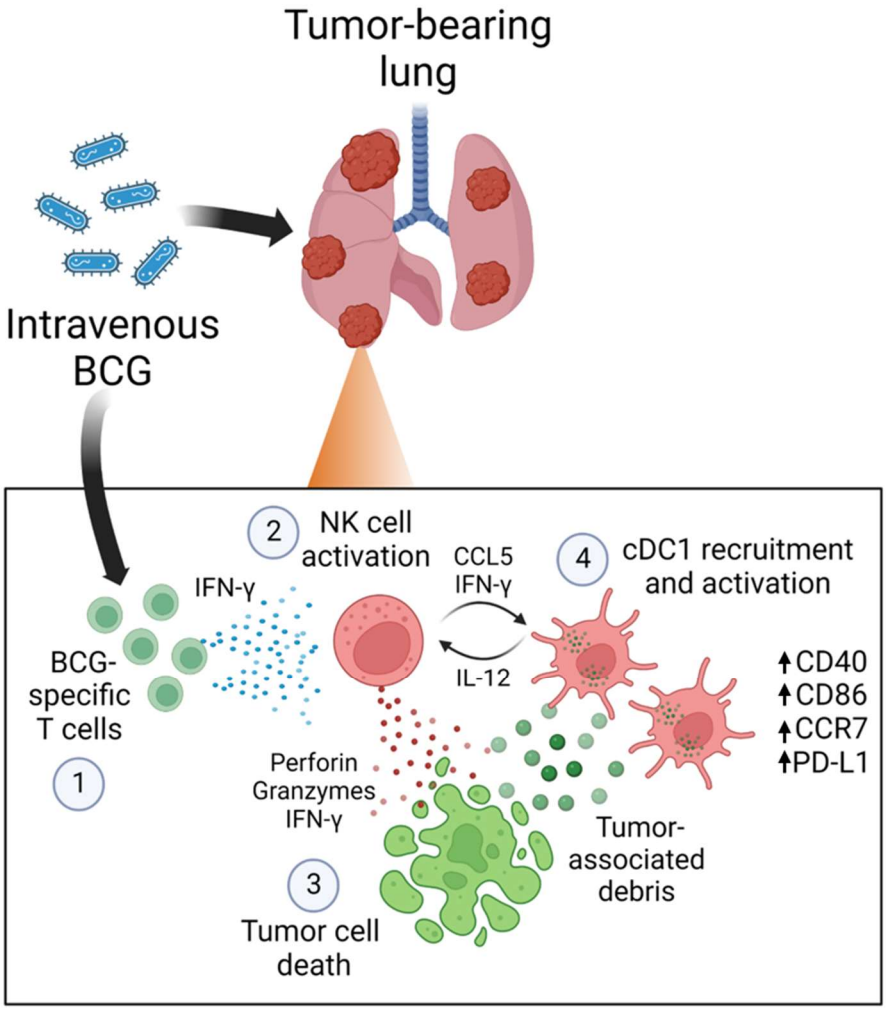

Second, previous sensitization to BCG by subcutaneous vaccination improved the efficacy of therapeutic ivBCG against B16-F10 lung metastases, meaning that boosting or accelerating the BCG-specific response can improve treatment efficacy.

Regardless of the mechanism, lung NK cells became activated by ivBCG treatment (2). We found that the role of NK cells in lung tumors was two-fold. First, stimulated lung NK cells with enhanced cytotoxic activity could be mediating tumor cell death (3), facilitating the upload of cDC1s with tumor cell-derived debris and the release of DAMPs, which would facilitate activation and maturation of these phagocytic cells. Secondly, we showed that NK cells were required for BCG-mediated recruitment of cDC1s to lung tumors by a mechanism which could involve CCL5 secretion (4). Furthermore, BCG-stimulated NK cells also facilitated IL-12 expression by cDC1s. Finally, BCG treatment increased the expression of the immunostimulatory molecules CD86 and CD40, but also of PD-L1, in lung cDC1s, evidencing an enhanced activation status. Elevated CCR7 expression in this cellular subset could also facilitate their migration to draining LNs.

2) *Induction of tumor-specific responses in the mediastinal lymph node*

Once in the draining lymph nodes (mediastinal LNs in the case of the lung), antigen loaded and activated cDC1s would prime naïve T cells. Owing to enhanced activation status (CD40, CD86, IL-12) and higher uptake of tumor-antigens, cDC1s in ivBCG mice could be responsible for priming improved tumor-specific $CD4^+$ and $CD8^+$ T cell responses. However, immune interactions in the mediastinal LN in the context of BCG vaccination need to be better characterized, as well as the requirement for T cell priming in the LN for treatment efficacy.

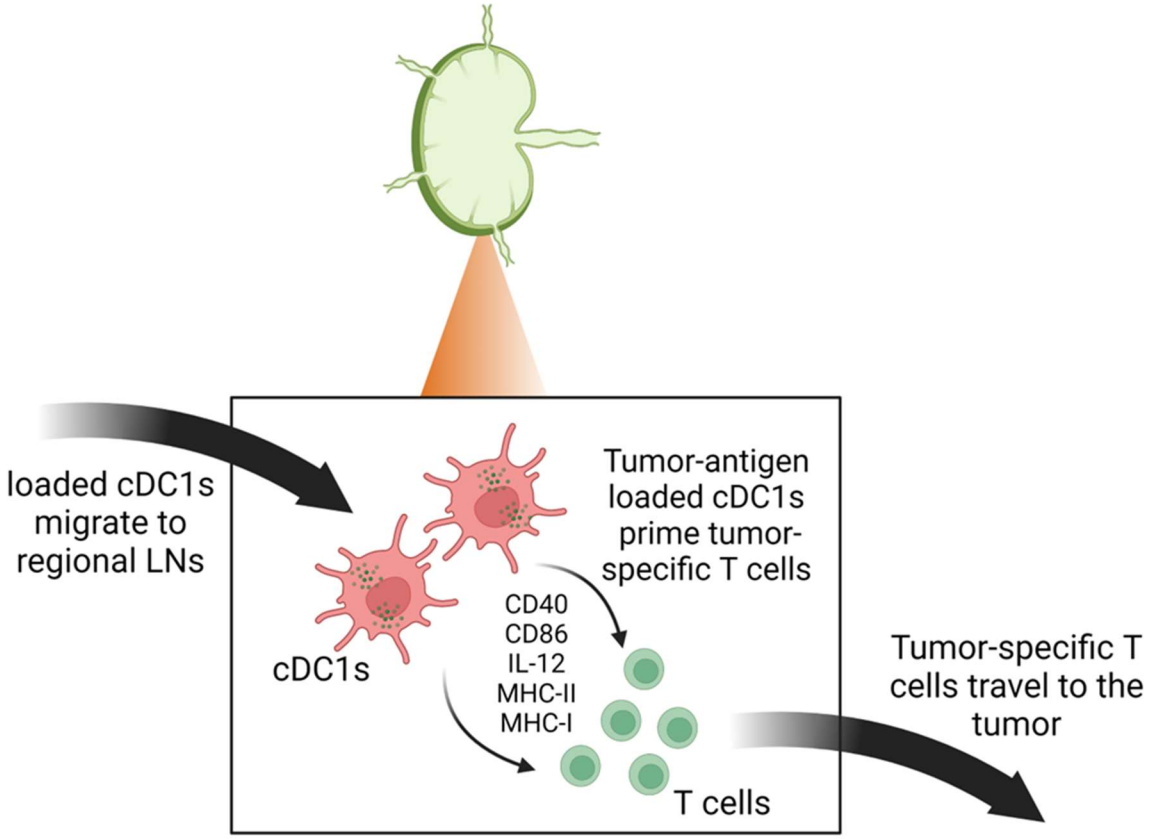

3) *ivBCG reprograms the lung TME, favoring effective antitumor T cell responses, which are further boosted by PD-L1 blockade.*

Following priming in the mediastinal LN, tumor-specific T cells travel to the tumor site, where they exert cytolytic roles as well as aid in the activation of other cellular subsets, such as macrophages or NK cells (1). Interestingly, both $CD4^+$ and $CD8^+$ were needed for ivBCG treatment success in late stages of tumor growth (day 17 onwards). Whether the role of $CD4^+$ T cells is circumscribed to helping the development of $CD8^+$ T cell mediated responses, or whether they exert direct antitumor activities or even cytotoxicity remains to be studied. Although not formally tested, it is probable that the observed shift in TAM phenotype towards a more immune-stimulatory profile further enables the activity of T cells at the tumor site (2). Lastly, as an unwanted consequence of ivBCG treatment, we observed widespread upregulation of PD-L1 in the TME, which could be hindering the full potential of this therapy. Consequently, combination of PD-L1 blocking antibodies with ivBCG treatment (3) greatly enhanced antitumor responses and overall improved mouse survival in three different models of lung tumors (4).

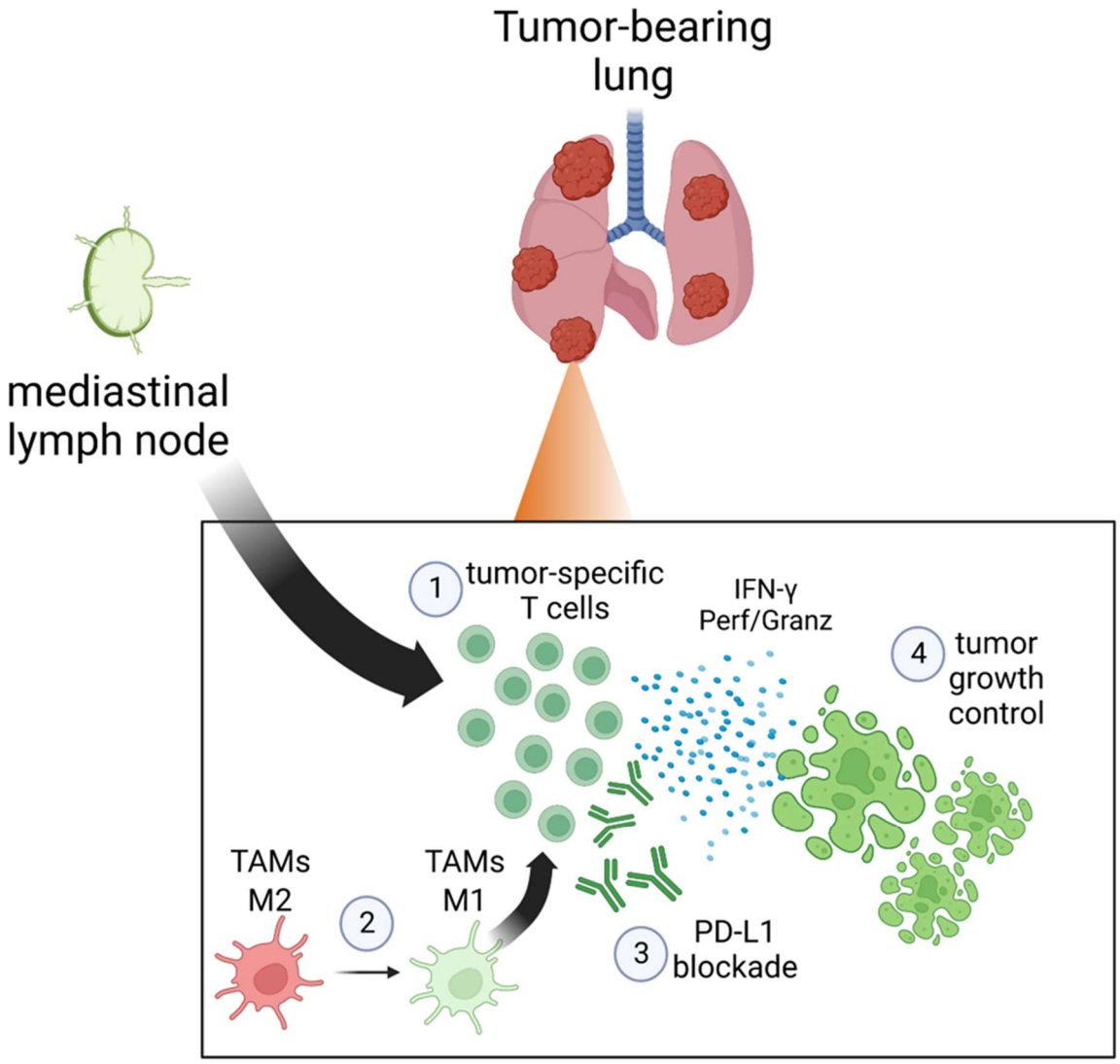

Therefore, here we have described a novel cancer immunotherapy approach based on intravenous administration of the live tuberculosis vaccine BCG, which triggered both adaptive and innate immune responses targeting tumors growing in the lung. BCG treatment stimulated multiple immune cell populations, including both T and NK cells as well as Batf3-dependent cDC1s, leading to the generation of functional tumor-specific adaptive immune responses.

cDC1s are critical mediators of antitumor immunity. Indeed, cDC1 abundance in the tumor is a good prognostic factor for favorable outcome in multiple human cancers[415,417,480], and is associated with immune-mediated control in mice[521–523]. On the contrary, paucity or a systemic dysfunctional state of cDC1s driven by tumorigenesis abrogates both

immunosurveillance and responses to immunotherapy[62,524]. Therefore, therapies that both expand and induce maturation of this cellular subset are capable of unleashing potent tumor-specific responses, as is the case with a combination of fms-like tyrosine kinase 3 ligand (Flt3l) and polyI:C[521], or a mix of Flt3l, anti-CD40 and radiotherapy for pancreatic cancer[62], which rendered tumors responsive to PD-L1 blockade. Here, we showed that ivBCG treatment efficacy critically relied on Batf3-dependent cDC1s, as is the case with other immunotherapies[204,444,522,525] and MTBVAC immunotherapy for bladder cancer[526], and rendered lung tumors responsive to antiPD-L1 blockade. Not only did ivBCG treatment augment cDC1 numbers in the tumor-bearing lung, but also induced their activation and licensing, concretely their expression of costimulatory ligands for T cell activation, their upload with tumor-associated material and their migration to draining LNs by increasing CCR7 expression, which evidences that BCG immunotherapy can improve cDC1 function. This could potentially be attributed to the ability of BCG to function as a source of PAMPs as well as of potent IFN-γ-producing cellular responses, both of which influence cDC1 function[475]. The BCG-induced upregulation of CD40 in cDC1s could also drive improved intratumoral survival of this cellular subset, since it is regulated by CD40/NF-kB signalling[527]. Indeed, it has been recently shown that Bcl-xL expression induced by CD40 signaling enhanced survival of cross-priming cDC1s in tumor draining LNs, contributing to tumor rejection[78].

Interestingly, although most work regarding cDC1s has been carried out using subcutaneously transplanted tumors, recent findings show that cDC1 recruitment (by exogenous CCL7 administration)[528] or expansion/stimulation (by Flt3l/anti-CD40 treatment)[529] can also boost antitumor immune responses in genetically engineered mouse models of lung adenocarcinoma. Indeed, it would be important to determine whether ivBCG also shows antitumor efficacy in these more restrictive mouse models, and it is an ongoing focus in our laboratory. For instance, ivBCG treatment alone was not able to slow tumor growth in the KC8.1 mouse model we developed, although further research is needed to explain the lack of efficacy in this scenario.

NK cell presence correlates with $BDCA3^+$ DCs (human cDC1s) frequency in several human cancers, and the abundance of both cellular subsets is associated with responses to αPD-1 immunotherapy and overall higher survival in melanoma patients[128], while paucity

of cDC1s in lung adenocarcinoma has been attributed to a lack of intratumoral NK cells[530]. Therefore, therapies that target NK cells and cDC1s, as we show here with ivBCG, can critically complement T cell directed immunotherapies. Interestingly, besides their ability to secrete CCL5, NK cells have been described to enhance frequencies of intratumoral cDC1 by establishing close contacts with them in the tumor and secreting the cDC1 prosurvival factor Flt3l[128]. It would be interesting to study whether NK cell derived Flt3l in the context of ivBCG treatment could also be facilitating cDC1 survival or differentiation from pre-cDC precursors[531], be it in the tumor or in the bone marrow, especially since ivBCG can alter other branches of hematopoiesis[260]. It is also tempting to speculate that ivBCG could counteract the immunosuppressive effects that the tumor exerts onto cDC1 progenitors, based on G-CSF mediated downregulation of interferon regulatory factor-8 (IRF8)[63] responsible for cDC1 development, especially since ivBCG upregulates IRF8 in myeloid progenitors in other contexts[260], perhaps by a mechanism driven by NK cell derived IFN-γ.

Another NK cell derived chemokine responsible of recruiting cDC1s is XCL1[127]. Although in our study we did not evaluate XCL1 production by NK cells, we did explore the other side of the axis, finding enhanced XCR1 expression by cDC1s in the TME, which could facilitate their XCL1-mediated retention in the tumor or their recruitment from circulation or surrounding tissue. In this regard, it would be interesting to determine whether ivBCG also affects the phenotype of circulating cDC1s, facilitating their recruitment to lung tumors by increasing their expression of chemokine receptors. Although CCL5 can mediate recruitment of cDC1s, they are not the only CCR5-expressing cellular subset. Tumor promoting immune cells such as macrophages or Tregs can also be recruited by CCL5 into the tumor[532,533], although in our context the benefits of CCL5-mediated cDC1 recruitment seem to outweigh hypothetical recruitment of immunosuppressive macrophages, especially since ivBCG can reprogram them into an immunostimulatory profile. Although we propose that NK cell derived CCL5 is responsible for ivBCG-mediated cDC1 recruitment into lung tumors, administration of neutralizing antibodies targeting CCL5, XCL1 and Flt3l would be needed to determine their individual contributions to this effect. In this regard, in a recent study the antitumoral efficacy of an adenoviral vector expressing IL-12, whose efficacy was ascribed to recruitment of cDC1s by NK cell derived CCL5, was abrogated when CCL5 neutralizing antibodies were administered[503]. Therapeutic strategies involving CCL5

are being increasingly harnessed in preclinical models and await testing in human clinical trials[503,534].

Another interesting aspect of ivBCG treatment was that NK cells not only facilitated cDC1 recruitment, but also contributed to production of IL-12 and expression of PD-L1 by this cellular subset. This could be attributed to enhanced production of IFN-γ by NK cells following ivBCG therapy. An important question that arises is the mechanism behind the strong relationship between NK cells and cDC1s in tumors. NK cells and cDC1s have been shown to establish close contacts in tumors[127], facilitated by chemotactic cues produced by NK cells and chemokines such as CXCL9 or CXCL10 secreted by cDC1s[523,535], which ensures further communication between these two cell types and explains the influence that they exert into each other. Indeed, activation of NK cells by cDC1-derived IL-12 and induction of IL-12 secretion in cDC1 by NK cell-derived IFN-have been described in independent scenarios[476,536], and we propose that this bidirectional relationship is enhanced in lung tumors by ivBCG treatment, enabling efficient antitumor immunity.

An unexpected finding from our study was that activation of NK cells by ivBCG seemed to rely on T cell derived IFN-γ, as lack of host IFN-γ expression or $CD4^+$ /$CD8^+$ T cell depletion abrogated NK cell recruitment and stimulation by ivBCG. In this regard, a previous study showed that a *Salmonella*-based bacterial immunotherapy for the prevention of lung metastasis critically relied on host IFN-γ, which was responsible for recruiting and enhancing the cytotoxic activity of NK cells[537], although in this work the cellular source of IFN-γ was not identified and bacteria were administered before tumor cells, representing a different scenario than therapeutic administration. Nevertheless, we have observed that ivBCG also prevents experimental metastasis to the lung in a similar manner to *Salmonella* (data not shown). Importantly, a previous study showed that IFN-γ indirectly modulated NK cell accumulation by inducing local expression of CXCR3 ligands[535]. Therefore, the mechanism of action of bacterial immunotherapies could be based on IFN-γ mediated recruitment and stimulation of NK cell function. Interestingly, accelerating the production of IFN-γ by BCG-specific T cells by previous subcutaneous immunization, which in our hands enhanced ivBCG antitumor efficacy, could result in faster mobilization of NK cells (and other innate immune cells) by IFN-γ producing memory T cells, something that has

already been described in the context of infection[538] and which is an ongoing topic of research in our laboratory.

Focusing on the traditional cytolytic role of NK cells, lymphocyte-mediated killing of tumor cells can induce immunogenic cell death, generating tumor cell debris and releasing damage associated molecular patterns (DAMPs), such as calreticulin or HMGB1[539,540]. These events are required for the priming of adaptive immune responses[471]. Interestingly, cDC1s acquire tumor cell-debris generated by NK cell-mediated killing more avidly than by freeze-thaw cycles, chemotherapy or even $CD8^+$ T cell-mediated cytotoxicity[540], suggesting a privileged ability of NK cells to generate immunogenic cargo for cDC1s at early stages of tumor growth to kickstart adaptive immune responses. Importantly, mice immunized with tumor cell debris generated by NK cell-mediated cytotoxicity required Batf3-dependent cDC1s for the cross-presentation of tumor-associated antigens and generation of tumor-specific adaptive immune responses[539,540]. In a similar way, we found that BCG-stimulated NK cells generated an in-situ vaccination effect, favoring the priming of tumor-specific $CD8^+$ T cells. In our model, perforin-mediated cytotoxicity by NK cells was needed for the generation of tumor cell-derived material and T cell priming, suggesting a minor role of other killing mechanisms such as FAS/FASL or TRAIL/DR, which can contribute to tumor growth control by the immune system in other contexts[541–543].

An interesting aspect of enhancing NK-cell antitumor activity is its potential to overcome T-cell associated immune evasion. Tumor cells can become resistant to $CD8^+$ T cell targeting by selection of MHC-I deficient clones, which increases their sensitivity to NK cell killing[544]. Indeed, loss of β2-microglobulin in human tumors has been proposed as a mechanism of immunotherapy resistance[420,545]. This has also been observed in human lung cancer[546]. Our results show that MHC-I deficient lung (and bladder) tumors still responded to BCG-treatment, which highlights that therapies that engage both T and NK cell-mediated immunity could overcome tumor immune escape. In our scenario, it would be interesting to further test whether the ivBCG + antiPD-L1 therapeutic approach relies on NK cells, T cells, or both. In a similar manner, we are currently testing whether the ivBCG + antiPD-L1 combination is effective against MHC class I deficient tumors. These experiments will provide functional evidence of whether antiPD-L1 boosts NK cell antitumor activity in our

experimental settings, either directly by blocking PD-1/PD-L1 interactions or indirectly by stimulating cytokine secretion by T cells or other innate subsets.

Acquisition of tumor resistance to immune checkpoint inhibition therapies has been attributed to several mechanisms, such as $CD8^+$ T cell exclusion from the tumor[523,547], a weak preexisting or dysfunctional $CD8^+$ T cell antitumor response[465], a "regulatory" profile or lack of infiltration into the tumor of cDC1s[62,127,506], or an immune-suppressive tumor microenvironment driven by myeloid cells[548]. Our results suggest that ivBCG could be overcoming several of these mechanisms. As already discussed, BCG treatment favored cDC1 recruitment to the tumor-bearing lung and their activation. Additionally, we observed a lack of acquisition of effector function by lung $CD8^+$ T cells from untreated mice bearing B16-F10 lung tumors. Indeed, $CD8^+$ T cells from untreated mice failed to acquire CD69, Granzyme B, IFN-γ or TIM-3 expression and remained $TCF1^+$, suggesting an already described dysfunctional state that arises specifically in response to lung but not to flank tumors, and that may explain their lack of response to checkpoint blockade therapy[465]. Interestingly, in that work, lung tumor-specific $CD8^+$ T cells were effectively primed, but did not become cytotoxic effectors[465]. Here, we show that following ivBCG therapy, lung-infiltrating $CD8^+$ T cells managed to acquire an effector phenotype, which concurred with tumor growth control in treated mice. Although our analysis of IFN-γ expression by lung T cell populations includes those which are BCG-specific, gp33-tumor specific $CD8^+$ T cells also upregulated Granzyme B upon treatment, and even to a higher extent when antiPD-L1 treatment was added. This result demonstrates that ivBCG and antiPD-L1 treatment affect the functionality of tumor-specific $CD8^+$ T cells.

Although we propose that enhanced generation of tumor antigens by the action of BCG-primed NK cells and subsequent priming in the mLN is the mechanism behind the enhancement of tumor-specific $CD8^+$ T cells responses, this requires further testing, for example by treating mice with FTY720 during the therapy course. This approach would allow us to determine whether priming and migration of $CD8^+$ T cells from the mLN to the tumor are required for treatment efficacy, as opposed to enhanced proliferation of tumor-specific clones in the TME. It would also be interesting to analyze the phenotype of tumor-specific T cells in the mLN of mice undergoing ivBCG or BCG + antiPDL1 treatment combination, as well as in the TME, with additional markers as IFN-γ, PD-1, TOX or Ki-

67. Enhanced effector function of tumor specific $CD8^+$ T cells could be driven by NK cells, as was shown in a lung adenocarcinoma model engineered to express NK cell stimulatory ligands[549]. In this regard, it would be compelling to analyze the effects of ivBCG on tumor cells themselves, as different activation or inhibitory ligands for NK cells could be modulated in response to treatment.

We observed that IFN-γ produced in response to ivBCG treatment increased PD-L1 expression in multiple immune cell populations of the TME, as well as in $CD45^-$ cells, which would include tumor cells themselves. This suggests the generation of an inflamed TME. However, such high levels of PD-L1 induced in the TME and in mLNs could be hindering the cytotoxic potential of T and NK cells by inhibitory PD-1/PD-L1 interactions. In concordance with this observation, different studies in mice and humans have found a correlation between PD-L1 expression on tumor-associated immune cells with better prognosis and response to immune checkpoint blockade therapy[157–160,446,550]. Moreover, in NSCLC patients, high PD-L1 expression on tumor cells or immune cells predicts response to immune checkpoint blockade[550–553]. On the contrary, NSCLC tumors with low PD-L1 expression were refractory to checkpoint blockade, even when those tumors were T cell-infiltrated[446,554–556]. Therefore, presence of T cells in the TME is not sufficient to drive responses to checkpoint blockade, and appropriately primed T cells which have acquired an effector phenotype are needed for treatment success. Therefore, PD-L1 expression in the tumor or in host immune cells works a surrogate marker of the functionality of infiltrating effector T cells. Our results showed that PD-L1 upregulation in the tumor and in host immune cells in response to BCG was driven by a combined action of $CD4^+$, $CD8^+$ T and NK cells, since depletion of each population alone did not completely abrogate the observed phenotype.

Primary and secondary immune organs as the bone marrow (BM) and the spleen are targeted by tumor-derived factors that induce an immune suppressive micro- and macroenvironment[557]. In this regard, previous data has evidenced that BCG administered by the IV route efficiently reaches both organs, where it can persist for several weeks[218,454]. For instance, as already discussed, ivBCG enhances in BM hematopoietic progenitors the expression of the transcription factor IRF8, which is implicated in myeloid cell differentiation and lineage commitment[260], and whose downregulation by tumor-derived

G-CSF and GM-CSF also leads to accumulation of poorly differentiated myeloid-derived MDSCs, which can suppress T and NK cell-mediated immunity[558]. Indeed, we found that TAMs of tumor-bearing mice treated with BCG were skewed into an immune-stimulatory profile, with heightened CD86, iNOS and MHC-II expression, and reduced CD206, although we did not functionally test their immune-suppressive or stimulatory activity in classical *in vitro* assays. TAMs in lung cancer have been shown to originate both from recruited BM-derived monocytes and from resident interstitial populations[514], and influence tumor progression by modulating adaptive immune responses[515–517]. In this regard, we have not tested whether ivBCG therapy is activating lung-resident macrophages or favoring the migration of trained monocytes from the BM, which would differentiate into immune stimulatory TAMs when recruited to lung tumors. It will be interesting to determine whether recruited "trained" monocytes from the BM contribute to ivBCG-driven antitumor immunity in the lung, for example by using $CCR2^{-/-}$ mice, in which monocyte migration is ablated[559]. Indeed, training of BM progenitors can slow the growth of transplanted tumors in mice[276,278]. However, our results here show that BCG efficacy is higher when administered by the IV route compared to IN, hinting that the antitumor effect of BCG against lung tumors is not only a consequence of the activation of lung-resident populations, something efficiently achieved by the IN route[264,512], but that it may additionally rely on facilitating systemic immunity, which is heavily altered by tumor derived factors[560–562].

Almost complete depletion of lung eosinophils by ivBCG treatment in tumor-bearing mice was also an interesting finding in our study. The ability of mycobacteria to reduce lung eosinophilia by abrogating eosinophilopoiesis has been studied for the treatment of allergic diseases[512,563]. Eosinophils have been described to possess both anti- and pro-tumorigenic roles in the TME[564]. Of particular interest is their ability to interact with ILCs, T and NK cells and modulate their antitumoral activity. Notably, following induction of allergic inflammation in the lungs of mice, eosinophils were reported to suppress NK cell cytotoxic activity, causing increased tumor burden in a B16-F10 lung metastasis model[497]. Therefore, it would be interesting to study whether ivBCG treatment could revert eosinophil-mediated suppression of NK cells in the context of lung allergic inflammation, especially since this axis facilitated the growth of lung metastases. Further analysis on the role of eosinophil

depletion by ivBCG in treatment efficacy will be needed, especially since immune-stimulatory functions of eosinophils have also been described[565–567].

Our results evidence that the highest antitumoral effect of BCG for lung tumors in mice was obtained when it was inoculated by the intravenous route, and not by the intranasal or subcutaneous. Therefore, there is an important component of safety in a potential implementation of this therapeutic approach to real patients. In this regard, even though our experiments were not specifically designed to evaluate safety, we did not observe any signs of a decrease in the health status of mice, or the induction of acute toxicities associated with the treatment. However, experiments to carefully assess potential toxicity issues of ivBCG and the ivBCG+PD-L1 combination in mice are undergoing. In this regards, published data in mouse and non-human primate models[218,260,568,569], and even for the treatment of canine osteosarcomas[570], suggests that ivBCG could be safe. Interestingly, ivBCG administration has also been performed in humans, and was found well tolerated across several studies in the last century, with doses as high as 10^8 bacilli in BCG-presensitized patients[571,572]. A common adverse effect found across humans, macaques and dogs was transient pyrexia the day following BCG administration. Although further research regarding the long-term effects of ivBCG administration is needed, the existing data suggests that translation of ivBCG to patients might be feasible. This, together with the strong antitumoral activity based on both NK and T cell stimulation described in our study, supports further exploration of ivBCG as a therapeutic strategy for lung cancer as well as for the prevention of metastatic outgrowth in this organ.

5.18 Conclusions

1. Therapeutic intravenous administration of live BCG delays the growth of pulmonary metastatic melanoma and orthotopic lung adenocarcinoma in mice by inducing tumor-specific immune responses in the lungs.

2. The antitumoral effect of intravenous BCG required NK lymphocytes, $CD4^+$ and $CD8^+$ T cells and Batf3-dependent cDC1s, as well as host IFN-γ and perforin expression, suggesting a crucial role of the immune system.

3. Mechanistically, intravenous BCG stimulates lung NK cells, which perform two separate tasks: 1) killing of tumor cells and 2) recruitment and activation of cDC1s, possibly by CCL5 and IFN-γ- dependent mechanisms. Additionally

4. Lung NK cells activated by intravenous BCG facilitated the loading of cDC1s with tumor-associated material by killing tumor cells in a perforin-dependent manner, which in turn augmented $CD8^+$ T cell dependent tumor-specific immune responses.

5. Administration of BCG by the intravenous route modulated the myeloid cell compartment in the lungs of tumor-bearing mice, shifting the phenotype of tumor-associated macrophages from tumor-promoting to immune-stimulatory.

6. Intravenous BCG upregulated surface PD-L1 expression in multiple immune and non-immune cellular populations in the lungs of tumor-bearing mice.

7. Consequently, combination of intravenous BCG with the administration of PD-L1 blocking antibodies improved mice survival in the B16-F10, LLC and KC8.1 models.

8. The stimulation of NK cell antitumor function could be ascribed to T cell-derived IFN-γ in response to intravenous BCG

References

1. Hanahan, D. & Weinberg, R. A. The Hallmarks of Cancer. *Cell* **100**, 57–70 (2000).

2. Klein, G. Tumor Antigens. *Annu Rev Microbiol* **20**, 223–252 (1966).

3. van der Bruggen, P. *et al.* A Gene Encoding an Antigen Recognized by Cytolytic T Lymphocytes on a Human Melanoma. *Science (1979)* **254**, 1643–1647 (1991).

4. Old, L. J. Cancer immunology: the search for specificity--G. H. A. Clowes Memorial lecture. *Cancer Res* **41**, 361–75 (1981).

5. Paul Ehrlich. *Über den jetzigen Stand der Karzinomforschung*. (1909).

6. Burnet, M. Cancer--A Biological Approach: III. Viruses Associated with Neoplastic Conditions. IV. Practical Applications. *BMJ* **1**, 841–847 (1957).

7. Old, L. J. & Boyse, E. A. Immunology of Experimental Tumors. *Annu Rev Med* **15**, 167–186 (1964).

8. Vesely, M. D., Kershaw, M. H., Schreiber, R. D. & Smyth, M. J. Natural Innate and Adaptive Immunity to Cancer. *Annu Rev Immunol* **29**, 235–271 (2011).

9. Street, S. E. A., Cretney, E. & Smyth, M. J. Perforin and interferon-γ activities independently control tumor initiation, growth, and metastasis. *Blood* **97**, 192–197 (2001).

10. Kaplan, D. H. *et al.* Demonstration of an interferon γ-dependent tumor surveillance system in immunocompetent mice. *Proceedings of the National Academy of Sciences* **95**, 7556–7561 (1998).

11. Shankaran, V. *et al.* IFNγ and lymphocytes prevent primary tumour development and shape tumour immunogenicity. *Nature* **410**, 1107–1111 (2001).

12. Smyth, M. J. *et al.* Perforin-Mediated Cytotoxicity Is Critical for Surveillance of Spontaneous Lymphoma. *Journal of Experimental Medicine* **192**, 755–760 (2000).

13. Bolitho, P. *et al.* Perforin-mediated suppression of B-cell lymphoma. *Proceedings of the National Academy of Sciences* **106**, 2723–2728 (2009).

14. Dunn, G. P. *et al.* A critical function for type I interferons in cancer immunoediting. *Nat Immunol* **6**, 722–729 (2005).

15. Liu, J., Xiang, Z. & Ma, X. Role of IFN Regulatory Factor-1 and IL-12 in Immunological Resistance to Pathogenesis of *N* -Methyl- *N* -Nitrosourea-Induced T Lymphoma. *The Journal of Immunology* **173**, 1184–1193 (2004).

16. Smyth, M. J., Crowe, N. Y. & Godfrey, D. I. NK cells and NKT cells collaborate in host protection from methylcholanthrene-induced fibrosarcoma. *Int Immunol* **13**, 459–463 (2001).

17. Schreiber, R. D., Old, L. J. & Smyth, M. J. Cancer Immunoediting: Integrating Immunity's Roles in Cancer Suppression and Promotion. *Science (1979)* **331**, 1565–1570 (2011).

18. Dighe, A. S., Richards, E., Old, L. J. & Schreiber, R. D. Enhanced in vivo growth and resistance to rejection of tumor cells expressing dominant negative IFNγ receptors. *Immunity* **1**, 447–456 (1994).

19. Dighe, A. S., Farrar, M. A. & Schreiber, R. D. Inhibition of cellular responsiveness to interferon-gamma (IFN gamma) induced by overexpression of inactive forms of the IFN gamma receptor. *J Biol Chem* **268**, 10645–53 (1993).

20. Dunn, G. P., Old, L. J. & Schreiber, R. D. The Three Es of Cancer Immunoediting. *Annu Rev Immunol* **22**, 329–360 (2004).

21. Bromberg, J. F., Horvath, C. M., Wen, Z., Schreiber, R. D. & Darnell, J. E. Transcriptionally active Stat1 is required for the antiproliferative effects of both interferon alpha and interferon gamma. *Proceedings of the National Academy of Sciences* **93**, 7673–7678 (1996).

22. Chin, Y. E., Kitagawa, M., Kuida, K., Flavell, R. A. & Fu, X. Y. Activation of the STAT signaling pathway can cause expression of caspase 1 and apoptosis. *Mol Cell Biol* **17**, 5328–5337 (1997).

23. Luster, A. D. & Leder, P. IP-10, a -C-X-C- chemokine, elicits a potent thymus-dependent antitumor response in vivo. *Journal of Experimental Medicine* **178**, 1057–1065 (1993).

24. Voest, E. E. *et al.* Inhibition of Angiogenesis In Vivo by Interleukin 12. *JNCI Journal of the National Cancer Institute* **87**, 581–586 (1995).

25. Alspach, E., Lussier, D. M. & Schreiber, R. D. Interferon γ and Its Important Roles in Promoting and Inhibiting Spontaneous and Therapeutic Cancer Immunity. *Cold Spring Harb Perspect Biol* **11**, a028480 (2019).

26. Boshoff, C. & Weiss, R. Aids-related malignancies. *Nat Rev Cancer* **2**, 373–382 (2002).

27. Enzler, T. *et al.* Deficiencies of GM-CSF and Interferon γ Link Inflammation and Cancer. *Journal of Experimental Medicine* **197**, 1213–1219 (2003).

28. Sepich-Poore, G. D. *et al.* The microbiome and human cancer. *Science (1979)* **371**, (2021).

29. Nejman, D. *et al.* The human tumor microbiome is composed of tumor type–specific intracellular bacteria. *Science (1979)* **368**, 973–980 (2020).

30. Li, X. & Saxena, D. The tumor mycobiome: A paradigm shift in cancer pathogenesis. *Cell* **185**, 3648–3651 (2022).

31. Dunn, G. P., Bruce, A. T., Ikeda, H., Old, L. J. & Schreiber, R. D. Cancer immunoediting: from immunosurveillance to tumor escape. *Nat Immunol* **3**, 991–998 (2002).

32. Dunn, G. P., Old, L. J. & Schreiber, R. D. The Three Es of Cancer Immunoediting. *Annu Rev Immunol* **22**, 329–360 (2004).

33. Krysko, D. v. *et al.* Immunogenic cell death and DAMPs in cancer therapy. *Nat Rev Cancer* **12**, 860–875 (2012).

34. Sims, G. P., Rowe, D. C., Rietdijk, S. T., Herbst, R. & Coyle, A. J. HMGB1 and RAGE in Inflammation and Cancer. *Annu Rev Immunol* **28**, 367–388 (2010).

35. Fuertes, M. B. *et al.* Host type I IFN signals are required for antitumor CD8+ T cell responses through CD8α+ dendritic cells. *Journal of Experimental Medicine* **208**, 2005–2016 (2011).

36. Diamond, M. S. *et al.* Type I interferon is selectively required by dendritic cells for immune rejection of tumors. *Journal of Experimental Medicine* **208**, 1989–2003 (2011).

37. López-Soto, A., Huergo-Zapico, L., Acebes-Huerta, A., Villa-Alvarez, M. & Gonzalez, S. NKG2D signaling in cancer immunosurveillance. *Int J Cancer* **136**, 1741–1750 (2015).

38. Guerra, N. *et al.* NKG2D-Deficient Mice Are Defective in Tumor Surveillance in Models of Spontaneous Malignancy. *Immunity* **28**, 571–580 (2008).

39. Han, J., Khatwani, N., Searles, T. G., Turk, M. J. & Angeles, C. v. Memory CD8+ T cell responses to cancer. *Semin Immunol* **49**, 101435 (2020).

40. DuPage, M. *et al.* Endogenous T cell responses to antigens expressed in lung adenocarcinomas delay malignant tumor progression. *Cancer Cell* **19**, 72–85 (2011).

41. DuPage, M., Mazumdar, C., Schmidt, L. M., Cheung, A. F. & Jacks, T. Expression of tumour-specific antigens underlies cancer immunoediting. *Nature* **482**, 405–9 (2012).

42. O'Sullivan, T. *et al.* Cancer immunoediting by the innate immune system in the absence of adaptive immunity. *Journal of Experimental Medicine* **209**, 1869–1882 (2012).

43. Schumacher, T. N. & Schreiber, R. D. Neoantigens in cancer immunotherapy. *Science (1979)* **348**, 69–74 (2015).

44. Boon, T., Cerottini, J.-C., van den Eynde, B., van der Bruggen, P. & van Pel, A. Tumor Antigens Recognized by T Lymphocytes. *Annu Rev Immunol* **12**, 337–365 (1994).

45. Sha, D. *et al.* Tumor Mutational Burden as a Predictive Biomarker in Solid Tumors. *Cancer Discov* **10**, 1808–1825 (2020).

46. Łuksza, M. *et al.* Neoantigen quality predicts immunoediting in survivors of pancreatic cancer. *Nature* **606**, 389–395 (2022).

47. Koebel, C. M. *et al.* Adaptive immunity maintains occult cancer in an equilibrium state. *Nature* **450**, 903–907 (2007).

48. Saudemont, A. & Quesnel, B. In a model of tumor dormancy, long-term persistent leukemic cells have increased B7-H1 and B7.1 expression and resist CTL-mediated lysis. *Blood* **104**, 2124–2133 (2004).

49. Loeser, S. *et al.* Spontaneous tumor rejection by cbl-b–deficient CD8+ T cells. *Journal of Experimental Medicine* **204**, 879–891 (2007).

50. Eyles, J. *et al.* Tumor cells disseminate early, but immunosurveillance limits metastatic outgrowth, in a mouse model of melanoma. *Journal of Clinical Investigation* **120**, 2030–2039 (2010).

51. Müller-Hermelink, N. *et al.* TNFR1 Signaling and IFN-γ Signaling Determine whether T Cells Induce Tumor Dormancy or Promote Multistage Carcinogenesis. *Cancer Cell* **13**, 507–518 (2008).

52. Meng, S. *et al.* Circulating Tumor Cells in Patients with Breast Cancer Dormancy. *Clinical Cancer Research* **10**, 8152–8162 (2004).

53. MacKie, R. M., Reid, R. & Junor, B. Fatal Melanoma Transferred in a Donated Kidney 16 Years after Melanoma Surgery. *New England Journal of Medicine* **348**, 567–568 (2003).

54. Mantovani, A. & Sica, A. Macrophages, innate immunity and cancer: balance, tolerance, and diversity. *Curr Opin Immunol* **22**, 231–237 (2010).

55. Gajewski, T. F., Fuertes, M., Spaapen, R., Zheng, Y. & Kline, J. Molecular profiling to identify relevant immune resistance mechanisms in the tumor microenvironment. *Curr Opin Immunol* **23**, 286–292 (2011).

56. Beatty, G. L. & Gladney, W. L. Immune Escape Mechanisms as a Guide for Cancer Immunotherapy. *Clinical Cancer Research* **21**, 687–692 (2015).

57. Spranger, S. & Gajewski, T. F. Tumor-intrinsic oncogene pathways mediating immune avoidance. *Oncoimmunology* **5**, e1086862 (2016).

58. Collier, J. L., Weiss, S. A., Pauken, K. E., Sen, D. R. & Sharpe, A. H. Not-so-opposite ends of the spectrum: CD8+ T cell dysfunction across chronic infection, cancer and autoimmunity. *Nature Immunology* vol. 22 809–819 Preprint at https://doi.org/10.1038/s41590-021-00949-7 (2021).

59. Vignali, D. A. A., Collison, L. W. & Workman, C. J. How regulatory T cells work. *Nat Rev Immunol* **8**, 523–532 (2008).

60. Veglia, F., Sanseviero, E. & Gabrilovich, D. I. Myeloid-derived suppressor cells in the era of increasing myeloid cell diversity. *Nat Rev Immunol* **21**, 485–498 (2021).

61. Condamine, T., Ramachandran, I., Youn, J.-I. & Gabrilovich, D. I. Regulation of Tumor Metastasis by Myeloid-Derived Suppressor Cells. *Annu Rev Med* **66**, 97–110 (2015).

62. Hegde, S. *et al.* Dendritic Cell Paucity Leads to Dysfunctional Immune Surveillance in Pancreatic Cancer. *Cancer Cell* **37**, 289-307.e9 (2020).

63. Meyer, M. A. *et al.* Breast and pancreatic cancer interrupt IRF8-dependent dendritic cell development to overcome immune surveillance. *Nat Commun* **9**, 1250 (2018).

64. DeNardo, D. G. & Ruffell, B. Macrophages as regulators of tumour immunity and immunotherapy. *Nature Reviews Immunology* vol. 19 369–382 Preprint at https://doi.org/10.1038/s41577-019-0127-6 (2019).

65. Xiang, X., Wang, J., Lu, D. & Xu, X. Targeting tumor-associated macrophages to synergize tumor immunotherapy. *Signal Transduction and Targeted Therapy* vol. 6 Preprint at https://doi.org/10.1038/s41392-021-00484-9 (2021).

66. Tzetzo, S. L. & Abrams, S. I. Redirecting macrophage function to sustain their "defender" antitumor activity. *Cancer Cell* **39**, 734–737 (2021).

67. Chen, D. S. & Mellman, I. Oncology Meets Immunology: The Cancer-Immunity Cycle. *Immunity* **39**, 1–10 (2013).

68. Ferguson, T. A., Choi, J. & Green, D. R. Armed response: how dying cells influence T-cell functions. *Immunol Rev* **241**, 77–88 (2011).

69. Fucikova, J. *et al.* Detection of immunogenic cell death and its relevance for cancer therapy. *Cell Death Dis* **11**, 1013 (2020).

70. de Miguel, D. *et al.* Inflammatory cell death induced by cytotoxic lymphocytes: a dangerous but necessary liaison. *FEBS J* **289**, 4398–4415 (2022).

71. Galluzzi, L., Petroni, G. & Kroemer, G. Immunogenicity of cell death driven by immune effectors. *J Immunother Cancer* **8**, e000802 (2020).

72. Wculek, S. K. *et al.* Dendritic cells in cancer immunology and immunotherapy. *Nat Rev Immunol* **20**, 7–24 (2020).

73. Hildner, K. *et al.* Batf3 deficiency reveals a critical role for CD8α+ dendritic cells in cytotoxic T cell immunity. *Science (1979)* **322**, 1097–1100 (2008).

74. Wu, R. & Murphy, K. M. DCs at the center of help: Origins and evolution of the three-cell-type hypothesis. *Journal of Experimental Medicine* **219**, (2022).

75. Sancho, D. *et al.* Identification of a dendritic cell receptor that couples sensing of necrosis to immunity. *Nature* **458**, 899–903 (2009).

76. Theisen, D. J. *et al.* WDFY4 is required for cross-presentation in response to viral and tumor antigens. *Science (1979)* **362**, 694–699 (2018).

77. Thaiss, C. A., Semmling, V., Franken, L., Wagner, H. & Kurts, C. Chemokines: A New Dendritic Cell Signal for T Cell Activation. *Front Immunol* **2**, (2011).

78. Wu, R. *et al.* Mechanisms of CD40-dependent cDC1 licensing beyond costimulation. *Nat Immunol* (2022) doi:10.1038/s41590-022-01324-w.

79. Ferris, S. T. *et al.* cDC1 prime and are licensed by CD4+ T cells to induce anti-tumour immunity. *Nature* **584**, 624–629 (2020).

80. Alspach, E. *et al.* MHC-II neoantigens shape tumour immunity and response to immunotherapy. *Nature* **574**, 696–701 (2019).

81. Franciszkiewicz, K., Boissonnas, A., Boutet, M., Combadière, C. & Mami-Chouaib, F. Role of Chemokines and Chemokine Receptors in Shaping the Effector Phase of the Antitumor Immune Response. *Cancer Res* **72**, 6325–6332 (2012).

82. Melero, I., Rouzaut, A., Motz, G. T. & Coukos, G. T-Cell and NK-Cell Infiltration into Solid Tumors: A Key Limiting Factor for Efficacious Cancer Immunotherapy. *Cancer Discov* **4**, 522–526 (2014).

83. Bejarano, L., Jordão, M. J. C. & Joyce, J. A. Therapeutic Targeting of the Tumor Microenvironment. *Cancer Discov* **11**, 933–959 (2021).

84. Bald, T., Krummel, M. F., Smyth, M. J. & Barry, K. C. The NK cell–cancer cycle: advances and new challenges in NK cell–based immunotherapies. *Nat Immunol* **21**, 835–847 (2020).

85. Liao, N.-S., Bix, M., Zijlstra, M., Jaenisch, R. & Raulet, D. MHC Class I Deficiency: Susceptibility to Natural Killer (NK) Cells and Impaired NK Activity. *Science (1979)* **253**, 199–202 (1991).

86. Pende, D. *et al.* Killer Ig-Like Receptors (KIRs): Their Role in NK Cell Modulation and Developments Leading to Their Clinical Exploitation. *Front Immunol* **10**, (2019).

87. Yokoyama, W. M. & Seaman, W. E. The Ly-49 and NKR-P1 Gene Families Encoding Lectin-Like Receptors on Natural Killer Cells: The NK Gene Complex. *Annu Rev Immunol* **11**, 613–635 (1993).

88. Johansson, S. *et al.* Natural killer cell education in mice with single or multiple major histocompatibility complex class I molecules. *Journal of Experimental Medicine* **201**, 1145–1155 (2005).

89. Horowitz, A. *et al.* Genetic and Environmental Determinants of Human NK Cell Diversity Revealed by Mass Cytometry. *Sci Transl Med* **5**, (2013).

90. Lanier, L. L. NK CELL RECOGNITION. *Annu Rev Immunol* **23**, 225–274 (2005).

91. Bhatnagar, N. *et al.* FcγRIII (CD16)-mediated ADCC by NK cells is regulated by monocytes and FcγRII (CD32). *Eur J Immunol* **44**, 3368–3379 (2014).

92. Bald, T., Krummel, M. F., Smyth, M. J. & Barry, K. C. The NK cell–cancer cycle: advances and new challenges in NK cell–based immunotherapies. *Nat Immunol* **21**, 835–847 (2020).

93. Raulet, D. H., Gasser, S., Gowen, B. G., Deng, W. & Jung, H. Regulation of Ligands for the NKG2D Activating Receptor. *Annu Rev Immunol* **31**, 413–441 (2013).

94. http://www.stream.wum.edu.pl/en/knowledge-base/96-nk-cells-applications-in-immuno-oncology.

95. López-Soto, A., Gonzalez, S., Smyth, M. J. & Galluzzi, L. Control of Metastasis by NK Cells. *Cancer Cell* **32**, 135–154 (2017).

96. Chockley, P. J. *et al.* Epithelial-mesenchymal transition leads to NK cell–mediated metastasis-specific immunosurveillance in lung cancer. *Journal of Clinical Investigation* **128**, 1384–1396 (2018).

97. Lo, H. C. *et al.* Resistance to natural killer cell immunosurveillance confers a selective advantage to polyclonal metastasis. *Nat Cancer* **1**, 709–722 (2020).

98. López-Soto, A. *et al.* Epithelial–Mesenchymal Transition Induces an Antitumor Immune Response Mediated by NKG2D Receptor. *The Journal of Immunology* **190**, 4408–4419 (2013).

99. Diefenbach, A., Jensen, E. R., Jamieson, A. M. & Raulet, D. H. Rae1 and H60 ligands of the NKG2D receptor stimulate tumour immunity. *Nature* **413**, 165–171 (2001).

100. Spiegel, A. *et al.* Neutrophils Suppress Intraluminal NK Cell–Mediated Tumor Cell Clearance and Enhance Extravasation of Disseminated Carcinoma Cells. *Cancer Discov* **6**, 630–649 (2016).

101. Street, S. E. A., Cretney, E. & Smyth, M. J. Perforin and interferon-γ activities independently control tumor initiation, growth, and metastasis. *Blood* **97**, 192–197 (2001).

102. Smyth, M. J. *et al.* Perforin is a major contributor to NK cell control of tumor metastasis. *J Immunol* **162**, 6658–62 (1999).

103. Takeda, K. *et al.* Involvement of tumor necrosis factor-related apoptosis-inducing ligand in surveillance of tumor metastasis by liver natural killer cells. *Nat Med* **7**, 94–100 (2001).

104. Viel, S. *et al.* TGF-β inhibits the activation and functions of NK cells by repressing the mTOR pathway. *Sci Signal* **9**, (2016).

105. Chan, C. J. *et al.* The receptors CD96 and CD226 oppose each other in the regulation of natural killer cell functions. *Nat Immunol* **15**, 431–438 (2014).

106. Gotthardt, D. *et al.* Loss of STAT3 in murine NK cells enhances NK cell–dependent tumor surveillance. *Blood* **124**, 2370–2379 (2014).

107. van Helden, M. J. *et al.* Terminal NK cell maturation is controlled by concerted actions of T-bet and Zeb2 and is essential for melanoma rejection. *Journal of Experimental Medicine* **212**, 2015–2025 (2015).

108. van der Weyden, L. *et al.* Genome-wide in vivo screen identifies novel host regulators of metastatic colonization. *Nature* **541**, 233–236 (2017).

109. Delconte, R. B. *et al.* CIS is a potent checkpoint in NK cell–mediated tumor immunity. *Nat Immunol* **17**, 816–824 (2016).

110. Paolino, M. *et al.* The E3 ligase Cbl-b and TAM receptors regulate cancer metastasis via natural killer cells. *Nature* **507**, 508–512 (2014).

111. Smyth, M. J., Crowe, N. Y. & Godfrey, D. I. NK cells and NKT cells collaborate in host protection from methylcholanthrene-induced fibrosarcoma. *Int Immunol* **13**, 459–463 (2001).

112. Guillerey, C. *et al.* Toll-like receptor 3 regulates NK cell responses to cytokines and controls experimental metastasis. *Oncoimmunology* **4**, e1027468 (2015).

113. Senovilla, L. *et al.* Trial watch. *Oncoimmunology* **1**, 1323–1343 (2012).

114. Judge, S. J. *et al.* Minimal PD-1 expression in mouse and human NK cells under diverse conditions. *Journal of Clinical Investigation* **130**, 3051–3068 (2020).

115. Huntington, N. D., Cursons, J. & Rautela, J. The cancer–natural killer cell immunity cycle. *Nat Rev Cancer* **20**, 437–454 (2020).

116. Bald, T., Krummel, M. F., Smyth, M. J. & Barry, K. C. The NK cell–cancer cycle: advances and new challenges in NK cell–based immunotherapies. *Nat Immunol* **21**, 835–847 (2020).

117. Marcus, A. *et al.* Tumor-Derived cGAMP Triggers a STING-Mediated Interferon Response in Non-tumor Cells to Activate the NK Cell Response. *Immunity* **49**, 754-763.e4 (2018).

118. Swann, J. B. *et al.* Type I IFN Contributes to NK Cell Homeostasis, Activation, and Antitumor Function. *The Journal of Immunology* **178**, 7540–7549 (2007).

119. Barber, G. N. STING: infection, inflammation and cancer. *Nat Rev Immunol* **15**, 760–770 (2015).

120. Woo, S.-R. *et al.* STING-Dependent Cytosolic DNA Sensing Mediates Innate Immune Recognition of Immunogenic Tumors. *Immunity* **41**, 830–842 (2014).

121. Nicolai, C. J. *et al.* NK cells mediate clearance of CD8 $^{+}$ T cell–resistant tumors in response to STING agonists. *Sci Immunol* **5**, (2020).

122. Shimasaki, N., Jain, A. & Campana, D. NK cells for cancer immunotherapy. *Nat Rev Drug Discov* **19**, 200–218 (2020).

123. Martínez-Lostao, L., Anel, A. & Pardo, J. How Do Cytotoxic Lymphocytes Kill Cancer Cells? *Clinical Cancer Research* **21**, 5047–5056 (2015).

124. Wolf, N. K., Kissiov, D. U. & Raulet, D. H. Roles of natural killer cells in immunity to cancer, and applications to immunotherapy. *Nat Rev Immunol* (2022) doi:10.1038/s41577-022-00732-1.

125. Adam, C. *et al.* DC-NK cell cross talk as a novel CD4+ T-cell–independent pathway for antitumor CTL induction. *Blood* **106**, 338–344 (2005).

126. Mocikat, R. *et al.* Natural Killer Cells Activated by MHC Class ILow Targets Prime Dendritic Cells to Induce Protective CD8 T Cell Responses. *Immunity* **19**, 561–569 (2003).

127. Böttcher, J. P. *et al.* NK Cells Stimulate Recruitment of cDC1 into the Tumor Microenvironment Promoting Cancer Immune Control. *Cell* **172**, 1022-1037.e14 (2018).

128. Barry, K. C. *et al.* A natural killer–dendritic cell axis defines checkpoint therapy–responsive tumor microenvironments. *Nat Med* **24**, 1178–1191 (2018).

129. Wilson, J. L. *et al.* Targeting of human dendritic cells by autologous NK cells. *J Immunol* **163**, 6365–70 (1999).

130. Starnes, C. O. Coley's toxins. *Nature* **360**, 23–23 (1992).

131. Zhang, Y. & Zhang, Z. The history and advances in cancer immunotherapy: understanding the characteristics of tumor-infiltrating immune cells and their therapeutic implications. *Cell Mol Immunol* **17**, 807–821 (2020).

132. Pol, J. *et al.* Trial Watch—Oncolytic viruses and cancer therapy. *Oncoimmunology* **5**, e1117740 (2016).

133. Lawler, S. E., Speranza, M.-C., Cho, C.-F. & Chiocca, E. A. Oncolytic Viruses in Cancer Treatment. *JAMA Oncol* **3**, 841 (2017).

134. Gatti-Mays, M. E., Redman, J. M., Collins, J. M. & Bilusic, M. Cancer vaccines: Enhanced immunogenic modulation through therapeutic combinations. *Hum Vaccin Immunother* **13**, 2561–2574 (2017).

135. Forbes, N. S. *et al.* White paper on microbial anti-cancer therapy and prevention. *J Immunother Cancer* **6**, 78 (2018).

136. Ribas, A. *et al.* Oncolytic Virotherapy Promotes Intratumoral T Cell Infiltration and Improves Anti-PD-1 Immunotherapy. *Cell* **170**, 1109-1119.e10 (2017).

137. Zamarin, D. *et al.* Localized Oncolytic Virotherapy Overcomes Systemic Tumor Resistance to Immune Checkpoint Blockade Immunotherapy. *Sci Transl Med* **6**, (2014).

138. Dougan, M., Dranoff, G. & Dougan, S. K. Cancer Immunotherapy: Beyond Checkpoint Blockade. *Annu Rev Cancer Biol* **3**, 55–75 (2019).

139. Mullard, A. Can innate immune system targets turn up the heat on 'cold' tumours? *Nat Rev Drug Discov* **17**, 3–5 (2018).

140. Alvarez, M. *et al.* Intratumoral co-injection of the poly I:C-derivative BO-112 and a STING agonist synergize to achieve local and distant anti-tumor efficacy. *J Immunother Cancer* **9**, e002953 (2021).

141. Kaczanowska, S., Joseph, A. M. & Davila, E. TLR agonists: our best *frenemy* in cancer immunotherapy. *J Leukoc Biol* **93**, 847–863 (2013).

142. Chin, E. N. *et al.* Antitumor activity of a systemic STING-activating non-nucleotide cGAMP mimetic. *Science (1979)* **369**, 993–999 (2020).

143. Pan, B.-S. *et al.* An orally available non-nucleotide STING agonist with antitumor activity. *Science (1979)* **369**, (2020).

144. Heidegger, S. *et al.* RIG-I activation is critical for responsiveness to checkpoint blockade. *Sci Immunol* **4**, (2019).

145. Such, L. *et al.* Targeting the innate immunoreceptor RIG-I overcomes melanoma-intrinsic resistance to T cell immunotherapy. *Journal of Clinical Investigation* (2020) doi:10.1172/JCI131572.

146. Doorduijn, E. M. *et al.* CD4+ T Cell and NK Cell Interplay Key to Regression of MHC Class Ilow Tumors upon TLR7/8 Agonist Therapy. *Cancer Immunol Res* **5**, 642–653 (2017).

147. Sun, L. *et al.* Activating a collaborative innate-adaptive immune response to control metastasis. *Cancer Cell* **39**, 1361-1374.e9 (2021).

148. Jahrsdörfer, B. & Weiner, G. J. CpG oligodeoxynucleotides as immunotherapy in cancer. *Update Cancer Ther* **3**, 27–32 (2008).

149. Aznar, M. A. *et al.* Intratumoral Delivery of Immunotherapy—Act Locally, Think Globally. *The Journal of Immunology* **198**, 31–39 (2017).

150. Melero, I., Castanon, E., Alvarez, M., Champiat, S. & Marabelle, A. Intratumoural administration and tumour tissue targeting of cancer immunotherapies. *Nat Rev Clin Oncol* **18**, 558–576 (2021).

151. Chambers, C. A., Kuhns, M. S., Egen, J. G. & Allison, J. P. CTLA-4-Mediated Inhibition in Regulation of T Cell Responses: Mechanisms and Manipulation in Tumor Immunotherapy. *Annu Rev Immunol* **19**, 565–594 (2001).

152. Leach, D. R., Krummel, M. F. & Allison, J. P. Enhancement of Antitumor Immunity by CTLA-4 Blockade. *Science (1979)* **271**, 1734–1736 (1996).

153. Baumeister, S. H., Freeman, G. J., Dranoff, G. & Sharpe, A. H. Coinhibitory Pathways in Immunotherapy for Cancer. *Annu Rev Immunol* **34**, 539–573 (2016).

154. Ribas, A. & Wolchok, J. D. Cancer immunotherapy using checkpoint blockade. *Science (1979)* **359**, 1350–1355 (2018).

155. Spranger, S. *et al.* Up-regulation of PD-L1, IDO, and Tregs in the melanoma tumor microenvironment is driven by CD8+ T cells. *Sci Transl Med* **5**, 1–21 (2013).

156. Ribas, A. Adaptive Immune Resistance: How Cancer Protects from Immune Attack. *Cancer Discov* **5**, 915–919 (2015).

157. Lau, J. *et al.* Tumour and host cell PD-L1 is required to mediate suppression of anti-tumour immunity in mice. *Nat Commun* **8**, 14572 (2017).

158. Lin, H. *et al.* Host expression of PD-L1 determines efficacy of PD-L1 pathway blockade–mediated tumor regression. *Journal of Clinical Investigation* **128**, 805–815 (2018).

159. Tang, H. *et al.* PD-L1 on host cells is essential for PD-L1 blockade–mediated tumor regression. *Journal of Clinical Investigation* **128**, 580–588 (2018).

160. Oh, S. A. *et al.* PD-L1 expression by dendritic cells is a key regulator of T-cell immunity in cancer. *Nat Cancer* **1**, 681–691 (2020).

161. Wei, S. C., Duffy, C. R. & Allison, J. P. Fundamental Mechanisms of Immune Checkpoint Blockade Therapy. *Cancer Discov* **8**, 1069–1086 (2018).

162. Kallies, A., Zehn, D. & Utzschneider, D. T. Precursor exhausted T cells: key to successful immunotherapy? *Nat Rev Immunol* **20**, 128–136 (2020).

163. Im, S. J. *et al.* Defining CD8+ T cells that provide the proliferative burst after PD-1 therapy. *Nature* **537**, 417–421 (2016).

164. Huang, Q. *et al.* The primordial differentiation of tumor-specific memory CD8+ T cells as bona fide responders to PD-1/PD-L1 blockade in draining lymph nodes. *Cell* **185**, 4049-4066.e25 (2022).

165. Fransen, M. F. *et al.* Tumor-draining lymph nodes are pivotal in PD-1/PD-L1 checkpoint therapy. *JCI Insight* **3**, (2018).

166. Wu, T. D. *et al.* Peripheral T cell expansion predicts tumour infiltration and clinical response. *Nature* **579**, 274–278 (2020).

167. Dammeijer, F. *et al.* The PD-1/PD-L1-Checkpoint Restrains T cell Immunity in Tumor-Draining Lymph Nodes. *Cancer Cell* **38**, 685-700.e8 (2020).

168. Gordon, S. R. *et al.* PD-1 expression by tumour-associated macrophages inhibits phagocytosis and tumour immunity. *Nature* **545**, 495–499 (2017).

169. Strauss, L. *et al.* Targeted deletion of PD-1 in myeloid cells induces antitumor immunity. *Sci Immunol* **5**, (2020).

170. Zhang, Q. *et al.* Blockade of the checkpoint receptor TIGIT prevents NK cell exhaustion and elicits potent anti-tumor immunity. *Nat Immunol* **19**, 723–732 (2018).

171. Pesini, C. *et al.* PD-1 is expressed in cytotoxic granules of NK cells and rapidly mobilized to the cell membrane following recognition of tumor cells. *Oncoimmunology* **11**, (2022).

172. Trefny, M. P. *et al.* PD-1+ natural killer cells in human non-small cell lung cancer can be activated by PD-1/PD-L1 blockade. *Cancer Immunology, Immunotherapy* **69**, 1505–1517 (2020).

173. Hsu, J. *et al.* Contribution of NK cells to immunotherapy mediated by PD-1/PD-L1 blockade. *Journal of Clinical Investigation* **128**, 4654–4668 (2018).

174. Mantovani, A., Allavena, P., Marchesi, F. & Garlanda, C. Macrophages as tools and targets in cancer therapy. *Nat Rev Drug Discov* **21**, 799–820 (2022).

175. Ruffell, B. & Coussens, L. M. Macrophages and Therapeutic Resistance in Cancer. *Cancer Cell* **27**, 462–472 (2015).

176. Murray, P. J. *et al.* Macrophage Activation and Polarization: Nomenclature and Experimental Guidelines. *Immunity* vol. 41 14–20 Preprint at https://doi.org/10.1016/j.immuni.2014.06.008 (2014).

177. Tzetzo, S. L. & Abrams, S. I. Redirecting macrophage function to sustain their "defender" antitumor activity. *Cancer Cell* **39**, 734–737 (2021).

178. DeNardo, D. G. & Ruffell, B. Macrophages as regulators of tumour immunity and immunotherapy. *Nat Rev Immunol* (2019) doi:10.1038/s41577-019-0127-6.

179. Anderson, N. R., Minutolo, N. G., Gill, S. & Klichinsky, M. Macrophage-based approaches for cancer immunotherapy. *Cancer Research* vol. 81 1201–1208 Preprint at https://doi.org/10.1158/0008-5472.CAN-20-2990 (2021).

180. Zhang, B. *et al.* B cell-derived GABA elicits IL-10+ macrophages to limit anti-tumour immunity. *Nature* **599**, 471–476 (2021).

181. Consonni, F. M. *et al.* Heme catabolism by tumor-associated macrophages controls metastasis formation. *Nat Immunol* **22**, 595–606 (2021).

182. Nywening, T. M. *et al.* Targeting both tumour-associated CXCR2 $^{+}$ neutrophils and CCR2 $^{+}$ macrophages disrupts myeloid recruitment and improves chemotherapeutic responses in pancreatic ductal adenocarcinoma. *Gut* **67**, 1112–1123 (2018).

183. Qian, B.-Z. *et al.* CCL2 recruits inflammatory monocytes to facilitate breast-tumour metastasis. *Nature* **475**, 222–225 (2011).

184. Bonapace, L. *et al.* Cessation of CCL2 inhibition accelerates breast cancer metastasis by promoting angiogenesis. *Nature* **515**, 130–133 (2014).

185. Fridlender, Z. G. *et al.* CCL2 Blockade Augments Cancer Immunotherapy. *Cancer Res* **70**, 109–118 (2010).

186. Ruffell, B. *et al.* Macrophage IL-10 Blocks CD8+ T Cell-Dependent Responses to Chemotherapy by Suppressing IL-12 Expression in Intratumoral Dendritic Cells. *Cancer Cell* **26**, 623–637 (2014).

187. Mitchem, J. B. *et al.* Targeting Tumor-Infiltrating Macrophages Decreases Tumor-Initiating Cells, Relieves Immunosuppression, and Improves Chemotherapeutic Responses. *Cancer Res* **73**, 1128–1141 (2013).

188. Germano, G. *et al.* Role of Macrophage Targeting in the Antitumor Activity of Trabectedin. *Cancer Cell* **23**, 249–262 (2013).

189. Zhu, Y. *et al.* CSF1/CSF1R Blockade Reprograms Tumor-Infiltrating Macrophages and Improves Response to T-cell Checkpoint Immunotherapy in Pancreatic Cancer Models. *Cancer Res* **74**, 5057–5069 (2014).

190. Pyonteck, S. M. *et al.* CSF-1R inhibition alters macrophage polarization and blocks glioma progression. *Nat Med* **19**, 1264–1272 (2013).

191. Pfirschke, C. *et al.* Macrophage-Targeted Therapy Unlocks Antitumoral Cross-talk between IFNγ-Secreting Lymphocytes and IL12-Producing Dendritic Cells. *Cancer Immunol Res* **10**, 40–55 (2022).

192. Cannarile, M. A. *et al.* Colony-stimulating factor 1 receptor (CSF1R) inhibitors in cancer therapy. *J Immunother Cancer* **5**, 53 (2017).

193. Ries, C. H. *et al.* Targeting Tumor-Associated Macrophages with Anti-CSF-1R Antibody Reveals a Strategy for Cancer Therapy. *Cancer Cell* **25**, 846–859 (2014).

194. Sun, L. *et al.* Activating a collaborative innate-adaptive immune response to control metastasis. *Cancer Cell* **39**, 1361-1374.e9 (2021).

195. Müller, E. *et al.* Toll-like receptor ligands and interferon-γ synergize for induction of antitumor M1 macrophages. *Front Immunol* **8**, (2017).

196. Müller, E. *et al.* Both type I and type II interferons can activate antitumor M1 macrophages when combined with TLR stimulation. *Front Immunol* **9**, (2018).

197. Lum, H. D. *et al.* Tumoristatic effects of anti-CD40 mAb-activated macrophages involve nitric oxide and tumour necrosis factor-α. *Immunology* **118**, 261–270 (2006).

198. Hoves, S. *et al.* Rapid activation of tumor-associated macrophages boosts preexisting tumor immunity. *Journal of Experimental Medicine* **215**, 859–876 (2018).

199. Murgaski, A. *et al.* Efficacy of CD40 Agonists Is Mediated by Distinct cDC Subsets and Subverted by Suppressive Macrophages. *Cancer Res* **82**, 3785–3801 (2022).

200. Sum, E. *et al.* The tumor-targeted CD40 agonist CEA-CD40 promotes T cell priming via a dual mode of action by increasing antigen delivery to dendritic cells and enhancing their activation. *J Immunother Cancer* **10**, e003264 (2022).

201. Wiehagen, K. R. *et al.* Combination of CD40 Agonism and CSF-1R Blockade Reconditions Tumor-Associated Macrophages and Drives Potent Antitumor Immunity. *Cancer Immunol Res* **5**, 1109–1121 (2017).

202. Winograd, R. *et al.* Induction of T-cell Immunity Overcomes Complete Resistance to PD-1 and CTLA-4 Blockade and Improves Survival in Pancreatic Carcinoma. *Cancer Immunol Res* **3**, 399–411 (2015).

203. Beatty, G. L. *et al.* CD40 Agonists Alter Tumor Stroma and Show Efficacy Against Pancreatic Carcinoma in Mice and Humans. *Science (1979)* **331**, 1612–1616 (2011).

204. Garris, C. S., Wong, J. L., Ravetch, J. v. & Knorr, D. A. Dendritic cell targeting with Fc-enhanced CD40 antibody agonists induces durable antitumor immunity in humanized mouse models of bladder cancer. *Sci Transl Med* **13**, (2021).

205. Nishiga, Y. *et al.* Radiotherapy in combination with CD47 blockade elicits a macrophage-mediated abscopal effect. *Nat Cancer* **3**, 1351–1366 (2022).

206. Willingham, S. B. *et al.* The CD47-signal regulatory protein alpha (SIRPa) interaction is a therapeutic target for human solid tumors. *Proceedings of the National Academy of Sciences* **109**, 6662–6667 (2012).

207. Guerriero, J. L. *et al.* Class IIa HDAC inhibition reduces breast tumours and metastases through anti-tumour macrophages. *Nature* **543**, 428–432 (2017).

208. Kaneda, M. M. *et al.* PI3Kγ is a molecular switch that controls immune suppression. *Nature* **539**, 437–442 (2016).

209. PEARL, R. CANCER AND TUBERCULOSIS*. *Am J Epidemiol* **9**, 97–159 (1929).

210. Pearl, R. On the Pathological Relations Between Cancer and Tuberculosis. *Exp Biol Med* **26**, 73–75 (1928).

211. Oettinger, T., Jørgensen, M., Ladefoged, A., Hasløv, K. & Andersen, P. Development of the Mycobacterium bovis BCG vaccine: review of the historical and biochemical evidence for a genealogical tree. *Tubercle and Lung Disease* **79**, 243–250 (1999).

212. Brosch, R. *et al.* Genome plasticity of BCG and impact on vaccine efficacy. *Proceedings of the National Academy of Sciences* **104**, 5596–5601 (2007).

213. Behr, M. A. BCG — different strains, different vaccines? *Lancet Infect Dis* **2**, 86–92 (2002).

214. Trunz, B. B., Fine, P. & Dye, C. Effect of BCG vaccination on childhood tuberculous meningitis and miliary tuberculosis worldwide: a meta-analysis and assessment of cost-effectiveness. *The Lancet* **367**, 1173–1180 (2006).

215. Colditz, G. A. *et al.* Efficacy of BCG vaccine in the prevention of tuberculosis. Meta-analysis of the published literature. *JAMA* **271**, 698–702 (1994).

216. Ritz, N., Hanekom, W. A., Robins-Browne, R., Britton, W. J. & Curtis, N. Influence of BCG vaccine strain on the immune response and protection against tuberculosis. *FEMS Microbiol Rev* **32**, 821–841 (2008).

217. Aguilo, N. *et al.* Pulmonary but Not Subcutaneous Delivery of BCG Vaccine Confers Protection to Tuberculosis-Susceptible Mice by an Interleukin 17–Dependent Mechanism. *Journal of Infectious Diseases* **213**, 831–839 (2016).

218. Darrah, P. A. *et al.* Prevention of tuberculosis in macaques after intravenous BCG immunization. *Nature* **577**, 95–102 (2020).

219. Uthayakumar, D. *et al.* Non-specific Effects of Vaccines Illustrated Through the BCG Example: From Observations to Demonstrations. *Front Immunol* **9**, (2018).

220. Moorlag, S. J. C. F. M., Arts, R. J. W., van Crevel, R. & Netea, M. G. Non-specific effects of BCG vaccine on viral infections. *Clinical Microbiology and Infection* **25**, 1473–1478 (2019).

221. OLD, L. J., CLARKE, D. A. & BENACERRAF, B. Effect of Bacillus Calmette-Guérin Infection on Transplanted Tumours in the Mouse. *Nature* **184**, 291–292 (1959).

222. Old, L. J. Immunotherapy for Cancer. *Sci Am* **275**, 136–143 (1996).

223. Nathan, C. F. Secretion of oxygen intermediates: role in effector functions of activated macrophages. *Fed Proc* **41**, 2206–11 (1982).

224. Carswell, E. A. *et al.* An endotoxin-induced serum factor that causes necrosis of tumors. *Proceedings of the National Academy of Sciences* **72**, 3666–3670 (1975).

225. Old, L. J. Tumor Necrosis Factor (TNF). *Science (1979)* **230**, 630–632 (1985).

226. Morales, A., Eidinger, D. & Bruce, A. W. Intracavitary Bacillus Calmette-guerin in the Treatment of Superficial Bladder Tumors. *Journal of Urology* **116**, 180–182 (1976).

227. Zbar, B. & Tanaka, T. Immunotherapy of Cancer: Regression of Tumors after Intralesional Injection of Living *Mycobacterium bovis*. *Science (1979)* **172**, 271–273 (1971).

228. Zbar, B., Bernstein, I. D. & Rapp, H. J. Suppression of tumor growth at the site of infection with living Bacillus Calmette-Guérin. *J Natl Cancer Inst* **46**, 831–9 (1971).

229. Zbar, B., Bernstein, I., Tanaka, T. & Rapp, H. J. Tumor Immunity Produced by the Intradermal Inoculation of Living Tumor Cells and Living *Mycobacterium bovis* (Strain BCG). *Science (1979)* **170**, 1217–1218 (1970).

230. Bast, R. C., Zbar, B., Borsos, T. & Rapp, H. J. BCG and Cancer. *New England Journal of Medicine* **290**, 1413–1420 (1974).

231. Bast, R. C., Zbar, B., Borsos, T. & Rapp, H. J. BCG and Cancer. *New England Journal of Medicine* **290**, 1458–1469 (1974).

232. Herr, H. W. & Morales, A. History of Bacillus Calmette-Guerin and Bladder Cancer: An Immunotherapy Success Story. *Journal of Urology* **179**, 53–56 (2008).

233. Mathé, G., Halle-Pannenko, O. & Bourut, C. BCG in cancer immunotherapy: results obtained with various BCG preparations in a screening study for systemic adjuvants applicable to cancer immunoprophylaxis or immunotherapy. *Natl Cancer Inst Monogr* **39**, 107–13 (1973).

234. Mathé, G. *et al.* ACTIVE IMMUNOTHERAPY FOR ACUTE LYMPHOBLASTIC LEUKÆMIA. *The Lancet* **293**, 697–699 (1969).

235. Morton, D. L. *et al.* Immunological Factors in Human Sarcomas and Melanomas. *Ann Surg* **172**, 740–749 (1970).

236. Dekernion, J. B., Golub, S. H., Gupta, R. K., Silverstein, M. & Morton, D. L. Successful transurethral intralesional BCG therapy of a bladder melanoma. *Cancer* **36**, 1662–1667 (1975).

237. Yasumoto, K. *et al.* Nonspecific adjuvant immunotherapy of lung cancer with cell wall skeleton of Mycobacterium bovis Bacillus Calmette-Guérin. *Cancer Res* **39**, 3262–7 (1979).

238. Maurer, L. H. *et al.* Combined modality therapy with radiotherapy, chemotherapy, and immunotherapy in limited small-cell carcinoma of the lung: a Phase III cancer and Leukemia Group B Study. *Journal of Clinical Oncology* **3**, 969–976 (1985).

239. Steven, A., Fisher, S. A. & Robinson, B. W. Immunotherapy for lung cancer. *Respirology* **21**, 821–833 (2016).

240. Usher, N. T. *et al.* Association of BCG Vaccination in Childhood With Subsequent Cancer Diagnoses. *JAMA Netw Open* **2**, e1912014 (2019).

241. Rosenthal, S. R. *et al.* BCG vaccination and leukemia mortality. *JAMA* **222**, 1543–4 (1972).

242. Davignon, L., Robillard, P., Lemonde, P. & Frappier, A. B.C.G. VACCINATION AND LEUKÆMIA MORTALITY. *The Lancet* **296**, 638 (1970).

243. Robinson, M. R., Rigby, C. C., Pugh, R. C. & Dumonde, D. C. Prostate carcinoma: intratumor BCG immunotherapy. *Natl Cancer Inst Monogr* 351–3 (1978).

244. Guinan, P. D., John, T., Nagale, V. & Ablin, R. J. BCG adjuvant immunotherapy in carcinoma of the prostate: an interim report. *Allergol Immunopathol (Madr)* **6**, 293–6 (1978).

245. Guinan, P., Toronchi, E., Shaw, M., Crispin, R. & Sharifi, R. Bacillus Calmette-Guerin (BCG) adjuvant therapy in stage D prostate cancer. *Urology* **20**, 401–403 (1982).

246. Kremenovic, M., Schenk, M. & Lee, D. J. Clinical and molecular insights into BCG immunotherapy for melanoma. *J Intern Med* **288**, 625–640 (2020).

247. Nathanson, L. Regression of intradermal malignant melanoma after intralesional injection of Mycobacterium bovis strain BCG. *Cancer Chemother Rep* **56**, 659–65 (1972).

248. MORTON, D. L. *et al.* BCG lmmunotherapy of Malignant Melanoma. *Ann Surg* **180**, 635–643 (1974).

249. TAN, J. K. L. & HO, V. C. Pooled Analysis of the Efficacy of Bacille Calmette-Guerin (BCG) Immunotherapy in Malignant Melanoma. *J Dermatol Surg Oncol* **19**, 985–990 (1993).

250. Kibbi, N., Ariyan, S., Faries, M. & Choi, J. N. Treatment of In-Transit Melanoma With Intralesional Bacillus Calmette-Guérin (BCG) and Topical Imiquimod 5% Cream. *Journal of Immunotherapy* **38**, 371–375 (2015).

251. Kidner, T. B. *et al.* Combined Intralesional Bacille Calmette-Guérin (BCG) and Topical Imiquimod for In-transit Melanoma. *Journal of Immunotherapy* **35**, 716–720 (2012).

252. da Gama Duarte, J. *et al.* Autoantibodies May Predict Immune-Related Toxicity: Results from a Phase I Study of Intralesional Bacillus Calmette–Guérin followed by Ipilimumab in Patients with Advanced Metastatic Melanoma. *Front Immunol* **9**, (2018).

253. Goodridge, H. S. *et al.* Harnessing the beneficial heterologous effects of vaccination. *Nat Rev Immunol* **16**, 392–400 (2016).

254. Netea, M. G. *et al.* Defining trained immunity and its role in health and disease. *Nat Rev Immunol* **20**, 375–388 (2020).

255. Aaby, P. *et al.* Vaccinia scars associated with better survival for adults. *Vaccine* **24**, 5718–5725 (2006).

256. Jensen, K. J. *et al.* Heterologous Immunological Effects of Early BCG Vaccination in Low-Birth-Weight Infants in Guinea-Bissau: A Randomized-controlled Trial. *J Infect Dis* **211**, 956–967 (2015).

257. de Castro, M. J., Pardo-Seco, J. & Martinón-Torres, F. Nonspecific (Heterologous) Protection of Neonatal BCG Vaccination Against Hospitalization Due to Respiratory Infection and Sepsis. *Clinical Infectious Diseases* **60**, 1611–1619 (2015).

258. Giamarellos-Bourboulis, E. J. *et al.* Activate: Randomized Clinical Trial of BCG Vaccination against Infection in the Elderly. *Cell* **183**, 315-323.e9 (2020).

259. Divangahi, M. *et al.* Trained immunity, tolerance, priming and differentiation: distinct immunological processes. *Nat Immunol* **22**, 2–6 (2021).

260. Kaufmann, E. *et al.* BCG Educates Hematopoietic Stem Cells to Generate Protective Innate Immunity against Tuberculosis. *Cell* **172**, 176-190.e19 (2018).

261. Mitroulis, I. *et al.* Modulation of Myelopoiesis Progenitors Is an Integral Component of Trained Immunity. *Cell* **172**, 147-161.e12 (2018).

262. Khan, N. *et al.* M. tuberculosis Reprograms Hematopoietic Stem Cells to Limit Myelopoiesis and Impair Trained Immunity. *Cell* **183**, 752-770.e22 (2020).

263. Yao, Y. *et al.* Induction of Autonomous Memory Alveolar Macrophages Requires T Cell Help and Is Critical to Trained Immunity. *Cell* **175**, 1634-1650.e17 (2018).

264. Mata, E. *et al.* Pulmonary BCG induces lung-resident macrophage activation and confers long-term protection against tuberculosis. *Sci Immunol* **6**, (2021).

265. Kleinnijenhuis, J. *et al.* BCG-induced trained immunity in NK cells: Role for non-specific protection to infection. *Clinical Immunology* **155**, 213–219 (2014).

266. Naik, S. & Fuchs, E. Inflammatory memory and tissue adaptation in sickness and in health. *Nature* **607**, 249–255 (2022).

267. Walk, J. *et al.* Outcomes of controlled human malaria infection after BCG vaccination. *Nat Commun* **10**, 874 (2019).

268. Arts, R. J. W. *et al.* BCG Vaccination Protects against Experimental Viral Infection in Humans through the Induction of Cytokines Associated with Trained Immunity. *Cell Host Microbe* **23**, 89-100.e5 (2018).

269. Bannister, S. *et al.* Neonatal BCG vaccination is associated with a long-term DNA methylation signature in circulating monocytes. *Sci Adv* **8**, (2022).

270. Kleinnijenhuis, J. *et al.* Bacille Calmette-Guérin induces NOD2-dependent nonspecific protection from reinfection via epigenetic reprogramming of monocytes. *Proceedings of the National Academy of Sciences* **109**, 17537–17542 (2012).

271. Mulder, W. J. M., Ochando, J., Joosten, L. A. B., Fayad, Z. A. & Netea, M. G. Therapeutic targeting of trained immunity. *Nat Rev Drug Discov* **18**, 553–566 (2019).

272. Netea, M. G., Joosten, L. A. B. & van der Meer, J. W. M. Hypothesis: stimulation of trained immunity as adjunctive immunotherapy in cancer. *J Leukoc Biol* **102**, 1323–1332 (2017).

273. van Puffelen, J. H. *et al.* Trained immunity as a molecular mechanism for BCG immunotherapy in bladder cancer. *Nat Rev Urol* **17**, 513–525 (2020).

274. Buffen, K. *et al.* Autophagy Controls BCG-Induced Trained Immunity and the Response to Intravesical BCG Therapy for Bladder Cancer. *PLoS Pathog* **10**, e1004485 (2014).

275. van Puffelen, J. H. *et al.* Intravesical BCG in patients with non-muscle invasive bladder cancer induces trained immunity and decreases respiratory infections. *bioRxiv* 2022.02.21.480081 (2022) doi:10.1101/2022.02.21.480081.

276. Kalafati, L. *et al.* Innate Immune Training of Granulopoiesis Promotes Anti-tumor Activity. *Cell* **183**, 771-785.e12 (2020).

277. Geller, A. E. *et al.* The induction of peripheral trained immunity in the pancreas incites anti-tumor activity to control pancreatic cancer progression. *Nat Commun* **13**, 759 (2022).

278. Priem, B. *et al.* Trained Immunity-Promoting Nanobiologic Therapy Suppresses Tumor Growth and Potentiates Checkpoint Inhibition. *Cell* **183**, 786-801.e19 (2020).

279. Koelwyn, G. J. *et al.* Myocardial infarction accelerates breast cancer via innate immune reprogramming. *Nat Med* **26**, 1452–1458 (2020).

280. Bhattacharya, S. & Singh, L. Anatomy of Urinary Bladder, Urethra and Pelvic Ureter. in *Urogynecology and Pelvic Reconstructive Surgery* 13–13 (Jaypee Brothers Medical Publishers (P) Ltd., 2016). doi:10.5005/jp/books/12783_3.

281. Jemal, A. *et al.* Global cancer statistics. *CA Cancer J Clin* **61**, 69–90 (2011).

282. Burger, M. *et al.* Epidemiology and Risk Factors of Urothelial Bladder Cancer. *Eur Urol* **63**, 234–241 (2013).

283. Sanli, O. *et al.* Bladder cancer. *Nat Rev Dis Primers* **3**, 17022 (2017).

284. Pettenati, C. & Ingersoll, M. A. Mechanisms of BCG immunotherapy and its outlook for bladder cancer. *Nat Rev Urol* **15**, 615–625 (2018).

285. Comprehensive molecular characterization of urothelial bladder carcinoma. *Nature* **507**, 315–322 (2014).

286. Knowles, M. A. & Hurst, C. D. Molecular biology of bladder cancer: new insights into pathogenesis and clinical diversity. *Nat Rev Cancer* **15**, 25–41 (2015).

287. Kiavash Nikkhou MD. https://www.nikkhoumd.com/.

288. https://training.seer.cancer.gov/bladder/abstract-code-stage/keys.html.

289. Power, N. E. & Izawa, J. Comparison of Guidelines on Non-Muscle Invasive Bladder Cancer (EAU, CUA, AUA, NCCN, NICE). *Bladder Cancer* **2**, 27–36 (2016).

290. Babjuk, M. *et al.* EAU Guidelines on Non–Muscle-Invasive Urothelial Carcinoma of the Bladder, the 2011 Update. *Eur Urol* **59**, 997–1008 (2011).

291. EAU Guidelines. Edn. presented at the EAU Annual Congress Amsterdam 2022. ISBN 978-94-92671-16-5. in.

292. Martínez-Pin˜eiro, J. A. *et al.* Long-term follow-up of a randomized prospective trial comparing a standard 81 mg dose of intravesical bacille Calmette-Guérin with a reduced dose of 27 mg in superficial bladder cancer. *BJU Int* **89**, 671–680 (2002).

293. Rentsch, C. A. *et al.* Bacillus Calmette-Guérin Strain Differences Have an Impact on Clinical Outcome in Bladder Cancer Immunotherapy. *Eur Urol* **66**, 677–688 (2014).

294. Gan, C., Mostafid, H., Khan, M. S. & Lewis, D. J. M. BCG immunotherapy for bladder cancer - The effects of substrain differences. *Nat Rev Urol* **10**, 580–588 (2013).

295. Biot, C. Claire Biot. BCG immunotherapy for bladder cancer : characterization and modeling of the bladder immune response to BCG identify strategies for improving anti-tumor activity. (2012).

296. García Rodríguez, J. F. G. J. M. E. B. S. G. Á. R. C. J. M. A. M. G. F. J. S. T. A. & R. S. J. Terapia endovesical: influencia sobre la recidiva en el cáncer vesical superficial. *Archivos Españoles de Urología (Ed. impresa)* **60**, 36–42 (2007).

297. HERR, H. W. Tumour progression and survival in patients with T1G3 bladder tumours: 15-year outcome. *BJU Int* **80**, 762–765 (1997).

298. Kamat, A. M. *et al.* Consensus statement on best practice management regarding the use of intravesical immunotherapy with BCG for bladder cancer. *Nat Rev Urol* **12**, 225–235 (2015).

299. Kates, M. *et al.* Adaptive Immune Resistance to Intravesical BCG in Non–Muscle Invasive Bladder Cancer: Implications for Prospective BCG-Unresponsive Trials. *Clinical Cancer Research* **26**, 882–891 (2020).

300. Shore, N. D. *et al.* Non-muscle-invasive bladder cancer: An overview of potential new treatment options. *Urologic Oncology: Seminars and Original Investigations* **39**, 642–663 (2021).

301. Rentsch, C. A., Hayoz, S. & Cathomas, R. Pembrolizumab monotherapy for high-risk, non-muscle-invasive bladder cancer. *Lancet Oncol* **22**, e379 (2021).

302. Meghani, K. *et al.* First-in-human Intravesical Delivery of Pembrolizumab Identifies Immune Activation in Bladder Cancer Unresponsive to Bacillus Calmette-Guérin. *Eur Urol* **82**, 602–610 (2022).

303. Gomes-Giacoia, E. *et al.* Intravesical ALT-803 and BCG Treatment Reduces Tumor Burden in a Carcinogen Induced Bladder Cancer Rat Model; a Role for Cytokine Production and NK Cell Expansion. *PLoS One* **9**, e96705 (2014).

304. Margolin, K. *et al.* Phase I Trial of ALT-803, A Novel Recombinant IL15 Complex, in Patients with Advanced Solid Tumors. *Clinical Cancer Research* **24**, 5552–5561 (2018).

305. Wong, J. L. *et al.* Phase I study of intravesical anti-CD40 agonist antibody 2141-V11 for non-muscle invasive bladder cancer unresponsive to Bacillus Calmette-Guerin (BCG) therapy. *Journal of Clinical Oncology* **40**, TPS4616–TPS4616 (2022).

306. Boorjian, S. A. *et al.* Intravesical nadofaragene firadenovec gene therapy for BCG-unresponsive non-muscle-invasive bladder cancer: a single-arm, open-label, repeat-dose clinical trial. *Lancet Oncol* **22**, 107–117 (2021).

307. Ramesh, N. *et al.* CG0070, a Conditionally Replicating Granulocyte Macrophage Colony-Stimulating Factor–Armed Oncolytic Adenovirus for the Treatment of Bladder Cancer. *Clinical Cancer Research* **12**, 305–313 (2006).

308. Packiam*, V. T. *et al.* MP43-02 CG0070, AN ONCOLYTIC ADENOVIRUS, FOR BCG-UNRESPONSIVE NON-MUSCLE-INVASIVE BLADDER CANCER (NMIBC): 18 MONTH FOLLOW-UP FROM A MULTICENTER PHASE II TRIAL. *Journal of Urology* **201**, (2019).

309. Li, R. *et al.* CORE1: Phase 2, single-arm study of CG0070 combined with pembrolizumab in patients with nonmuscle-invasive bladder cancer (NMIBC) unresponsive to bacillus Calmette-Guerin (BCG). *Journal of Clinical Oncology* **40**, 4597–4597 (2022).

310. Salomé, B. *et al.* NKG2A and HLA-E define an alternative immune checkpoint axis in bladder cancer. *Cancer Cell* **40**, 1027-1043.e9 (2022).

311. Ranti, D., Bieber, C., Wang, Y.-S., Sfakianos, J. P. & Horowitz, A. Natural killer cells: unlocking new treatments for bladder cancer. *Trends Cancer* **8**, 698–710 (2022).

312. Ranti, D. *et al.* Elevated HLA-E and NKG2A as a Consequence of Chronic Immune Activation Defines Resistance to M. bovis BCG Immunotherapy in Non-Muscle-Invasive Bladder Cancer. *bioRxiv* 2022.03.06.483198 (2022) doi:10.1101/2022.03.06.483198.

313. Durek, C. *et al.* The fate of bacillus Calmette-Guerin after intravesical instillation. *J Urol* **165**, 1765–8 (2001).

314. Abou-Zeid, C. *et al.* Characterization of fibronectin-binding antigens released by Mycobacterium tuberculosis and Mycobacterium bovis BCG. *Infect Immun* **56**, 3046–3051 (1988).

315. Ratliff, T. L., Palmer, J. O., McGarr, J. A. & Brown, E. J. Intravesical Bacillus Calmette-Guérin Therapy for Murine Bladder Tumors: Initiation of the Response by Fibronectin-mediated Attachment of Bacillus Calmette-Guérin. *Cancer Res* **47**, 1762–1766 (1987).

316. Huang, G., Redelman-Sidi, G., Rosen, N., Glickman, M. S. & Jiang, X. Inhibition of Mycobacterial Infection by the Tumor Suppressor PTEN. *Journal of Biological Chemistry* **287**, 23196–23202 (2012).

317. Redelman-Sidi, G., Iyer, G., Solit, D. B. & Glickman, M. S. Oncogenic activation of Pak1-dependent pathway of macropinocytosis determines BCG entry into bladder cancer cells. *Cancer Res* **73**, 1156–1167 (2013).

318. Rouanne, M. *et al.* BCG therapy downregulates HLA-I on malignant cells to subvert antitumor immune responses in bladder cancer. *Journal of Clinical Investigation* (2022) doi:10.1172/JCI145666.

319. de Queiroz, N. M. G. P., Marinho, F. v., de Araujo, A. C. V. S. C., Fahel, J. S. & Oliveira, S. C. MyD88-dependent BCG immunotherapy reduces tumor and regulates tumor microenvironment in bladder cancer murine model. *Sci Rep* **11**, 15648 (2021).

320. Zhang, G., Chen, F., Cao, Y., Johnson, B. & See, W. A. HMGB1 Release by Urothelial Carcinoma Cells is Required for the In Vivo Antitumor Response to Bacillus Calmette-Guérin. *Journal of Urology* **189**, 1541–1546 (2013).

321. Suriano, F. *et al.* Tumor associated macrophages polarization dictates the efficacy of BCG instillation in non-muscle invasive urothelial bladder cancer. *Journal of Experimental & Clinical Cancer Research* **32**, 87 (2013).

322. Pichler, R. *et al.* Tumor-infiltrating immune cell subpopulations influence the oncologic outcome after intravesical Bacillus Calmette-Guérin therapy in bladder cancer. *Oncotarget* **7**, 39916–39930 (2016).

323. de Boer, E. C. *et al.* Presence of activated lymphocytes in the urine of patients with superficial bladder cancer after intravesical immunotherapy with bacillus Calmette-Guérin. *Cancer Immunology, Immunotherapy* **33**, 411–416 (1991).

324. Kemp, T. J. *et al.* Neutrophil stimulation with Mycobacterium bovis bacillus Calmette-Guérin (BCG) results in the release of functional soluble TRAIL/Apo-2L. *Blood* **106**, 3474–3482 (2005).

325. Siracusano, S. *et al.* The Role of Granulocytes Following Intravesical BCG Prophylaxis. *Eur Urol* **51**, 1589–1599 (2007).

326. Suttmann, H. *et al.* Neutrophil Granulocytes Are Required for Effective *Bacillus Calmette-Guérin* Immunotherapy of Bladder Cancer and Orchestrate Local Immune Responses. *Cancer Res* **66**, 8250–8257 (2006).

327. García-Cuesta, E. M. *et al.* Characterization of a human anti-tumoral NK cell population expanded after BCG treatment of leukocytes. *Oncoimmunology* **6**, e1293212 (2017).

328. Sonoda, T., Sugimura, K., Ikemoto, S.-I., Kawashima, H. & Nakatani, T. Significance of target cell infection and natural killer cells in the anti-tumor effects of bacillus Calmette-Guerin in murine bladder cancer. *Oncol Rep* **17**, 1469–74 (2007).

329. Brandau, S. & Böhle, A. Activation of Natural Killer Cells by Bacillus Calmette–Guérin. *Eur Urol* **39**, 518–524 (2001).

330. Brandau, S. *et al.* In Vitro Generation of Bacillus Calmette-Guérin-Activated Killer Cells. *Clinical Infectious Diseases* **31**, S94–S100 (2000).

331. Brandau, S. *et al.* Perforin-mediated lysis of tumor cells by Mycobacterium bovis Bacillus Calmette-Guérin-activated killer cells. *Clin Cancer Res* **6**, 3729–38 (2000).

332. Brandau, S. *et al.* NK cells are essential for effective BCG immunotherapy. *Int J Cancer* **92**, 697–702 (2001).

333. Beatty, J. D., Islam, S., North, M. E., Knight, S. C. & Ogden, C. W. Urine dendritic cells: a noninvasive probe for immune activity in bladder cancer? *BJU Int* **94**, 1377–1383 (2004).

334. Naoe, M. *et al.* Bacillus Calmette-Guérin-pulsed dendritic cells stimulate natural killer T cells and γδT cells. *International Journal of Urology* **14**, 532–538 (2007).

335. Ratliff, T. L., Gillen, D. & Catalona, W. J. Requirement of a thymus dependent immune response for BCG-mediated antitumor activity. *Journal of Urology* **137**, 155–158 (1987).

336. Ratliff, T. L., Ritchey, J. K., Yuan, J. J. J., Andriole, G. L. & Catalona, W. J. T-cell subsets required for intravesical BCG immunotherapy for bladder cancer. *Journal of Urology* **150**, 1018–1023 (1993).

337. Boccafoschi, C. *et al.* Immunophenotypic Characterization of the Bladder Mucosa Infiltrating Lymphocytes after Intravesical BCG Treatment for Superficial Bladder Carcinoma. *Eur Urol* **21**, 304–308 (1992).

338. Kamat, A. M. *et al.* Cytokine Panel for Response to Intravesical Therapy (CyPRIT): Nomogram of Changes in Urinary Cytokine Levels Predicts Patient Response to Bacillus Calmette-Guérin. *Eur Urol* **69**, 197–200 (2016).

339. Riemensberger, J., Böhle, A. & Brandau, S. IFN-gamma and IL-12 but not IL-10 are required for local tumour surveillance in a syngeneic model of orthotopic bladder cancer. *Clin Exp Immunol* **127**, 20–26 (2002).

340. Biot, C. *et al.* Preexisting BCG-Specific T Cells Improve Intravesical Immunotherapy for Bladder Cancer. *Sci Transl Med* **4**, (2012).

341. Ji, N. *et al.* γδ T Cells Support Antigen-Specific αβ T cell–Mediated Antitumor Responses during BCG Treatment for Bladder Cancer. *Cancer Immunol Res* **9**, 1491–1503 (2021).

342. Antonelli, A. C., Binyamin, A., Hohl, T. M., Glickman, M. S. & Redelman-Sidi, G. Bacterial immunotherapy for cancer induces CD4-dependent tumor-specific immunity through tumor-intrinsic interferon-γ signaling. *Proceedings of the National Academy of Sciences* **117**, 18627–18637 (2020).

343. Arbues, A. *et al.* Construction, characterization and preclinical evaluation of MTBVAC, the first live-attenuated M. tuberculosis-based vaccine to enter clinical trials. *Vaccine* **31**, 4867–4873 (2013).

344. Gonzalo-Asensio, J., Marinova, D., Martin, C. & Aguilo, N. MTBVAC: Attenuating the Human Pathogen of Tuberculosis (TB) Toward a Promising Vaccine against the TB Epidemic. *Front Immunol* **8**, (2017).

345. Marinova, D., Gonzalo-Asensio, J., Aguilo, N. & Martin, C. MTBVAC from discovery to clinical trials in tuberculosis-endemic countries. *Expert Rev Vaccines* **16**, 565–576 (2017).

346. Martín, C., Marinova, D., Aguiló, N. & Gonzalo-Asensio, J. MTBVAC, a live TB vaccine poised to initiate efficacy trials 100 years after BCG. *Vaccine* **39**, 7277–7285 (2021).

347. Tameris, M. *et al.* Live-attenuated Mycobacterium tuberculosis vaccine MTBVAC versus BCG in adults and neonates: a randomised controlled, double-blind dose-escalation trial. *Lancet Respir Med* **7**, 757–770 (2019).

348. Aguilo, N. *et al.* MTBVAC vaccine is safe, immunogenic and confers protective efficacy against Mycobacterium tuberculosis in newborn mice. *Tuberculosis* **96**, 71–74 (2016).

349. Roy, A. *et al.* Evaluation of the immunogenicity and efficacy of BCG and MTBVAC vaccines using a natural transmission model of tuberculosis. *Vet Res* **50**, 82 (2019).

350. White, A. D. *et al.* MTBVAC vaccination protects rhesus macaques against aerosol challenge with M. tuberculosis and induces immune signatures analogous to those observed in clinical studies. *NPJ Vaccines* **6**, 1–10 (2021).

351. Spertini, F. *et al.* Safety of human immunisation with a live-attenuated Mycobacterium tuberculosis vaccine: a randomised, double-blind, controlled phase I trial. *Lancet Respir Med* **3**, 953–962 (2015).

352. Aguilo, N. *et al.* Reactogenicity to major tuberculosis antigens absent in BCG is linked to improved protection against Mycobacterium tuberculosis. *Nat Commun* **8**, (2017).

353. Covián, C. *et al.* BCG-Induced Cross-Protection and Development of Trained Immunity: Implication for Vaccine Design. *Front Immunol* **10**, (2019).

354. Tarancón, R. *et al.* New live attenuated tuberculosis vaccine MTBVAC induces trained immunity and confers protection against experimental lethal pneumonia. *PLoS Pathog* **16**, e1008404 (2020).

355. Alvarez-Arguedas, S. *et al.* Therapeutic efficacy of the live-attenuated Mycobacterium tuberculosis vaccine, MTBVAC, in a preclinical model of bladder cancer. *Translational Research* **197**, 32–42 (2018).

356. Markman, J. L. *et al.* Loss of testosterone impairs anti-tumor neutrophil function. *Nat Commun* **11**, 1613 (2020).

357. Summerhayes, I. C. & Franks, L. M. Effects of donor age on neoplastic transformation of adult mouse bladder epithelium in vitro. *J Natl Cancer Inst* **62**, 1017–23 (1979).

358. Domingos-Pereira, S. *et al.* Intravesical Ty21a vaccine promotes dendritic cells and T cell–mediated tumor regression in the MB49 bladder cancer model. *Cancer Immunol Res* **7**, 621–629 (2019).

359. Fidler, I. J. Biological behavior of malignant melanoma cells correlated to their survival in vivo. *Cancer Res* **35**, 218–24 (1975).

360. Prévost-Blondel, A. *et al.* Tumor-infiltrating lymphocytes exhibiting high ex vivo cytolytic activity fail to prevent murine melanoma tumor growth in vivo. *J Immunol* **161**, 2187–94 (1998).

361. Bertram, J. S. & Janik, P. Establishment of a cloned line of Lewis Lung Carcinoma cells adapted to cell culture. *Cancer Lett* **11**, 63–73 (1980).

362. Zal, T., Volkmann, A. & Stockinger, B. Mechanisms of tolerance induction in major histocompatibility complex class II-restricted T cells specific for a blood-borne self-antigen. *Journal of Experimental Medicine* **180**, 2089–2099 (1994).

363. Morales, A., Eidinger, D. & Bruce, A. W. Intracavitary Bacillus Calmette Guerin in the treatment of superficial bladder tumors. *Journal of Urology* **116**, 180–182 (1976).

364. Babjuk, M. *et al.* EAU Guidelines on Non–Muscle-Invasive Urothelial Carcinoma of the Bladder, the 2011 Update. *Eur Urol* **59**, 997–1008 (2011).

365. Wang, Y. *et al.* Recombinant bacillus Calmette-Guérin in urothelial bladder cancer immunotherapy: Current strategies. *Expert Rev Anticancer Ther* **15**, 85–93 (2014).

366. Oliveira, T. L., Rizzi, C. & Dellagostin, O. A. Recombinant BCG vaccines: molecular features and their influence in the expression of foreign genes. *Appl Microbiol Biotechnol* **101**, 6865–6877 (2017).

367. Luo, Y., Henning, J. & O'Donnell, M. A. Th1 cytokine-secreting recombinant Mycobacterium bovis bacillus Calmette-Guérin and prospective use in immunotherapy of bladder cancer. *Clin Dev Immunol* **2011**, (2011).

368. Nieuwenhuizen, N. E. *et al.* The recombinant bacille Calmette-Guérin vaccine VPM1002: Ready for clinical efficacy testing. *Front Immunol* **8**, 1–9 (2017).

369. Rentsch, C. A. *et al.* A Phase 1/2 Single-arm Clinical Trial of Recombinant Bacillus Calmette-Guérin (BCG) VPM1002BC Immunotherapy in Non–muscle-invasive Bladder Cancer Recurrence After Conventional BCG Therapy: SAKK 06/14. *Eur Urol Oncol* **5**, 195–202 (2022).

370. Singh, A. K. *et al.* Re-engineered BCG overexpressing cyclic di-AMP augments trained immunity and exhibits improved efficacy against bladder cancer. *Nat Commun* **13**, 878 (2022).

371. Singh, A. *et al.* Recombinant BCG overexpressing STING agonist elicits trained immunity and improved antitumor efficacy in non-muscle invasive bladder cancer. *Urologic Oncology: Seminars and Original Investigations* **38**, 899 (2020).

372. Luo, Y., Chen, X., Han, R. & O'Donnell, M. A. Recombinant bacille Calmette–Guérin (BCG) expressing human interferon-alpha 2B demonstrates enhanced immunogenicity. *Clin Exp Immunol* **123**, 264–270 (2001).

373. Noguera-Ortega, E. *et al.* Nonpathogenic Mycobacterium brumae Inhibits Bladder Cancer Growth In Vitro, Ex Vivo, and In Vivo. *Eur Urol Focus* **2**, 67–76 (2016).

374. Noguera-Ortega, E. *et al.* Intravesical Mycobacterium brumae triggers both local and systemic immunotherapeutic responses against bladder cancer in mice. *Sci Rep* **8**, 1–9 (2018).

375. Witjes, J. A. *et al.* The efficacy of BCG Tice and BCG Connaught in a cohort of 2099 T1G3 non-muscle invasive bladder cancer patients. *Urol oncol* **34**, 484 (2016).

376. Devaud, C. *et al.* Tissues in Different Anatomical Sites Can Sculpt and Vary the Tumor Microenvironment to Affect Responses to Therapy. *Molecular Therapy* **22**, 18–27 (2014).

377. Guerin, M. v, Finisguerra, V., van den Eynde, B. J., Bercovici, N. & Trautmann, A. Preclinical murine tumor models: A structural and functional perspective. *Elife* **9**, (2020).

378. Loskog, A. *et al.* Optimization of the MB49 mouse bladder cancer model for adenoviral gene therapy. *Lab Anim* **39**, 384–393 (2005).

379. Günther, J. H. *et al.* Optimizing syngeneic orthotopic murine bladder cancer (MB49). *Cancer Res* **59**, 2834–7 (1999).

380. Sin Mun, T., Kesavan, E. & Mahendran, R. A Murine Orthotopic Bladder Tumor Model and Tumor Detection System. *Journal of Visualized Experiments* (2017) doi:10.3791/55078.

381. Günther, J. H. *et al.* Optimizing syngeneic orthotopic murine bladder cancer (MB49). *Cancer Res* **59**, 2834–7 (1999).

382. Sin Mun, T., Kesavan, E. & Mahendran, R. A Murine Orthotopic Bladder Tumor Model and Tumor Detection System. *Journal of Visualized Experiments* (2017) doi:10.3791/55078.

383. Erman, A. *et al.* How Cancer Cells Invade Bladder Epithelium and Form Tumors: The Mouse Bladder Tumor Model as a Model of Tumor Recurrence in Patients. *Int J Mol Sci* **22**, 6328 (2021).

384. Redelman-Sidi, G., Glickman, M. S. & Bochner, B. H. The mechanism of action of BCG therapy for bladder cancer—a current perspective. *Nat Rev Urol* **11**, 153–162 (2014).

385. Zhao, W. *et al.* Role of a bacillus calmette-guerin fibronectin attachment protein in BCG-induced antitumor activity. *Int J Cancer* **86**, 83–88 (2000).

386. Fleischmann, J. D., Park, M.-C. & Hassan, M. O. Fibronectin Expression on Surgical Specimens Correlated with the Response to Intravesical Bacillus Calmette-Guerin Therapy. *Journal of Urology* **149**, 268–271 (1993).

387. Bevers, R. F. M., Kurth, K.-H. & Schamhart, D. H. J. Role of urothelial cells in BCG immunotherapy for superficial bladder cancer. *Br J Cancer* **91**, 607–612 (2004).

388. Wolf, A. J. *et al.* Initiation of the adaptive immune response to Mycobacterium tuberculosis depends on antigen production in the local lymph node, not the lungs. *Journal of Experimental Medicine* **205**, 105–115 (2008).

389. Teppema, J. S., de Boer, E. C., Steerenberg, P. A. & van der Meijden, A. P. M. Morphological aspects of the interaction of Bacillus Calmette-Guérin with urothelial bladder cells in vivo and in vitro: relevance for antitumor activity? *Urol Res* **20**, 219–228 (1992).

390. Kuroda, K., Brown, E. J., Telle, W. B., Russell, D. G. & Ratliff, T. L. Characterization of the internalization of bacillus Calmette-Guerin by human bladder tumor cells. *Journal of Clinical Investigation* **91**, 69–76 (1993).

391. Naito, M., Ohara, N., Matsumoto, S. & Yamada, T. The Novel Fibronectin-binding Motif and Key Residues of Mycobacteria. *Journal of Biological Chemistry* **273**, 2905–2909 (1998).

392. Kinhikar, A. G. *et al.* Potential role for ESAT6 in dissemination of M. tuberculosis via human lung epithelial cells. *Mol Microbiol* **75**, 92–106 (2010).

393. Pym, A. S., Brodin, P., Brosch, R., Huerre, M. & Cole, S. T. Loss of RD1 contributed to the attenuation of the live tuberculosis vaccines Mycobacterium bovis BCG and Mycobacterium microti. *Mol Microbiol* **46**, 709–717 (2002).

394. Copin, R., Coscollá, M., Efstathiadis, E., Gagneux, S. & Ernst, J. D. Impact of in vitro evolution on antigenic diversity of Mycobacterium bovis bacillus Calmette-Guerin (BCG). *Vaccine* **32**, 5998–6004 (2014).

395. Pichler, R. *et al.* Tumor-infiltrating immune cell subpopulations influence the oncologic outcome after intravesical Bacillus Calmette-Guérin therapy in bladder cancer. *Oncotarget* **7**, 39916–39930 (2016).

396. Riemensberger, J., Böhle, A. & Brandau, S. IFN-gamma and IL-12 but not IL-10 are required for local tumour surveillance in a syngeneic model of orthotopic bladder cancer. *Clin Exp Immunol* **127**, 20–26 (2002).

397. Cao, X. *et al.* Granzyme B and Perforin Are Important for Regulatory T Cell-Mediated Suppression of Tumor Clearance. *Immunity* **27**, 635–646 (2007).

398. Pardoll, D. M. The blockade of immune checkpoints in cancer immunotherapy. *Nat Rev Cancer* **12**, 252–264 (2012).

399. Chen, D. S. & Mellman, I. Oncology Meets Immunology: The Cancer-Immunity Cycle. *Immunity* **39**, 1–10 (2013).

400. Suttmann, H. *et al.* Neutrophil Granulocytes Are Required for Effective *Bacillus Calmette-Guérin* Immunotherapy of Bladder Cancer and Orchestrate Local Immune Responses. *Cancer Res* **66**, 8250–8257 (2006).

401. Antonelli, A. C., Binyamin, A., Hohl, T. M., Glickman, M. S. & Redelman-Sidi, G. Bacterial immunotherapy for cancer induces CD4-dependent tumor-specific immunity through tumor-intrinsic interferon-γ signaling. *Proc Natl Acad Sci U S A* **117**, 18627–18637 (2020).

402. Loskog, A. *et al.* Optimization of the MB49 mouse bladder cancer model for adenoviral gene therapy. *Lab Anim* **39**, 384–393 (2005).

403. Perez-Diez, A. *et al.* CD4 cells can be more efficient at tumor rejection than CD8 cells. *Blood* **109**, 5346–5354 (2007).

404. Kershaw, M. H. *et al.* Immunization against endogenous retroviral tumor-associated antigens. *Cancer Res* **61**, 7920–4 (2001).

405. White, H. D., Roeder, D. A. & Green, W. R. An immunodominant Kb-restricted peptide from the p15E transmembrane protein of endogenous ecotropic murine leukemia virus (MuLV) AKR623 that restores susceptibility of a tumor line to anti-AKR/Gross MuLV cytotoxic T lymphocytes. *J Virol* **68**, 897–904 (1994).

406. Ye, X. *et al.* Endogenous retroviral proteins provide an immunodominant but not requisite antigen in a murine immunotherapy tumor model. *Oncoimmunology* **9**, (2020).

407. Griffin, G. K. *et al.* Epigenetic silencing by SETDB1 suppresses tumour intrinsic immunogenicity. *Nature* **595**, 309–314 (2021).

408. Vandeveer, A. J. *et al.* Systemic Immunotherapy of Non-Muscle Invasive Mouse Bladder Cancer with Avelumab, an Anti–PD-L1 Immune Checkpoint Inhibitor. *Cancer Immunol Res* **4**, 452–462 (2016).

409. Reyes, R. M. *et al.* CD122-directed interleukin-2 treatment mechanisms in bladder cancer differ from αPD-L1 and include tissue-selective γδ T cell activation. *J Immunother Cancer* **9**, e002051 (2021).

410. Gubin, M. M. *et al.* High-Dimensional Analysis Delineates Myeloid and Lymphoid Compartment Remodeling during Successful Immune-Checkpoint Cancer Therapy. *Cell* **175**, 1014-1030.e19 (2018).

411. Philip, M. & Schietinger, A. CD8+ T cell differentiation and dysfunction in cancer. *Nat Rev Immunol* **22**, 209–223 (2022).

412. Liakou, C. I. *et al.* CTLA-4 blockade increases IFNγ-producing $CD4^{+}$ $ICOS^{hi}$ cells to shift the ratio of effector to regulatory T cells in cancer patients. *Proceedings of the National Academy of Sciences* **105**, 14987–14992 (2008).

413. Duhen, R. *et al.* PD-1 and ICOS coexpression identifies tumor-reactive CD4+ T cells in human solid tumors. *Journal of Clinical Investigation* **132**, (2022).

414. Metzger, T. C. *et al.* ICOS Promotes the Function of CD4+ Effector T Cells during Anti-OX40–Mediated Tumor Rejection. *Cancer Res* **76**, 3684–3689 (2016).

415. Broz, M. L. *et al.* Dissecting the Tumor Myeloid Compartment Reveals Rare Activating Antigen-Presenting Cells Critical for T Cell Immunity. *Cancer Cell* **26**, 638–652 (2014).

416. Ruhland, M. K. *et al.* Visualizing Synaptic Transfer of Tumor Antigens among Dendritic Cells. *Cancer Cell* **37**, 786-799.e5 (2020).

417. Roberts, E. W. *et al.* Critical Role for CD103+/CD141+ Dendritic Cells Bearing CCR7 for Tumor Antigen Trafficking and Priming of T Cell Immunity in Melanoma. *Cancer Cell* **30**, 324–336 (2016).

418. Dunn, G. P., Old, L. J. & Schreiber, R. D. The Three Es of Cancer Immunoediting. *Annu Rev Immunol* **22**, 329–360 (2004).

419. Roh, W. *et al.* Integrated molecular analysis of tumor biopsies on sequential CTLA-4 and PD-1 blockade reveals markers of response and resistance. *Sci Transl Med* **9**, (2017).

420. Zaretsky, J. M. *et al.* Mutations Associated with Acquired Resistance to PD-1 Blockade in Melanoma. *New England Journal of Medicine* **375**, 819–829 (2016).

421. Sokol, L. *et al.* Loss of tapasin correlates with diminished CD8+ T-cell immunity and prognosis in colorectal cancer. *J Transl Med* **13**, 279 (2015).

422. Gao, J. *et al.* Loss of IFN-γ Pathway Genes in Tumor Cells as a Mechanism of Resistance to Anti-CTLA-4 Therapy. *Cell* **167**, 397-404.e9 (2016).

423. Maruhashi, T. *et al.* Binding of LAG-3 to stable peptide-MHC class II limits T cell function and suppresses autoimmunity and anti-cancer immunity. *Immunity* **55**, 912-924.e8 (2022).

424. Yang, R. *et al.* Galectin-9 interacts with PD-1 and TIM-3 to regulate T cell death and is a target for cancer immunotherapy. *Nat Commun* **12**, 832 (2021).

425. Kamat, A. M. *et al.* Expert consensus document: Consensus statement on best practice management regarding the use of intravesical immunotherapy with BCG for bladder cancer. *Nat Rev Urol* **12**, 225–235 (2015).

426. Raj, G. v. *et al.* Treatment Paradigm Shift May Improve Survival of Patients With High Risk Superficial Bladder Cancer. *Journal of Urology* **177**, 1283–1286 (2007).

427. Ikeda, N., Honda, I., Yano, I., Koyama, A. & Toida, I. Bacillus Calmette-Guerin Tokyo172 substrain for superficial bladder cancer: Characterization and antitumor effect. *Journal of Urology* **173**, 1507–1512 (2005).

428. Decaestecker, K. & Oosterlinck, W. Managing the adverse events of intravesical bacillus Calmette–Guï¿½rin therapy. *Res Rep Urol* **7**, 157–163 (2015).

429. Redelman-Sidi, G., Glickman, M. S. & Bochner, B. H. The mechanism of action of BCG therapy for bladder cancer-A current perspective. *Nat Rev Urol* **11**, 153–162 (2014).

430. Kelley, D. R. *et al.* Intravesical Bacillus Calmette-Guerin Therapy for Superficial Bladder Cancer: Effect of Bacillus Calmette-Guerin Viability on Treatment Results. *Journal of Urology* **134**, 48–53 (1985).

431. Bevers, R. F., de Boer, E. C., Kurth, K. H. & Schamhart, D. H. BCG-induced interleukin-6 upregulation and BCG internalization in well and poorly differentiated human bladder cancer cell lines. *Eur Cytokine Netw* **9**, 181–6 (1998).

432. Bevers, R. F. M., Kurth, K.-H. & Schamhart, D. H. J. Role of urothelial cells in BCG immunotherapy for superficial bladder cancer. *Br J Cancer* **91**, 607–612 (2004).

433. Teppema, J. S., de Boer, E. C., Steerenberg, P. A. & van der Meijden, A. P. M. Morphological aspects of the interaction of Bacillus Calmette-Guérin with urothelial bladder cells in vivo and in vitro: relevance for antitumor activity? *Urol Res* **20**, 219–228 (1992).

434. Mora-Bau, G. *et al.* Macrophages Subvert Adaptive Immunity to Urinary Tract Infection. *PLoS Pathog* **11**, e1005044 (2015).

435. Lacerda Mariano, L. *et al.* Functionally distinct resident macrophage subsets differentially shape responses to infection in the bladder. *Sci Adv* **6**, (2020).

436. Bisiaux, A. *et al.* Molecular Analyte Profiling of the Early Events and Tissue Conditioning Following Intravesical Bacillus Calmette-Guerin Therapy in Patients With Superficial Bladder Cancer. *Journal of Urology* **181**, 1571–1580 (2009).

437. Bao, Y., Wang, L. & Sun, J. A Small Protein but with Diverse Roles: A Review of EsxA in Mycobacterium–Host Interaction. *Cells* **10**, 1645 (2021).

438. Khan, H. S. *et al.* Identification of scavenger receptor B1 as the airway microfold cell receptor for Mycobacterium tuberculosis. *Elife* **9**, (2020).

439. Rousselle, P. & Scoazec, J. Y. Laminin 332 in cancer: When the extracellular matrix turns signals from cell anchorage to cell movement. *Semin Cancer Biol* **62**, 149–165 (2020).

440. Sjödahl, G. *et al.* A Molecular Taxonomy for Urothelial Carcinoma. *Clinical Cancer Research* **18**, 3377–3386 (2012).

441. Mooberry, L. K., Sabnis, N. A., Panchoo, M., Nagarajan, B. & Lacko, A. G. Targeting the SR-B1 Receptor as a Gateway for Cancer Therapy and Imaging. *Front Pharmacol* **7**, (2016).

442. Zhang, Y. *et al.* FimH confers mannose-targeting ability to Bacillus Calmette-Guerin for improved immunotherapy in bladder cancer. *J Immunother Cancer* **10**, e003939 (2022).

443. Oh, D. Y. *et al.* Intratumoral CD4+ T Cells Mediate Anti-tumor Cytotoxicity in Human Bladder Cancer. *Cell* **181**, 1612-1625.e13 (2020).

444. Sánchez-Paulete, A. R. *et al.* Cancer immunotherapy with immunomodulatory anti-CD137 and anti–PD-1 monoclonal antibodies requires BATF3-dependent dendritic cells. *Cancer Discov* **6**, 71–79 (2016).

445. Saito, R. *et al.* Molecular Subtype-Specific Immunocompetent Models of High-Grade Urothelial Carcinoma Reveal Differential Neoantigen Expression and Response to Immunotherapy. *Cancer Res* **78**, 3954–3968 (2018).

446. Herbst, R. S. *et al.* Predictive correlates of response to the anti-PD-L1 antibody MPDL3280A in cancer patients. *Nature* **515**, 563–567 (2014).

447. Yu, J., Song, Y. & Tian, W. How to select IgG subclasses in developing anti-tumor therapeutic antibodies. *J Hematol Oncol* **13**, 45 (2020).

448. Overdijk, M. B. *et al.* Crosstalk between Human IgG Isotypes and Murine Effector Cells. *The Journal of Immunology* **189**, 3430–3438 (2012).

449. Tsuji, S. *et al.* Intravesical VAX014 Synergizes with PD-L1 Blockade to Enhance Local and Systemic Control of Bladder Cancer. *Cancer Immunol Res* **10**, 978–995 (2022).

450. Holm, G., Stejskal, V. & Perlmann, P. Cytotoxic effects of activated lymphocytes and their supernatants. *Clin Exp Immunol* **14**, 169–79 (1973).

451. Singh, A. K., Netea, M. G. & Bishai, W. R. BCG turns 100: its nontraditional uses against viruses, cancer, and immunologic diseases. *Journal of Clinical Investigation* **131**, (2021).

452. Janker, F., Weder, W., Jang, J.-H. & Jungraithmayr, W. Preclinical, non-genetic models of lung adenocarcinoma: a comparative survey. *Oncotarget* **9**, 30527–30538 (2018).

453. Agalioti, T. *et al.* Mutant KRAS promotes malignant pleural effusion formation. *Nat Commun* **8**, 15205 (2017).

454. Mittrücker, H.-W. *et al.* Poor correlation between BCG vaccination-induced T cell responses and protection against tuberculosis. *Proceedings of the National Academy of Sciences* **104**, 12434–12439 (2007).

455. Shapiro, A., Ratliff, T. L., Oakley, D. M. & Catalona, W. J. Reduction of bladder tumor growth in mice treated with intravesical Bacillus Calmette-Guérin and its correlation with Bacillus Calmette-Guérin viability and natural killer cell activity. *Cancer Res* **43**, 1611–5 (1983).

456. Cuff, S., Dolton, G., Matthews, R. J. & Gallimore, A. Antigen Specificity Determines the Pro- or Antitumoral Nature of CD8 $^{+}$ T Cells. *The Journal of Immunology* **184**, 607–614 (2010).

457. Takeda, K. *et al.* IFN-γ production by lung NK cells is critical for the natural resistance to pulmonary metastasis of B16 melanoma in mice. *J Leukoc Biol* **90**, 777–785 (2011).

458. Prévost-Blondel, A., Roth, E., Rosenthal, F. M. & Pircher, H. Crucial Role of TNF-α in CD8 T Cell-Mediated Elimination of 3LL-A9 Lewis Lung Carcinoma Cells In Vivo. *The Journal of Immunology* **164**, 3645–3651 (2000).

459. Young, T. M. *et al.* Autophagy protects tumors from T cell–mediated cytotoxicity via inhibition of TNFα-induced apoptosis. *Sci Immunol* **5**, (2020).

460. Montfort, A. *et al.* The TNF Paradox in Cancer Progression and Immunotherapy. *Front Immunol* **10**, (2019).

461. Bertrand, F. *et al.* TNFα blockade overcomes resistance to anti-PD-1 in experimental melanoma. *Nat Commun* **8**, 2256 (2017).

462. Otano, I. *et al.* Human CD8 T cells are susceptible to TNF-mediated activation-induced cell death. *Theranostics* **10**, 4481–4489 (2020).

463. Liao, W., Lin, J.-X. & Leonard, W. J. Interleukin-2 at the Crossroads of Effector Responses, Tolerance, and Immunotherapy. *Immunity* **38**, 13–25 (2013).

464. Kaptein, P. *et al.* Addition of interleukin-2 overcomes resistance to neoadjuvant CTLA4 and PD1 blockade in ex vivo patient tumors. *Sci Transl Med* **14**, (2022).

465. Horton, B. L. *et al. Lack of CD8 + T cell effector differentiation during priming mediates checkpoint blockade resistance in non-small cell lung cancer*. *Sci. Immunol* vol. 6 https://www.science.org (2021).

466. Anderson, K. G. *et al.* Intravascular staining for discrimination of vascular and tissue leukocytes. *Nat Protoc* **9**, 209–222 (2014).

467. Borst, J., Ahrends, T., Bąbała, N., Melief, C. J. M. & Kastenmüller, W. CD4+ T cell help in cancer immunology and immunotherapy. *Nat Rev Immunol* **18**, 635–647 (2018).

468. Nishimura, T. *et al.* Distinct Role of Antigen-Specific T Helper Type 1 (Th1) and Th2 Cells in Tumor Eradication in Vivo. *Journal of Experimental Medicine* **190**, 617–628 (1999).

469. Kurtulus, S. & Hildeman, D. Assessment of CD4+ and CD8+ T Cell Responses Using MHC Class I and II Tetramers. in 71–79 (2013). doi:10.1007/978-1-62703-290-2_8.

470. MacNabb, B. W. *et al.* Dendritic cells can prime anti-tumor CD8+ T cell responses through major histocompatibility complex cross-dressing. *Immunity* **55**, 982-997.e8 (2022).

471. Galluzzi, L., Buqué, A., Kepp, O., Zitvogel, L. & Kroemer, G. Immunogenic cell death in cancer and infectious disease. *Nat Rev Immunol* **17**, 97–111 (2017).

472. Edelson, B. T. *et al.* Peripheral CD103+ dendritic cells form a unified subset developmentally related to CD8α+ conventional dendritic cells. *Journal of Experimental Medicine* **207**, 823–836 (2010).

473. Engelhardt, J. J. *et al.* Marginating Dendritic Cells of the Tumor Microenvironment Cross-Present Tumor Antigens and Stably Engage Tumor-Specific T Cells. *Cancer Cell* **21**, 402–417 (2012).

474. Fuertes, M. B. *et al.* Host type I IFN signals are required for antitumor CD8+ T cell responses through CD8α+ dendritic cells. *Journal of Experimental Medicine* **208**, 2005–2016 (2011).

475. Garris, C. S. *et al.* Successful Anti-PD-1 Cancer Immunotherapy Requires T Cell-Dendritic Cell Crosstalk Involving the Cytokines IFN-γ and IL-12. *Immunity* **49**, 1148-1161.e7 (2018).

476. Mittal, D. *et al.* Interleukin-12 from CD103+ Batf3-Dependent Dendritic Cells Required for NK-Cell Suppression of Metastasis. *Cancer Immunol Res* **5**, 1098–1108 (2017).

477. Gurka, S., Hartung, E., Becker, M. & Kroczek, R. A. Mouse Conventional Dendritic Cells Can be Universally Classified Based on the Mutually Exclusive Expression of XCR1 and SIRPÎ±. *Front Immunol* **6**, (2015).

478. Crozat, K. *et al.* The XC chemokine receptor 1 is a conserved selective marker of mammalian cells homologous to mouse CD8α+ dendritic cells. *Journal of Experimental Medicine* **207**, 1283–1292 (2010).

479. Bachem, A. *et al.* Expression of XCR1 Characterizes the Batf3-Dependent Lineage of Dendritic Cells Capable of Antigen Cross-Presentation. *Front Immunol* **3**, (2012).

480. Böttcher, J. P. *et al.* NK Cells Stimulate Recruitment of cDC1 into the Tumor Microenvironment Promoting Cancer Immune Control. *Cell* **172**, 1022-1037.e14 (2018).

481. Mashayekhi, M. *et al.* CD8α+ Dendritic Cells Are the Critical Source of Interleukin-12 that Controls Acute Infection by Toxoplasma gondii Tachyzoites. *Immunity* **35**, 249–259 (2011).

482. Ruffell, B. *et al.* Macrophage IL-10 Blocks CD8+ T Cell-Dependent Responses to Chemotherapy by Suppressing IL-12 Expression in Intratumoral Dendritic Cells. *Cancer Cell* **26**, 623–637 (2014).

483. Tugues, S. *et al.* New insights into IL-12-mediated tumor suppression. *Cell Death Differ* **22**, 237–246 (2015).

484. Hsieh, C.-S. *et al.* Development of T_H 1 $CD4^+$ T Cells Through IL-12 Produced by *Listeria* -Induced Macrophages. *Science (1979)* **260**, 547–549 (1993).

485. Kobayashi, M. *et al.* Identification and purification of natural killer cell stimulatory factor (NKSF), a cytokine with multiple biologic effects on human lymphocytes. *Journal of Experimental Medicine* **170**, 827–845 (1989).

486. Nastala, C. L. *et al.* Recombinant IL-12 administration induces tumor regression in association with IFN-gamma production. *J Immunol* **153**, 1697–706 (1994).

487. del Vecchio, M. *et al.* Interleukin-12: Biological Properties and Clinical Application. *Clinical Cancer Research* **13**, 4677–4685 (2007).

488. Kerkar, S. P. *et al.* IL-12 triggers a programmatic change in dysfunctional myeloid-derived cells within mouse tumors. *Journal of Clinical Investigation* **121**, 4746–4757 (2011).

489. Ma, X. *et al.* The interleukin 12 p40 gene promoter is primed by interferon gamma in monocytic cells. *Journal of Experimental Medicine* **183**, 147–157 (1996).

490. Hayes, M. P., Wang, J. & Norcross, M. A. Regulation of interleukin-12 expression in human monocytes: selective priming by interferon-gamma of lipopolysaccharide-inducible p35 and p40 genes. *Blood* **86**, 646–50 (1995).

491. Takeda, K. *et al.* IFN-γ production by lung NK cells is critical for the natural resistance to pulmonary metastasis of B16 melanoma in mice. *J Leukoc Biol* **90**, 777–785 (2011).

492. Wiltrout, R. H. *et al.* Role of organ-associated NK cells in decreased formation of experimental metastases in lung and liver. *J Immunol* **134**, 4267–75 (1985).

493. Esteso, G. *et al.* Natural Killer Anti-Tumor Activity Can Be Achieved by In Vitro Incubation With Heat-Killed BCG. *Front Immunol* **12**, (2021).

494. Kleinnijenhuis, J. *et al.* BCG-induced trained immunity in NK cells: Role for non-specific protection to infection. *Clinical Immunology* **155**, 213–219 (2014).

495. Suliman, S. *et al.* Bacillus Calmette–Guérin (BCG) Revaccination of Adults with Latent *Mycobacterium tuberculosis* Infection Induces Long-Lived BCG-Reactive NK Cell Responses. *The Journal of Immunology* **197**, 1100–1110 (2016).

496. Kim, S. *et al.* In vivo developmental stages in murine natural killer cell maturation. *Nat Immunol* **3**, 523–528 (2002).

497. Schuijs, M. J. *et al.* ILC2-driven innate immune checkpoint mechanism antagonizes NK cell antimetastatic function in the lung. *Nat Immunol* **21**, 998–1009 (2020).

498. Elpek, K. G., Rubinstein, M. P., Bellemare-Pelletier, A., Goldrath, A. W. & Turley, S. J. Mature natural killer cells with phenotypic and functional alterations accumulate upon sustained stimulation with IL-15/IL-15Rα complexes. *Proceedings of the National Academy of Sciences* **107**, 21647–21652 (2010).

499. Brownlie, D. *et al.* Expansions of adaptive-like NK cells with a tissue-resident phenotype in human lung and blood. *Proceedings of the National Academy of Sciences* **118**, (2021).

500. Sojka, D. K. *et al.* Tissue-resident natural killer (NK) cells are cell lineages distinct from thymic and conventional splenic NK cells. *Elife* **3**, (2014).

501. Peng, H. *et al.* Liver-resident NK cells confer adaptive immunity in skin-contact inflammation. *Journal of Clinical Investigation* **123**, 1444–1456 (2013).

502. Karlhofer, F. M., Ribaudo, R. K. & Yokoyama, W. M. MHC class I alloantigen specificity of Ly-49+ IL-2-activated natural killer cells. *Nature* **358**, 66–70 (1992).

503. Kirchhammer, N. *et al.* NK cells with tissue-resident traits shape response to immunotherapy by inducing adaptive antitumor immunity. *Sci Transl Med* **14**, (2022).

504. Tang, Z., Kang, B., Li, C., Chen, T. & Zhang, Z. GEPIA2: an enhanced web server for large-scale expression profiling and interactive analysis. *Nucleic Acids Res* **47**, W556–W560 (2019).

505. Cursons, J. *et al.* A Gene Signature Predicting Natural Killer Cell Infiltration and Improved Survival in Melanoma Patients. *Cancer Immunol Res* **7**, 1162–1174 (2019).

506. Maier, B. *et al.* A conserved dendritic-cell regulatory program limits antitumour immunity. *Nature* **580**, 257–262 (2020).

507. Huntington, N. D., Cursons, J. & Rautela, J. The cancer–natural killer cell immunity cycle. *Nat Rev Cancer* **20**, 437–454 (2020).

508. Horowitz, A., Stegmann, K. A. & Riley, E. M. Activation of natural killer cells during microbial infections. *Front Immunol* **2**, 88 (2011).

509. Alspach, E., Lussier, D. M. & Schreiber, R. D. Interferon γ and its important roles in promoting and inhibiting spontaneous and therapeutic cancer immunity. *Cold Spring Harb Perspect Biol* **11**, (2019).

510. Herbst, S., Schaible, U. E. & Schneider, B. E. Interferon Gamma Activated Macrophages Kill Mycobacteria by Nitric Oxide Induced Apoptosis. *PLoS One* **6**, e19105 (2011).

511. Moliva, J. I., Turner, J. & Torrelles, J. B. Immune Responses to Bacillus Calmette–Guérin Vaccination: Why Do They Fail to Protect against Mycobacterium tuberculosis? *Front Immunol* **8**, (2017).

512. Tarancón, R. *et al.* Therapeutic efficacy of pulmonary live tuberculosis vaccines against established asthma by subverting local immune environment. *EBioMedicine* **64**, 103186 (2021).

513. MITCHELL, M. S., KIRKPATRICK, D., MOKYR, M. B. & GERY, I. On the Mode of Action of BCG. *Nat New Biol* **243**, 216–218 (1973).

514. Loyher, P.-L. *et al.* Macrophages of distinct origins contribute to tumor development in the lung. *J Exp Med* **215**, 2536–2553 (2018).

515. Casanova-Acebes, M. *et al.* Tissue-resident macrophages provide a pro-tumorigenic niche to early NSCLC cells. *Nature* **595**, 578–584 (2021).

516. Fritz, J. M. *et al.* Depletion of Tumor-Associated Macrophages Slows the Growth of Chemically Induced Mouse Lung Adenocarcinomas. *Front Immunol* **5**, (2014).

517. Sharma, S. K. *et al.* Pulmonary Alveolar Macrophages Contribute to the Premetastatic Niche by Suppressing Antitumor T Cell Responses in the Lungs. *The Journal of Immunology* **194**, 5529–5538 (2015).

518. Arendt, K. A. M. *et al.* An In Vivo Inflammatory Loop Potentiates KRAS Blockade. *Biomedicines* **10**, 592 (2022).

519. Pfirschke, C. *et al.* Immunogenic Chemotherapy Sensitizes Tumors to Checkpoint Blockade Therapy. *Immunity* **44**, 343–354 (2016).

520. Hsu, J. *et al.* Contribution of NK cells to immunotherapy mediated by PD-1/PD-L1 blockade. *Journal of Clinical Investigation* **128**, 4654–4668 (2018).

521. Salmon, H. *et al.* Expansion and Activation of CD103+ Dendritic Cell Progenitors at the Tumor Site Enhances Tumor Responses to Therapeutic PD-L1 and BRAF Inhibition. *Immunity* **44**, 924–938 (2016).

522. Spranger, S., Dai, D., Horton, B. & Gajewski, T. F. Tumor-Residing Batf3 Dendritic Cells Are Required for Effector T Cell Trafficking and Adoptive T Cell Therapy. *Cancer Cell* **31**, 711-723.e4 (2017).

523. Spranger, S., Bao, R. & Gajewski, T. F. Melanoma-intrinsic β-catenin signalling prevents anti-tumour immunity. *Nature* **523**, 231–235 (2015).

524. Lin, J. H. *et al.* Type 1 conventional dendritic cells are systemically dysregulated early in pancreatic carcinogenesis. *Journal of Experimental Medicine* **217**, (2020).

525. Teijeira, A. *et al.* Depletion of conventional type-1 dendritic cells in established tumors suppresses immunotherapy efficacy. *Cancer Res* (2022) doi:10.1158/0008-5472.CAN-22-1046.

526. Moreo, E. *et al.* Novel intravesical bacterial immunotherapy induces rejection of BCG-unresponsive established bladder tumors. *J Immunother Cancer* **10**, e004325 (2022).

527. Miga, A. J. *et al.* Dendritic cell longevity and T cell persistence is controlled by CD154-CD40 interactions. *Eur J Immunol* **31**, 959–965 (2001).

528. Zhang, M. *et al.* CCL7 recruits cDC1 to promote antitumor immunity and facilitate checkpoint immunotherapy to non-small cell lung cancer. *Nat Commun* **11**, 6119 (2020).

529. Schenkel, J. M. *et al.* Conventional type I dendritic cells maintain a reservoir of proliferative tumor-antigen specific TCF-1+ CD8+ T cells in tumor-draining lymph nodes. *Immunity* **54**, 2338-2353.e6 (2021).

530. Lavin, Y. *et al.* Innate Immune Landscape in Early Lung Adenocarcinoma by Paired Single-Cell Analyses. *Cell* **169**, 750-765.e17 (2017).

531. Pulendran, B. *et al.* Distinct dendritic cell subsets differentially regulate the class of immune response *in vivo*. *Proceedings of the National Academy of Sciences* **96**, 1036–1041 (1999).

532. Tan, M. C. B. *et al.* Disruption of CCR5-Dependent Homing of Regulatory T Cells Inhibits Tumor Growth in a Murine Model of Pancreatic Cancer. *The Journal of Immunology* **182**, 1746–1755 (2009).

533. Halama, N. *et al.* Tumoral Immune Cell Exploitation in Colorectal Cancer Metastases Can Be Targeted Effectively by Anti-CCR5 Therapy in Cancer Patients. *Cancer Cell* **29**, 587–601 (2016).

534. Tian, L. *et al.* Specific targeting of glioblastoma with an oncolytic virus expressing a cetuximab-CCL5 fusion protein via innate and adaptive immunity. *Nat Cancer* **3**, 1318–1335 (2022).

535. Wendel, M., Galani, I. E., Suri-Payer, E. & Cerwenka, A. Natural Killer Cell Accumulation in Tumors Is Dependent on IFN-γ and CXCR3 Ligands. *Cancer Res* **68**, 8437–8445 (2008).

536. Alexandre, Y. O. *et al.* XCR1+ dendritic cells promote memory CD8+ T cell recall upon secondary infections with Listeria monocytogenes or certain viruses. *Journal of Experimental Medicine* **213**, 75–92 (2016).

537. Lin, Q. *et al.* IFN-γ-dependent NK cell activation is essential to metastasis suppression by engineered Salmonella. *Nat Commun* **12**, 2537 (2021).

538. Soudja, S. M. *et al.* Memory-T-Cell-Derived Interferon-γ Instructs Potent Innate Cell Activation for Protective Immunity. *Immunity* **40**, 974–988 (2014).

539. Jaime-Sanchez, P. *et al.* Cell death induced by cytotoxic CD8 $^{+}$ T cells is immunogenic and primes caspase-3–dependent spread immunity against endogenous tumor antigens. *J Immunother Cancer* **8**, e000528 (2020).

540. Minute, L. *et al.* Cellular cytotoxicity is a form of immunogenic cell death. *J Immunother Cancer* **8**, e000325 (2020).

541. Martínez-Lostao, L., Anel, A. & Pardo, J. How Do Cytotoxic Lymphocytes Kill Cancer Cells? *Clinical Cancer Research* **21**, 5047–5056 (2015).

542. de Miguel, D. *et al.* Inflammatory cell death induced by cytotoxic lymphocytes: a dangerous but necessary liaison. *FEBS J* **289**, 4398–4415 (2022).

543. Smyth, M. J. *et al.* Tumor Necrosis Factor–Related Apoptosis-Inducing Ligand (Trail) Contributes to Interferon γ–Dependent Natural Killer Cell Protection from Tumor Metastasis. *Journal of Experimental Medicine* **193**, 661–670 (2001).

544. Freeman, A. J. *et al.* Natural Killer Cells Suppress T Cell-Associated Tumor Immune Evasion. *Cell Rep* **28**, 2784-2794.e5 (2019).

545. Restifo, N. P. *et al.* Loss of Functional Beta2-Microglobulin in Metastatic Melanomas From Five Patients Receiving Immunotherapy. *JNCI Journal of the National Cancer Institute* **88**, 100–108 (1996).

546. Korkolopoulou, P., Kaklamanis, L., Pezzella, F., Harris, A. & Gatter, K. Loss of antigen-presenting molecules (MHC class I and TAP-1) in lung cancer. *Br J Cancer* **73**, 148–153 (1996).

547. Joyce, J. A. & Fearon, D. T. T cell exclusion, immune privilege, and the tumor microenvironment. *Science (1979)* **348**, 74–80 (2015).

548. Altorki, N. K. *et al.* The lung microenvironment: an important regulator of tumour growth and metastasis. *Nat Rev Cancer* **19**, 9–31 (2019).

549. Schmidt, L. *et al.* Enhanced adaptive immune responses in lung adenocarcinoma through natural killer cell stimulation. *Proceedings of the National Academy of Sciences* **116**, 17460–17469 (2019).

550. Liu, Y. *et al.* Immune Cell PD-L1 Colocalizes with Macrophages and Is Associated with Outcome in PD-1 Pathway Blockade Therapy. *Clinical Cancer Research* **26**, 970–977 (2020).

551. Kowanetz, M. *et al.* Differential regulation of PD-L1 expression by immune and tumor cells in NSCLC and the response to treatment with atezolizumab (anti–PD-L1). *Proceedings of the National Academy of Sciences* **115**, (2018).

552. Reck, M. *et al.* Pembrolizumab versus Chemotherapy for PD-L1–Positive Non–Small-Cell Lung Cancer. *New England Journal of Medicine* **375**, 1823–1833 (2016).

553. Brody, R. *et al.* PD-L1 expression in advanced NSCLC: Insights into risk stratification and treatment selection from a systematic literature review. *Lung Cancer* **112**, 200–215 (2017).

554. Herbst, R. S. *et al.* Atezolizumab for First-Line Treatment of PD-L1–Selected Patients with NSCLC. *New England Journal of Medicine* **383**, 1328–1339 (2020).

555. Brahmer, J. R. *et al.* The Society for Immunotherapy of Cancer consensus statement on immunotherapy for the treatment of non-small cell lung cancer (NSCLC). *J Immunother Cancer* **6**, 75 (2018).

556. Tokito, T. *et al.* Predictive relevance of PD-L1 expression combined with CD8+ TIL density in stage III non-small cell lung cancer patients receiving concurrent chemoradiotherapy. *Eur J Cancer* **55**, 7–14 (2016).

557. Hiam-Galvez, K. J., Allen, B. M. & Spitzer, M. H. Systemic immunity in cancer. *Nat Rev Cancer* **21**, 345–359 (2021).

558. Waight, J. D. *et al.* Myeloid-derived suppressor cell development is regulated by a STAT/IRF-8 axis. *Journal of Clinical Investigation* **123**, 4464–4478 (2013).

559. Kurihara, T., Warr, G., Loy, J. & Bravo, R. Defects in Macrophage Recruitment and Host Defense in Mice Lacking the CCR2 Chemokine Receptor. *Journal of Experimental Medicine* **186**, 1757–1762 (1997).

560. Wu, W.-C. *et al.* Circulating hematopoietic stem and progenitor cells are myeloid-biased in cancer patients. *Proceedings of the National Academy of Sciences* **111**, 4221–4226 (2014).

561. Allen, B. M. *et al.* Systemic dysfunction and plasticity of the immune macroenvironment in cancer models. *Nat Med* **26**, 1125–1134 (2020).

562. Casbon, A.-J. *et al.* Invasive breast cancer reprograms early myeloid differentiation in the bone marrow to generate immunosuppressive neutrophils. *Proceedings of the National Academy of Sciences* **112**, (2015).

563. Tarancón, R., Uranga, S., Martín, C. & Aguiló, N. *Mycobacterium tuberculosis* infection prevents asthma and abrogates eosinophilopoiesis in an experimental model. *Allergy* **74**, 2512–2514 (2019).

564. Grisaru-Tal, S., Rothenberg, Marc. E. & Munitz, A. Eosinophil–lymphocyte interactions in the tumor microenvironment and cancer immunotherapy. *Nat Immunol* **23**, 1309–1316 (2022).

565. Mattes, J. *et al.* Immunotherapy of Cytotoxic T Cell–resistant Tumors by T Helper 2 Cells. *Journal of Experimental Medicine* **197**, 387–393 (2003).

566. O'Flaherty, S. M. *et al.* TLR-Stimulated Eosinophils Mediate Recruitment and Activation of NK Cells *In Vivo*. *Scand J Immunol* **85**, 417–424 (2017).

567. Qi, L. *et al.* Interleukin-33 activates and recruits natural killer cells to inhibit pulmonary metastatic cancer development. *Int J Cancer* **146**, 1421–1434 (2020).

568. Hilligan, K. L. *et al.* Intravenous administration of BCG protects mice against lethal SARS-CoV-2 challenge. *Journal of Experimental Medicine* **219**, (2022).

569. Barclay, W. R., Anacker, R. L., Brehmer, W., Leif, W. & Ribi, E. Aerosol-Induced Tuberculosis in Subhuman Primates and the Course of the Disease After Intravenous BCG Vaccination. *Infect Immun* **2**, 574–582 (1970).

570. Owen, L. N. & Bostock, D. E. *Effects of Intravenous BCG in Normal Dogs and in Dogs with Spontaneous Osteosarcoma*. J. Cancer* vol. 10 (1974).

571. Schwarzenberg, L., Simmler, M. C. & Pico, J. L. Human toxicology of BCG applied in cancer immunotherapy. *Cancer Immunology, Immunotherapy* **1–1**, 69–76 (1976).

572. Holmgren, I. Employment of B. C. G., especially in Intravenous Injection. *Acta Med Scand* **90**, 350–361 (1936).